Modelling the radio synchrotron outbursts from the nova-like variable star AE Aquarii

Louis Albert Venter

This thesis is submitted to fulfill the requirements
for the qualification Master of Science
in the
Faculty of Natural and Agricultural Sciences,
Department of Physics
of the University of the Free State.

Supervisor : Dr P.J. Meintjes

Date of submission : 2003/05/30

Acknowledgments

I would like to thank Dr. Pieter Meintjes for his initiative and excellent leadership in this study.

I gratefully acknowledge the financial support of the NRF during the period of 2002-2003.

Die werk en kennis waarmee ek in die soeke na 'n model vir die radio waarnemings van AE Akwarius in aanraking gekom het, was hoogs leersaam. Dit is steeds byna onbegryplik hoeveel verder, wyer en dieper nog gedelf kan word in enige van die oneindige aantal spesialiteitsvelde van die fisiese wetenkappe. Uitdagings sal nooit skaars raak nie.

Graag bedank ek Dr. Meintjes vir sy inisiatief en onontbeerlike raad en leiding in die voltooiing van hierdie verhandeling met goeie werk altyd as oogmerk.

Verder bedank ek ook my ouers en broers vir hulle ondersteuning oor jare van studie. Hulle was en is 'n seën in my lewe.

Al die eer en dank kom toe aan ons Vader in die hemel vir sy sorg en seën in sy onbegryplike groot genade, liefde en wysheid.

Abstract

This thesis proposes a model for the origin of the observed radio outbursts of the binary star AE Aquarii. The system consists of a white dwarf (WD) and a red dwarf (RD) orbiting each other with a period of P_{orb} ~10 h. The compact white dwarf and its relatively strong ($B_* \sim 10^6$ G) magnetic field rotates about its spin axes with period P_{WD} ~ 33 s.

Plasma clouds fall from the RD to the WD and a part of this mass transfer reaches the surface of the WD where X-ray and optical emission results. An important aspect for the model is that most of the transfer flow is expelled from the system by the rapidly rotating magnetosphere of the WD. An assumtion of the model is that a part of the transfer is magnetized with a field strength of up to B_{blob} = 3000 G. This magnetic field in the transfer originates on the red dwarf star. The blobs originate at the point where the gravitational and centrifugal forces of the two star combination is in equilibrium and where plasma is pushed from the RD to the WD by pressure gradients between the RD's surface and the vacuum-like space around the WD. In this process the RD's magnetic field is pinched into the clouds and electrons are accelerated to mildly relativistic energies (1-15 MeV). These electrons in the the magnetic field then radiate via the synchrotron emission process in the radio to infra-red frequency range.

The radiation loses intensity as the blobs expand due to the weakening field and the electrons losing energy. However, in the model it is suggested that the electrons are re-accelerated in the propeller ejection process. The electrons are energized by the compressing action of the magnetophere on the blobs in terms of acceleration mechanisms like shock drift acceleration and magnetic pumping.

It is also assumed that the magnetic field is tangled in the blobs in a highly turbulent medium. The tangled field ensures knots of high magnetic energy density where acceleration can take place. The field also weakens slower with expansion.

The combination of the re-acceleration and the strengthened field means that a blob can stay a radio source for a longer time. This prolonged life time of a radio blob is important to explain the observed time variation of the radio flux from AE Aquarii.

The Van der Laan model describes the time evolution of a synchrotron cloud due to its expansion. This idea is applied to the plasma blobs of AE Aqr that are ejected from the system and expand as they drift away.

The flux is calculated for a single blob in the radio to IR frequency range. The flux from blobs at different stages of expansion are integrated in all frequency bands above the plasma frequency of each individual blob. The result is a spectrum that can be compared to the average observed spectrum.

Key terms : radio flares, synchrotron blobs, magnetic propeller, particle acceleration, flux integration, average spectrum, van der Laan mechanism

Contents

Chapter 1

Introduction

It is estimated that up to 70% of stars are double or multiple (Warner 1995). These binary star systems are classified in many different categories according to a variety of criteria. However, the closer the stars are to each other, the better the chances of strong interaction between them which will result in more spectacular emission. The systems with the smallest separation are called close binaries and since AE Aqr falls into this category, a basic introductory discussion will be given of close binary systems mostly concerning aspects relevant to this study.

1.1 Close Binary Stars

1.1.1 Basic principles

A close binary system consists of two orbiting stars very close to each other, comparable to the Earth-Moon system, resulting in very strong tidal interaction between them. If the physical dimensions of the two orbiting stars are significant fractions of the orbital separation, the outer layers of the stars will be severely distorted by the gravitational interaction between the two stars. This tidal interaction between two such close orbiting stars is illustrated in Figure 1a. However, close binary systems may also exist in a configuration where one of the components is a compact star like a white dwarf, neutron star or black hole, orbiting a main sequence star. The orbital motion of the two stars occur about the centre of mass of the system as shown in Figure 1b.

Furthermore, stellar rotation periods may be synchronized with the orbital period of the system as a result of the tidal forces between the stars. The theoretical description of the gravitational interaction in binary stars in general was given by Edouard Albert Roche,

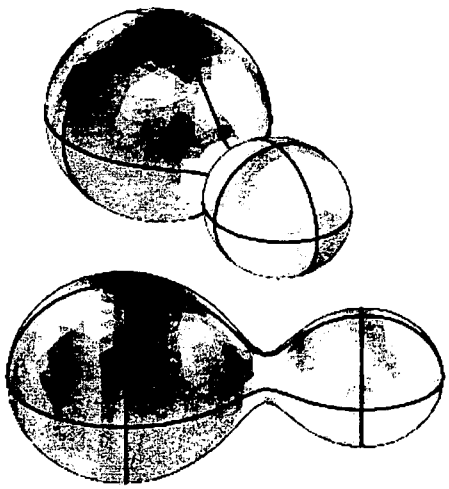

Figure 1a : The distortion of two stars in a close binary due to their strong gravitational interaction (two viewing angles). (Hendry & Mochnacki 2000)

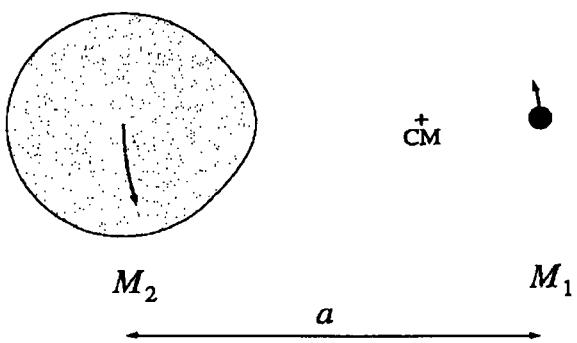

Figure 1b : A binary system consisting of a compact star of mass M_1 and a sun-like star of mass M_2. The binary separation a, is the distance between the centres of the stars. (Frank, King and Raine 1992)

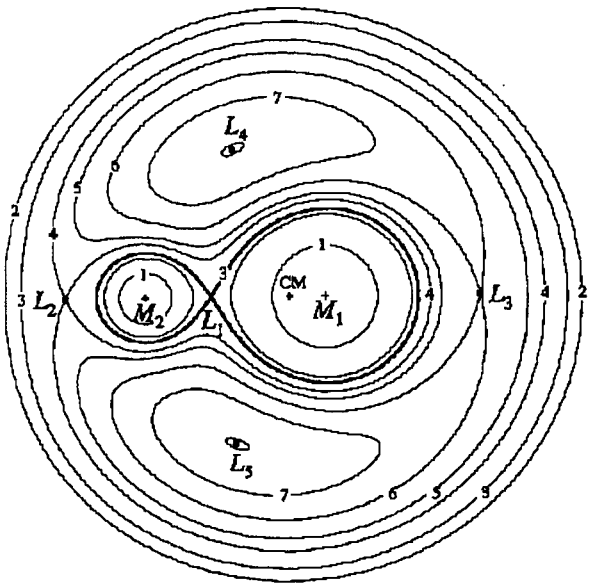

Figure 2: Illustration of the equipotential surfaces of the Roche potential for a specific mass ratio between the two stars. (Frank, King & Raine 1992)

a French mathematician, in 1873. In Roche's model, which is still used today, the stellar components are treated as gravitational point sources to give, relative to a Cartesian reference frame centered on the primary star and rotating with the binary the total potential. This potential is the sum of the gravitational potentials and the centrifugal potential and is given by

$$\Phi_R(\bar{r}) = \frac{-\mathrm{GM}_1}{\bar{r}-\bar{r}_1} - \frac{\mathrm{GM}_2}{\bar{r}-\bar{r}_2} - \frac{1}{2}(\omega \times \bar{r})^2. \tag{1.1}$$

For circular orbits time independent equipotentials can be found. Near the stellar centres these equipotential surfaces are spherical, but become pear-shaped further away. Critical surfaces result where the apexes of the equipotentials of each star touch. These surfaces contain the masses of their respective gravitational sources, i.e. stars, and are referred to as the Roche lobes of the stars. The point of contact of the Roche lobes is called the inner Lagrangian point, L1, which is an unstable equilibrium position. This equilibrium point is where the gravitational and centrifugal forces of the two stars are in equilibrium and therefore material at the L1 point will be weightless with respect to both stars. Figure 2 shows the general form of the Roche equipotentials in a binary.

Before the 20th century it was thought that this model was only a special limiting case of the gravitational interaction between binary components whose mass is concentrated in their centres. However, by the second decade of the 20th century it was realized that a large fraction of the

mass of ordinary main sequence stars is in fact concentrated in the centre, and consequently the gravitational potential does not deviate significantly from that of a point source, as seen from outside the star. This is true for all tidally and rotationally distorted stars since the outer tenuous layers, contribute very weakly to the total gravitational potential of the star (Campbell 1997). More refined models, e.g. Chandrasekhar (1933) and Plavec (1958), indicate that the equipotentials of distorted stars in close tidally interacting binaries approach those of the Roche model to a high degree of accuracy.

The interaction of the two stars in a close binary through mass transfer leads to spectacular emission phenomena, characteristic of these type of stellar systems. The mass transfer in such a binary system is closely related to the physical evolution of the two stars. Mass transfer is most effective when at least one of the stars comes into contact with its Roche lobe. In this process the high thermal velocities of the gas particles in the outer envelope (near L1) will carry them over the L1 point into the gravitational potential well of the companion star. Gas is therefore transferred from a 'mass donating'star to the Roche lobe of its companion. This process will be discussed in more detail below.

Roche lobe contact (the star surface touching its own Roche lobe) of stars in binary systems can be established and maintained through various mechanisms. Main sequence stars burning hydrogen in their centres increase in size by up to 60% relative to their Zero Age Main Sequence size (Iben 1967). Therefore, these stars can 'swell-up'into their Roche surface. Post main-sequence evolution also results in an increase in the dimensions of the star which can result in Roche lobe contact. Complementing stellar evolution, angular momentum losses from the binary system, as a result of stellar wind and gravitational radiation losses, shrinks the Roche lobe so that Roche lobe contact can also be established and maintained in this fashion.

It was suggested (Wood 1950) that close binary stars can be divided into two classes; one containing systems in which both stellar components lie beneath their respective Roche surfaces, known as detached systems, and the other, containing binaries in which at least one binary component fills its Roche lobe. Kopal (1955) suggested further dividing the latter class into two groups, the first containing systems in which only one stellar component fills its Roche lobe, known as semi-detached systems, while in the second group both components fill their Roche surfaces to form contact binaries (Campbell 1997). The basic configuration of a semi-detached binary is illustrated in Figure 3.

Fascinating phenomena occur in semi-detached binary systems in which an ordinary main sequence star fills its Roche surface while orbiting a more massive compact object like a black hole,

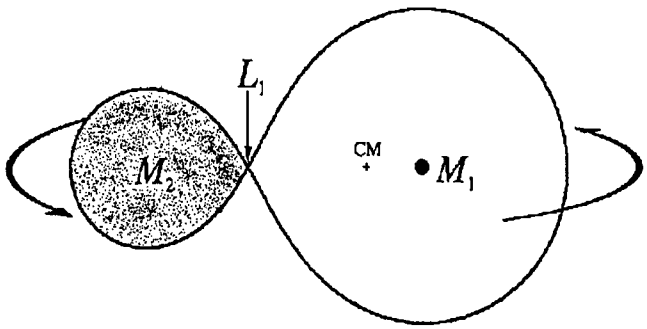

Figure 3: Illustration of a typical semi-detached close binary. CM indicates the centre of mass of the system. The primary star is the more massive star and mass can escape from the secondary through the L1 region towards the primary. (Frank , King & Raine 1992)

neutron star or white dwarf. The lobe filling main sequence star is called **the secondary star**, while the compact object is called **the primary star**. Semi-detached binaries where the compact object is a neutron star or black hole, are usually referred to as X-ray binaries, while systems with a white dwarf as the primary, are in broad terms referred to as cataclysmic variables. The name refers to some emission properties of these systems.

If the initial pre semi-detached evolution of the close binary brought the outer tenuous layers of the secondary star near the inner Lagrangian point, gas particles can as a result of their high thermal velocities escape from the atmosphere of the secondary into the Roche lobe of the primary compact object, initiating mass transfer from the secondary to the primary. Figure 4 illustrates the flow of the mass from the secondary star through the L1 'nozzle' into the primary's Roche lobe.

1.1.2 Mass transfer in close binaries

Roche contact in a semi-detached binary system initiates the mass transfer phase; a fascinating period in the evolution of the system. The subsequent gas flow from the inner Lagrangian point resembles the escape of a gas through a nozzle into a vacuum. The flow velocity through the nozzle is to order of magnitude equal to the thermal velocity of the gas. As the stream of gas flows away from the L1 point the stream is deflected by the Coriolis effect through an angle(θ) with respect to the line of centres of the two stars (see Figure 4).

The stream follows a ballistic trajectory, expanding also transversely with the speed of sound and therefore pressure forces in the stream quickly become negligible. Therefore, the stream

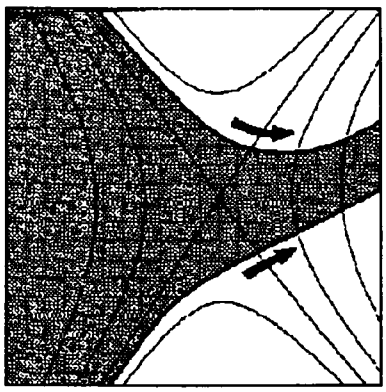

Figure 4: The flow of gas from the secondary through the L1 region into the Roche lobe of the primary star. The deviation in direction on just entering the lobe is the result of the Coriolis force. (from Pringle 1985)

trajectory is well described by single particle trajectories of individual particles ejected from L1 in all directions, but in the general direction of the stream, at sonic velocities (see Warner 1995 for a discussion). As can be seen from Figure 5 the stream, when initiated, still remains in tact after the first passage past the primary star. The stream trajectory can be found by integrating the equations of motion for a single particle in the rotating binary frame, keeping in mind conservation of total mechanical energy of the particles, i.e.

$$\frac{1}{2}\dot{r}^2 + \Phi_R = \text{const} \tag{1.2}$$

where $\dot{r}$ is the particle velocity and Φ_R is the Roche potential.

Particles starting off with low velocities, i.e. approximately equal to the speed of sound, at the inner Lagrangian point L1, do not have sufficient energy to cross the Roche surface at any other point in the Roche lobe of the primary (Flannery 1975, Warner 1995). This is because the potential well of the primary star, which is usually a more massive compact object, is significantly deeper than the potential well of the secondary. Therefore, the trajectories of these particles lie completely within the Roche lobe of the primary. When the particles approach the Roche lobe of the primary, they do it with very low velocities. Therefore, the Roche lobe is known as a *zero velocity surface.* The stream has a distance of closest approach from the centre of the primary (Lubow & Shu 1975, Warner 1995) which is given by

$$\frac{r_{min}}{a} \approx 0.05\mathrm{q}^{-0.464} \tag{1.3}$$

for $0.05 < \mathrm{q} = \frac{\mathrm{M_2}}{\mathrm{M_1}} < 1$, where $\mathrm{M_2}$ and $\mathrm{M_1}$ represent the masses of the secondary and primary respectively. The larger q is, the smaller r_{min} is. In this relation a represents the binary separation

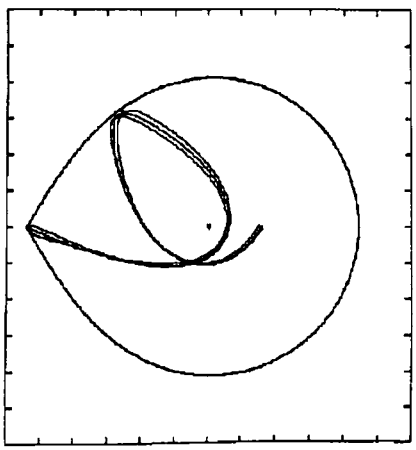

Figure 5: Illustration of the initial encircling of the primary and the formation of a ring. (Flannery 1975)

(see Frank, King & Raine 1992), which for close binaries with orbital periods of the order of a few hours, can be written as

$$a = 3.5 \times 10^{10} \left(\frac{M_1}{M_\odot}\right)^{1/3} (1+q)^{1/3} P_{orb,hr}^{2/3} \text{ cm} \tag{1.4}$$

Since for most semi-detached binaries the primary star is a compact object with dimension $R_* \leq 10^9$ cm, and $q \leq 1$, it can be seen that in all cases under consideration the distance of closest approach $r_{min} > R_*$ (Warner 1995). Therefore, interaction of the stream with the compact primary star is very unlikely unless the primary has a very strong magnetic field which can intercept the flow at some point. Examples of this is found in certain magnetic cataclysmic variables which will be discussed later. As the trajectory of the stream lies totally within the Roche lobe of the primary star, and is confined to the orbital plane, it will intersect itself at a point well within the Roche surface of the primary (see Fig.6). This collision at supersonic speed shocks the gas to high temperatures, thereby radiating away the surplus thermal energy of the impact. However, angular momentum is conserved and since a circular orbit has the least energy for a given angular momentum, the dissipation of energy in this initial process will tend to produce a ring of gas orbiting the compact object with a circular orbit. The initial ring therefore forms at the so called circularization radius where the specific angular momentum of the gas flow is the same as the specific angular momentum at the L1 point.

However, unless an effective mechanism exists that drains away angular momentum from the accretion ring, no direct mass accretion onto the compact object can occur, unless of course, the

compact object possesses a significant magnetic field as was mentioned above.

1.1.3 Basic principles of mass accretion onto a compact object

Suppose a ring of matter is orbiting a central compact object of mass M in a circular orbit of inner radius r. By balancing the gravitational force against the centrifugal force one can show that the angular velocity of orbiting particles is given by

$$\Omega(r) = \left(\frac{GM_*}{r^3}\right)^{1/2} \tag{1.5}$$

where G and M_* represent the universal gravitational constant and the mass of the central compact object respectively. The angular velocity of the planets around the Sun also varies as $\Omega \propto r^{-3/2}$ leading to Kepler's third law of planetary motion and therefore the associated motion is called Keplerian motion. In a gaseous ring around a central gravitating object such a relation implies a high velocity shear within the ring. Then, as a result of viscosity, we can expect angular momentum to be transferred from the faster moving inner regions of the ring to the slower moving outer regions. As matter in the inner regions loses angular momentum it spirals inward, closer to the central gravitating object. Outer regions, gaining angular momentum, will spread out towards the mass donating star. Hence it is viscosity that determines the rate at which gravitational PE is converted into heat and radiation when the material is eventually accreted onto the surface of the compact object. The whole process of ring and disc formation and eventual mass accretion onto the compact object is illustrated in Figure 6.

Therefore, accretion discs are highly efficient machines that drain away the angular momentum of the mass transfer from a companion star, enabling it to accrete onto the surface of a compact object, liberating its enormous amount of gravitational PE as radiation. It can be shown that for an accreting body of mass M_* the total amount of gravitational PE released from accreting material can be calculated as the total amount of work done by the gravitational field in bringing the gas pockets to the surface from $R \rightarrow \infty$ (since the field weakens rapidly with radial distance) or $\int_\infty^r \mathbf{F}_{grav}.d\mathbf{r}$ and therefore

$$\begin{aligned} \Delta E_{acc} &= -\int_{R_*}^{\infty} \mathbf{F}_{grav}.d\mathbf{r} \\ &= \frac{GM_*m}{R_*}. \end{aligned} \tag{1.6}$$

The amount of gravitational PE released when a mass of 1 g accretes onto a one Solar mass white dwarf with radius R_* is

$$\Delta E_{grav} \approx 10^{17} \left(\frac{M_*}{M_\odot}\right) \left(\frac{m}{1\,g}\right) \left(\frac{R_*}{10^9\,cm}\right)^{-1} \text{erg.} \tag{1.7}$$

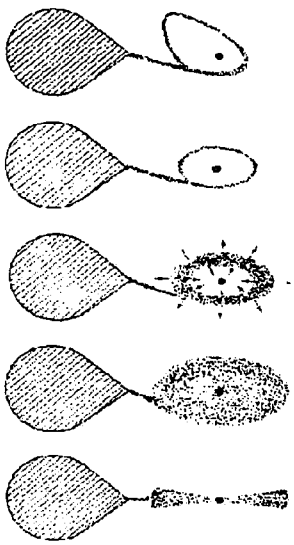

Figure 6: Illustration of the formation of the ring and subsequently the disc in a close binary. The disc makes accretion onto the primary star possible. The last sketch is a side view. (Verbunt 1982)

This energy is released mainly in the form of electromagnetic radiation and heat. The same amount of material, i.e. hydrogen, when converted into helium by thermonuclear reactions, will release

$$\begin{aligned} \Delta E_{nuc} &= 7 \times 10^{-3} \mathrm{mc}^2 \\ &= 10^{18} \left(\frac{\mathrm{m}}{1\,\mathrm{g}} \right) \mathrm{erg}, \end{aligned} \tag{1.8}$$

showing that accretion onto a compact object like a white dwarf will release, to order of magnitude, the same amount of energy as a nuclear fusion reaction. The effectiveness of converting gravitational PE into radiation is significantly higher when the accreting object is a very compact object like a 10 km, one Solar mass, neutron star. In such a case the ratio of accretion power to fusion power of one gram of material is approximately

$$\alpha = \left(\frac{\Delta E_{acc}}{\Delta E_{nuc}} \right) \approx 16. \tag{1.9}$$

Accretion onto a compact object is therefore a very efficient mechanism of converting gravitational potential energy into heat and radiation. One can easily show that the rate at which gravitational potential energy is released as heat and radiation is given by

$$\mathrm{L}_{acc} = \left(\frac{dE_{acc}}{dt} \right) = \frac{d}{dt} \left(\frac{\mathrm{GMm}}{\mathrm{R}_*} \right) \tag{1.10}$$

which results in

$$L_{acc} = \left(\frac{GM\dot{m}}{R_*}\right) \tag{1.11}$$

where $\dot{m}$ represents the mass accretion rate onto the poles of the compact object.

It can be shown that mass accretion onto a one Solar mass white dwarf or neutron star can result in accretion induced luminosities of the order of

$$L_{acc} \approx 10^{34} \left(\frac{\dot{m}}{10^{17}\,\mathrm{g\,s^{-1}}}\right)\left(\frac{M_*}{M_\odot}\right)\left(\frac{R_*}{10^9\,\mathrm{cm}}\right)^{-1} \mathrm{erg\,s^{-1}} \tag{1.12}$$

and

$$L_{acc} \approx 10^{37} \left(\frac{\dot{m}}{10^{17}\,\mathrm{g\,s^{-1}}}\right)\left(\frac{M_*}{M_\odot}\right)\left(\frac{R_*}{10^6\,\mathrm{cm}}\right)^{-1} \mathrm{erg\,s^{-1}} \tag{1.13}$$

respectively. If this luminosity, which is released on the compact object, is compared to the total integrated luminosity of the Sun, i.e.

$$L_\odot = 3.86 \times 10^{33}\,\mathrm{erg\,s^{-1}}, \tag{1.14}$$

it can be seen that mass accretion can be a very efficient source of emission in astrophysical objects. This simple example shows that mass accretion onto compact objects is a very interesting mechanism for the release of gravitational potential energy since these systems are as a result amongst the most luminous systems in the galaxy. These systems also display a plethora of transient accretion related emission phenomena which is why they are among the most studied objects in observational and theoretical astrophysics (see Warner 1995).

Up to this point the discussion regarding close binaries has been very general and concentrated on the most basic properties of mass transfer and mass accretion in these systems. Since this study concerns the non-thermal properties of the magnetic cataclysmic variable AE Aquarii, a more detailed discussion regarding the various aspects of mass transfer and mass accretion falls outside the scope of this thesis. Since AE Aquarii is a member of the cataclysmic variable stars, more specifically the magnetic cataclysmic variables, we will now shift our attention to some of their most basic properties.

1.1.4 Cataclysmic Variables

Cataclysmic variables (see Warner 1995, Lang 1991) consist of a white dwarf star (primary) and a relatively small companion star (secondary) orbiting their common centre of mass. The companion star is usually a cool main-sequence star (red dwarf) of late spectral type G, K or M. These systems have orbital periods lying between 1 and 15 hours. The orbital period is an indicator of the binary

separation. The binary separation and the mass ratio of the two stars (i.e. $q = \frac{M_2}{M_1}$) are such that the secondary star fills its Roche lobe causing gas to flow from its tenuous outer envelope to the degenerate primary star, i.e. the white dwarf. In the absence of a strong magnetic field on the white dwarf, the gas can form an accretion disc around the white dwarf. The disc may then extend down to the white dwarf surface, where the accretion power is released in a very thin boundary layer (Frank King & Raine 1992). If the white dwarf has a significant magnetic field, the magnetosphere (the spatial confinement or influence sphere of the magnetic field) influences the gas flow before the gas reaches the surface of the white dwarf (see §1.2). In extreme cases, which will be discussed later, the formation of a disc may be prevented by the strong magnetosphere.

The magnetosphere-disc interface will be a region of pressure equilibrium between the gas and magnetosphere. If this pressure equilibrium exists at radial distances from the white dwarf which lies within the corotation radius (r_{co}), i.e. where the Keplerian velocity of the orbiting gas equals the rotation of the white dwarf and its magnetosphere, gas parcels can attach onto the field lines and be guided to the surface of the star where they can accrete. The Keplerian velocity increases the closer a particle gets to a gravitating object (the white dwarf) and thus at some radial distance (r_{co}) this velocity will equal the rotation velocity of the white dwarf. No accretion can occur from outside the corotation radius since the gas parcels cannot overcome the centrifugal barrier posed by the faster rotating magnetosphere in this region.

The cataclysmic variables are classified according to the character of their light variations, resulting from gigantic outbursts (hence the name cataclysmic variables) on the surface of the accreting white dwarf or in the accretion disc. These outbursts can be linked to the various mechanisms involved in the mass accretion process onto the surface of the white dwarf. One class, called novae or classical novae, displays very luminous outbursts that are in some cases visible to the unaided eye. These nova outbursts have usually been observed only once, and are believed to be the result of the sudden nuclear fusion of hydrogen in the hot dense envelope formed by mass accretion on the surface of the white dwarf. Classical novae occur in our galaxy at the rate of approximately 73 per year (Lang 1991), which makes them about 3300 times more common than supernovae in our galaxy (Lang 1991, and references therein). Each nova explosion releases about 5×10^{-5} Solar masses of ejected gas. Recurrent novae have also been recorded and they usually display more than one outburst of smaller amplitude than nova eruptions, with the interval between nova eruptions of the order of 10 to 50 years.

Another class, the dwarf novae, have weaker but more frequent outbursts, with amplitudes ranging between 2 and 6 magnitudes. The interval between outbursts ranges from days to months

or years in some cases (Warner 1995, Lang 1991). The dwarf nova outbursts are attributed to the increase in accretion rate onto the white dwarf as a result of an increase in disc viscosity, which is still a very poorly understood process. A sudden increase in disc viscosity results in an enhanced accretion rate onto the white dwarf (Frank King & Raine 1992) according to

$$\nu\Sigma = \frac{\dot{m}}{3\pi}\left(1 - \left(\frac{R_*}{R}\right)^{1/2}\right) \tag{1.15}$$

where ν and Σ represent the disc viscosity and surface density (gcm^{-2}) respectively, and $\dot{m}$ represents the mass accretion rate. The correlation between high disc viscosity and enhanced mass accretion can be understood by noting that the higher the gas viscosity in the disc, the more efficient is the angular momentum transfer from the faster rotating inner layers of the disc to the slower rotating outer layers. A higher disc viscosity results in the quick spreading of the disc, the inner layers (losing angular momentum) towards the compact degenerate star, and the outer layers (gaining angular momentum) towards the mass donating star, feeding angular momentum back to the binary. Angular momentum loss from the inner layers as a result of enhanced viscosity (see Frank, King & Raine 1992 for a detailed discussion) will result in a dramatic increase in the accretion rate onto the white dwarf which will result in a dwarf nova outburst. Dwarf novae have been divided into three subtypes according to the light curve of their stellar prototypes, i.e. the U Geminorum, Z Camelopardalis and SU Ursae Majoris subtypes (Smak 1984, Lang 1991). A more detailed discussion of these systems and their properties falls outside the scope of this thesis.

1.2 The Magnetic Cataclysmic Variables (mcvs)

Stellar magnetic fields can be intensely amplified during stellar evolution to the white dwarf stage, resulting in the surface magnetic field of the white dwarf to be amplified to values $B_* \geq 10^7$ Gauss. Therefore some cataclysmic variables consist of an intensely magnetized white dwarf primary star and a red-dwarf secondary that fills its Roche lobe. In these systems the magnetic field of the primary starts to influence the flow of gas at large distances from the white dwarf, as was briefly mentioned earlier. Based mainly upon the surface magnetic field of the white dwarf, the mcvs are divided into three main categories, the polars, intermediate polars and the DQ Herculis systems.

1.2.1 Polars (AM Herculis systems)

These systems contain the most intensely magnetized white dwarfs, with surface fields of $B_* > 10^7$ G, resulting in a magnetic moment ($\mu = B_* R_*^3$), i.e. an indication of the extent of the magnetosphere

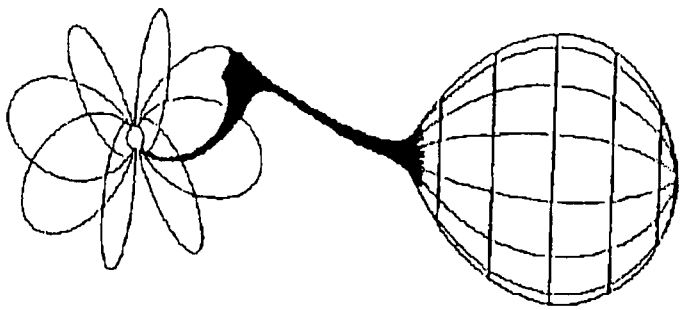

Figure 7 : A sketch of a typical polar illustrating the flow of plasma along the field lines of the white dwarf's magnetic field.(Warner 1995, adapted from Cropper 1990)

(Warner 1995), of

$$\mu > 10^{34} \left(\frac{B_*}{10^7\,G}\right)\left(\frac{R_*}{10^9\,cm}\right)^3 G\ cm^3. \tag{1.16}$$

They are also very compact binary systems with the red dwarf and white dwarf orbiting their common centre of mass with periods $P_{orb} < 4$ hours, resulting in a binary separation (Warner 1995)

$$a < 9 \times 10^{10} \left(\frac{P_{orb}}{4\,h}\right)^{2/3} cm, \tag{1.17}$$

which implies that these systems can easily fit into the Sun, i.e. $(a/D_\odot) < 0.7$, where $D_\odot$ represents the Sun's diameter. As a result of the very strong white dwarf surface field, as well as the compactness of the system, the magnetosphere of the white dwarf exceeds the binary separation, resulting in the magnetosphere of the white dwarf intercepting the gas stream from the Roche filling secondary (see Figure 7).

Since the magnetic pressure dominates the gas pressure the gas flow is guided towards the polar cap regions of the white dwarf where accretion can occur after the supersonic flow is thermalized in a stand-off shock where it passes from supersonic to subsonic speeds (see Figure 8) before accreting onto the poles. The temperature in the shock is determined by the mass and radius of the white dwarf (Frank King & Raine 1992) according to

$$k_B T_s \approx 35 \left(\frac{M_1}{M_\odot}\right)\left(\frac{R_*}{10^9\,cm}\right)^{-1} keV \tag{1.18}$$

for a one solar mass white dwarf. Temperatures in the region of 1 keV or more produce strong X-ray emission, which is in fact how these systems were discovered (Warner 1995). The optical light emitted from the accretion zone above the polar cap contains a high degree of circular polarization

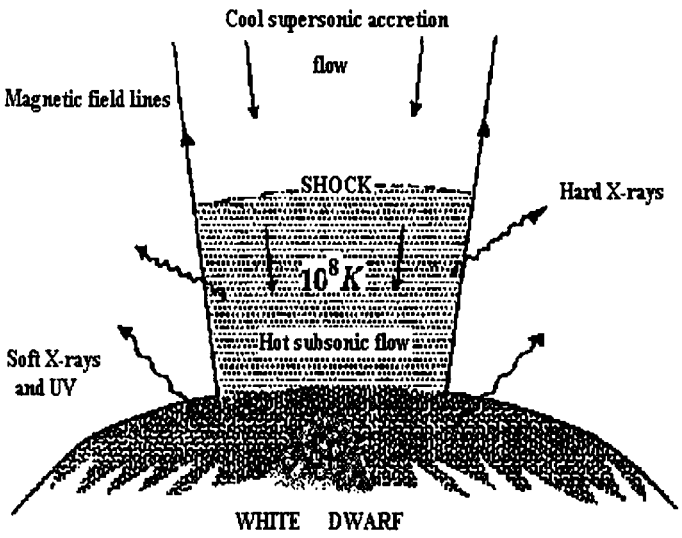

Figure 8 : A sketch of the typical structure of the shock region formed in an accretion column on a white dwarf (Patterson 1994)

as a result of cyclotron emission from thermal electrons trapped in the strong field. The high degree of circular polarization is also the reason why these systems are called polars.

The compactness of these systems, coupled with the fact that the white dwarf magnetosphere exceeds the binary separation, results in the tidal interaction and magnetic torques between the white dwarf and secondary to synchronize the orbital and rotation periods of both stars. Therefore, these systems are also sometimes called synchronous mcvs.

1.2.2 Intermediate Polars

TV Col and AO Psc were the first two members of this class of cataclysmic variables discovered, which are now designated as intermediate polars (Campbell 1997). In contrast to the polars, these systems show no detectable circular polarization in the optical light, indicating a weaker field. In the intermediate polars the white dwarf is slightly less magnetized, with fields of the order of $B_* < 10^7$ G, resulting in a magnetic moment

$$\mu < 10^{34}\,\mathrm{G\ cm^3}. \tag{1.19}$$

These binaries are wider than the polars, with orbital periods of the order of $P_{orb} > 3.5$ hours. The weaker field combined with the wider binary separation result in the rotation of the primary

not being synchronized with the orbital period. The spin periods of the white dwarfs are typically of the order of $P_* >> 100$ s. In general it is found that the ratio of the spin and orbital periods in most of the intermediate polars seems to obey the relation $P_* \sim 0.1\ P_{orb}$. This relation was shown to result from the mass transfer between the secondary and the compact primary being fragmented into large diamagnetic blobs (diamagnetic: not easily penetrated by external magnetic fields) (King & Lasota 1991; King 1993; Wynn & King 1995). A consequence of this mode of mass transfer is that large blobs can stay in tact without being disrupted or influenced by the white dwarf magnetosphere at distances further than the circularization radius. This is where the accretion flow forms a ring conserving the specific angular momentum the transfer had at the L1 point. If the circularization radius is inside the corotation radius, the white dwarf can accrete material that has the same specific angular momentum as the binary system. The accretion of orbital angular momentum results in a gradual spin-up of the white dwarf to an equilibrium period $P_{eq} \sim 0.1\ P_{orb}$.

However, depending on variations in the mass transfer rate from the secondary as well as the magnetic field strength of the white dwarf, these systems can also accrete via an accretion disc if the following condition (Warner & Wickramasinghe 1991) is satisfied

$$\frac{\mu_{34}}{\sqrt{\dot{m}_{18}}} < 0.4 \left(\frac{P_{orb}}{4\,h}\right)^{7/6} M_1^{5/6} \tag{1.20}$$

where μ_{34} is the magnetic moment of the white dwarf in units of 10^{34} G cm^3, $\dot{m}_{18}$ represents the mass accretion rate in units of 10^{18} g s^{-1} and M_1 represents the white dwarf mass in solar units. It can be seen that this condition depends rather sensitively on the magnetic moment of the white dwarf, as well as on the mass transfer rate from the companion star, albeit to a somewhat lesser degree. The presence of an accretion disc in the intermediate polars can result in significant deviations in the relation $P_* \sim 0.1\ P_{orb}$ as a result of star-disc torques spinning the white dwarf up or down. Table 1 lists the observed periods and rates of spin-down or -up of the intermediate polars.

To put this into context a brief overview of the interaction between the white dwarf magnetosphere and an accretion disc will be given to highlight the most important aspects that dominate the angular momentum exchange between the magnetized white dwarf and accretion disc. The net torque on the magnetized white dwarf can either result in the spinning-up (rotates faster) or spinning-down (rotates slower) of the accreting white dwarf, and is the sum of the angular momentum flux from the disc inner edge as a result of mass accretion from regions inside the corotation radius (spin-up) and the drag the white dwarf experiences from the coupling of the magnetosphere

with the disc outside the corotation radius (spin-down) (Ghosh & Lamb 1978, 1979a,b, Wang 1987).

Name	P(hr)	P_R(min)	$\dot{P}_R/P_R(yr^{-1})$
Gk Per	47.92	5.86	-2.2×10^{-6}
V1062 Tau	9.95	62.00	
XY Ari	6.06	3.44	
TX Col	5.72	31.84	
TV Col	5.49	31.83	
PQ Gem	5.18	13.89	
FO Aqr	4.85	20.91	8.6×10^{-7}
YY Dra	3.91	8.82	
AO Psc	3.59	13.42	-2.6×10^{-6}
V1223 Sgr	3.370	12.42	9.7×10^{-7}
BG CMi	3.24	15.22	2.0×10^{-8}
EX Hya	1.63	67.03	-3.0×10^{-7}

Table 1. This table lists the orbital and rotation periods as well as the observed spin-up or -down of some intermediate polars (Campbell 1997).

The net torque on the compact accreting white dwarf is given by the expression (Wang 1987)

$$N = \dot{m}(GM_1R_c)^{1/2} f(x_o), \tag{1.21}$$

where $\dot{m}$, M_1, R_c represents the accretion rate from the disc inner edge, the mass of the white dwarf and the corotation radius respectively, with the dimensionless function given by

$$f(x_o) = \left(x_o^{1/2} + \frac{2}{9} x_o^{31/80} \left[1 - x_o^{3/2} - \frac{x_o^{9/4}}{(1 - x_o^{3/2})^{1/2}} \right] \right) \tag{1.22}$$

with $x_o = (R_o/R_c)) \leq 1$. Here R_o is the radial distance where the gas flow is dominated by the white dwarf magnetic field (in the vicinity of the disc inner edge) and R_c is the corotation radius. Wang (1987) showed that $f(x_o) > 0$ for all $x_o < 0.971$ resulting in a positive net torque and a subsequent spin-up of the accreting compact object. Since $f(x_o) < 0$ (negative net torque) for all $0.971 < x_o \leq 1$, the compact object will spin down. The equilibrium period, reached when spin-up and spin-down torques are in balance, is obtained at $x_o = 0.971$. The rate of change of the white dwarf period is then

$$\left(\frac{-\dot{P}_*}{P_*} \right) = \left(\frac{N}{I\Omega_*} \right) \approx \frac{5}{2} \left(\frac{\dot{m}}{M_1} \right) \left(\frac{R_c}{R_*} \right) f(x_o), \tag{1.23}$$

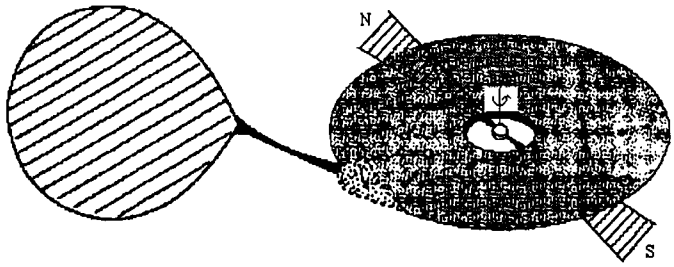

Figure 9 : An illustration of the supposed configuration of an oblique rotator, as proposed for DQ Her and AE Aqr. (Patterson 1979, 1994)

where N, I, $\dot{m}$, M_1 and R_* represent the net torque, moment of inertia of the white dwarf, mass accretion rate, white dwarf mass and white dwarf radius, respectively. The total timescale of change of the white dwarf period in these systems is $\tau = P_*/|\dot{P}_*|$. It can be seen that these systems can actually fluctuate between states of spin-up and spin-down depending on the mass transfer rate from the secondary star since this will influence the position of the disc inner edge (where pressure equilibrium exists between the disc and magnetosphere) and hence the ratio x_o as well as $f(x_o)$.

The long term monitoring of these systems, paying special attention to the evolution of the spin period of the accreting white dwarfs, can provide valuable information about possible variations in the mass transfer, which is closely linked to the evolution of these systems.

1.2.3 DQ Herculis (DQ Her) systems

The DQ Her binaries are a subset of the intermediate polars. They have short primary rotation periods ($P_* < 100$ s) and lack hard X-ray emission. In terms of the standard model, the short rotation period $P_* \ll 0.1\ P_{orb}$ hints that these systems may be disc accretors. To put the pulsed emission of DQ Her, the prototype of this class, into perspective, the oblique disc rotator model was developed by Bath, Evans & Pringle (1974), which could be a representative model for all disc accreting magnetic cataclysmic variables (Figure 9).

In this model the pulsed emission from disc accreting DQ Her stars, as well as the intermediate polars, is the direct result of the accretion of gas onto the exposed magnetic pole of a magnetized white dwarf, which is tilted with respect to the rotation axis (see Figures 9, 10). Rotation of the compact object will cause the pole heated by accretion to continually move into and out of the field of view of an observer, resulting in pulsed emission modulated with the spin period of the magnetized white dwarf.

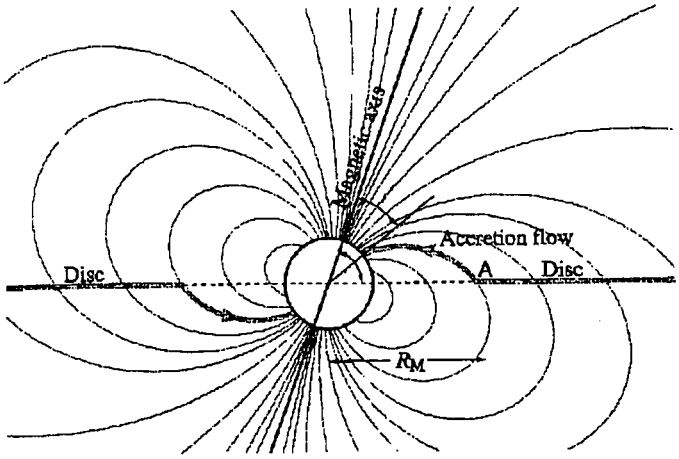

Figure 10 : An illustration of the basic orientation of the accreting pole and accretion disc for an oblique rotator. (Frank, King & Raine 2002)

This subclass contains only three systems, AE Aquarii (AE Aqr), DQ Herculis (DQ Her) and V533 Herculis (V533 Her). Their basic properties are listed in Table 2.

Name	P(hr)	P_R(min)	$\dot{P}_R/P_R(yr^{-1})$
AE Aqr	9.88	0.55	5.4×10^{-6}
V533 Her	5.04	1.06	1.5×10^{-7}
DQ Her	4.65	1.18	-3.6×10^{-7}

Table 2. The characteristic periods of the three DQ Her systems. (Campbell 1997)

These binaries played an extremely important role in the early pioneering work regarding the development of a general model for the cataclysmic variables. AE Aqr was shown to be a spectroscopic binary by Joy (1954) and was subsequently used by Crawford & Kraft (1956) towards deriving the basic model for the cataclysmic variables. DQ Her is the remnant of Nova Herculis 1934 and was identified by Walker (1954) as an eclipsing binary with an orbital period of P_{orb} = 4 hr 39 min (Campbell 1997).

The discussion above regarding the various magnetic cataclysmic variables, illuminating just some of their most important properties, paved the way for our focus to shift to AE Aquarii. The rapid and continuous variability of this system makes it a very peculiar source, which is why is has been scrutinized in all available wavelengths, from radio to TeV gamma-rays.

1.3 The Nova-Like Variable AE Aquarii

1.3.1 The basic properties of the binary system

AE Aquarii was first discovered on photographic plates (Zinner 1938). The peculiar variability of this system stimulated intense follow-up studies. The picture that immerged is that AE Aquarii consists of a white dwarf primary and K4-K5 red dwarf secondary orbiting their common centre of mass with a period of $P_{orb} \approx 9.88$ h. The inferred distance to AE Aqr is approximately D = 100 pc (Welsh, Horne & Oke 1993). The total optical emission from the system is dominated by the red dwarf secondary, but superimposed on this, flares with magnitudes $\Delta m_v \leq 2$ occur on a nearly continuous basis, causing the visible magnitude to fluctuate continuously between $m_v \sim 12$ (quiescence) and $m_v \sim 10$ (flares). Figure 11 shows some example of optical lightcurves.

The first systematic study of the nature of the pulsed optical emission (Patterson 1979) revealed steady but rather weak (amplitudes between 0.1-0.2 %, increasing to 0.6 % during flares) pulsations at periods of $P_o = 33.08$ s and $P_1 = 16.54$ s (first harmonic of P_o), with a wealth of quasi periodic oscillations (QPOs) which seem to be associated with the optical emission during outbursts (see Figure 12a).

In terms of the standard model for accreting systems, i.e. the oblique rotator model (Bath, Evans & Pringle 1974), adopted by Patterson (1979), the two fundamental pulses were explained as the spin period of the white dwarf ($P_* = P_o$), with the first harmonic($P_1 = 16.54$ s) the result of illumination of the disc inner edge by the second pole facing the other way. The QPOs were explained in terms of self luminous blobs orbiting the disc with Keplerian periods, during periods of enhanced mass accretion leading to outbursts. The very short period of $P_* = 33.08$ s means that AE Aquarii possesses the fastest rotating accreting white dwarf known.

AE Aquarii was also detected in X-ray wavelengths by the *EINSTEIN* satellite in the *wavelength* range 0.1 - 4 keV (Patterson et al. 1980). The X-ray emission resembles a 1 keV thermal bremsstrahlung spectrum with an inferred luminosity of $L_X \sim 5 \times 10^{30}(D/100\ pc)^2$ erg s^{-1} (Patterson et al. 1980). The $P_* = 33.08$ s spin period of the white dwarf is visible in the *EINSTEIN* observations, but no hint of the first overtone at 16.54 s is found. The strong periodic nature of the X-ray emission at the observed optical and supposed spin period of the white dwarf can be seen in Figure 12b.

Hubble Space Telescope (HST) observations of AE Aquarii in the ultra-violet wavelengths showed a very strong modulation at the 33 s rotation period of the white dwarf, but no significant increase in the signal is observed during strong outbursts (Eracleous et al. 1994).

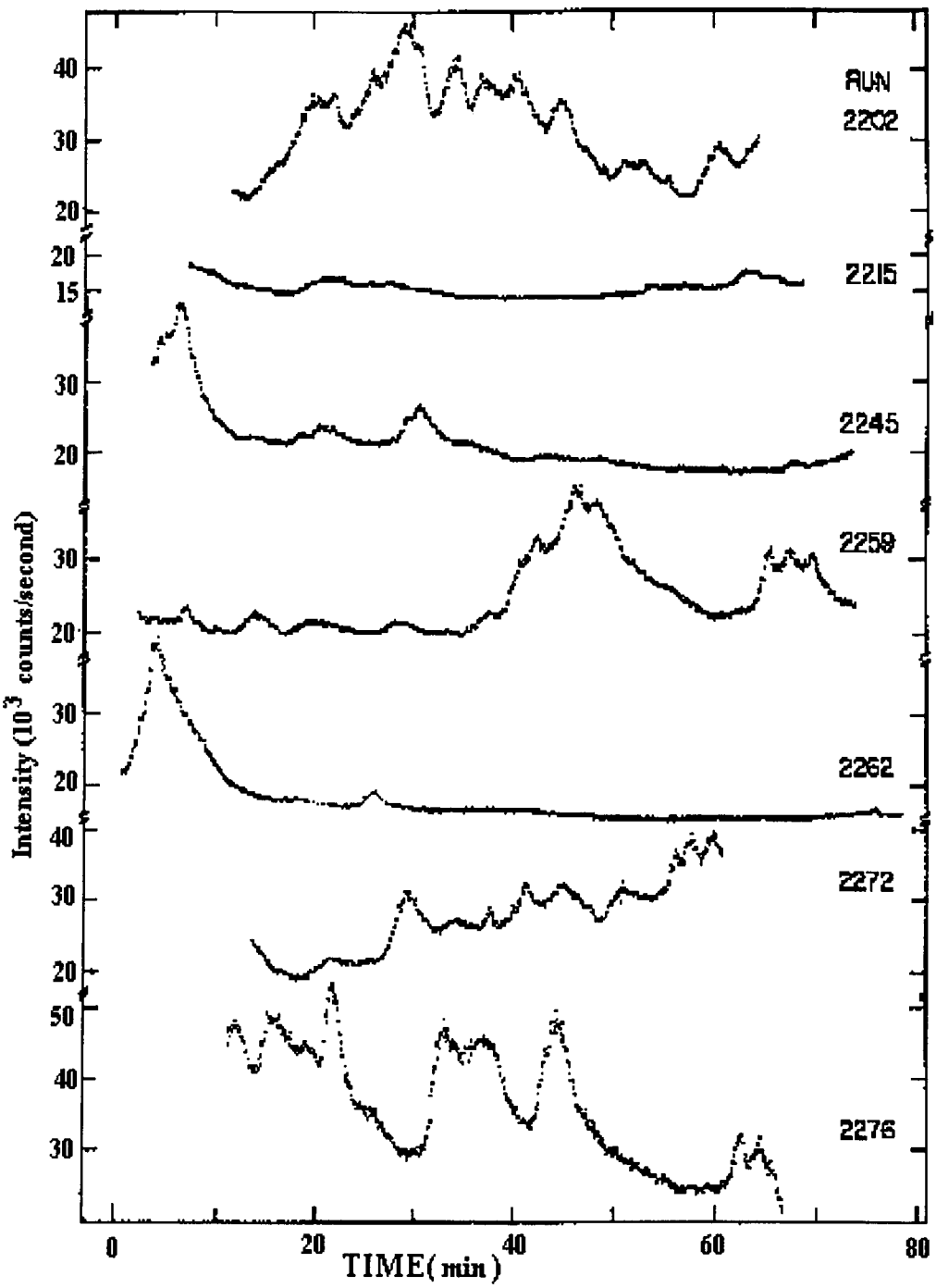

Figure 11 : Light curves of AE Aquarii in the optical band showing the variable nature of the emission from the system. (Patterson 1979)

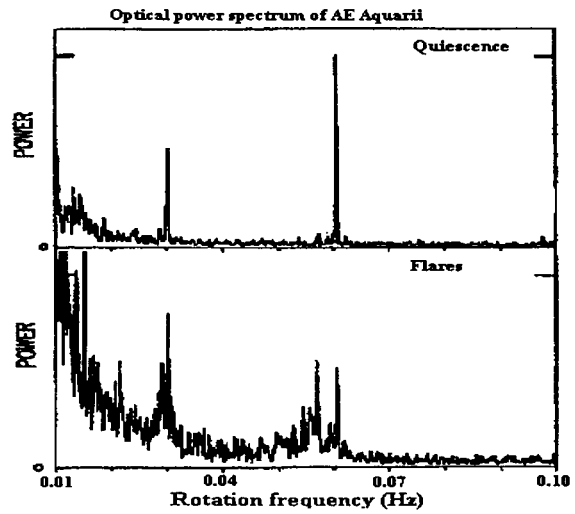

Figure 12a : Power spectra of AE Aquarii showing the strong signal at the spin period of the white dwarf of $P_o = 33.08$ s and the first harmonic $P_1 = 16.54$ s. The bottom panel also indicates the multitude of QPOs that appear in the flare state. (Patterson 1994)

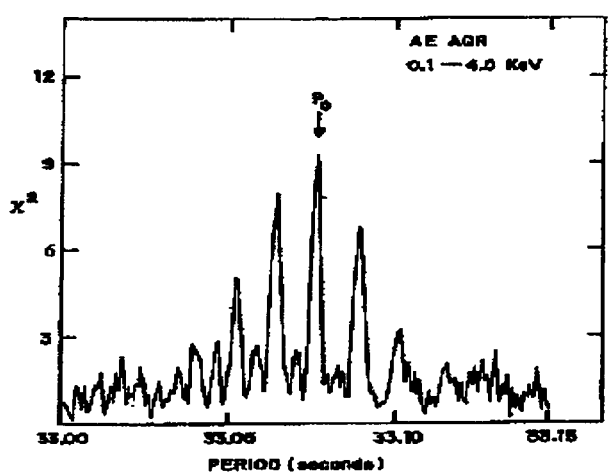

Figure 12b : Periodogram of the soft X-ray (0.1 - 0.4 keV) light curve of AE Aqr (1980 May 13-15). The central peak occurs at the optical period while the flanking peaks are aliases introduced by 24-hr gaps in the data. (de Jager 1991; Patterson 1994)

The average luminosity derived from the *HST* data is $L_{UV} \sim 2 \times 10^{31}(D/100\ pc)^2$ erg s^{-1}, which must be mainly the result of direct mass accretion onto the poles of the white dwarf, given the strong modulated signal at the spin period of the white dwarf. The lack of additional modulation at this period during outbursts was the first sign that enhanced accretion onto the white dwarf is not the mechanism behind the outbursts in AE Aquarii. *X-ray* and *HST* observations in the UV band confirm the spin of the white dwarf, but the relatively low X-ray luminosity of $L_X \sim 5 \times 10^{30}$ erg s^{-1}(Wynn, King and Horne 1997) implies a small accretion rate onto the poles of the white dwarf with $\dot{M} \leq 10^{14}$ g s^{-1}. The *HST* UV light curve suggested a quiescent UV luminosity which can be the result of mass accretion onto the poles of $L_{UV} \sim 1.7 \times 10^{31} \left(\frac{f}{1\ mJy}\right) \left(\frac{2000\ \mathring{A}}{\lambda}\right)$ erg s^{-1}. The authors estimate the accretion luminosity or rate as $L_{acc} \sim 3L_{UV} = 5 \times 10^{31}$ erg s^{-1}.

Spectroscopic studies (Jameson, King & Sherrington 1980) of AE Aqr show unusually strong UV emission lines of low and high ionization species. It is concluded that the emission lines originate at different sites in the system. Eracleous et al. (1994) reported a strong Lyα absorption line which is attributed to a white dwarf atmosphere with temperature T $\sim$ 26000 K. Line emission detected in spectroscopic observations (Eracleous & Horne 1996) implies gas densities of between $n \sim 10^9 - 10^{11}$ cm^{-3} and this in return indicates a minimum mass transfer flow of $\dot{M} \sim 4 \times 10^{17}$ g s^{-1}. Spectrophotometry of AE Aqr (Welsh, Horne & Gomer 1998), especially the Hα line emission, revealed a Doppler tomogram which is consistent with mass outflow from the system (see Figure 13). It was also shown that the observed flaring in the line emission from AE Aqr is consistent with radiative cooling of ejected gas blobs from the system, meaning as the blobs enlarge their surface area they become more luminous. This provides evidence that the flaring is not accretion driven but a result of radiative cooling. This puts the weak correlation between the pulsed 33 s signal and the flares into perspective.

A detailed pulse timing analysis (de Jager et al. 1994), using an optical data set spanning 14 years, revealed that the white dwarf is steadily spinning down at a rate of $\dot{P}_* = 5.64 \times 10^{-14}$ s s^{-1}, resulting in the white dwarf to lose rotational kinetic energy at a rate of

$$\begin{aligned} \dot{E}_{rot} &= I\Omega_*\dot{\Omega}_* \\ &\approx 10^{34} \left(\frac{I}{10^{50}\ g\ cm^2}\right) \left(\frac{P_*}{33\ s}\right)^{-3} \left(\frac{\dot{P}_*}{5.64 \times 10^{-14}\ s\ s^{-1}}\right) \text{ erg } s^{-1}, \end{aligned} \tag{1.24}$$

where I is the moment of inertia and $\Omega = (2\ \pi/P_*)$ is the angular frequency of the white dwarf.

By adopting an orbital inclination $i = 55°$ (Warner 1995) (the angle between the normal vector to the binary plane and observer), the pulse timing analysis (de Jager et al. 1994) constrained the

Figure 13 : Computer simulation of the ejected transfer flow from the red dwarf by the magnetic propeller of the white dwarf in AE Aquarii. (Frank, King & Raine 1992, image by Dr. G.A. Wynn)

masses of the secondary and primary to

$$\begin{aligned} \left(\frac{M_1}{M_\odot}\right) &\approx 0.9\left(\frac{\sin i}{\sin 55^\circ}\right)^{-3} \\ \left(\frac{M_2}{M_\odot}\right) &\approx 0.6\left(\frac{\sin i}{\sin 55^\circ}\right)^{-3} \end{aligned} \tag{1.25}$$

which results in a mass ratio of the binary of

$$q = \left(\frac{M_2}{M_1}\right) \approx 0.67. \tag{1.26}$$

The peculiarly weak amplitudes of the $P_* = 33.08$ s pulsed signal in the optical data, during periods of quiescence and flares, as well as the lack of additional modulation of the spin period in the *HST* data during outbursts, are however not reconcilable with the standard model (Patterson 1979), i.e. being the result of mass accretion onto the poles of an oblique rotating magnetized white dwarf from an accretion disc. Recent studies (Eracleous & Horne 1996, Wynn, King & Horne 1997; Meintjes & de Jager 2000; Meintjes 2002a,b) indicated that the mass transfer from the secondary star in AE Aquarii is far too low for an accretion disc to develop in the system. This is the case since the fast rotating white dwarf acts as a propeller flinging the gas flow from the system, resulting in very low mass accretion onto the polar caps of the white dwarf. This is consistent with the Doppler tomogram showing mass outflow from the system (see Figure 13).

The detailed mechanism through which the white dwarf magnetosphere ejects the mass transfer is not yet understood. It can be expected that the mass transfer is ionized to some extent and that

the magnetosphere applies some force on this material. The ionized material is also resistant to penetration by the magnetic field of the white dwarf and this may mean that currents flowing along the field lines also flow 'around'the blob-like material. Magnetic forces on the moving charges can then drive the material out of the system. The ionization of the mass transfer can be the result of heating by the emission from the white dwarf accretion hot-spot, interaction with the rotating magnetosphere, the formation of shocks in the transfer flow and current heating.

The minimum mass outflow required to explain the rapid and continuous variablity then is $\dot{M}_{eject} \geq 5 \times 10^{17}$ g s^{-1}, leaving the system with velocities $v_{eject} \geq v_{esc} \approx 1550$ km s^{-1}, resulting in a total loss of mechanical energy from the system of

$$\begin{aligned} L_{mech} &\approx \tfrac{1}{2}\dot{M}_{eject} v_{esc}^2 \\ &\geq 5 \times 10^{33} \left(\frac{\dot{M}_{eject}}{5\times10^{17}\ \mathrm{g\ s^{-1}}}\right)\left(\frac{v_{eject}}{v_{esc}}\right)^2 \mathrm{erg\ s^{-1}}. \end{aligned} \tag{1.27}$$

This corresponds well with the loss of rotational kinetic energy of the white dwarf as a result of the magnetohydrodynamic(MHD) propeller ejecting gas from the binary system. The dissipation of MHD power in the magnetosphere of the white dwarf in AE Aquarii as the result of propeller ejection of gas also provides a mechanism to explain the transient non-thermal emission from AE Aquarii in terms of the conversion of rotational kinetic energy into mass outflow and particle acceleration. Since this thesis involves the study of the non-thermal radio outbursts in AE Aquarii, a discussion of the non-thermal properties of AE Aquarii will be presented.

1.3.2 The non-thermal emission from AE Aquarii

The energy supply for the non-thermal emission in the system is the spin-down of the white dwarf and the ejection of mass by the magnetic propeller. Only a small amount of material reaches the surface of the primary, explaining the weak correlation between the pulsed amplitude and the flaring activity. The accretion power available in the mass transfer can be estimated by considering the potential energy per nucleon released in a strong shock(encounter with the magnetic propeller) at the distance of closest approach of blobs to the white dwarf, before being flung out of the system. The available accretion power (for radiation) is found to be of the order of $L_{acc} \approx$ few $\times 10^{33}$ erg s^{-1} (Eracleous & Horne 1996), considering a mass transfer rate of $\dot{M} \sim$ 4-5 $\times 10^{17}$ g s^{-1}. This means that most of the Roche lobe overflow is being thrown out of the system since such a luminosity is only observed during flares.

The total power budget in AE Aqr is $\dot{E}_{sp-d} \approx L_{mech} + L_{flares} + L_{other}$ and it is noticeable that the largest fraction of the spin down power ($\dot{E} \approx 10^{34}$ erg s^{-1}) of the white dwarf is converted to

the mechanical outflow of material ($L_{mech} \approx 5 \times 10^{33}$ erg s^{-1}), resulting in a reservoir available to drive among others the non-thermal power (radio, TeV γ-rays) from the system.

Observations have been made in the TeV γ-ray band (Meintjes et al. 1992, 1994; Bowden et al. 1992) and these show pulsation at or close to the spin period of the white dwarf. These γ-rays show some quasi-periodicity but also burst-like events. The strongest TeV flares ($\sim 10^{34}$ erg s^{-1}) can at times, it seems, use all of the spin-down power for particle acceleration. Some of the TeV emission events are characterized as 1 min. spikes (de Jager 1995; Bowden et al. 1992) and these spikes may appear once in 40–50 h. Similar spikes have also been seen in optical data (de Jager & Meintjes 1993). The production of γ-rays in the energy range $E_\gamma > 1$ GeV is mainly due to the decay of π°-mesons produced in the high energy collisions between beams of ultra-relativistic protons with target matter(gas) with an integrated surface density $\Sigma \approx 50$ g cm^{-2}. The propeller ejected blobs in AE Aqr may act as target material which is bombarded by beams of protons and ions, presumably produced in the "propeller zone"by mechanisms like magnetic reconnection (Meintjes & de Jager 2000 for a detailed discussion).

AE Aquarii was discovered to be a highly variable *radio* source by Bookbinder & Lamb(1987). The first observations at 1.4 GHz and 4.9 GHz revealed that the flux varied between 3–5 mJy[1]. The emission varied on time-scales of the order of ≤ 5 minutes with an implied source size of $r = 10^{11}$ cm. The variable nature of the radio emission can be seen from the radio (15 and 4.9 GHz) light curves in Figure 14.

The explanation put forward was incoherent (gyro-)synchrotron emission from mildly relativistic electrons. The source is also thought to be dynamic as was proposed by Bastian, Dulk and Chanmugam (1988)(BDC) in the sense that the radio flux results from the superposition of individual flare events. These authors explained the highly variable radio emission in terms of the expansion of synchrotron emitting clouds of relativistic electrons, i.e. the so-called Van der Laan mechanism. This mechanism was proposed (Van der Laan 1963, 1966) to explain synchrotron flares in radio galaxies. Such a process is however consistent with the ejection of gas blobs ('blobs'is used when meaning magnetized, propeller influenced clouds) from AE Aqr by the magnetic propeller. If the blobs are magnetized, it will provide an environment in which the radio-synchrotron flares can occur. BDC reported observations in the frequency range 4–22.5 GHz which show the continuous nature of the radio outbursts or flares. The radio emission shows no periodicity but strong flares are superimposed on a weak, slowly varying background flux. The observed source size implies a high brightness temperature, $T_B \geq 10^{10}$ K and the radio

[1] 1 Jy (Jansky) = 10^{-23} erg $cm^{-2}.s^{-1}Hz^{-1}$

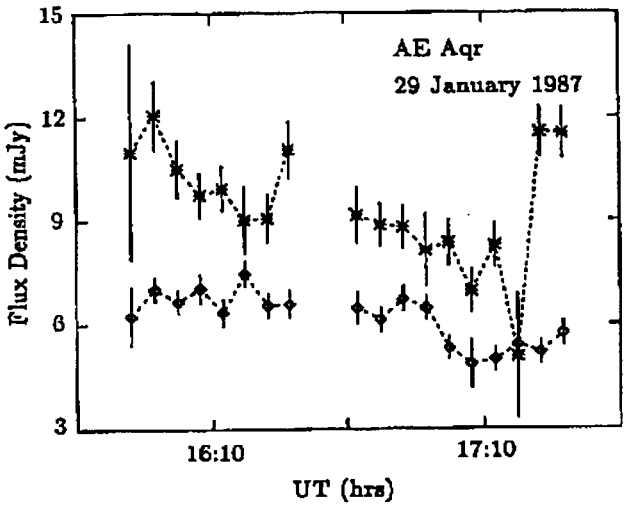

Figure 14 : Flux density of the 15 GHz (asterisks) and the 4.9 GHz (diamonds) emission of AE Aquarii obtained with the *VLA*. (Bastian, Dulk & Chanmugam 1988)

emission is therefore thought to be non-thermal in origin and specifically of synchrotron origin.

No polarization (or $< 10\%$) has been observed in this frequency range (1–22 GHz). Synchrotron radiation in a uniform magnetic field will be polarized to different degrees according to the orientation of the field with respect to the observer. The lack of polarization may indicate that the radio sources in AE Aqr contain randomly orientated magnetic fields with respect to one another and polarization is therefore lessened by the superposition of the emission from different sources.

Bastian, Beasley & Bookbinder (1996) found no variation in the radio emission at the orbital period (P_{orb} = 9.88 h) or at the spin period (P_{spin} = 33 s) of the white dwarf. The emission is therefore not dependent on the orbital phase of the system, thus consistent with radiation coming from blobs being thrown from the system on a continuous basis. Abada-Simon et al. (1993) observed at frequencies (4.9, 8.4, 15, 22.5, 88 and 240 GHz) and found variations of 1–2 hr and occasional short $\sim$ 5 min. variations. They also found that flux levels observed in May 1991 were appreciably lower than that of Oct. 1991. The emission thus seems to vary on more than one time-scale, minutes to hours but also months. The spectrum (a log(S)-log(ν) plot) of the average measurements is consistent with a power law for the flux , $S = S_o \nu^{\alpha}$ with α = 0.34–0.59. The variation over the month time-scale can thus be seen in the variation of S_o.

Abada-Simon et al.(1995a,b) reported simultaneous optical and radio (*VLA*) observations which show no correlation between the flares in the observed frequency ranges (5–15 GHz for the radio). *IRAS* data(horizontal lines in Fig. 15) at 100, 60, 25 and 12 μm could only establish upper limits

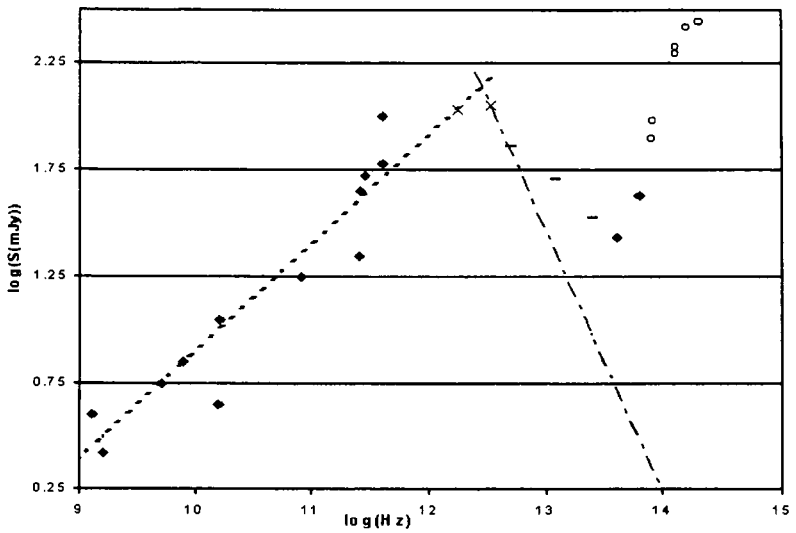

Figure 15 : The average radio-to-IR spectrum of AE Aquarii showing the optically thin and optically thick frequency ranges. (Adapted from Abada-Simon et al. 1999, 2002)

for the flux of 376, 73, 51 and 34 mJy respectively(Abada-Simon et al. 2003).

This constrains the highest frequency for the power law realistically to at most 60 μm (5000 GHz). The latest detections (Abada-Simon et al. 1999, 2002) revealed a flux density of 113 mJy at 90 μm (3330 GHz) at the 5σ confidence level and a 3σ upper limit of 108 mJy at 170 μm (1765 GHz). These two data points are indicated as X in Figure 15. The plot is of observations since 1981 from more than 10 different telescopes and instruments. The most recent being MERLIN, the Ryle telescope, the radio telescope in Nobeyama and instruments of the ISO (see Abada-Simon et al.2003 for details). Observations in the IR frequencies, dominated by the secondary star (indicated by open blocks)(Tanzi, Chincarini & Walker 1981), is also included in Figure 15. The dashed line is a fit to 14 average fluxes between 1.5 and 3330 GHz and has a slope of ($\sim$ +0.5). The dash-dot fit goes through the 90 μm and the 60 μm IRAS upperlimit and has a slope of -1.1 which would indicate an electron distribution index of $\delta = 3.2$ (see §3.1). On average the observations show variations in flux density by factors of up to 3 with time. The high variability in intensity can be seen from the detections of both 64 mJy and 107 mJy at 760 μm (400 GHz)(not averaged out).

The fact that the flux density increases with frequency beyond 400 GHz, already makes AE Aquarii unique among CVs. AE Aqr and AM Her are the only two CVs that are observed to be 'radio loud' (Beasley et al. 1994). The spectrum seems to have a turning point in the region of 90 μm. To actually pin down a specific turning point would in practice be difficult due to the

highly variable radio emission from the system. A possible average turning frequency and flux density may be found by modelling the radio spectrum of AE Aquarii.

An interesting observation was made by Niell(personal communication)(VLBI observation) of an expanding radio source with an average expansion velocity of $v_{exp} \sim 3000$ km s^{-1} to 4 times the binary separation a of the system. A peak flux of 24 mJy was measured for the initially unresolved radio source (3.6 cm / 8 GHz) and 7 mJy for a resolved source of $4 \times a$. This expansion occurred in about 30 minutes. This observation is consistent with a blob-like nature of the radio sources in AE Aqr and supports the scenario of expanding clouds of synchrotron emitting electrons. Abada-Simon et al. (1999) also explain observed dips in the radio data as eclipses by accreting gas blobs. This is consistent with the fact that the flaring radio sources (expanding clouds of relativistic electrons) are probably among the propeller outflow from the system, resulting in occasional eclipsing by other blobs. They constrain the radio source size to $R_s \leq 10^{10}$ cm which then means $T_B \geq 10^{12}$ K. This high brightness temperature could point to occasional coherent emission through a cyclotron or synchrotron maser which is not discussed here.

The radio emission, as was mentioned above, is considered to be non-thermal in origin. BDC(1988) considered this by looking at the range of brightness temperatures, T_B and the implied source size. T_B is given by

$$T_B = \frac{S_\nu c^2 D^2}{2k\nu^2 \pi r_s^2}$$

with k being Boltzmann's constant, πr_s^2 the projected source area and D the distance to the object. The brightness temperature gives an idea of the luminosity of a source in terms of a thermal blackbody description. A temperature of $T_B \approx 10^8$ K implies, with observed flux levels, that the source is quite large and should be a strong X-ray source which is not the case. If the temperature is lower the source must be even bigger and it cannot accommodate the observed variability time scales. They also rule out coherent emission on the grounds that no rapid temporal (time) variations or high degrees of circular polarization are seen. Therefore the radio emission is described as incoherent non-thermal radiation of synchrotron origin.

In this chapter a discussion of the basic principles governing cataclysmic variables was given with the aim to introduce the system AE Aquarii and to put it into perspective with respect to other mcvs. The radio to infra-red data specifically suggests a non-thermal origin and this implies the acceleration of thermal particles by non-thermal mechanisms. The question of particle acceleration in AE Aqr is therefore of importance to explain the radio and TeV outbursts. The next chapter will concentrate on this aspect.

1.4 Outline of the thesis

Chapter 2:

In this chapter particle acceleration mechanisms that operate in astrophysical environments are discussed. Particle acceleration is of importance in modelling the radio emission from AE Aqr in highly conducting plasma clouds thrown from the system by a magnetospheric propeller.

Chapter 3:

In this chapter an overview is given of some relevant theoretical aspects concerning the processes included in the model . These processes are the emission of synchrotron radiation by electrons and the Van der Laan model describing the evolution of the emission from an expanding synchrotron cloud. Since modelling of the radio flares in AE Aqr relies on the synchrotron emission from expanding magnetized clouds, the magnetic structure of the secondary star, from which the mass transfer flow originates, is investigated. This is done in an attempt to constrain the magnetic flux possibly frozen into the blobs leaving the secondary.

Chapter 4:

In this chapter a description is given of the proposed origin of the radio sources in AE Aquarii. The various contributors to the observed spectrum are discussed. These include plasma clouds or blobs, electrons of sufficient energy and acceleration mechanisms, magnetic fields of sufficient strength and the combination of these in an expanding cloud scenario.

Chapter 2

Particle acceleration

2.1 Propeller outflow and particle acceleration in AE Aquarii

In the previous chapter the enigmatic transient nature of the thermal and non-thermal emission from AE Aquarii was attributed to the propeller ejection of the mass transfer stream from the secondary star. The propeller ejection of material is the result of intense magnetohydrodynamic (mhd) interaction between the fast rotating white dwarf magnetosphere and the gas stream from the secondary. A detailed study (Meintjes & de Jager 2000) of the interaction between the magnetospheric propeller with slower orbiting gas near the circularization radius $R_c \sim 2 \times 10^{10}$ $(P_{orb}/9.88\ h)^{2/3}$ cm (Frank, King & Raine 1992) showed that a drag force is exerted on the white dwarf as a result of the magnetosphere's attempt to bring the gas into corotation. Shearing of the field will occur, resulting in the creation of a toroidal (azimuthal) magnetic field in the propeller zone (Meintjes & de Jager 2000) with strength of $B_\phi \sim (8\dot{m}v_{ff}/r^2)^{1/2}$ (v_{ff} is the free fall velocity), which is

$$B_\phi \approx 1000 \left(\frac{\dot{M}_{eject}}{5 \times 10^{17}\,g.s^{-1}}\right)^{1/2} \left(\frac{M_1}{0.9M_\odot}\right)^{1/4} \left(\frac{r}{R_c}\right)^{-5/4} G. \tag{2.1}$$

This results in the dissipation of power in the magnetosphere at a rate of $P_{mhd} \sim (B_\phi^2/8\pi)v_A R_c^2$ which is of the order of

$$P_{mhd} \approx 10^{34} \left(\frac{B_\phi}{1000\,G}\right)^3 \left(\frac{P_{orb}}{9.88\,h}\right)^{4/3} \left(\frac{n_g}{10^{10}\,cm^{-3}}\right)^{-1/2} erg\ s^{-1}, \tag{2.2}$$

similar to the spin down power as well as the rate of mass outflow from the system and where n_g is the density of the line emitting gas. The violent interaction between the magnetosphere and gas flow as a result of the dissipation of mhd power in this region may result in particle acceleration through various mechanisms, which will be discussed shortly.

Since the temperature in the magnetosphere of the white dwarf is nowhere below $T_m = 10^4$ K, the gas is highly conducting, with the Coulomb conductivity (Priest & Forbes 2000) nowhere below

$$\sigma \geq 3.22 \times 10^{12} \left(\frac{T_B}{10^4 \, K} \right)^{3/2} s^{-1}. \tag{2.3}$$

The Coulomb conductivity of the fluid severely influences the nature of particle acceleration through electrodynamic processes and needs to be discussed. In the next section the properties of highly conducting fluids and the influence it has on particle acceleration in general is discussed.

Since the nature of the non-thermal emission is highly variable on relatively short time scales, the particles also need to be energized over similar time scales. Therefore, impulsive electrodynamic processes must definitely play an important role in the initial energizing of charged particles. If these particles are trapped in the magnetosphere, shock acceleration and magnetic pumping mechanisms can also be fundamental processes in continuously energizing this population. The best known regions of particle acceleration in astrophysics are the Sun and the geomagnetic tail. It is expected that processes at work here are also applicable to AE Aquarii. A qualitative discussion of these processes will now be presented (Parker 1976 for a review).

2.2 Acceleration in a highly conducting fluid

Consider electromagnetic fields in a highly conducting fluid with small velocity $\mathbf{v}$ ($v \ll c$). These fields can be deduced from Maxwell's equations. In the frame of the fluid, Ohm's law states that the current density is related to the conductivity of the fluid (σ) through J' = σ E' with $\sigma = 3.22 \times 10^6 \, T_e^{3/2}$ (s^{-1}) representing the Coulomb conductivity. The transformation of the fields (Jackson 1975) from the laboratory frame or rest frame (i.e. K), to a reference frame comoving with the fluid (i.e. K$'$) is given by

$$\mathbf{E}' = \gamma[\mathbf{E} + \frac{1}{c}(\mathbf{v} \times \mathbf{B})]$$

and

$$\mathbf{B}' = \gamma[\mathbf{B} - \frac{1}{c}(\mathbf{v} \times \mathbf{E})].$$

where the primed quantities represent the fields in the comoving reference frame and the unprimed quantities represent the field in the laboratory system.

For $v/c \ll 1$, $\gamma \to 1$ and

$$\mathbf{E}' = \mathbf{E} + \frac{1}{c}(\mathbf{v} \times \mathbf{B})$$

and

$$\mathbf{B}' = \mathbf{B} - \frac{1}{c}(\mathbf{v} \times \mathbf{E}).$$

If the conductivity is high, any current in the fluid's frame can be supported by $\mathbf{E}' \rightarrow 0$, resulting in

$$\mathbf{E} = -\frac{1}{\mathrm{c}}(\mathbf{v} \times \mathbf{B}) \tag{2.4}$$

and

$$\begin{aligned}
\mathbf{B}' &= \mathbf{B} - \frac{1}{\mathrm{c}}(\mathbf{v} \times \mathbf{E}) \\
&= \mathbf{B} - \frac{1}{\mathrm{c}}(\mathbf{v} \times \left(-\frac{1}{\mathrm{c}}(\mathbf{v} \times \mathbf{B})\right) \\
&= \mathbf{B} - \frac{1}{\mathrm{c}^2}[\mathbf{v}(\mathbf{v}.\mathbf{B}) - \mathbf{B}(\mathbf{v}.\mathbf{v})] \;\; ; \;\; [\mathbf{a} \times (\mathbf{b} \times \mathbf{c}) = \mathbf{b}(\mathbf{a}.\mathbf{c}) - \mathbf{c}(\mathbf{a}.\mathbf{b})] \\
&= \mathbf{B} \;\; ; \;\; [\text{neglect } \mathrm{O(v/c)^2 terms}]
\end{aligned} \tag{2.5}$$

Let the characteristic scale of the field be L. Then if the characteristic time for adjustment in the field is $\tau = \mathrm{L/v}$, Ampère's law can be adapted as follows

$$\begin{aligned}
\nabla \times \mathbf{B} &= \frac{4\pi}{\mathrm{c}}\mathbf{J} + \frac{1}{\mathrm{c}}\frac{\partial \mathbf{E}}{\partial t} \\
\mathrm{c}\nabla \times \mathbf{B} &\approx 4\pi\mathbf{J} + \frac{\mathbf{E}}{\tau} \\
&= 4\pi\mathbf{J} + \frac{\mathrm{v}}{\mathrm{L}}\mathbf{E}
\end{aligned} \tag{2.6}$$

Now consider the dimensions of this equation

$$\left(\frac{\mathrm{cB}}{\mathrm{L}}\right) \approx 4\pi\mathrm{J} + \frac{v}{\mathrm{L}}E = 4\pi\mathrm{J} + \frac{v}{\mathrm{L}}\frac{\mathrm{vB}}{\mathrm{c}} = 4\pi\mathrm{J} + \frac{v^2}{\mathrm{c}^2}\left(\frac{\mathrm{cB}}{\mathrm{L}}\right)$$

The second term on the right $\left(\frac{v^2}{\mathrm{c}^2}\left(\frac{\mathrm{cB}}{\mathrm{L}}\right)\right)$ can be ignored when compared to the left side. The result is that in a highly conducting fluid the $\frac{d\mathbf{E}}{dt}$ term can be left out of Ampère's law, illustrating that electric induction will not occur in a highly conducting fluid.

Therefore

$$\nabla \times \mathbf{B} = \frac{4\pi}{\mathrm{c}}\mathbf{J}. \tag{2.7}$$

Any current produced through the rotation of $\mathbf{B}$ in a conducting fluid or plasma is then of order

$$\mathrm{J} \approx \frac{\mathrm{cB}}{4\pi\mathrm{L}}$$

Now we get back to Ohm's law $\mathbf{J}' = \sigma\mathbf{E}'$ and

$$\mathbf{J}' = \mathbf{J} = \sigma\mathbf{E}' \quad [\text{where } \mathbf{J}' = \mathbf{J} \text{ in a slow moving plasma}]$$

Now

$$\begin{aligned} \mathbf{J} &= \sigma \mathbf{E}' \\ &= \sigma[\mathbf{E} + \frac{1}{\mathrm{c}}(\mathbf{v} \times \mathbf{B})] \quad ; \ \gamma \approx 1 \\ \Rightarrow \ \sigma \mathbf{E} &= \mathbf{J} - \sigma \frac{\mathbf{v}}{\mathrm{c}} \times \mathbf{B} \end{aligned}$$

so then

$$\begin{aligned} \mathbf{E} &= \frac{\mathbf{J}}{\sigma} - \frac{\mathbf{v}}{\mathrm{c}} \times \mathbf{B} \\ &= \frac{1}{\sigma}\left[\frac{\mathrm{c}}{4\pi}(\nabla \times \mathbf{B})\right] - \frac{\mathbf{v}}{\mathrm{c}} \times \mathbf{B} \ ; \ [\mathbf{J} \text{ from Eq.2.7}] \\ &= \frac{\mathrm{c}}{4\pi\sigma}\nabla \times \mathbf{B} - \frac{\mathbf{v}}{\mathrm{c}} \times \mathbf{B} \end{aligned} \tag{2.8}$$

This can now be substituted into Faraday's induction equation $\nabla \times \mathbf{E} = -\frac{1}{\mathrm{c}}\frac{\partial \mathbf{B}}{\partial t}$ to give

$$\begin{aligned} \frac{\partial \mathbf{B}}{\partial t} &= -\mathrm{c}\nabla \times \mathbf{E} \\ &= -\mathrm{c}\nabla \times [\frac{\mathrm{c}}{4\pi\sigma}\nabla \times \mathbf{B} - \frac{\mathbf{v}}{\mathrm{c}} \times \mathbf{B}] \\ \frac{\partial \mathbf{B}}{\partial t} &= \nabla \times \mathbf{v} \times \mathbf{B} - \nabla \times \eta\nabla \times \mathbf{B} \ ; \ [\eta = \frac{\mathrm{c}^2}{4\pi\sigma}] \end{aligned} \tag{2.9}$$

where η represents a resistive coefficient for diffusion of the magnetic field relative to the fluid supporting it. The second term of Eq.2.9 can be called the diffusion term.

Consider the equations

$$\frac{\partial \mathbf{B}}{\partial t} = \nabla \times \mathbf{v} \times \mathbf{B} - \nabla \times \eta\nabla \times \mathbf{B} \tag{2.10}$$

$$\mathbf{E} = \frac{\mathrm{c}}{4\pi\sigma}\nabla \times \mathbf{B} - \frac{\mathbf{v}}{\mathrm{c}} \times \mathbf{B} \quad ; \ [\mathbf{E} \perp \mathbf{B}] \tag{2.11}$$

Let us define the magnetic Reynolds number

$$R_m = \frac{\mathrm{L}v}{\eta}$$

Then

$$\begin{aligned} \frac{\partial \mathbf{B}}{\partial t} &= \nabla \times (\mathbf{v} \times \mathbf{B} - \eta\nabla \times \mathbf{B}) \\ \frac{\partial \mathrm{B}}{\partial t} &\approx \frac{1}{\mathrm{L}}(\mathrm{vB} - \eta\frac{\mathrm{B}}{\mathrm{L}}) \\ &\approx \frac{\mathrm{vB}}{\mathrm{L}} - \frac{1}{\mathrm{R}_m}\frac{\mathrm{vB}}{\mathrm{L}} \end{aligned} \tag{2.12}$$

Now for a highly conducting medium, $\sigma \to \infty$, hence $\eta \propto 1/\sigma \to 0$ and this results in $\mathrm{R}_m \to \infty$. This means that the diffusion term is smaller in magnitude than the first term in Eq.2.9 by the reciprocal of this large Reynolds number.

Now we look at the electric field, perpendicular or parallel to the magnetic field $\mathbf{B}$

$$\begin{aligned}
\mathbf{E}_\perp &= -\frac{\mathbf{v}}{\mathrm{c}} \times \mathbf{B} + \frac{\mathrm{c}}{4\pi\sigma} \nabla \times \mathbf{B} \\
&= -\frac{\mathbf{v}}{\mathrm{c}} \times \mathbf{B} + \frac{\eta}{\mathrm{c}} \nabla \times \mathbf{B} \\
&= -\frac{\mathbf{v}}{\mathrm{c}} \times \mathbf{B} + \frac{1}{R_m} \frac{\mathrm{Lv}}{\mathrm{c}} \nabla \times \mathbf{B}
\end{aligned} \tag{2.13}$$

If $R_m \to \infty$

$$\mathbf{E}_\perp \approx -\frac{1}{\mathrm{c}} \mathbf{v} \times \mathbf{B}$$

or $E_\perp \approx \frac{\mathrm{vB}}{\mathrm{c}}$.

The component parallel to the magnetic field gives

$$\mathbf{J}_\parallel = \sigma \mathbf{E}_\parallel$$

and thus

$$\begin{aligned}
\mathbf{E}_\parallel &= \mathbf{J}/\sigma \\
&= [\frac{\mathrm{c}}{4\pi} \nabla \times \mathbf{B}]_\parallel / \sigma \\
&= \frac{1}{R_m} \frac{\mathrm{Lv}}{\mathrm{c}} (\nabla \times \mathbf{B})
\end{aligned}$$

so then

$$E_\parallel \approx \frac{1}{R_m} \frac{\mathrm{Lv}}{\mathrm{c}} \frac{\mathrm{B}}{\mathrm{L}} \approx \frac{1}{R_m} \frac{\mathrm{vB}}{\mathrm{c}} \quad ; \quad [E_\perp \approx \frac{\mathrm{vB}}{\mathrm{c}}] \tag{2.14}$$

We therefore see that $E_\parallel \approx \frac{1}{R_m} E_\perp$ and thus

$$E_\parallel \ll E_\perp$$

Therefore in a highly conducting fluid the parallel component of the electric field can be neglected. We proceed by looking at the motion of a free particle due to these calculated fields in a fluid with velocity $\mathbf{v}$. The equation of motion for such a particle of mass m_p, charge q and velocity $\mathbf{w}_p$ is

$$\begin{aligned}
\mathrm{m}_p \frac{d\mathbf{w}_p}{dt} &= \mathbf{F}_{\mathrm{Lorentz}} \\
&= \mathrm{q}[\mathbf{E} + \left(\frac{\mathbf{w}_p}{\mathrm{c}} \times \mathbf{B}\right)] \\
&\approx \mathrm{q}(\mathbf{E}_\perp + \frac{\mathbf{w}_p}{\mathrm{c}} \times \mathbf{B}) \\
&\approx \mathrm{q}\left(-\frac{1}{\mathrm{c}} \mathbf{v} \times \mathbf{B} + \frac{\mathbf{w}_p}{\mathrm{c}} \times \mathbf{B}\right) \\
\mathrm{m}_p \frac{d\mathbf{w}_p}{dt} &\approx \frac{\mathrm{q}}{\mathrm{c}} ((\mathbf{w}_p - \mathbf{v}) \times \mathbf{B})
\end{aligned} \tag{2.15}$$

Then

$$m_p \frac{d\mathbf{w}_p}{dt}.\mathbf{w}_p = \frac{q}{c}((\mathbf{w}_p - \mathbf{v}) \times \mathbf{B}).\mathbf{w}_p$$

but we also have

$$\frac{d}{dt}(1/2 m_p w_p^2) = m_p \frac{d\mathbf{w}_p}{dt}.\mathbf{w}_p \tag{2.16}$$

Then we find

$$\begin{aligned} \frac{d}{dt}(1/2 m_p w_p^2) &= \frac{q}{c}((\mathbf{w}_p - \mathbf{v}) \times \mathbf{B}).\mathbf{w}_p \\ &= \frac{q}{c}[(\mathbf{w}_p \times \mathbf{B}).\mathbf{w}_p) - (\mathbf{v} \times \mathbf{B}).\mathbf{w}_p] \\ &= \frac{q}{c}[-(\mathbf{v} \times \mathbf{B}).\mathbf{w}_p] \quad ; [\text{since } (\mathbf{w_p} \times \mathbf{B}) \perp \mathbf{w_p}]. \end{aligned} \tag{2.17}$$

We can use the identity $\mathbf{a}.(\mathbf{b} \times \mathbf{c}) = \mathbf{b}.(\mathbf{c} \times \mathbf{a}) = \mathbf{c}.(\mathbf{a} \times \mathbf{b})$.
and thus

$$\begin{aligned} \frac{d}{dt}(1/2 m_p w_p^2) &= -\frac{q}{c}(\mathbf{v} \times \mathbf{B}).\mathbf{w}_p \\ &= \mathbf{v}.[\frac{q}{c}(\mathbf{w}_p \times \mathbf{B})] \\ &= \mathbf{v}.\mathbf{F}_{p,\text{Lorentz}} = v F_p \cos\theta \end{aligned} \tag{2.18}$$

The Lorentz force is always perpendicular to the particle velocity and the field direction. For q = -e and q = +e the maximum rate of energy transfer is $\frac{d}{dt}(1/2 m_p w_p^2)_{max} = v F_{p,Lor}$ with $\theta = \pi$ and 0 respectively. This means that the rate of kinetic energy increase is the same for the two charges, but the effective change in velocity is greater for the less massive electron. Now if θ is the angle between the fluid velocity and the B-field, the maximum acceleration of an electron occurs when the fluid tries to move the electron head-on against F_{Lor}. The B-field is frozen into the fluid and thus it can be said that the comoving fluid and field scatters the electron. This is basically a Fermi-type acceleration. In the case of the positive charge it is bumped by the field in the direction of the Lorentz force. We therefore see that any scattering of an electron relative to the fluid or magnetic field is likely to win the electron some energy or accelerate it.

2.3 Reduced conductivity and particle acceleration

The theoretical electrical conductivity for small current densities in an ionized gas is $\sigma = 10^7 T^{3/2}$ esu . It has been suggested (Parker 1976) that this value may be greatly reduced at critical points in the system where current densities are high. The implied enhanced resistivity would then increase the dissipation *and the electric field* across the reduced conductivity region to

keep the current constant (Meintjes & de Jager 2000) if it flows parallel to the magnetic field. If such regions of enhanced resistivity can be created, acceleration of particles can occur.

As an example, let the current density parallel to the B-field be so high that the electron drift velocity u exceeds the thermal ion velocity $v_{th} \approx \left(\frac{3kT}{m_i}\right)^{1/2}$. (The total translational (x, y, z) kinetic energy per particle is 3/2kT.) Then various micro-instabilities are invoked that greatly enhances the resistivity of the plasma and thus

$$E_{\parallel} = J_{\parallel}/\sigma \rightarrow \infty \quad (\sigma \rightarrow 0)$$

The current density is given by J = -$N_e$eu with N_e the electron density. Now if the magnetic field changes over a length scale l, from Ampère's law we get

$$J = \frac{cB}{4\pi l}$$

and so

$$\frac{cB}{4\pi l} = -N_e e u \Rightarrow u = -\frac{cB}{4\pi e N_e l} \tag{2.19}$$

If $N_e \rightarrow 0$, u can be larger than v_{th}.

So now let $u^2 > \frac{3kT}{m_i}$ or also

$$\frac{c^2B^2}{16\pi^2 e^2 N_e^2 l^2} > \frac{3kT}{m_i}.$$

The plasma frequency is $\omega_p = \left(\frac{4\pi N_e e^2}{m_e}\right)^{1/2}$.

Therefore

$$\begin{aligned}
\frac{c^2B^2}{4\pi^2 l^2 m_e}\left(\frac{m_e}{4\pi e^2 N_e}\right) &> \frac{3kT}{m_i} \\
\frac{c^2B^2}{4\pi^2 m_e l^2}\left(\frac{1}{\omega_p^2}\right) &> \frac{3kT}{m_i} \\
l^2\omega_p^2 &< \frac{c^2B^2}{4\pi^2 m_e}\frac{m_i}{3kT} \\
&< \left(\frac{\frac{B^2}{8\pi}}{3/2kT}\right)\frac{m_i}{m_e}c^2 \\
l\omega_p &< \left(\frac{P_{mag}}{P_{gas}}\right)^{1/2}\left(\frac{m_i}{m_e}\right)^{1/2} c \\
l\omega_p &< \left(\frac{m_i}{m_e}\right)^{1/2} c
\end{aligned} \tag{2.20}$$

The next step is to marginally quantify this condition which points to possibly enhanced resistivity. Currents produced by magnetic reconnection (discussed later) is dependent on the approach speed

v of the diffusing field lines over the length l. Therefore if $\mathrm{v} = \frac{\eta}{l}$, where η is the magnetic diffusion coefficient (see §2.1), then

$$l = \frac{\eta}{v} = \frac{\eta}{\epsilon v_A}.$$

But

$$\begin{aligned}
l\omega_p &< \left(\frac{\mathrm{m}_i}{\mathrm{m}_e}\right)^{1/2} \mathrm{c} \\
\frac{\eta}{\epsilon v_A}\omega_p &< \left(\frac{\mathrm{m}_i}{\mathrm{m}_e}\right)^{1/2} \mathrm{c} \\
\frac{1}{\epsilon}\frac{\mathrm{c}^2}{4\pi\sigma}\left(\frac{4\pi e^2 \mathrm{N}_e}{\mathrm{m}_e}\right)^{1/2}\left(\frac{\mathrm{B}^2}{4\pi \mathrm{N}_e \mathrm{m}_i}\right)^{-1/2} &< \left(\frac{\mathrm{m}_i}{\mathrm{m}_e}\right)^{1/2} \mathrm{c} \\
\frac{\mathrm{ceN}_e}{\sigma\epsilon\mathrm{B}} &< 1 \\
\frac{\mathrm{B}\sigma}{\mathrm{N}_e} &> \frac{ce}{\epsilon} \qquad (2.21) \\
\frac{\mathrm{B}\sigma}{\mathrm{N}_e} &> 10^2 \quad ; \ [\mathrm{c(cm\ s^{-1})};\ \mathrm{e(esu)}] \qquad (2.22)
\end{aligned}$$

This result indicates that the combination of strong fields and low electron densities are conducive to the enhancement of the resistivity in the plasma. The theoretical conductivity for small current densities in an ionized gas is $\sigma = 10^7 \mathrm{T}^{1/2}$ (Parker 1976), resulting in

$$\begin{aligned}
\frac{\mathrm{B}10^7\mathrm{T}^{1/2}}{\mathrm{N}_e} &> \frac{ce}{\epsilon} \\
\frac{\mathrm{BT}^{1/2}}{\mathrm{N}_e} &> \frac{ce}{10^7\epsilon} \qquad (2.23)
\end{aligned}$$

If these conditions are satisfied in a plasma the conductivity may be anomalously reduced in localized regions, resulting in particle acceleration.

The acceleration of particles through reduced conductivity in a highly conducting plasma is a very attractive mechanism to explain the non-thermal radio synchrotron outbursts from some astrophysical sources, like the Sun (during flares), quasars, radio stars and also AE Aquarii. The generation of strong electric fields in a plasma can lead to a phenomenon called "electron run-away acceleration", resulting in huge populations of electrons to be energized in a single "explosive" impulsive event (see e.g Benz 1994 for a detailed discussion). This occurs if the electric field generated in the plasma becomes greater than the so-called Dreicer field (Dreicer 1959), i.e. $\mathrm{E}_D \sim 2 \times 10^{-10}\ (\mathrm{N}_e/\mathrm{T})$ statvolt.cm^{-1}. For typical parameter values the Dreicer field is

$$\mathrm{E}_D \approx 6 \times 10^{-3}\left(\frac{\mathrm{N}}{10^9\,\mathrm{cm}^{-3}}\right)\left(\frac{\mathrm{T}}{10^4\,\mathrm{K}}\right)^{-1} \text{ Volt cm}^{-1} \qquad (2.24)$$

For all electric fields greater than the Dreicer field, the thermal electrons with velocities greater than the drift velocity of electrons relative to the heavier ions (Meintjes & de Jager 2000 for a detailed discussion), i.e. the high energy thermal tail of the MB distribution, will accelerate freely, experiencing virtually no friction as a result of ion-electron collisions. This will result in the whole high velocity thermal tail of the MB electron population to accelerate at once. The effectiveness of the acceleration process is then determined by the physical size of the medium, as well as energy loss processes of the electrons, like synchrotron emission and adiabatic losses.

2.4 Magnetic reconnection: Neutral sheet acceleration

The Sun's ever changing surface magnetism as a result of the continuous emergence of magnetic flux, generated by an internal dynamo mechanism, results in unremitting unrest above the Sun's surface. The reconnection of the newly immerged flux tubes with the existing flux tubes above the surface releases stored magnetic energy on an awesome scale, resulting in Solar flares. The amount of energy released through this process (i.e. magnetic reconnection) above the Sun's surface is equivalent to billions of thermonuclear explosions, raising the local temperature of Earth size regions in the Sun's atmosphere by tens of millions of degrees. Although the flares appear rather inconspicuous in visible light, they release enough energy in the X-ray and radio, through non-thermal radio synchrotron emission of vast amounts of relativistic electrons accelerated by electric fields and shocks in the acceleration zone (neutral sheet), to outshine the entire visible Sun.

Magnetic reconnection as the driving mechanism behind Solar flares and accompanying particle acceleration has been proposed by Parker (1957), refined by Petschek (1964) and has been extensively reviewed (Parker 1976; Benz 1994; Priest & Forbes 2000). The principle upon which the mechanism is based is the diffusion of magnetic regions of opposite polarity towards one another through a highly conducting plasma. The annihilation of magnetic flux in the merger will eventually be converted to kinetic and thermal energy of the plasma in the reconnection zone (see also Meintjes & de Jager 2000). The discussion that follows will illuminate only the basic principles of the reconnection process and acceleration, and is based on a general discussion of the Petschek model (Parker 1976).

Consider a magnetic field $\mathbf{B} = \mathrm{B(x)}\hat{\mathbf{e}}_z$ which is an odd function of x. The field approaches a uniform value $\pm\ \mathrm{B_o}$ for large x (see Figure 9).

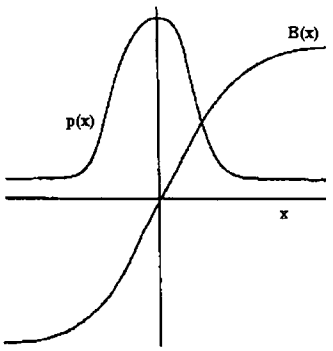

Figure 9 : Magnetic field strength and gas pressure with variation in x. (Parker 1976)

If hydrostatic equilibrium is to prevail in the x-direction the combination of the gas and field pressure must be uniform to avoid pressure gradients from forming, or

$$\mathrm{P}(x) + \frac{\mathrm{B}^2(x)}{8\pi} = \mathrm{P}_\circ \quad \text{(constant)} \tag{2.25}$$

Since B(x = 0) = 0, the gas pressure P(x) is a maximum at x = 0 to support the whole configuration. The result is that there is nothing to counteract the high pressure at x = 0, preventing the gas from flowing away. This configuration is illustrated in Figure 9.

Two scenarios are now possible. The gas can flow along the lines of force and escape at the edge of the field or in blobs through the B-field due to large scale magnetic instabilities. If the gas escapes, the regions of opposite field come closer together while the condition for hydrostatic equilibrium may still be satisfied. The escape can continue and as a result the field gradient becomes steeper and steeper. Now if the transition layer between the two opposite fields has thickness $2l$, Ampère's law gives the current density as

$$\begin{aligned} 4\pi\mathbf{J} &= \mathrm{c}\nabla \times \mathbf{B} \\ \mathbf{J} &= \frac{\mathrm{c}}{4\pi}\left[\frac{d\mathrm{B}(x)}{dy}\mathbf{i} - \frac{d\mathrm{B}(x)}{dx}\mathbf{j} + 0\mathbf{k}\right] \\ &= -\frac{\mathrm{c}}{4\pi}\frac{d\mathrm{B}(x)}{dx}\mathbf{j} \end{aligned} \tag{2.26}$$

Then

$$J = -\frac{\mathrm{c}}{4\pi}\frac{d\mathrm{B}(x)}{dx} = O(\frac{\mathrm{cB}(x)}{4\pi l}) \quad ; \text{[in the y-direction]} \tag{2.27}$$

We see that the current density increases as l decreases. The presence of a current flowing in the y-direction points to the presence of an electric field in that direction. This field is given by

$$\mathbf{E} = -\frac{\mathbf{v}}{\mathrm{c}} \times \mathbf{B} + \frac{\mathrm{c}}{4\pi\sigma}\nabla \times \mathbf{B}$$

and the E-field must be in the y-direction :

$$\begin{aligned} E\mathbf{j} &= -\left(-\frac{\mathrm{v(x)B(x)}}{\mathrm{c}}\right)\mathbf{j} - \frac{\mathrm{c}}{4\pi\sigma}\frac{dB(x)}{dx}\mathbf{j} \\ &= -\frac{\mathrm{c}}{4\pi\sigma}\frac{d\mathrm{B}(x)}{dx}\mathbf{j} + \frac{\mathrm{v(x)B(x)}}{\mathrm{c}}\mathbf{j} \end{aligned} \tag{2.28}$$

$$\Rightarrow \quad E = \frac{\eta}{\mathrm{c}}\frac{d\mathrm{B}(x)}{dx} + \frac{\mathrm{v(x)B(x)}}{\mathrm{c}} \quad ; \text{[in the y-direction]} \tag{2.29}$$

We can imagine steady conditions where the B-field and the gas is convected in from each side at a velocity v(x) as rapidly as it is expelled and dissipated (by reconnection) near x = 0. This would mean that $\frac{d\mathbf{B}}{dt} = 0$ and hence from Faraday's induction law $\nabla \times \mathbf{E} = -\frac{1}{\mathrm{c}}\frac{\partial \mathbf{B}}{\partial t}$, we see that $\nabla \times \mathbf{E} = 0$.

Furthermore since E $\equiv$ E_y, E is independent of x and z.

$$\nabla \times \mathbf{E} = -\frac{dE_y}{dz}\mathbf{i} - 0\mathbf{j} + \frac{dE_y}{dx}\mathbf{k} = 0\mathbf{i} - 0\mathbf{j} + 0\mathbf{k}$$

At x = 0 we get

$$E = -\frac{\eta}{\mathrm{c}}\left(\frac{d\mathrm{B}}{dx}\right)_{\circ} \quad ; \text{[in the y-direction; } \mathrm{B}(x=0) = 0] \tag{2.30}$$

For large x, B $\sim$ $\mathrm{B}_{\circ}$ and thus we have $(\frac{d\mathrm{B}}{dx}) = 0$ and

$$E = \frac{\mathrm{v(x)B(x)}}{\mathrm{c}} = \frac{\mathrm{v(x)B_{\circ}}}{\mathrm{c}} \tag{2.31}$$

or

$$v(x) = \frac{\mathrm{c}E}{\mathrm{B_{\circ}}} = \frac{\mathrm{c}}{\mathrm{B_{\circ}}}\left(\frac{-\eta}{\mathrm{c}}\left(\frac{d\mathrm{B}}{dx}\right)_{\circ}\right) = -\frac{\mathrm{c}^2/4\pi\sigma}{\mathrm{B_{\circ}}}\left(\frac{d\mathrm{B}}{dx}\right)_{\circ},$$

assuming a constant E-field in the whole region.

This indicates that a particle may attain a velocity v(x) depending on the gradient in the magnetic field $\frac{d\mathrm{B}}{dx}$, near the position x = 0. The electric field E in the y-direction may accelerate particles to high energies depending on the field's strength. The creation and maintenance of such a field in a highly conducting fluid is however a difficult task. The best scenario is a region where the opposite B-fields come into contact over a very narrow region forming a steep gradient in the process.

From above (Eq.2.30) we have

$$E = -\frac{\eta}{\mathrm{c}}\left(\frac{d\mathrm{B}}{dx}\right)_{\circ} = -\frac{\mathrm{c}}{4\pi\sigma}\left(\frac{d\mathrm{B}}{dx}\right)_{\circ}$$

and therefore if σ is large, we need $\left(\frac{d\mathrm{B}}{dx}\right)_{\circ} \to \infty$ to get E to be large. This scenario of the annihilation of the magnetic field over a small region (Δx $\to$ 0) is known as the Petschek mechanism.

and therefore if σ is large, we need $\left(\frac{dB}{dx}\right)_o \rightarrow \infty$ to get E to be large. This scenario of the annihilation of the magnetic field over a small region ($\Delta x \rightarrow 0$) is known as the Petschek mechanism.

The short region of contact causes the gas to squeeze out rapidly from between the fields. The scale length l may adjust to a value at which the fields near each other at $v_m = \epsilon v_A$ (merging speed) where $v_A = \frac{B}{\sqrt{4\pi\rho}}$ is the Alfvén speed of the medium, with $\epsilon = 0.1$ (e.g. Parker 1976; Priest 1981). The electric field generated in the merging region (MR) is then of the order of

$$E_{MR} = \frac{vB_o}{c} , = \frac{\epsilon v_A B_o}{c} \tag{2.32}$$

The energies particles can achieve with this mechanism depend on the length scale of the reconnection zone, which is still an unsolved theoretical dilemma. There is an alternative point of view regarding the actual acceleration of particles through magnetic reconnection (e.g Biskamp 1988; Lesch 1991), following directly from Faraday's induction law. These authors proposed that the actual site for particle acceleration is not the region where the merging fields approach one another, i.e. the merging region (MR), but the dissipation region (DR) where current flows along the field lines. In terms of this alternative description, it is proposed that a charged particle spiralling in the field in the MR will experience that the magnetic flux ($\Phi_m = B\pi R_L^2$) that passes through a hypothetical surface bounded by its orbit with Larmor radius R_L, will decrease at a rate $d\Phi_m/dt \sim -(B\pi R_L^2/\tau_r)$, where $\tau_r = R_L/v_m$. The work done per unit charge (emf) in one single orbit is (Biskamp 1988)

$$emf = 2\pi R_L E_{DR} = \frac{2\pi R_L \epsilon v_A B_o}{c} \tag{2.33}$$

where $E_{DR} = (1/\sigma)$ J is the accompanying electric field driving the current along the field lines away from the MR, with σ the conductivity of the plasma along the field. Effective particle acceleration will only occur if micro-instabilities are induced along the field as a result of the current, reducing σ to anomalously low values.

It is however generally accepted that magnetic reconnection is the mechanism behind the non-thermal outbursts on the Sun, as well as the particle acceleration in the geomagnetic tail. In the case of particle acceleration in the geomagnetic tail, for typical values of the magnetic field and particle density, i.e. $B_o = 2 \times 10^{-4}$ G and $n \approx 1$ cm^{-3} or $\rho \approx 6.67 \times 10^{-24}$ gcm^{-3}, it results in $v_A \approx 2.5 \times 10^7$ cm/s and $E \sim 10^{-9}$ statvolt/cm $= 5 \times 10^{-7}$ Volt/cm. If the length scale of acceleration is taken to be $\Delta L = 10^{11}$ cm, it can be shown that particles can be accelerated to energies like

$$\epsilon = e\Delta V \approx eE\Delta L \approx 10^4 \,\text{eV}$$

In Solar flares much higher energies can be achieved. The magnetic field in prominences is of the

order of B $\approx 10^4$ Gauss, with typical particle densities of n $\approx 10^{11}$ cm^{-3} ($v_A \approx 7 \times 10^8$ cm s^{-1}). If acceleration can occur over length scales ΔL = 10^8 cm, it can be shown that particles can be accelerated to energies of

$$\epsilon = e\Delta V \approx eE\Delta L \approx 10^{10}\,\mathrm{eV}$$

in these events. If a large population of run-away electrons with energies of the order of $\epsilon \approx 10$ GeV are produced in a flare event, it will explain the non-thermal radio synchrotron outbursts during Solar flares and this mechanism may well be applicable to AE Aquarii.

2.5 Double-layer formation and particle acceleration

The acceleration of particles along field lines (e.g in the DR) are closely linked to the formation of so-called double layers. A qualitative description of double layer formation will be presented next.

Consider a magnetic field **B** embedded in a highly conducting fluid. Let the fluid motion be along $\hat{e}_x$ for all z > h but no fluid motion for z < 0. The velocity is therefore $\mathbf{v} = v_x\hat{e}_x$. This motion has the effect of moving charges across the B-field (we consider a field in the z-direction, $\mathbf{B} = B_z\hat{e}_z$), resulting in an ϵmf which can drive a current. In a highly conducting fluid this is given by (as from Eq.2.4)

$$\mathbf{E} = -\frac{1}{c}\mathbf{v}\times\mathbf{B}$$

or

$$\begin{aligned}\mathbf{E} &= -\frac{1}{c}(v_x\hat{e}_x \times B_z\hat{e}_z)\\ &= -\frac{v_x B_z}{c}(-\hat{e}_y)\\ &= E_y\hat{e}_y \quad ;[E_y = \frac{v_x B_z}{c} = vB/c]\end{aligned} \tag{2.34}$$

In the gap (0 < z < h) we have

$$\mathbf{E} = -\nabla\phi$$

This electric field will drive a current at z > h.

But first

$$\begin{aligned}\mathbf{E} &= -\nabla\phi\\ (E_x\hat{e}_x + E_y\hat{e}_y + E_z\hat{e}_z) &= -\left(\frac{d\phi}{dx}\hat{e}_x + \frac{d\phi}{dy}\hat{e}_y + \frac{d\phi}{dz}\hat{e}_z\right)\end{aligned}$$

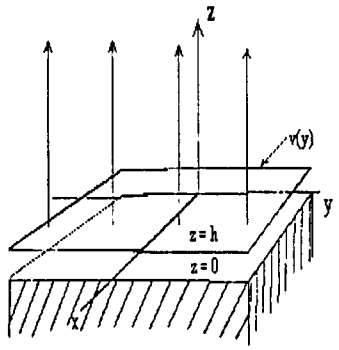

Figure 16 : A visualization of a double-layer. (Parker 1976)

$$\text{but} \quad E_x, E_z = 0 \ (z > h)$$

$$\mathbf{E} = \mathbf{E_y}\hat{\mathbf{e}}_\mathbf{y} \quad = \quad -\frac{d\phi}{dy}\hat{e}_y \tag{2.35}$$

So at z = h,

$$E_y = -\frac{\Delta\phi}{\Delta y} = -\left[\frac{\phi(y,h) - \phi(y=0,h)}{\Delta y}\right]$$

$$\begin{aligned} -\nabla\phi &= E_y \Delta y \\ -[\phi(y,h) - \phi(y=0,h)] &= \int_0^y E_y dy \\ \Rightarrow \quad \phi(y,h) &= \phi(y=0,h) - \int_0^y E_y dy \quad ;[\text{on } z = h] \end{aligned} \tag{2.36}$$

The scenario as described above is depicted in Figure 16.

Now for 0 < z < h

$$z = 0 \ ; E_y = 0$$

$$z = h \ ; E_y = -\frac{\Delta\phi}{\Delta y}$$

We also have

$$E_z = -\nabla\phi_{,z} = \frac{\partial\phi}{\partial z}\hat{e}_z$$

but we see that

$$E_z = -\frac{\Delta\phi}{\Delta z} \approx O\left(\frac{\phi}{h}\right) \tag{2.37}$$

and

$$E_y = -\frac{\Delta\phi}{\Delta y} \approx O\left(\frac{\phi}{l}\right) \tag{2.38}$$

where l is a length along the y-axis.

Therefore for $l \gg$ h

$$E_y \ll E_z.$$

The boundary conditions are now

$$z = 0 \quad ; \quad \phi(y, z = 0) = 0 \tag{2.39}$$

$$z = h \quad ; \quad \phi(y, h) = \phi(y = 0, h) - \int_0^y E_y dy. \tag{2.40}$$

In the z-direction we have

$$\begin{aligned} \Delta\phi_{,z} &= \phi(y, z = h) - \phi(y, z = 0) \\ &= [\phi(y = 0, h) - \int_0^y E_y dy] - \phi(y, z = 0) \\ &= \phi(y = 0, h) - \int_0^y E_y dy \\ &\approx -\int_0^y E_y dy. \end{aligned} \tag{2.41}$$

Then in the gap we get

$$\begin{aligned} E_z &= -\frac{\Delta\phi}{\Delta z} \\ &\approx \frac{\int_0^l E_y dy}{h} \\ &\approx \frac{\frac{\mathrm{vB}}{\mathrm{c}} \int_0^l dy}{h} \\ &= E_y \frac{l}{h} \end{aligned} \tag{2.42}$$

and then for z = h

$$E_y = \mathrm{vB/c}$$

and for z = 0

$$E_y = 0.$$

For 0 < z < h :

$$E_y(z) = \int_0^z \frac{E_y(z = h)}{h} dz = E_y \frac{z}{h}. \tag{2.43}$$

Thus in summary :

$$E_z \approx E_y \frac{l}{h}$$

$$E_y(z) \approx E_y \frac{z}{h}.$$

In the gap we have

$$E_z(z) \gg E_y(z) \quad \text{for} \quad l \gg z.$$

Figure 17 gives an idea of the electric field configuration in the case of a double layer.

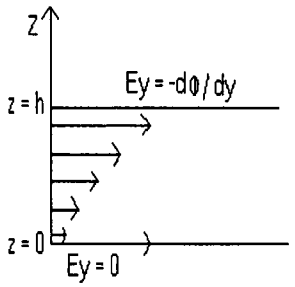

Figure 17 : The variation of the electric field in the gap.

One can see from this result that currents flowing in the B-field direction (z-direction) are generated outside the zone of cross-field motion.

$$E_{\|} = E_z = E_y(z \geq h)\frac{l}{h}$$

$$E_{\perp} = E_y(z \geq h)\frac{z}{h}$$

where E_y = vB/c. The electric fields generated through this process can result in particle acceleration, if the conductivity is reduced anomalously through the generation of micro-instabilities.

2.5.1 The electrostatic diode

A more detailed discussion can be given of a double layer by considering the example of the electrostatic diode. Let such a structure be between z = a and z = b. We consider the parameters $m_{i,e}$, $u_{i,e}(z)$ and $N_{i,e}(z)$ which represent for ions or electrons the mass, velocity and number density along the z-axis, respectively.

The flux of ions in the positive z-direction (upwards) is

$$\Phi(z) = N_i(z)u_i(z) \quad (cm^{-2}s^{-1}) \tag{2.44}$$

and similar for the electron flux, only in the opposite direction

$$\Phi(z) = N_e(z)u_e(z) \quad (cm^{-2}s^{-1}). \tag{2.45}$$

The total charge density then is

$$\begin{aligned} \rho(z) &= N_i(z)q_+ + N_e(z)q_- \\ &= [N_i(z) - N_e(z)]e. \end{aligned} \tag{2.46}$$

This leads to a current density of

$$\begin{aligned} J(z) &= q_+N_i(z)u_i(z) + q_-N_e(z)u_e(z) \\ &= [\Phi_i(z) - \Phi_e(z)]e \quad \text{(statampere cm}^{-2}\text{)}. \end{aligned} \tag{2.47}$$

If steady conditions are to prevail, Φ_i and Φ_e must be uniform over z and t. If this was not the case, charges would accumulate in different regions and electric fields would start currents flowing to reduce the imbalances.

The vertical electric field relates to the potential ϕ like

$$E(z) = -\frac{d\phi}{dz}.$$

The potential must also satisfy Poisson's equation.

$$\nabla^2\phi = -4\pi\rho. \tag{2.48}$$

If we ignore x and y dependence this gives

$$\frac{d^2\phi}{dz^2} = -4\pi\rho(z) = -4\pi(N_i(z) - N_e(z))e. \tag{2.49}$$

We now let ϕ vanish at z = b and let $\phi = \phi_o$ at z = a. As from above the ion flux is upwards and thus the electron flux is downwards. We consider negligible velocities for the ions and electrons as they enter the gap (a < z < b), ions from below and electrons from above. Therefore the velocities can be found as a function of z by considering the work-energy theorem

$$W_{\text{field}} = \Delta KE_{\text{particle}}.$$

This then gives

$$\begin{aligned} W &= \Delta(F_e z) \\ &= \Delta(qEz) = q\Delta(Ez) = q\Delta\phi. \end{aligned} \tag{2.50}$$

For protons (ions) we have

$$\Delta\phi(z) = \phi_o - \phi(z) > 0 \quad \text{[protons gain energy in the gap]}$$

and therefore

$$\begin{aligned} W = e(\phi_o - \phi(z)) &= 1/2m_iu_i^2(z) - 1/2m_iu_i^2 \ (z = a) \\ &= 1/2m_iu_i^2(z). \end{aligned} \tag{2.51}$$

And also for electrons

$$\Delta\phi(z) \;=\; \phi(z=b) - \phi(z) \;=\; -\phi(z)$$

and then to gain energy (choosing the sign correctly) in the gap

$$\begin{aligned} \mathrm{W} \;=\; -e(\Delta\phi(z)) \;&=\; 1/2\mathrm{m}_e u_e^2(z) - 1/2\mathrm{m}_e u_e^2 \;\; (z=b) \\ &=\; 1/2\mathrm{m}_e u_e^2(z) \end{aligned} \tag{2.52}$$

and therefore

$$e\phi(z) \;=\; 1/2\mathrm{m}_e u_e^2(z). \tag{2.53}$$

In summary then

$$\frac{1}{2}\mathrm{m}_i u_i^2(z) \;=\; e(\phi_\circ - \phi(z)) \tag{2.54}$$

$$\frac{1}{2}\mathrm{m}_e u_e^2(z) \;=\; e\phi(z)). \tag{2.55}$$

Now we can solve for the respective velocities.

$$u_i^2 \;=\; \frac{2e(\phi_\circ - \phi(z))}{\mathrm{m}_i} \tag{2.56}$$

$$u_e^2 \;=\; \frac{2e\phi(z)}{\mathrm{m}_e}. \tag{2.57}$$

We proceed with substitution into Poisson's equation as goal in mind.

Then from Eq.2.44 the respective densities for ions and electrons are

$$\mathrm{N}_i(z) \;=\; \frac{\Phi_i(z)}{u_i(z)} \quad ; \quad \mathrm{N}_e(z) \;=\; \frac{\Phi_e(z)}{u_e(z)}.$$

Therefore

$$\mathrm{N}_i(z) \;=\; \Phi_i(z)\left[\frac{\mathrm{m}_i}{2e(\phi_\circ - \phi(z))}\right]^{1/2} \tag{2.58}$$

$$\mathrm{N}_e(z) \;=\; \Phi_e(z)\left[\frac{\mathrm{m}_e}{2e\phi(z)}\right]^{1/2}. \tag{2.59}$$

This can be substituted into Poisson's equation

$$\begin{aligned} \frac{d^2\phi}{dz^2} \;&=\; -4\pi e(\mathrm{N}_i(z) - \mathrm{N}_e(z)) \\ &=\; -4\pi e\left[\Phi_i(z)\left(\frac{\mathrm{m}_i}{2e(\phi_\circ - \phi(z))}\right)^{1/2} - \Phi_e(z)\left[\frac{\mathrm{m}_e}{2e\phi(z)}\right]^{1/2}\right] \\ &=\; 4\pi e\left[\Phi_e(z)\left(\frac{\mathrm{m}_e}{2e\phi(z)}\right)^{1/2} - \Phi_i(z)\left(\frac{\mathrm{m}_i}{2e(\phi_\circ - \phi(z))}\right)^{1/2}\right]. \end{aligned} \tag{2.60}$$

Now consider the following

$$\frac{d}{dz}\left(\frac{d\phi}{dz}\right)^2 = 2\frac{d\phi}{dz}\frac{d^2\phi}{dz^2}$$

or

$$\Rightarrow \quad \frac{d^2\phi}{dz^2} = \frac{1}{2}\frac{dz}{d\phi}\frac{d}{dz}\left(\frac{d\phi}{dz}\right)^2 = \frac{1}{2}\frac{d}{d\phi}\left(\frac{d\phi}{dz}\right)^2.$$

So

$$\begin{aligned}
\frac{1}{2}\frac{d}{d\phi}\left(\frac{d\phi}{dz}\right)^2 &= 4\pi e\left[\Phi_e(z)\left(\frac{m_e}{2e\phi(z)}\right)^{1/2} - \Phi_i(z)\left(\frac{m_i}{2e(\phi_\circ - \phi(z))}\right)^{1/2}\right] \\
\int d\left(\frac{d\phi}{dz}\right)^2 &= \frac{8\pi e}{(2e)^{1/2}}\left[\Phi_e(z)m_e^{1/2}\int\frac{d\phi}{\phi^{1/2}(z)} - \Phi_i(z)m_i^{1/2}\int\frac{d\phi}{(\phi_\circ - \phi(z))^{1/2}}\right] \\
\left(\frac{d\phi}{dz}\right)^2 &= \frac{8\pi e}{(2e)^{1/2}}\left[\Phi_e(z)m_e^{1/2}\frac{\phi^{1/2}(z)}{1/2} - \Phi_i(z)m_i^{1/2}\int\frac{d\phi}{(-\phi(z)+\phi_\circ)^{1/2}}\right].
\end{aligned} \tag{2.61}$$

The second integral has a standard solution like $\int\frac{dx}{(ax+b)^{1/2}} = \frac{2\sqrt{ax+b}}{a}$, which in our case is = -2$(\phi_\circ - \phi(z))^{1/2}$.

Therefore

$$\begin{aligned}
\left(\frac{d\phi}{dz}\right)^2 &= \frac{8\pi e}{(2e)^{1/2}}\left[2\Phi_e(z)m_e^{1/2}\phi^{1/2}(z) + 2\Phi_i(z)m_i^{1/2}(\phi_\circ - \phi(z))^{1/2}\right] \\
&= 8\pi(2e)^{1/2}\left[\Phi_e(z)m_e^{1/2}\phi^{1/2}(z) + \Phi_i(z)m_i^{1/2}(\phi_\circ - \phi(z))^{1/2}\right].
\end{aligned} \tag{2.62}$$

If the ion mass is very high implying $u_i \ll u_e$ then

$$m_i^{1/2}\Phi_i(z) \ll m_e^{1/2}\Phi_e(z)$$

$$m_i^{1/2}N_i(z)u_i(z) \ll m_e^{1/2}N_e(z)u_e(z)$$

$$\Rightarrow \quad u_i(z) \ll u_e(z).$$

Therefore

$$\begin{aligned}
\left(\frac{d\phi}{dz}\right)^2 &\approx 8\pi(2e)^{1/2}(\Phi_e(z)m_e^{1/2}\phi^{1/2}(z)) \\
\frac{d\phi}{dz} &= \pm\left[8\pi(2e)^{1/2}(\Phi_e(z)m_e^{1/2}\phi^{1/2}(z))\right]^{1/2} \\
&= \pm\left[128\pi^2 e\Phi_e^2(z)m_e\phi(z)\right]^{1/4}.
\end{aligned} \tag{2.63}$$

Then

$$\int_0^{\phi(z)}\phi^{-1/4}(z)d\phi = -\left[128\pi^2 e\Phi_e^2(z)m_e\right]^{1/4}\int_b^z dz \quad ; \text{ [for a positive solution]}$$

$$\begin{aligned}\phi(z) &= (3/4)^{4/3}\left[128\pi^2 e\Phi_e^2(z)\mathrm{m}_e\right]^{1/3}(b-z)^{4/3} \\ &= \left[(81/2)\pi^2 e\Phi_e^2(z)\mathrm{m}_e(b-z)^4\right]^{1/3}\end{aligned}$$

resulting in

$$\begin{aligned}\phi(z) &= \left[\frac{81\pi^2}{2e}e^2\Phi_e^2(z)\mathrm{m}_e(b-z)^4\right]^{1/3} \\ &= \left(\frac{81\pi^2\mathrm{m}_e}{2e}\right)^{1/3}(e\Phi_e(z))^{2/3}(b-z)^{4/3} \\ &= 10^{-5}\mathrm{J}_e^{2/3}(z)(b-z)^{4/3} \quad \text{(statvolt)}\end{aligned}$$

$$\Rightarrow \quad \phi(z) = 3\times 10^{-3}\mathrm{J}_e^{2/3}(z)(b-z)^{4/3} \quad \text{(Volt)} \quad [1\,\text{statvolt} = 300\,\text{Volt}]. \tag{2.64}$$

One can illustrate this at the hand of double layer formation in prominences on the Sun during eruptions. For typical values we get from

$$\phi(z) = 3\times 10^{-3}\mathrm{J}_e^{2/3}(z)(b-a)^{4/3} \quad \text{Volt},$$

and for $\mathrm{J} \approx \frac{\mathrm{cB}}{4\pi l} \approx 2400\left(\frac{\mathrm{B}}{10\mathrm{G}}\right)\left(\frac{l}{10^7\mathrm{cm}}\right)^{-1}$ esu, it results in a potential difference of the order of

$$\phi(\text{gap}) \approx 1\,\text{GigaVolt}\left(\frac{\mathrm{J}_e}{2400\text{esu}}\right)^{2/3}\left(\frac{b-a}{10^7\text{cm}}\right)^{4/3}$$

and particle energies of

$$E_e = e\phi(\text{gap}) \approx 1\,\text{GeV}.$$

This mechanism therefore has the potential to accelerate electrons to high energies during Solar flares, explaining the non-thermal emission during these events.

2.6 Adiabatic compression in magnetic fields: Betatron Acceleration

Betatron acceleration is widely considered as the acceleration mechanism responsible for the acceleration of charged particles in the Earth's magnetosphere, as well as the mechanism responsible for the energy gain of relativistic electrons during their interaction with supernova envelopes at the later stages of the evolution of the envelope. The betatron process is based upon the conservation of the adiabatic invariant of a charged particle ($\mu = \mathrm{p}_\perp^2/\mathrm{B} = \text{const}$) when moving in a magnetic field of varying intensity. In this expression $\mathrm{p}_\perp = \mathrm{m}_p\,\mathrm{w}_\perp$ represents the component of momentum of the particle perpendicular to the field, and B the magnetic intensity. A discussion of this process will now be given.

Consider n(cm^{-3}) particles with particle mass m_p(g) and mean square velocity $< u^2 > = u^2$ in a certain direction. We calculate the pressure exerted by the particle in that direction.
The pressure generally is

$$\begin{aligned} P &= 1/3n < \mathbf{p}.\mathbf{v} > = 1/3n < m_p \mathbf{v}.\mathbf{v} > \\ &= 1/3nm_p < v^2 > \end{aligned} \tag{2.65}$$

but (for example) $< v^2 > = < v_x^2 + v_y^2 + v_z^2 > = < 3v_x^2 > = 3 < v_x^2 >$.
So in one dimension :

$$P = 1/3nm_p.3 < v_x^2 > = nm_p < v_x^2 > . \tag{2.66}$$

Thus

$$\Rightarrow \quad P = nm_p < u^2 > = nm_p u^2.$$

The first law of thermodynamics for adiabatic variations of a volume V is

$$dU + PdV = 0 \tag{2.67}$$

where U is the kinetic energy contained in the volume V. Using the expression for energy and pressure, this results in

$$d[(1/2nm_p u^2)V] + (nm_p u^2)dV = 0.$$

But $d(uv) = vdu + udv$

$$\begin{aligned} V d(1/2nm_p u^2) + 1/2nm_p u^2 dV + (nm_p u^2)dV &= 0 \\ \frac{d(1/2nm_p u^2)}{(1/2nm_p u^2)} + 3\frac{dV}{V} &= 0 \\ 3\int \frac{dV}{V} + \int \frac{d(1/2nm_p u^2)}{(1/2nm_p u^2)} &= \ln(\text{const}) \\ 3\ln V + \ln(1/2nm_p u^2) &= \ln(\text{const}) \\ \frac{1}{2} nm_p u^2 V^3 &= \text{const.} \end{aligned} \tag{2.68}$$

But

$$\frac{1}{2} m_p = \text{const}$$

$$\Rightarrow \quad nu^2 V^3 = \text{const.}$$

If the number of particles is conserved

$$N = n(cm^{-3})V(cm^3) = \text{const}$$

then the equation becomes

$$\begin{aligned} (nV)(u^2V^2) &= \text{const} \\ \rightarrow \quad (uV)^2 &= \text{const} \end{aligned} \tag{2.69}$$

or

$$uV = \text{const.} \tag{2.70}$$

When considering one-dimensional compression V can be replaced by l and thus

$$ul = \text{const}$$

where u is for motion parallel to l.

This applies to compression in the absence of a B-field and for compression parallel to a field since the motion of charged particles are confined by the field in the perpendicular direction. Now if the dimension l is confined (compression) then the velocity has to adjust.

$$\Rightarrow \quad l \rightarrow 0$$

$$\Rightarrow \quad u \rightarrow \infty \quad \text{(particles accelerate).}$$

The motions perpendicular to the magnetic field (x and y directions) are strongly coupled by the gyrations around field lines. This must be taken into account for the case of compression perpendicular to the magnetic field. We can consider the mean square particle velocity in either of the two directions to find the kinetic energy density.
Per particle we have :
(Let $\mathbf{B} = B\hat{e}_z$)

$$\begin{aligned} \text{KE} &= \frac{1}{2}\text{m}_p < v_x^2 + v_y^2 > \\ &= \frac{1}{2}\text{m}_p[< v_x^2 > + < v_y^2 >] \\ &\approx \text{m}_p < v_x^2 > \quad \text{[in direction of motion]} \end{aligned}$$

$$\Rightarrow \quad \text{KE} \approx \text{m}_p u^2. \tag{2.71}$$

The kinetic energy density then is

$$U = n\text{m}_p u^2. \tag{2.72}$$

Applying the first law of thermodynamics to this example gives

$$\begin{aligned} \mathrm{dU} + \mathrm{PdV} &= 0 \\ d(n\mathrm{m}_p u^2 V) + (n\mathrm{m}_p u^2)dV &= 0 \end{aligned}$$

like before :

$$\begin{aligned} V d(n\mathrm{m}_p u^2) + 2n\mathrm{m}_p u^2 dV &= 0 \\ \int \frac{d(n\mathrm{m}_p u^2)}{n\mathrm{m}_p u^2} + 2\int \frac{dV}{V} &= \ln(\mathrm{const}) \\ \Rightarrow \quad nu^2V^2 &= \mathrm{const} \\ \Rightarrow \quad u^2 V &= \mathrm{const} \quad ; (N = nV \text{ is conserved}). \end{aligned} \tag{2.73}$$

In terms of a two-dimensional motion with V $\propto l^2$

$$a) \quad \Rightarrow \quad u^2 l^2 = \mathrm{const.}$$

But the conservation of magnetic flux also requires that

$$b) \quad \Rightarrow \quad \mathrm{B}l^2 = \mathrm{const}$$

or

$$l^2 = \frac{\mathrm{const}}{\mathrm{B}}.$$

This is put into a) to give

$$\frac{u^2}{\mathrm{B}} = \mathrm{const.} \tag{2.74}$$

Usually the r.m.s velocity for the two directions $\perp$ to the field is written as $\mathrm{v}_\perp^2$.
Therefore if $\mathbf{B} = \mathrm{B}\hat{\mathbf{e}}_\mathbf{z}$ then the x- and y-directions are the $\perp$ directions and

$$\begin{aligned} 1/2 < v_x^2 + v_y^2 > &= 1/2 < v_\perp^2 > \\ &= 1/2(2 < u^2 >) = u^2. \end{aligned} \tag{2.75}$$

Now consider

$$\begin{aligned} < w_\perp^2 > &= 2u^2 \quad ; [\text{with definition : } < w_\perp^2 > = < u_x^2 + u_y^2 >] \\ w_\perp^2 &= 2u^2. \end{aligned} \tag{2.76}$$

Then $\frac{u^2}{\mathrm{B}} = \mathrm{const}$

$$\Rightarrow \quad \frac{1/2w_\perp^2}{\mathrm{B}} = \mathrm{const.}$$

$$\Rightarrow \quad \frac{1/2\mathrm{m}_p w_\perp^2}{\mathrm{B}} = \text{const} \;\; ; \;\; [\mathrm{m}_p = \text{const}, \text{non-relativistic case}]. \tag{2.77}$$

Particles that move parallel to the B-field with speed $\mathrm{u}_\parallel$ between approaching magnetic mirrors are also compressed to give, in the one-dimensional case,

$$n(\mathrm{cm}^{-1})l = \text{const} \quad ; \text{[conservation of particles]}$$

where l is the separation between the mirrors.

For simultaneous transverse and longitudinal compression we can write for such a 3D compression

$$V(\mathrm{cm}^3)n(\mathrm{cm}^{-3}) = \text{const}$$

and

$$V = A(\mathrm{cm}^2)l.$$

This then gives

$$n(\mathrm{cm}^{-3})A(\mathrm{cm}^2)l = \text{const.} \tag{2.78}$$

Conservation of B-flux requires

$$\mathrm{B}A = \text{const}$$

$$\mathrm{B}l^2 = \text{const.}$$

Then from above

$$a)(\text{Eq.2.76}) \quad \frac{w_\perp^2}{\mathrm{B}} = \text{const}$$

$$b) \quad w_\parallel l = \text{const} = \frac{w_\perp l^2}{l}.$$

Therefore from b) and Eq.2.77

$$\begin{aligned}
\frac{w_\parallel A n l}{n l^2} &= \text{const} \;\; ; \;\; [An = nl^2] \\
\frac{w_\parallel \text{const}}{n l^2} &= \text{const} \;\; ; \;\; [Anl = \text{const}] \\
\frac{w_\parallel \mathrm{B}}{\mathrm{n}\mathrm{B} l^2} &= \text{const} \\
\Rightarrow \quad \frac{w_\parallel \mathrm{B}}{n} &= \text{const} \;\; ; \;\; [\mathrm{B}l^2 = \text{const}].
\end{aligned} \tag{2.79}$$

Hence in summary

$$\frac{w_\perp^2}{\mathrm{B}} = \text{const} \tag{2.80}$$

$$\frac{w_\parallel \mathrm{B}}{n} = \text{const.} \tag{2.81}$$

The particle pressures are :

$$P_{\perp} = \frac{1}{2} n m_p w_{\perp}^2 \tag{2.82}$$

$$P_{\parallel} = n m_p w_{\parallel}^2. \tag{2.83}$$

Then

$$\frac{P_{\perp}}{nB} = \frac{1/2 n m_p w_{\perp}^2}{nB} = \frac{1/2 m_p w_{\perp}^2}{B} = \text{const.} \tag{2.84}$$

Also

$$\frac{P_{\parallel}}{nB} = \frac{n m_p w_{\parallel}^2}{nB} = \frac{n^2 m_p}{B^3} \frac{w_{\parallel}^2 B^2}{n^2} = \text{const} \frac{n^2 m_p}{B^3}. \tag{2.85}$$

Then

$$\frac{B^2 P_{\parallel}}{m_p n^3} = \text{const.}$$

Therefore in summary

$$\frac{P_{\parallel} B^2}{n^3} = \text{const} \tag{2.86}$$

$$\frac{P_{\perp}}{nB} = \text{const.} \tag{2.87}$$

We can therefore see that for magnetic compression of particles

we get

$$(nB) \rightarrow \infty \Rightarrow P_{\perp} = 1/2 n m_p w_{\perp}^2 \rightarrow \infty$$

resulting in

$$w_{\perp}^2 \rightarrow \infty.$$

The average KE of the particles increases to keep the ratio $\frac{P_{\perp}}{nB}$ constant.

Furthermore, for parallel compression we get if

$$n^3 \rightarrow \infty$$

$$P_{\parallel} B^2 \rightarrow \infty$$

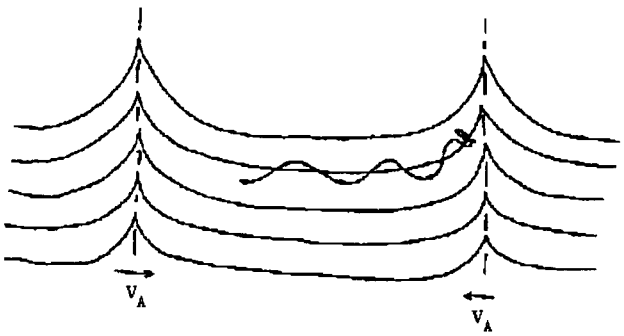

Figure 18 : A particle can be trapped between two approaching magnetic waves. (Parker 1976)

resulting in

$$n m_p w_{\parallel}^2 B^2 \rightarrow \infty$$

$$\Rightarrow \quad w_{\parallel}^2 \text{ will also increase.} \tag{2.88}$$

It must be kept in mind that this process is completely reversible, unless the particles can somehow leak out of the acceleration zone when they have higher energies, i.e. where the field gradient is largest. A specific example of the acceleration of particles by this process is the scattering of charged particles in a turbulent plasma from Alfvén waves, i.e.magnetic discontinuities propagating along field lines with a typical speed, the Alfvén speed. (Parker 1958; Parker 1976). A discussion of this process will now be presented.

Imagine a particle with pitch angle $\theta_o(t)$ in a field B_o. The particle is trapped between two approaching Alfvén waves with maximum field density $B_w > B_o$, where B_o is the field strength in the interwave zone. The condition for the particle to be trapped in these approaching fields is given by $\sin^2 \theta_o(t_o) > \frac{B_o}{B_w}$.

The particle is reflected back and forth between the two waves. A charge that approaches a wave crest 'tries' to follow the field line but gets flipped back in the process. A graphical representation is shown in Figure 18. The kinetic energy of the motion parallel to the field satisfies

$$\frac{1/2 m_p w_{\perp}^2}{B} = \text{const} \tag{2.89}$$

and this kinetic energy does not change between the waves or

$$w_{\perp}(t) = w_{\perp}(0).$$

For motion parallel to the field

$$w_{\parallel}(t) l(t) = \text{const},$$

where $l(t)$ is the separation between two waves.

The pitch angle θ is given by

$$\tan\theta = \frac{w_\perp}{w_\parallel}.$$

In the increased field of a wave the pitch angle increases from $\theta_\circ$ in the $B_\circ$ field to

$$\sin^2\theta(t) = \frac{B}{B_\circ}\sin^2\theta_\circ(t). \tag{2.90}$$

Considering the constant ratio (Eq.2.88), as $\mathbf{w_p}$ increases with successive reflections from head-on waves, the angle $\theta_\circ$(t) (the angle in the uniform field between the waves) will decrease. This process will continue until θ(t) fails to reach $\pi/2$ which is the reflection angle. The field is $B = B_w$ at this flip back stage and therefore the critical pitch angle is reached for

$$\begin{aligned}\sin^2\theta_\circ(t) &= \frac{B_\circ}{B_w}\sin^2\theta(t)\\ &\leq \frac{B_\circ}{B_w} \quad ; [\sin^2\theta \leq 1\ ; \theta \leq \pi/2].\end{aligned} \tag{2.91}$$

At this stage the parallel velocity of the deflected particle is

$$\begin{aligned}\tan\theta_\circ(t) &= \frac{w_\perp}{w_\parallel}\\ w_\parallel^2 &= \frac{\cos^2\theta_\circ(t)}{\sin^2\theta_\circ(t)}w_\perp^2\\ &= w_\perp^2\frac{1-\sin^2\theta_\circ}{\sin^2\theta_\circ}\\ &= w_\perp^2\left[\frac{B_w}{B_\circ}-1\right].\end{aligned} \tag{2.92}$$

Also

$$\begin{aligned}w^2(t) &= w_\parallel^2(t) + w_\perp^2(t)\\ &= w_\perp^2(t)\left[\frac{B_w}{B_\circ}-1\right] + w_\perp^2(t)\\ &= w_\perp^2(t)\frac{B_w}{B_\circ} = w_\perp^2(t)[\cot^2\theta_\circ(t)+1].\end{aligned} \tag{2.93}$$

If the initial pitch angle was $\theta_\circ(t_\circ)$ when the particle entered the region between the waves, the critical velocity was

$$\begin{aligned}w^2(t_\circ) &= w_\parallel^2(t_\circ) + w_\perp^2(t_\circ)\\ &= w_\perp^2(t_\circ)\left[\frac{B_w}{B_\circ}-1\right] + w_\perp^2(t_\circ)\\ &= w_\perp^2(t_\circ)[\cot^2\theta_\circ(t_\circ)+1].\end{aligned} \tag{2.94}$$

The gain in KE before the particle escapes is therefore

$$\begin{aligned}\frac{w^2(t)}{w^2(t_\circ)} &= \frac{w_\perp^2(t)[\cot^2\theta_\circ(t)+1]}{w_\perp^2(t_\circ)[\cot^2\theta_\circ(t_\circ)+1]} \\ &= \frac{\frac{\cos^2\theta_\circ(t)+1}{\sin^2\theta_\circ(t)}+1}{\frac{\cos^2\theta_\circ(t_\circ)+1}{\sin^2\theta_\circ(t_\circ)}+1} \\ &= \frac{\mathrm{B}_w}{\mathrm{B}_\circ}\sin^2\theta_\circ(t_\circ). \end{aligned} \tag{2.95}$$

If, for example, $\theta_\circ(t_\circ) = \pi/3$ and $\frac{\mathrm{B}_w}{\mathrm{B}_\circ} \approx 2$ then

$$\frac{w^2(t)}{w^2(t_\circ)} \approx 1.5$$

or the kinetic energy increases by 50 % before the particle escapes. However, if the particles that are trapped in the wave zone (between approaching crests) have their pitch angles continuously isotropized as a result of scattering off whistler waves and other particles, the energy gained before they tunnel out can be substantially greater. This process can play a very important role in the continuous acceleration of charged particles that are trapped inside magnetized gas that are continuously battered by a magnetospheric propeller, like proposed for AE Aquarii.

2.7 Fermi acceleration

The Fermi mechanism was first proposed by Fermi (1949) as a stochastic means by which particles colliding with clouds or inhomogeneities in the interstellar medium (ISM) could be accelerated to very high energies, accounting for the high energy cosmic rays observed in ground based and balloon experiments. In a collision of a particle with a moving inhomogeneity, the magnitude of the relative velocity remains unchanged. This is the same concept as the elastic collision between a particle and a moving piston.

Therefore

$$|v_{\mathrm{rel}}(\mathrm{before})| = |v_{\mathrm{rel}}(\mathrm{after})|.$$

Consider an overtaking type of collision (see Figure 19) :

$$v_{\mathrm{rel}}(\mathrm{before}) = w_p\cos\theta - u$$

$$v_{\mathrm{rel}}(\mathrm{after}) = w_p'\cos\theta' + u.$$

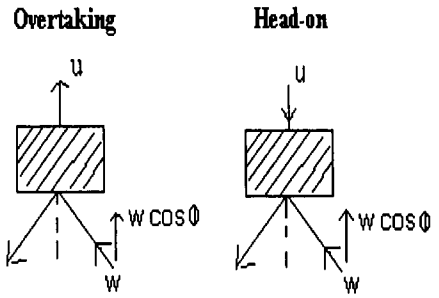

Figure 19 : The difference in the head-on and the overtaking types of collisions.

Then

$$\begin{aligned} w_p \cos\theta - u &= w_p' \cos\theta' + u \\ w_p' \cos\theta' &= w_p \cos\theta - 2u. \end{aligned} \tag{2.96}$$

The other possibility is a head-on collision :

$$v_{\text{rel}}(\text{before}) = w_p \cos\theta + u$$

$$v_{\text{rel}}(\text{after}) = w_p' \cos\theta' - u.$$

Then

$$w_p' \cos\theta' = w_p \cos\theta + 2u. \tag{2.97}$$

Now consider the one-dimensional case :

$$w_p' = w_p + 2u \quad [\text{head-on}]$$

$$w_p' = w_p - 2u \quad [\text{overtaking}].$$

A particle in the fixed frame (its own stationary frame of reference) gains kinetic energy T for Head-on:

$$\begin{aligned} \Delta\mathrm{T} &= \frac{1}{2}\mathrm{m}_p(w_p')^2 - \frac{1}{2}\mathrm{m}_p(w_p)^2 \\ &= \frac{1}{2}\mathrm{m}_p(w_p + 2u)^2 - \frac{1}{2}\mathrm{m}_p w_p^2 \\ &= 2\mathrm{m}_p u(w_p + u) \end{aligned} \tag{2.98}$$

and for Overtaking:

$$\begin{aligned}\Delta \mathrm{T} &= \frac{1}{2}\mathrm{m}_p(w_p')^2 - \frac{1}{2}\mathrm{m}_p(w_p)^2 \\ &= \frac{1}{2}\mathrm{m}_p(w_p - 2u)^2 - \frac{1}{2}\mathrm{m}_p w_p^2 \\ &= -2\mathrm{m}_p u(w_p - u). \end{aligned} \tag{2.99}$$

We next calculate the mean rate-of-change of a particle's kinetic energy between head-on and overtaking type scatterings.

This gives

$$\frac{\Delta \mathrm{T}}{\Delta t} = \frac{1}{2}\left[\left(\frac{\Delta \mathrm{T}}{\Delta t}\right)_{\text{H-on}} + \left(\frac{\Delta \mathrm{T}}{\Delta t}\right)_{\text{overt}}\right]. \tag{2.100}$$

The rates for the two types of collision are roughly

$$\left(\frac{1}{\Delta t}\right)_{\text{H-on}} \approx \frac{w_p + u}{\mathrm{L}} \tag{2.101}$$

$$\left(\frac{1}{\Delta t}\right)_{\text{Overt}} \approx \frac{w_p - u}{\mathrm{L}}. \tag{2.102}$$

Then

$$\begin{aligned}\left(\frac{\Delta \mathrm{T}}{\Delta t}\right) &= \frac{1}{2}\left[\left(\frac{w_p + u}{\mathrm{L}}\right)(2\mathrm{m}_p u(w_p + u)) + \left(\frac{w_p - u}{\mathrm{L}}\right)(-2\mathrm{m}_p u(w_p - u))\right] \\ &= \frac{1}{2}\left[\frac{2\mathrm{m}_p u}{\mathrm{L}}(w_p + u))^2 - \frac{2\mathrm{m}_p u}{\mathrm{L}}(w_p - u))^2\right] \\ &= \frac{\mathrm{m}_p u}{\mathrm{L}}(4w_p u) \end{aligned} \tag{2.103}$$

or

$$\dot{T} = \frac{4\mathrm{m}_p u^2 w_p}{\mathrm{L}}.$$

This then gives

$$\begin{aligned}\frac{\dot{T}}{T} = \frac{1}{T}\frac{\Delta T}{\Delta t} &= \frac{(4\mathrm{m}_p u^2 w_p/\mathrm{L})}{(1/2\mathrm{m}_p w_p^2)} \\ &= 8\left(\frac{u}{w_p}\right)^2\left(\frac{w_p}{\mathrm{L}}\right) \quad ; [\frac{w_p}{\mathrm{L}} \approx \text{collision rate}]. \end{aligned} \tag{2.104}$$

The constant in the equation is ~ 2 in the 3-D case.

We see that the mean fractional change in KE per collision is of the order of $\left(\frac{u}{w_p}\right)^2$. The result is a net gain because head-on collisions are more probable than overtaking collisions. Overtaking requires a particle to catch up with an inhomogeneity.

In the extreme relativistic case we have

$$\frac{1}{\mathrm{T}}\frac{d\mathrm{T}}{dt} = \mathrm{s}\left(\frac{\mathrm{c}}{\mathrm{L}}\right)\frac{v^2}{\mathrm{c}^2}$$

with s of order unity.

Now let F(T)dt represent the number of particles in the energy interval (T, T + dT) in a region of a turbulent magnetic field.

Conservation of particles leads to

$$\begin{aligned} dF &= \frac{\partial F}{\partial t}dt + \frac{\partial F}{\partial \mathrm{T}}\frac{d\mathrm{T}}{dt}dt = 0 \\ \frac{dF}{dt} &= \frac{\partial F}{\partial t} + \frac{\partial F}{\partial \mathrm{T}}\frac{d\mathrm{T}}{dt} = 0 \\ &= \frac{\partial F}{\partial t} + \frac{\partial}{\partial \mathrm{T}}(F\frac{d\mathrm{T}}{dt}) = 0 \end{aligned} \tag{2.105}$$

since

$$\begin{aligned} \frac{\partial}{\partial \mathrm{T}}(F\frac{d\mathrm{T}}{dt}) &= \frac{\partial F}{\partial \mathrm{T}}\frac{d\mathrm{T}}{dt} + F\frac{\partial^2 \mathrm{T}}{\partial t \partial \mathrm{T}} \\ &= \frac{\partial F}{\partial \mathrm{T}}\frac{d\mathrm{T}}{dt} \quad ;[\text{to first order}]. \end{aligned} \tag{2.106}$$

Now if $\frac{\partial F}{\partial t} = 0$, we get

$$\begin{aligned} \Rightarrow \quad \frac{\partial}{\partial \mathrm{T}}(F\frac{d\mathrm{T}}{dt}) &= 0 \\ \int d(F\frac{d\mathrm{T}}{dt}) &= \text{const} \quad ; [\text{with } \frac{\partial \text{const}}{\partial \mathrm{T}} = 0] \\ F\frac{d\mathrm{T}}{dt} &= \text{const} \end{aligned} \tag{2.107}$$

and thus

$$F(\mathrm{T}) = \frac{\text{const}}{\frac{d\mathrm{T}}{dt}}. \tag{2.108}$$

Now let

$$\frac{d\mathrm{T}}{dt} = \alpha \mathrm{T} \quad (\mathrm{T}_\circ < \mathrm{T} < \mathrm{T}_1) \quad (\alpha(\mathrm{s}^{-1})$$

then

$$F(\mathrm{T}) = \frac{\text{const}}{\alpha \mathrm{T}}. \tag{2.109}$$

Consider a rate of injection $\mathrm{N}_\circ$ of particles at the energy $\mathrm{T}_\circ$

$$\begin{aligned} \mathrm{N}_\circ &= F(\mathrm{T}_\circ)\left(\frac{d\mathrm{T}}{dt}\right)_\circ = F(\mathrm{T}_\circ)\alpha \mathrm{T}_\circ \\ \Rightarrow \quad F(\mathrm{T}_\circ) &= \frac{\mathrm{N}_\circ}{\alpha \mathrm{T}_\circ} \end{aligned} \tag{2.110}$$

and therefore the condition in (2.107) is

$$\text{const} = \mathrm{N_o}$$

$$\Rightarrow \quad F(\mathrm{T}) = \frac{\mathrm{N_o}}{\alpha \mathrm{T}} = \frac{\mathrm{N_o}}{\alpha \mathrm{T_o}} \frac{\mathrm{T_o}}{\mathrm{T}}.$$

This then gives

$$F(\mathrm{T}) \propto \mathrm{T}^{-1}. \tag{2.111}$$

In general the spectrum is not as flat as this result would suggest meaning the decline in number of particles with energy T is not as gradual as the result suggests. If a particle has a mean life time in the shock region the spectrum changes.

Suppose a particle has a mean life in such a region with characteristic time τ.

Then

$$\begin{aligned} dF &= \frac{\partial F}{\partial t}dt + \frac{\partial F}{\partial \mathrm{T}}\frac{d\mathrm{T}}{dt}dt + \frac{F}{\tau}dt = 0 \\ \frac{dF}{dt} &= \frac{\partial F}{\partial t} + \frac{\partial F}{\partial \mathrm{T}}\frac{d\mathrm{T}}{dt} + \frac{F}{\tau} = 0 \\ &= \frac{\partial F}{\partial t} + \frac{\partial}{\partial \mathrm{T}}(F\frac{d\mathrm{T}}{dt}) + \frac{F}{\tau} = 0. \end{aligned} \tag{2.112}$$

In a steady state with $\frac{\partial F}{\partial t} = 0$:

$$\begin{aligned} \frac{\partial}{\partial \mathrm{T}}\left(F\frac{d\mathrm{T}}{dt}\right) + \frac{F}{\tau} &= 0 \\ d\left(F\frac{d\mathrm{T}}{dt}\right) + \frac{F}{\tau}d\mathrm{T} &= 0 \\ \alpha \mathrm{T}dF + Fd(\alpha \mathrm{T}) + \frac{F}{\tau}d\mathrm{T} &= 0 \\ \frac{dF}{F} + \frac{d\mathrm{T}}{\mathrm{T}} + \frac{1}{\alpha\tau}\frac{d\mathrm{T}}{\mathrm{T}} &= 0 \end{aligned}$$

Integration gives:

$$\begin{aligned} (\ln F - \ln F_o) + (\ln \mathrm{T} - \ln \mathrm{T_o}) + \frac{1}{\alpha\tau}(\ln \mathrm{T} - \ln \mathrm{T_o}) &= 0 \\ \ln(F\mathrm{T}^{(1+\frac{1}{\alpha\tau})}) &= \ln(F_o \mathrm{T_o}^{(1+\frac{1}{\alpha\tau})}) \\ F\mathrm{T}^{(1+\frac{1}{\alpha\tau})} &= F_o \mathrm{T_o}^{(1+\frac{1}{\alpha\tau})} \end{aligned}$$

and finally, resulting in

$$\begin{aligned} F &= F_o\left(\frac{\mathrm{T_o}}{\mathrm{T}}\right)^{(1+\frac{1}{\alpha\tau})} \\ &= \frac{\mathrm{N_o}}{\alpha \mathrm{T_o}}\left(\frac{\mathrm{T_o}}{\mathrm{T}}\right)^{(1+\frac{1}{\alpha\tau})}. \end{aligned} \tag{2.113}$$

This spectrum then is steeper than the previous one by a factor $\frac{1}{\alpha\tau}$. This means that the population of accelerated particles depends on the influx of 'fresh'particles into the shock acceleration region, the initial energies of these particles and the time they remain in the acceleration region.

2.8 Shock-waves and fast particles: Shock drift acceleration

The acceleration of charged particles as a results of criss-crossing magnetohydrodynamic wave fronts has been extensively documented, see for example Toptyghin (1980)(review article). In this section we will concentrate however, only on the reflection of a charged particle with a high velocity, oblique shock (see Figure 20), resulting in acceleration of the particle through the so-called shock drift acceleration process or fast-Fermi process (Benz 1994).

If charged particles have gyroradii which are much smaller than the thickness of a magnetohydrodynamic disturbance propagating through the plasma, the shock will act as a magnetic mirror since there is an increase in the magnetic field across a shock for fast-mode shocks (Benz 1994). The acceleration of the particle in the particle-shock interaction is basically the result of the conservation of the magnetic moment, as was discussed earlier. It can be shown that, from the condition

$$\frac{p_\perp^2}{B} = \text{const}$$

for non-relativistic particles

$$\begin{aligned} E_\perp &= \frac{1}{2}m_o v_\perp^2 \quad \Rightarrow \quad 2E_\perp m_o = (m_o v_\perp)^2 \\ p_\perp^2 &= 2m_o E_\perp \qquad (2.114) \\ \Rightarrow \quad \frac{2m_o E_\perp}{B} &= \text{const} \\ \Rightarrow \quad \frac{E_{\perp 2}}{B_2} &= \frac{E_{\perp 1}}{B_1} \\ \Rightarrow \quad \frac{E_{\perp 2}}{E_{\perp 1}} &= \frac{B_2}{B_1}. \qquad (2.115) \end{aligned}$$

Similarly for relativistic particles from the condition :

$$\frac{p_\perp^2}{B} = \text{const}$$

where

$$E_\perp \approx p_\perp c \quad \Rightarrow \quad p_\perp = \frac{E_\perp}{c}.$$

Then

$$\frac{(E_\perp/c)^2}{B} = \text{const}$$

$$\Rightarrow \quad \frac{E_{\perp}^2}{B} = \text{const.} \tag{2.116}$$

This then gives

$$\begin{aligned} \frac{E_{\perp 2}^2}{B_2} &= \frac{E_{\perp 1}^2}{B_1} \\ \Rightarrow \quad \frac{E_{\perp 2}}{E_{\perp 1}} &= \left(\frac{B_2}{B_1}\right)^{1/2}. \end{aligned} \tag{2.117}$$

Therefore we have

$$\begin{aligned} \text{non-relativistic:} \quad \frac{E_{\perp 2}}{E_{\perp 1}} &= \frac{B_2}{B_1} \\ \text{relativistic} \quad \frac{E_{\perp 2}}{E_{\perp 1}} &= \left(\frac{B_2}{B_1}\right)^{1/2}. \end{aligned} \tag{2.118}$$

From these equations one can see that the interaction of the particles with magnetic compressions in shock fronts in astrophysical plasmas will result in the increase of the energy of the particles. The probability that a charged particle is reflected by a shock front is determined by estimating the critical pitch angle of the particle with respect to the field as a function of the magnetic compression in a shock front. We showed earlier that for particles trapped between approaching magnetic inhomogeneities (magnetic compressions, which can be produced by shock fronts propagating through the plasma), the particles will be trapped if

$$\left(\frac{v_{\parallel o}}{v_{\perp o}}\right)^2 < \frac{B_m}{B_o} - 1. \tag{2.119}$$

We have $v_{\parallel o}^2 = v_{po}^2 - v_{\perp o}^2$ so

$$\begin{aligned} \frac{v_{po}^2 - v_{\perp o}^2}{v_{\perp o}^2} &< \frac{B_m}{B_o} - 1 \\ \left(\frac{v_{po}}{v_{\perp o}}\right)^2 &< \frac{B_m}{B_o} \\ \left(\frac{v_{\perp o}}{v_{po}}\right)^2 &> \frac{B_o}{B_m} \\ \sin^2\theta &> \frac{B_o}{B_m} \\ \cos\theta_o &> \left(1 - \frac{B_o}{B_m}\right)^{1/2}. \end{aligned} \tag{2.120}$$

This means that if, for example, $\frac{B_o}{B_m} \approx 4$, then $\theta_o > 30°$. The trapping of a particle between moving inhomogeneities (shocks) in a plasma secures the continuous interaction of the particle with the shock, which will result in the net gain of kinetic energy of the particle.

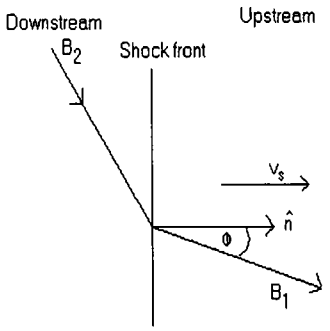

Figure 20 : An oblique shock moves at an angle with respect to the upstream B-field.

Energy may be gained by particles that are reflected repeatedly by the shock while conserving their magnetic moments $p_\perp^2/B$. A detailed analysis showed that the maximum energy transfer to a particle in a single crossing of the shock is (Toptyghin 1980, Priest & Forbes 2000)

$$\frac{\Delta E_{max}}{E_i} = \left(4\left(\frac{B_d}{B_u}\right) - 3\right) \text{ (thermal)}$$

and

$$\frac{\Delta E_{max}}{E_i} = \left(2\left(\frac{B_d}{B_u}\right) - 1\right) \text{ (relativistic)}$$

where B_d and B_u are the up and down stream magnetic fields respectively. Strong shocks give $B_d/B_u \rightarrow 4$, and thus the energy of thermal and mildly relativistic electrons can be increased by factors of $(\Delta\ E_{max}/E_i) \rightarrow 13$ and $(\Delta\ E_{max}/E_i) \rightarrow 7$ respectively, in a single encounter with a strong shock.

In this chapter a description was given of a variety of scenarios in which particle acceleration can occur in highly conducting and turbulent media. The mhd propeller in AE Aquarii, expelling blobs of plasma from the fast rotating white dwarf magnetosphere, is conducive to mechanisms such as reconnection, adiabatic compression as well as the generation of shock waves in the plasma. The efficiency of these processes in producing populations of high energy particles is limited, but as will be shown the model for the radio emission from AE Aqr does not require high efficiency. Even limited efficiency in terms of acceleration of some fraction of the thermal population of electrons in the plasma blobs is sufficient to drive the non-thermal outbursts from AE Aquarii, from the radio to infrared frequencies. These aspects will be addressed in the next chapter. The discussions that follow form the foundation of the model developed to explain the synchrotron flares from AE Aquarii, as is documented in the paper, *Meintjes P.J. & Venter L.A. 2003, Modelling the continuous radio outbursts in AE Aquarii, MNRAS, 341, 891.* The paper is included at the back.

Chapter 3

Propeller Outflow and Radio-Synchrotron emission

The highly variable radio-infrared (IR) outbursts from AE Aquarii are most probably of non-thermal origin as can be concluded from the high brightness temperature of the radio source, ruling out any thermal origin of the emission. A *VLBI* observation showed indications of an expanding radio synchrotron source (Abada-Simon et al. 1999, 2002; A.E. Niell, private communication), which may be an observational indicator that the non-thermal radio synchrotron emission originates from expanding synchrotron emitting clouds, probably in terms of a Van der Laan mechanism (Van der Laan 1963, 1966). The Van der Laan mechanism describes the radio synchrotron emission from expanding magnetized clouds, which can be incorporated within the basic theoretical framework of the propeller ejection of gas from the binary system, provided the gas contains magnetic flux frozen into it. The model proposed for the non-thermal radio outbursts from AE Aquarii is based upon the integration of the concepts of propeller ejection of magnetized gas clouds from the system with a Van der Laan radio-synchrotron process. It will be shown that the mass transfer flow from the secondary may contain substantial magnetic flux since the mass transfer originates from a secondary K4-5 star, which usually have deep convective envelopes, in which a magnetic field can be generated through some dynamo process. Therefore, some fraction of the mass transfer from the secondary may have magnetic flux frozen into it.

The radio flares from AE Aquarii is modelled in terms of expanding magnetized synchrotron emitting plasma clouds ejected from the binary system by a mhd propeller mechanism. However, the energetics involved in the synchrotron process, i.e. magnetic and particle energy, and the Van der Laan mechanism is also used extensively to constrain some determining parameters like relativistic electron density and blob magnetic fields. Complementing this, the magnetized mass

transfer is independently constrained through the magnetic braking of the mass donating star (dependent on the surface field strength), which drives the mass transfer in the binary system. Since the radio synchrotron flares and the surface magnetic fields, constrained by the magnetic braking of the secondary, are interlinked in our modelling of the flares, a short but relevant discussion of these will be presented.

3.1 Synchrotron emission process

Only some basic principles of the synchrotron process, relevant to the study, will be highlighted in the following discussion.

Synchrotron radiation, also known as magneto-bremsstrahlung, occurs as the result of the motion of charged particles in a magnetic field. In the case of non-relativistic particles this radiation is called cyclotron radiation and the frequency of the radiation is the gyration frequency of the particles around the field lines, or $\omega_B = \frac{\mathrm{qB}}{\gamma \mathrm{mc}}$ with $\gamma = (1 - \frac{v^2}{\mathrm{C}^2})^{-1/2}$. If the particles are relativistic, the frequency spectrum becomes extended by the inclusion of many harmonics of the fundamental gyration, or cyclotron frequency and the result is synchrotron radiation. The modification of the simple cyclotron frequency is the result of relativistic beaming of the emitted radiation from relativistic particles spiraling in the magnetic field.

The power radiated by a single charged particle in a magnetic field can be written as

$$\begin{aligned} \mathrm{P} &= \text{Const } 1\frac{\mathrm{B}^2 v_\perp^2}{\mathrm{m}_p^2 \gamma^2} \\ &= \text{Const } 2\beta_\perp^2 \gamma^2 \mathrm{B}^2 \\ &= 2 \times 10^{-3} \mathrm{B}^2 E^2 \mathrm{ergs}^{-1} \end{aligned} \tag{3.1}$$

where m_p is the mass of a radiating particle, $\mathrm{v}_\perp$ ($\beta_\perp = \mathrm{v}_\perp/\mathrm{c}$) represents the perpendicular component of the particle's velocity with respect to the B-field and γ (the Lorentz factor) [or E (erg)] is the particles's relativistic energy. This expression shows that relativistic electrons are much stronger synchrotron radiators than relativistic protons. Therefore, the observed emission from synchrotron radio sources is dominated by the emission of large ensembles of relativistic magnetically confined electrons in these objects.

Cosmic ray studies and observations of Solar flares, to name two examples, indicate that nature favors a mechanism that produces a power-law distribution of accelerated particles and hence the particle energy distribution is usually assumed to be a power law where the number of particles

with energies between E and E + dE can be expressed as

$$N(E)dE = CE^{-\delta}dE$$

for energies in the range $E_1 < E < E_2$ and δ the spectral index. The index δ, is not always well quantifiable but in most astrophysical applications may be in a range $\delta = 2$ - 3.2. Cosmic ray studies indicate $\delta = 2.5$ - 2.75. The radiated power then depends on frequency like $P(\omega) \propto \nu^{-(\delta-1)/2}$.

A synchrotron source has a total volume emissivity as a result of the total number density of synchrotron emitting electrons given by

$$\mathrm{L} = \int \mathrm{n}(E) \left(\frac{-dE}{dt}\right) dE \tag{3.2}$$

where n(E) represents the power-law relativistic electron number density and the rate at which an electron loses energy is $\frac{dE}{dt} = -2.4 \times 10^{-3} B^2 E^2$ erg s^{-1} (see Pacholzyk 1970; Lang 1998). The critical frequency, at which most power is radiated per single electron, is $\nu_c = c_1 \mathrm{B}E^2$ ($c_1 = 6.27 \times 10^{18}$). The spectral luminosity L_ν from a synchrotron source allows an estimate of the total amount of energy it contains in the form of relativistic electrons (Pacholzyk 1970). By integrating the total energy spectrum

$$W = \int_{E1}^{E2} E\mathrm{n}(E)d(E)$$

one gets

$$E_{e^-} = \frac{C}{2-\delta}\left[E_2^{2-\delta} - E_1^{2-\delta}\right] \text{ erg cm}^{-3}$$

This allows the determination of the constant C in terms of the electron energies involved. Integrating the synchrotron emissivity between the same two energies/frequencies gives

$$\mathrm{L} = \frac{2 \times 10^{-3} C \mathrm{B}_\perp^2}{3-\delta}\left[E_2^{3-\delta} - E_1^{3-\delta}\right] \text{ erg cm}^{-3}\text{s}^{-1}$$

Substituting C, obtained from the previous integration, and simplifying gives

$$E_e(\mathrm{erg}) = \frac{\mathrm{L}(\mathrm{erg\ s}^{-1})}{2 \times 10^{-3}}\left(\frac{3-\delta}{2-\delta}\right) c_1^{1/2} \mathrm{B}^{-3/2} \frac{\nu_\circ^{\frac{2-\delta}{2}} - \nu^{\frac{2-\delta}{2}}}{\nu_\circ^{\frac{3-\delta}{2}} - \nu^{\frac{3-\delta}{2}}} \tag{3.3}$$

where energy was written in terms of observed synchrotron frequency.

The total magnetic energy in the source is $E_B(\mathrm{erg}) = \frac{\mathrm{B}^2 \mathrm{R}^3 \Phi}{6}$ with Φ the fraction of volume occupied by both the field and the relativistic particles (Pacholzyk 1970). Then ignoring particles other than electrons it can be shown (Pacholzyk 1970) that equipartition between the magnetic field and the particle energy (minimizing the energy with respect to the B-field), gives

$$\mathrm{B}_{min} = \left[\frac{3}{4}\frac{C_e(\delta)}{8\pi}\frac{\mathrm{L}(\mathrm{erg\ s}^{-1})}{\mathrm{V}_{source}}\right]^{2/7}. \tag{3.4}$$

The observed radio to IR spectrum (Abada-Simon et al. 1999, 2002) implies a maximum luminosity in the range of $L_{max} \sim 5 \times 10^{30}$ erg s^{-1}, which is dominated by emission in the near IR from blobs with typical sizes $r_o = 10^8 - 10^9$ cm (Abada-Simon et al. 1999, 2002). If a large fraction of the luminosity is confined to a single blob of these dimensions, magnetic fields of the order of $B_{blob} = (650 - 2 \times 10^4)$ G are required to confine the electrons.

This indicates that the synchrotron blobs probably must be magnetized with a relatively high field strength to explain the radio emission. Part of the requirements for a model will therefore be to account for the presence of a sufficiently strong B-field in the synchrotron source. This must be done in context with the available energies and densities with an assumed initial size r_o of the blobs.

The origin of the blob fields is dependent on the surface field strength of the secondary star, especially the distribution of the field over the stellar surface. The magnetic activity of the secondary can be constrained by the magnetic braking of the secondary star, which drives the mass transfer in most close binaries. The attraction of this approach is that the mass transfer, which is an observably constrainable quantity, can be used to limit the surface field strength of the secondary star, which may provide an indication of the magnetic field strength to be expected in the mass transfer. It was proposed in a recent mcv conference (Cape Town Dec. 2002) that magnetic structures like star spots and prominences can have a severe influence on the mass transfer process. It was proposed (Hessman(2002) personal communication) that extended gas filled magnetic structures on the secondary (prominences) can pinch off gravitationally into the Roche lobe of the primary as they drift towards the L1 point. This will provide a natural mechanism to generate magnetized blobs in the mass transfer flow.

The actual surface field of the secondary that can possibly be transferred to the flow can be estimated by carefully evaluating the magnetic braking process that drives the mass transfer in the system. Since this forms an integral part of the model, a short discussion will follow.

3.2 Magnetic Braking of the Secondary Star: Surface Field Strength

A significant pressure gradient between the surface of a star and the interstellar medium(ISM) can result in the escape of the stellar atmosphere from the star. If the star has a magnetic field, the atmosphere can flow away along the "open" field lines, pushed along by the pressure gradient between the stellar atmosphere and the ISM. The magnetosphere of the star will corotate with the star. However, the flux of particles flowing away from the rotating star, also carrying angular

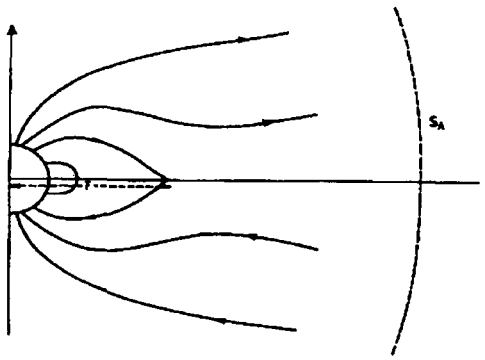

Figure 21 : Schematic of the magnetic field structure in a magnetic stellar wind showing the dead zone and open field lines. (Campbell 1997 from Mestel & Spruit 1987)

momentum away, will result in a braking torque on the rotating star as the star tries to keep the magnetically guided out flowing atmosphere in corotation.

Angular momentum loss through a stellar wind in these stars will result in tidal torques acting between the primary and secondary attempting to keep the braking star synchronous with the binary period, causing the binary system to shrink physically and the binary period to decrease. Paradoxically, this tidal interaction will then result in the secondary to rotate faster. The tidal spin-up of a satellite losing altitude as its orbit decays away as a result of frictional forces can serve as an analogy.

The decrease in the binary period, and hence the orbital separation, will also shrink the respective Roche lobes of the secondary and primary stars. This will severely influence the mass transfer rate and is basically the mechanism driving mass transfer in most binary systems. Therefore, the orbital evolution of the system can be used as a diagnostic tool in constraining the mass transfer in close binaries and hence the magnetic braking process for a system with a given mass ratio. This then provides an independent constraint of the surface magnetic field strength of the secondary star that can somehow be transferred to the mass flow between the secondary and primary.

Magnetic braking as a mechanism driving mass transfer in a binary system has been extensively discussed in literature. The basic theoretical framework for this discussion is the defining paper by Mestel & Spruit (1987) (see also Campbell (1997); Mestel (1999) for an encyclopedic overview).

In models of magnetic winds (Mestel & Spruit 1987; Campbell 1997; Mestel 1999) the wind carries the field lines with it. Figure 21 shows the structure of the magnetic wind. The mass loss in the wind is driven by thermal pressure gradients and centrifugal acceleration which is not balanced by the interstellar medium pressure. The kinetic energy density of the out flowing wind

material becomes comparable with the poloidal magnetic energy density ($\rho v_r^2 = \frac{B^2}{4\pi}$) at the Alfvén radius (defining the surface S_A) where the velocity reaches $v_A = \left(\frac{B_p^2}{4\pi\rho}\right)^{1/2}$ with ρ the density of the wind material. If the flow reaches v_A before the magnetic loops close, the field is dragged out with the flow. Close to the star the magnetic pressure dominates the gas pressure and closed flux tubes trap hot gas in the so-called dead zone with radius $\bar{r}$, in the equatorial plane. Outside the dead zone the field is nearly radial with flux tubes being pulled open as a result of the centrifugal acceleration of the wind along the field lines. The total braking torque (Mestel & Spruit 1987) is calculated by integrating the total angular momentum flux carried jointly by the wind and the magnetic stresses along fluid stream lines following the open field lines, over the entire Alfvén sphere, with surface S_A, which is permeated by open field lines. Without digressing into the detail of the calculation, which is quite cumbersome, it can be shown that the total angular momentum loss through magnetic braking is

$$-\dot{J}_{mb} = \frac{2}{3}\left(\frac{2}{3}\right)^{2/3}\left(\frac{\bar{r}}{R_s}\right)^{-4/3}\left(\frac{B_o}{B_\odot}\right)^{4/3}\left(\frac{\dot{M}_w}{\dot{M}_\odot}\right)^{1/3} B_\odot^{4/3}\dot{M}_\odot^{1/3}R_s^{8/3}\Omega_s^{1/3}, \tag{3.5}$$

scaled with respect to the mass loss from the Sun, where B_o represents the polar surface field strength of the secondary ($B_\odot$ the corresponding value for the Sun), $\dot{M}_w$ representing the wind loss rate from the secondary ($\dot{M}_\odot$ the corresponding value for the Sun), R_s the radius of the secondary ($R_\odot$ the Solar radius) and $\Omega = (2\pi/P_{rot})$ the rotation period of the secondary, which is synchronized with the binary period. This angular momentum loss will result in a drain of orbital angular momentum, which is given by

$$J_{orb} = 1.49\left(\frac{G\,R_\odot}{M_\odot}\right)^{1/2} q^{1/2}M_1\frac{M_2^{4/3}}{(M_1+M_2)^{1/3}} \tag{3.6}$$

where $q = (M_2/M_1)$ represents the mass ratio of the binary.

It was shown by Meintjes (2002a,b) that the AE Aquarii binary system is most probably currently in a converging phase of its evolution (King 1988), resulting in the mass transfer between the secondary and the highly magnetized white dwarf being between 4×10^{17} g.s$^{-1} \leq \dot{M}_2 \leq 2 \times 10^{18}$ g.s^{-1}. Mass transfer in this range is too low for the development of an accretion disc in the system given the fast rotation period of the spun-up white dwarf. The relatively low mass transfer from the secondary in the current phase results in propeller driven mass ejection from the system, with a total mechanical outflow power exceeding the power released by mass accretion by a factor of of $\kappa = \left(\frac{\text{outflow power}}{\text{accretion power}}\right) \approx 250$ (Wynn, King & Horne 1997; Meintjes & de Jager 2000; Meintjes 2002a,b). In recent papers (Kuijpers & Pringle 1982; Frank, King & Lasota 1988; King & Lasota 1991; King 1993; Wynn & King 1995) it was

pointed out that the mass transfer flow from the secondary to the primary in the intermediate polar and polar subclasses of magnetic cataclysmic variables may be clumpy or blob-like. A detailed study of the densities of the gas blobs from the secondary star in AM Her was carried out by Beardmore & Osborne (1997). They described the variability in the hard X-ray observations from AM Her, made by *Ginga*, as shot noise caused by inhomogeneous accretion of blobs with typical densities of $N_{blob} \sim 10^{15}$ - 10^{17} cm^{-3}. For these densities the blobs are probably diamagnetic, i.e. not easily penetrated by the magnetic field of the white dwarf. They may however be magnetized themselves, i.e. having a frozen-in magnetic field from the K4-5 secondary star, which may have a substantial surface magnetic field strength.

The surface field of the K4-5 secondary star in AE Aquarii, i.e. the mass donor, is obtained from the condition of stable mass transfer in binary systems where the mass transfer process is driven by magnetic braking. For a mass losing system like AE Aquarii, detailed calculations (Wynn & King 1995, Meintjes 2002b, King & Lasota 1991, King 1993, Wynn & King 1995) showed that stable mass transfer in the converging phase of a binary system's evolution must satisfy the condition

$$\left(\frac{-\dot{J}_{mb}}{J}\right) \geq \left[1 - q_i(1-\alpha) - \frac{\alpha}{2}\left(\frac{M_2}{M}\right) - \eta\left(\frac{M}{M_1}\right)^{1/2}\left(\frac{R_{circ}}{a}\right)^{1/2}\right]\left(\frac{-\dot{M}_{2,i}}{M_{2,i}}\right) \qquad (3.7)$$

where η is the fraction of the angular momentum, in terms of Roche lobe overflow across L1 being ejected from the binary, and where α is the fraction of the mass overflow from the secondary being propelled out of the system by the propeller. In the current propeller phase of AE Aquarii we have $\eta \approx 1$ and $\alpha \approx 1$.

The mass transfer rate in AE Aquarii is constrained by the minimum required mass transfer that can explain the emission lines from the system, i.e. $\dot{M}_2 \geq 4 \times 10^{17}$ g.s^{-1} (Eracleous & Horne 1996) and the maximum allowed rate that would still result in a converging evolution $\dot{M}_2 \leq 2 \times 10^{18}$ g.s^{-1} (Mcdermott & Taam 1989; Meintjes 2002b). By adopting the Mestel & Spruit (1987) stellar wind model of magnetic braking in the fast rotator limit, i.e. $(\Omega_2/\Omega_\odot) = (P_\odot/P_2) >> 1$ (applicable to AE Aqr), assuming the secondary star's rotation period is tidally locked with the orbital period of the system, the orbital angular momentum loss via stellar wind from the secondary in AE Aquarii, and hence magnetic braking, is derived from the basic stellar wind equations (Campbell 1997)

$$\frac{\dot{J}_{mb}}{J_{orb}} \approx 5.8\times10^{-21}\left(\frac{\bar{r}}{R_2}\right)^{-5/3}\left(\frac{P_{orb}}{9.88\,\mathrm{hr}}\right)^{8/3}\left(\frac{M_1}{0.9\,M_\odot}\right)^{-1}\left(\frac{M_2}{0.6\,M_\odot}\right)^{-4/3}\left(\frac{M}{1.5\,M_\odot}\right)^{1/3}\left(\frac{B_\circ}{B_\odot}\right)^{(4n+2)/3n} \qquad (3.8)$$

for a stellar field depending on the dynamo number n. As an independent check, the same calculation was repeated for a model where the stellar field scales with the inverse turbulent Rossby

number (Saar 1991; Campbell 1997)

$$\frac{\dot{J}_{mb}}{J_{orb}} \approx 4.2 \times 10^{-21} \left(\frac{\bar{r}}{\mathrm{R}_2}\right)^{-5/3} \left(\frac{\mathrm{P}_{orb}}{9.88\,\mathrm{hr}}\right)^{20/9} \left(\frac{\mathrm{M}_1}{0.9\,\mathrm{M}_\odot}\right)^{-1} \left(\frac{\mathrm{M}_2}{0.6\,\mathrm{M}_\odot}\right)^{-4/9} \left(\frac{\mathrm{M}}{1.5\,\mathrm{M}_\odot}\right)^{1/3} \left(\frac{\mathrm{B}_\circ}{\mathrm{B}_\odot}\right)^2 \tag{3.9}$$

where in both models $\bar{r}/\mathrm{R}_2$ represents the ratio of the wind dead zone to stellar radius for the secondary star (Mestel & Spruit 1987; Campbell 1997; Mestel 1999), and where $(\mathrm{B}_\circ/\mathrm{B}_\odot)$ is the ratio of the stellar to solar surface polar magnetic field strength. The condition for stable mass transfer in AE Aquarii in the current propeller driven mass losing phase ($\alpha \approx 1$; $\eta \approx 1$) is

$$\frac{\dot{J}_{mb}}{J} \geq 5.25 \times 10^{-16} \left(\frac{\dot{M}_2}{2 \times 10^{18}\,\mathrm{g\ s^{-1}}}\right) \left(\frac{\mathrm{M}_2}{0.6\,\mathrm{M}_\odot}\right)^{-1} \mathrm{s}^{-1} \tag{3.10}$$

In the fast rotator limit $(P_\odot/P_2) \approx 70$, applicable to AE Aquarii, the ratio $(\bar{r}/\mathrm{R}_2) \approx 3$ - 5 (Campbell 1997). This results in an estimate for the polar value of the secondary star's magnetic field, for a linear $n = 1$ dynamo model and the inverse Rossby number law respectively, which are

$$\mathrm{B}_\circ \geq 1900 \left(\frac{\mathrm{B}_\odot}{2\,\mathrm{G}}\right) \left(\frac{\dot{M}_2}{2 \times 10^{18}\,\mathrm{g\ s^{-1}}}\right)^{1/2} \left(\frac{\mathrm{P}_{orb}}{9.88\,\mathrm{hr}}\right)^{-8/6} \mathrm{G} \tag{3.11}$$

and

$$\mathrm{B}_\circ \geq 2245 \left(\frac{\mathrm{B}_\odot}{2\,\mathrm{G}}\right) \left(\frac{\dot{M}_2}{2 \times 10^{18}\,\mathrm{g\ s^{-1}}}\right)^{1/2} \left(\frac{\mathrm{P}_{orb}}{9.88\,\mathrm{hr}}\right)^{-20/18} \mathrm{G} \tag{3.12}$$

using $(\mathrm{M}_2/0.6\,\mathrm{M}_\odot)$, $(\mathrm{M}_1/0.9\,\mathrm{M}_\odot)$ and $(\mathrm{M}/1.5\,\mathrm{M}_\odot)$. Both estimates show that the polar value for the surface field of the secondary star can reach values up to $B_\circ \approx 2000$ G for a Mestel & Spruit (1987) stellar wind model.

These estimates just show that the secondary is magnetized, having a reasonably high polar surface field. The actual distribution of magnetic flux across the stellar surface will actually determine the average field strength of the secondary star. The Sun, which has a polar field strength between $\mathrm{B}_\odot$ = 1 - 5 Gauss (Parker 1979), however has a far more magnetically active equatorial belt as a result of the faster rotation at the equator, which may also apply to magnetic secondary stars in binary systems that transfer mass to a compact primary. Assuming the secondary is magnetized, with a magnetically active equatorial zone, one can envisage a scenario where star spots or prominences may frequently drift into regions close to L1, where they can be gravitationally pulled into the Roche lobe of the primary star. This mechanism may ensure that a fraction of the clumpy mass transfer flow from the secondary to the primary consists of highly conducting, magnetized blobs.

Values obtained for the surface field strength of the secondary star ($\mathrm{B}_\circ = \mathrm{B}_{blob} \sim 2000$ G) are then taken as limiting values for the fields imbedded in the blobs. The estimates of the surface

field and the blob fields from the synchrotron constraints (from above), are consistent with these values and therefore it is assumed that initial blob field strengths of $B_{blob} \geq 2000$ G are acceptable. If the electron population in these blobs can be energized to relativistic energies, these blobs may be strong synchrotron sources.

It was shown before that the violent interaction of magnetized blobs with the propeller may result in particle acceleration through various mechanisms like magnetic reconnection, magnetic pumping and shock drift acceleration. The efficiency of the last two processes in accelerating electrons from a thermal population to relativistic energies is very low, but increases dramatically if electrons can be injected into pumping sites and shock fronts with energies significantly above the thermal energy of the plasma, ideally energies as high and above ≥ 1 MeV.

3.3 Particle Acceleration and the Van der Laan(VDL) model

The model proposes that dense, strongly magnetized, gas blobs may be among the stream of ejected mass transfer propelled out of the system by the propeller mechanism. It is proposed that particle acceleration can occur in the blobs as a result of the severe battering from the propeller, leading to radio flares as these blobs expand. To order of magnitude, one can estimate the energy pumped into these expanding blobs as the white dwarf magnetic field sweeps over and tries to compress them. The mhd power pumped into expanding blobs by the rotating magnetic field of the white dwarf can be estimated as

$$\begin{aligned} L_{blob} &\approx \left(\frac{B^2(r)}{8\pi}\right)\left(\frac{4\pi}{3}\right) R_b^3 \Omega_* \\ &\leq 10^{32}\left(\frac{B_*}{2\times 10^6\,G}\right)^2\left(\frac{P_{wd}}{33\,S}\right)^{-1}\left(\frac{R_{wd}}{10^9\,cm}\right)^3 \text{ erg s}^{-1}. \end{aligned} \tag{3.13}$$

The energizing is the result of the transfer of the magnetic energy of the magnetosphere to the blobs over time scales equal to the rotation period of the white dwarf, i.e. P_{wd}. This power is sufficient to drive the non-thermal radio-synchrotron emission in the system.

It will be shown that processes like magnetic reconnection can provide a quick impulsive energizing phase of the thermal electron population in these blobs to energies of approximately 1-2 MeV, and that continuous re-acceleration occurs in the blobs via processes like shock drift acceleration in oblique shock fronts, adiabatic compression and magnetic pumping via Alfvén waves, resulting in heating of electrons to energies approaching $\gamma \approx 20$ as the blobs reach $\rho = (r/r_o) \approx 400$. The radio spectrum is then a superposition of several ($N \leq 20$) radio emitting expanding blobs in different stages of their evolution. Since the initial acceleration and the continued re-acceleration of the electron population in the blobs play such an important role in the model, a qualitative discussion will be given of the various processes and stages that are relevant for the model.

3.3.1 Particle Acceleration Processes in Magnetized Blobs

Phase I: magnetic reconnection

Magnetic reconnection (see §2.4) as a mechanism to convert magnetic energy to particle energy in the form of thermal heating and possibly also acceleration is well documented (e.g. Priest & Forbes 2000 and references therein). The mechanism occurs when field lines of opposite polarity merges at neutral points where B = 0. In the standard steady state Sweet-Parker model (Sweet 1958; Parker 1958,1963) the rate at which magnetic fields merge in a highly conducting fluid scales as $M_m \propto (R_m)^{-1/2}$ (Priest & Forbes 2000 for a discussion), with R_m the magnetic Reynolds number, which can be very large for perfectly conducting fluids. In terms of the Petschek model (Petschek 1964) the diffusion region of the magnetic field (where the field lines locally approach one another) is much smaller than the global length scale of the field. Merging of field lines are facilitated by shocks, accelerating the fluid from the diffusion region and therefore also accelerating the inflow of the fields of opposing polarity towards one another. This results in the rate of merging to scale according to $M_m \propto (\log(R_m))^{-1}$ (Priest & Forbes 2000 for a discussion). This will dramatically increase the effectivity of reconnection as a mechanism for converting magnetic energy to thermal particle heating and possibly also acceleration.

We argue that magnetic reconnection through the fast Petschek (1964) mechanism as a result of turbulent fluid motions in fragments of the mass transfer flow can be initiated in localized regions within a blob. It can be shown (Parker 1976 for a discussion) that the electric field generated through this process is of the order of

$$E \approx -\frac{c}{4\pi\sigma}\left(\frac{\partial B}{\partial x}\right)_{\circ} \tag{3.14}$$

where $\sigma \approx 3.22 \times 10^6\ T^{3/2}$ esu (Benz 1994) is the Coulomb conductivity of the fluid, and $\left(\frac{\partial B}{\partial x}\right)_{\circ}$ represents the magnetic flux gradient near the neutral point in the reconnection zone. Since the electrical conductivity of astrophysical fluids is very high, the Petschek mechanism is only effective in producing strong electric fields if the magnetic reconnection takes place over a very small scale length in comparison to the dimension of the blob (Petschek 1964; Parker 1976; Priest & Forbes 2000). To convert magnetic field energy through reconnection into relativistic particles, instead of Ohmic heating of gas, reconnection has to occur in regions where the plasma is magnetically dominated instead of gas dominated, i.e. $\beta = (8\ \pi n k_B T\ /\ B^2) < 1$. Therefore, for Petschek reconnection in localized regions in blobs where $\beta \leq 1$ (magnetic knots), satisfying the condition that the reconnection length (l_{rec}) and acceleration length (l_{acc}) should comprise a very small fraction of the initial blob size, e.g. $(\frac{l_{rec}}{r_{\circ}})$ and $(\frac{l_{acc}}{r_{\circ}}) \leq 10^{-2}$, one can show that for initial blob dimensions of the order of

$r_o \approx 10^9$ cm and a typical blob field of $B_{eq} \approx 2300$ G, magnetic reconnection can accelerate charged particles like electrons to energies of the order of (from Eq. 3.14)

$$\varepsilon_e \leq 1.6 \left(\frac{B_{eq}}{2300\,G}\right) \left(\frac{T_b}{10^5\,K}\right)^{-1/2} \left(\frac{l_{rec}}{10^{-2} r_o}\right)^{-1} \left(\frac{l_{acc}}{10^{-2} r_o}\right) \text{MeV} \tag{3.15}$$

Initially, in a highly magnetized $B_{b,i} \approx 2000$ G, dense $N_{p,i} \approx 10^{16}$ cm^{-3} plasma, synchrotron losses of mildly relativistic electrons will be the dominant energy loss mechanism. For sufficient acceleration initially, reconnection must occur on a shorter timescale than the synchrotron loss timescale (Lang 1998) for $\varepsilon_e \sim 1$ MeV electrons, which is

$$t_{s,i} \approx 60 \left(\frac{\gamma}{2}\right)^{-1} \left(\frac{B}{2300\,G}\right)^{-2} \text{sec.} \tag{3.16}$$

Reconnection can typically occur on timescales $\tau_{rec} \approx (l_{rec}/v_i)$ where l_{rec} and v_i represent the length scale of magnetic reconnection and speed at which the field lines approach one another, typically a fraction ($\beta \sim 0.1$) of the Alfvén speed ($v_A = (B/\sqrt{4\pi\rho})$, i.e. $v_i \approx 0.1\ (B/\sqrt{4\pi\rho})$ (Parker 1976; Priest 1981). Since we consider $l_{rec} \approx 10^{-2}\ r_o$, we can see that the reconnection and hence acceleration timescale is approximately

$$\tau_{rec} \approx 20 \left(\frac{l_{rec}}{10^{-2} r_o}\right) \left(\frac{v_i}{0.1\,v_A}\right)^{-1} \text{sec} \tag{3.17}$$

which is significantly shorter than the synchrotron loss timescale.

Phase II: Shock drift acceleration and magnetic pumping

As the battered magnetic blobs are heated and expand, the frozen-in magnetic field of the blob will decrease correspondingly as the blobs grow in size. Magnetic reconnection in regions where $\beta \leq 1$ could have energized a fraction of the blobs' electron population, i.e. the suprathermal tail of the MB distribution in reconnection zones, which can be re-accelerated as the blobs expand. In this phase expansion losses ($t_{exp} \sim r/v_{exp}$) of the blobs take over from synchrotron losses as the dominant energy loss mechanism, i.e.

$$t_s \approx 50 \left(\frac{\gamma}{20}\right)^{-1} \left(\frac{B}{100\,G}\right)^{-2} \text{min} \tag{3.18}$$

$$t_{exp} \approx 30 \left(\frac{r(t)}{4\,a}\right) \left(\frac{v_{exp}}{0.01\,c}\right)^{-1} \text{min} \tag{3.19}$$

where t_{exp} corresponds to a *VLBI* radio measurement (A.E. Niell, personal communication) of a typical expanding synchrotron emitting cloud, expanding with a speed $v_{exp} \sim 0.01$ c until it reaches a size of approximately $\rho = (r/r_o) \rightarrow 400$, corresponding to a size of approximately 4 times

the binary separation (a) of the system (Frank, King & Raine 1992), where the binary separation is approximately

$$a \approx 10^{11} \left(\frac{\mathrm{P}_{orb}}{9.88\,\mathrm{hr}} \right)^{2/3} \mathrm{cm}. \tag{3.20}$$

These relatively slow losses during the expansion phase of the blobs may be instrumental in the net gain of electron energies through the processes described below.

Acceleration of electrons is often observed in astrophysical sites where strong oblique shocks (with respect to magnetic field) are generated in $\beta \leq 1$ plasmas (Benz 1994, Priest & Forbes 2000, Eilek & Hughes 1991). This mechanism, sometimes referred to as shock drift acceleration or the fast Fermi process(see §2.8), is responsible for huge populations of mildly relativistic electrons at interplanetary shocks (Sarris & Krimigis 1985). The maximum energization of particles by this mechanism is caused by the reflection of a particle from a mirror or shock which propagates through a medium at an angle θ with respect to field lines (Holman & Pesses 1983). In the rest frame of a particle on a field line, the shock or mirror approaches with a speed $\mathrm{v}_{\|} = \mathrm{v}_s \sec\theta$, with v_s the shock velocity. A condition for a particle to be reflected from the mirror is if $\mathrm{v}_s \sec\theta < (\mathrm{B}_u/\mathrm{B}_d)\ \mathrm{v}_i$ with B_u, B_d and v_i representing the upstream and downstream magnetic fields and the upstream particle speed respectively. Reflection of thermal and mildly relativistic electrons (Toptyghin 1980) from a mirror point results in a maximum energy transfer per scattering of

$$\frac{\Delta E_{max}}{E_i} = \left(4 \left(\frac{\mathrm{B}_d}{\mathrm{B}_u} \right) - 3 \right) \text{ (thermal)} \tag{3.21}$$

$$\frac{\Delta E_{max}}{E_i} = \left(2 \left(\frac{\mathrm{B}_d}{\mathrm{B}_u} \right) - 1 \right) \text{ (relativistic)} \tag{3.22}$$

Since for strong shocks $(\mathrm{B}_d/\mathrm{B}_u) \rightarrow 4$, this mechanism implies that the energy of thermal and mildly relativistic electrons can be increased respectively by factors of $(\Delta\ \mathrm{E}_{max}/\mathrm{E}_i) \rightarrow 13$ and $(\Delta\ \mathrm{E}_{max}/\mathrm{E}_i) \rightarrow 7$ in a single encounter with a strong shock. This can result in a relatively quick energizing of the electron population that can compete with the energy loss timescales in this phase of the blobs' evolution. Given the short rotation period of the white dwarf ($\mathrm{P}_{rot} \approx 33$ s) and the strong white dwarf field ($\mathrm{B}_{wd} \approx 10^6$ G) it is expected that the fast periodic sweeping of the white dwarf field across blobs can generate intense shocks in the blobs that can result in effective acceleration of particles like electrons in regions where the shocks are collisionless (de Jager 2002, personal communication), i.e. where $\beta \leq 1$ in the blob. One can also see that the rate at which energy is pumped into the expanding blobs(see Eq. 3.13) is sufficient to drive the total observed non-thermal radio to IR emission in AE Aquarii. In particular, because of the sec θ factor, this mechanism can have a profound effect on the effective acceleration of particles with $\mathrm{v}_{u,i} > \mathrm{v}_s$, i.e.

the suprathermal tail of the MB distribution. Shock fronts in the blobs may result in fast repeated scattering of the electron population to energies of the order of $\gamma \leq 20$ for all $\rho \rightarrow 400$.

Additional acceleration mechanisms that may work in tandem with the fast Fermi process in regions where $\beta \leq 1$ in the blob is electron heating through adiabatic compression in a magnetic field and scattering of electrons off Alfvén waves (Parker 1976). Both these processes can in principle be considered as magnetic pumping of electrons. Magnetic pumping of electrons through adiabatic compression is in principle a reversible process but it can be made irreversible by wave turbulence and scattering which may isotropize the pitch angle distribution, resulting in a net acceleration of particles even during expansion. If the shock or magnetic mirror thickness is larger than the gyroradius of the particles, particles penetrating the shock will conserve their magnetic moment, resulting in

$$\frac{\mathrm{p}_{\perp,d}^2}{\mathrm{B}_d} = \frac{\mathrm{p}_{\perp,u}^2}{\mathrm{B}_u}. \tag{3.23}$$

Compression parallel to the field can also occur, resulting in

$$\mathrm{p}_{\parallel,d}\mathrm{L}_d = \mathrm{p}_{\parallel,u}\mathrm{L}_u \tag{3.24}$$

where L represents the longitudinal space in which the particle is confined in the field. Magnetic pumping can also be produced by travelling Alfvén waves in the magnetized plasma. In this process, which is in principle very similar to the processes described above, magnetic disturbances in the magnetic field take on the role of magnetic pumps. Electrons can be accelerated by this mechanism and subsequently scattered in pitch angle by whistler waves. This process will result in an average energy gain by the particles

$$\left(\frac{E(t)}{E_\circ}\right) = \left(\frac{\mathrm{B}_w}{\mathrm{B}_u}\right) \sin^2 \theta_\circ(t_\circ) \tag{3.25}$$

before they tunnel through the magnetic disturbance. In this equation B_w, B_u and $\theta_\circ$ represent the magnitude of the magnetic disturbance in the wave, the upstream unperturbed magnetic field and the initial pitch angle of the particle upstream of the approaching wave, respectively. Maximum gain in energy will occur for $\theta_\circ \rightarrow \pi/2$ and $(\mathrm{B}_w/\mathrm{B}_\circ) \rightarrow 4$. For continued pumping and isotropizing of pitch angles by whistler waves or turbulence in the blobs, the particle population may be sufficiently heated to mildly relativistic energies $\gamma \leq 20$ while the blobs expand.

Since the blobs that are propelled out of the system will be subjected to continuous battering by the propeller, the mechanisms proposed above may all occur simultaneously to pump-up the electron energies to $\gamma \sim 20$ as the blobs expand. In our modelling of the radio outbursts of AE Aquarii the electron energy as a function of $\rho = (\mathrm{r}/\mathrm{r}_\circ)$ approached $\gamma \sim 20$ asymptotically in smaller

increments as $\rho \rightarrow 400$. It can be shown that the electron gyro radii $r_e = 2.4 \times 10^9$ (ε/B) cm (Lang 1998) inside the blobs scale as

$$r_e \approx 1 \left(\frac{\varepsilon}{1\,\mathrm{MeV}}\right)\left(\frac{\mathrm{B}_{eq}}{2300\,\mathrm{G}}\right)^{-1} \mathrm{cm} \quad (\rho \rightarrow 1) \tag{3.26}$$

$$r_e \approx 3 \times 10^5 \left(\frac{\varepsilon}{20\,\mathrm{MeV}}\right)\left(\frac{\mathrm{B}_{eq}}{0.28\,\mathrm{G}}\right)^{-1} \mathrm{cm} \quad (\rho \rightarrow 400) \tag{3.27}$$

clearly showing that for all $\rho = 1 \rightarrow 400$, $r_e \ll r_{blob}$, but for $\rho > 400$ the gyro radius is increasing, reaching sizes $r_e \gg 1$ km which may result in the electron not seeing shocks in the plasma as sharp discontinuities any more and hence limiting the energy increase per interaction. However it will be shown that electron energies of the order of $\gamma = 20$ are more than adequate to simulate the observed non-thermal radio to infra-red fluxes from 1 GHz to 3000 GHz.

3.3.2 The VDL model Parameterization of a single radio blob

The Van der Laan (1963) model gives a parameterization of a single synchrotron flare from an ensemble of electrons.

VDL (1963) gives

$$\mathrm{S}(\nu) = k_1 \mathrm{B}^{-1/2}\theta^2\nu^{5/2} \quad ; [\nu \ll \nu_m] \tag{3.28}$$

and

$$\mathrm{S}(\nu) = k_2 C \mathrm{B}^{(\delta+1)/2}\theta^3\nu^{-(\delta-1)/2} \quad ; [\nu \gg \nu_m] \tag{3.29}$$

where k_1 and k_2 are constants and C is the coefficient in the energy distribution

$$N(E)dE = CE^{-\delta}dE.$$

Here it can be seen that a synchrotron spectrum has distinctive power law indexes associated with the two frequency ranges and a turning point where the flux is a maximum.

The following is also assumed :

$$\begin{aligned} \mathrm{B} &= \mathrm{B}_\circ(r/r_\circ)^{-2} \\ E &= E_\circ(r/r_\circ)^{-1} \quad ; \text{[for a single particle]} \end{aligned}$$

and

$$\theta = \theta_\circ(r/r_\circ)$$

indicating that the magnetic flux is conserved, the gas cools adiabatically and the angular diameter of the source varies with r. The ratio $r/r_\circ$ is also written as ρ.

We know that the source function of synchrotron emission is

$$B_\nu \propto \nu^{5/2}$$

and then the intensity of the source is

$$S_\nu = B_\nu(1 - e^{-\tau_\nu}). \quad \text{(Rybicki \& Lightman 1979)} \tag{3.30}$$

The amount of $B_\nu e^{-\tau_\nu}$ is absorbed along the line of sight in the source.
Thus

$$S_\nu \propto \nu^{5/2}(1 - e^{-\tau_\nu}) \tag{3.31}$$

and then we have

$$S(\nu_m, \rho) \propto \nu_m^{5/2}(1 - e^{-\tau_{\nu_m}}) \tag{3.32}$$

This then gives

$$\begin{aligned} \frac{S(\nu,\rho)}{S(\nu_m,\rho)} &= \left(\frac{\nu}{\nu_m}\right)^{5/2}\left[\frac{1-e^{-\tau_\nu}}{1-e^{-\tau_{\nu_m}}}\right] \\ S(\nu,\rho) &= S_{mo}\rho^{\frac{-(7\delta+3)}{(\delta+4)}}\left[\frac{\nu}{\nu_{mo}\rho^{-(4\delta+6)/(\delta+4)}}\right]^{5/2}\left[\frac{1-e^{-\tau_\nu}}{1-e^{-\tau_{\nu_m}}}\right] \end{aligned}$$

and this reduces to

$$S(\nu,\rho) = S_{mo}\left(\frac{\nu}{\nu_{mo}}\right)^{5/2}\rho^3\left[\frac{1-e^{-\tau_\nu}}{1-e^{-\tau_{\nu_m}}}\right] \tag{3.33}$$

Now the optical depth τ_ν depends on the absorption coefficient k_ν as follows (Pacholzyk 1970)

$$\begin{aligned} \tau_\nu &= \int_0^s k_\nu dl \\ &= \frac{c_s(\delta)sCB^{(\delta+2)/2}}{(2c_1)^{-(\delta+4)/2}}\nu^{-(\delta+4)/2} \end{aligned}$$

and therefore

$$\frac{\tau_\nu}{\tau_{\nu_m}} = \frac{\nu^{-(\delta+4)/2}}{\nu_m^{-(\delta+4)/2}} \tag{3.34}$$

and then also

$$\begin{aligned} \tau_\nu &= \tau_{\nu_m}\left(\frac{\nu}{\nu_m}\right)^{-(\delta+4)/2} \\ &= \tau_{\nu_m}\left(\frac{\nu}{\nu_{mo}}\right)^{-(\delta+4)/2}\rho^{-(2\delta+3)} \end{aligned} \tag{3.35}$$

The optical depth τ_ν, is a measure of the transparency of a blob to its own emitted radiation. For an optically thin source, in other words a source that is transparent to its own radiation, $\tau \leq 1$. For an expanding synchrotron source most of the radiation comes from such optically thin regions.

Therefore the flux density is given by (VDL 1963; BDC 1988)

$$S(\nu,\rho) = S_{mo}\left(\frac{\nu}{\nu_{mo}}\right)^{5/2}\rho^3\frac{1-e^{-\tau_{\nu_m}\left(\frac{\nu}{\nu_{mo}}\right)^{-(\delta+4)/2}\rho^{-(2\delta+3)}}}{1-e^{-\tau_{\nu_m}}} \tag{3.36}$$

where S_{mo} is the maximum flux density at initial time t_o, ν_{mo} is the frequency at this maximum and τ_m is the optical depth at this frequency. The optical depth τ_ν, is frequency dependent but most of the emission is emitted for $\tau_\nu \approx \tau_m \approx 1$.

Now if $\nu \ll \nu_m$: $\frac{\nu}{\nu_{mo}} \to 0$ and the exponential term in the numerator of Eq. 3.36 vanishes. Thus

$$S(\nu,\rho) = S(\nu)\rho^3 \qquad [\nu \ll \nu_m] \tag{3.37}$$

Then if $\nu \gg \nu_m$ or $\nu \gg \nu_{mo}$:

$$\tau_m(\nu/\nu_{mo})^{-(\delta+4)/2}\rho^{-(2\delta+3)}$$

becomes small and thus we can use $e^x = 1+x$ for small x.

Therefore

$$\begin{aligned} S(\nu,\rho) &= S_{mo}\rho^3\frac{\tau_m(\nu/\nu_{mo})^{-(\delta+4)/2}\rho^{-(2\delta+3)}}{1-exp(-\tau_m)} \\ &= S(\nu)\rho^{-2\delta} \quad ; [\nu \gg \nu_m] \end{aligned} \tag{3.38}$$

VDL(1963) gives the relation of the radius to the expansion time as

$$\rho = \left(1+\frac{tv_o}{\beta r_o}\right)^\beta \tag{3.39}$$

with v_o the initial velocity of expansion and β a constant dependent on the medium the cloud is expanding into ($\beta = 1$ for constant expansion velocity, $\beta = 2/5$, asymptotically, in a uniform medium and $\beta = 2/3$, asymptotically, into a stellar wind (Woodsworth & Hughes 1976)).

Now initially (for small t) we have that

$$\rho \approx \left(1+\frac{(t=0)v_o}{\beta r_o}\right)^\beta + \beta\left(1+\frac{(t=0)v_o}{\beta r_o}\right)^{\beta-1}\frac{v_o}{\beta r_o}t$$

and thus

$$\rho \propto t \quad \Rightarrow \quad \rho^3 \propto t^3$$

Also at later times (large t) :

$$\rho \approx \left(\frac{tv_o}{\beta r_o}\right)^{\beta} \quad \Rightarrow \quad \rho \propto t^{\beta}$$

and thus $\rho^{-2\delta} \propto t^{-2\beta\delta}$.

Therefore we see that the flux density for a frequency $\nu < \nu_{mo}$, initially increases approximately like $\rho^3 \propto t^3$ to reach a maximum when $\tau_\nu = \tau_m \approx 1$.
After this the flux diminishes like $\rho^{-2\delta} \propto t^{-2\beta\delta}$ in an optically thin medium.

The time evolution of such a synchrotron source (not considered in this thesis) will be important in modelling the 'real' evolution of the emission from a blob-like source with time. Such an evolution could then be compared to the observed temporal evolution at specific frequencies.

The frequency ν_m depends on radius as

$$\nu_m(\rho) = \nu_{mo}\rho^{-(4\delta+6)/(\delta+4)}. \tag{3.40}$$

This means that $\nu_m \leq \nu_{mo}$.

Eq. 3.38 and Eq. 3.40 also gives :

$$\begin{aligned} \mathrm{S}(\nu = \nu_m, \rho) &= \mathrm{S_o}(\nu = \nu_m)\rho^{-2\delta} \\ &= k_1 C \mathrm{B_o}^{(\delta+1)/2}\theta_o^3 \nu_m^{-(\delta-1)/2}\rho^{-2\delta} \\ &= k_1 C \mathrm{B_o}^{(\delta+1)/2}\theta_o^3 [\nu_{mo}\rho^{-(4\delta+6)/(\delta+4)}]^{-(\delta-1)/2}\rho^{-2\delta} \\ &= \mathrm{S_o}(\nu = \nu_{mo})\rho^{\frac{-(7\delta+3)}{(\delta+4)}} \end{aligned} \tag{3.41}$$

The frequency of the maximum flux is given by (Dulk 1985) as

$$\nu_{mo} \approx 2.8 \times 10^7 \left(\frac{\mathrm{E_c}}{1\mathrm{MeV}}\right)^{(2\delta-2)/(\delta+4)} \left(\frac{\delta-1}{\delta+2}\mathrm{N_o}r_{11}\right)^{2/(\delta+4)} \mathrm{B_o}^{(\delta+2)/(\delta+4)} \tag{3.42}$$

An average value of $<\theta> = 60°$ is assumed for the angle between the magnetic field and the line of sight. Define the source radius as r_{ν_m}. Then from Eq. 3.40 we have

$$r_{\nu_m} = r_o \left(\frac{\nu_m}{\nu_{mo}}\right)^{-(\delta+4)/(4\delta+6)} \tag{3.43}$$

The initial parameters of a synchrotron blob is taken as r_o, $\mathrm{B_o}$ and $\mathrm{N_o}$.
ν_{mo} can therefore be calculated from Eq. 3.42 for assumed values of $\mathrm{E_c}$, δ and $\mathrm{N_o}$.

The brightness temperature of the source is expressed as

$$\mathrm{T}_B = \frac{\mathrm{S}_\nu \mathrm{c}^2 D^2}{2\mathrm{k}\nu^2 \pi r_s^2}. \tag{3.44}$$

πr_s^2 is the projected source area, D is the distance to the source and k is Boltzmann's constant.

Now we get

$$S_{\nu_m} = 2kT_B \frac{\nu_m^2}{c^2} \frac{\pi r_{\nu_m}^2}{D^2} \tag{3.45}$$

We consider the case $\tau_\nu \approx 1$ and then $T_B \approx T_{eff}$.

Then this gives (Dulk 1985)

$$T_{eff} \approx 2.8 \times 10^9 \times 2^{-\delta/2} \left(\frac{\nu}{\nu_B}\right)^{1/2}. \tag{3.46}$$

$\nu_B = eB/2\pi m_e c$ is the gyrofrequency.

The maximum flux density (zero expansion, $\rho = 1$) can be estimated from Dulk (1985), which is summarized in Bastian, Dulk & Chanmugam (1988).

For single flare events we have

$$S_{m,o} = A_1 \left[A_2 \frac{\delta - 1}{\delta + 2} \left(\frac{E_c}{1\,\mathrm{MeV}}\right)^{\delta-1} N_o\right]^{3/(2\delta+3)} \left[r_o^{(4\delta+9)/3} B_o^{(\delta+3)/6}\right]^{3/(2\delta+3)} \nu_m^{(7\delta+3)/(4\delta+6)} \tag{3.47}$$

with $A_1 = 3.3 \times 10^6 \times 2^{-\delta/2} \pi k/c^2 D^2$, $A_2 = (2.8 \times 10^7)^{(\delta+4)/2}/10^{11}$ and

$$N_o = A_3 \left[\frac{\delta + 2}{\delta - 1} \left(\frac{E_c}{1\,\mathrm{MeV}}\right)^{-(\delta-1)} \frac{B_o^{2\delta+9}}{r_o}\right]^{1/(\delta+5)} \tag{3.48}$$

where N_o represents the electron number density assuming equipartition between the magnetic and relativistic electron energy densities or

$$\frac{B_o^2}{8\pi} = N_o k T_{eff}.$$

The constant A_3 above is $A_3 = [3.2 \times 10^4 \times 2^{\delta/2} (10^{11})^{1/(\delta+4)}]^{(\delta+4)/(\delta+5)}$.

By substituting Eq. 3.42, Eq. 3.47 and Eq. 3.48 into Eq. 3.36, the expected flux densities of individual flare events can be calculated.

Chapter 4

Modelling of the radio-to-IR outbursts

The radio emission of AE Aqr consists of nearly continuous (random) outbursts or flares superimposed on a weak quiescent flux level. The simulation of individual flares was not attempted here. Instead, the emphasis of this study was on an attempt to construct a theoretical framework to explain the flare-like and quiescent non-thermal emission of AE Aqr in terms of the propeller ejected outflow of diamagnetic blobs from the system. In terms of the model proposed, the flare-like emission is the result of an expanding magnetized synchrotron emitting clouds, i.e. a VDL description (§3.3.2). These clouds are activated by the interaction with the MHD propeller and the emission is superimposed on the non-thermal emission of a diffuse remnant surrounding the system. The remnant is believed to be the result of the confluence of expanded blobs leaving the system. It will be shown that the diffuse remnant can account for the quiescent emission in the low frequency (few GHz) range of the radio observations (BDC 1988, Abada-Simon et al.1999, 2002). Furthermore, the superposition of expanding synchrotron sources in different phases of their evolution could provide a natural platform explaining the self-absorbed spectrum from radio to IR frequencies. Within this framework the turning point of the spectrum, i.e. changing from optically thick to optically thin, could be constrained.

The model of the synchrotron emission from individual blobs in the superposition is dependent on the embedded magnetic fields and the electron energies. In the VDL model the B-field falls like $1/r^2$ with expansion. As an illustration the evolution of the flux density of a single blob as a function of $\rho = (r/r_o)$ for initial parameters $B_o = 2000$ G and peak electron energy $\varepsilon_e = 1$ MeV is presented in Figure 22a. In this scenario the electron energy diminishes with increasing ρ as a result of adiabatic expansion.

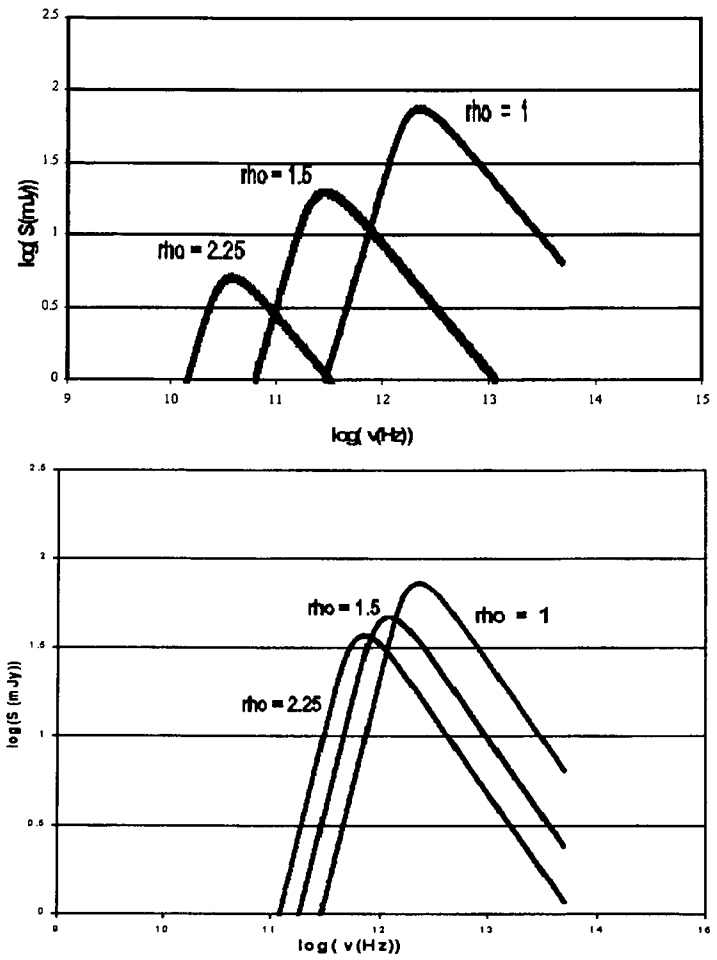

Figure 22a: The evolution of the flux density (mJy) of a single blob as a function of $\rho = (r/r_o)$ for initial parameters $B_o = 2000$ G and peak electron energy $\varepsilon_e = 1$ MeV. In this scenario the electron energy diminishes with increasing ρ as a result of adiabatic losses.

Figure 22b: The evolution of the flux density (mJy) as a function of $\rho = (r/r_o)$ for initial parameters $B_o = 2000$ G and peak electron energy of $\varepsilon_e = 1$ MeV which was kept constant as the blob expanded. This represents an electron population which is continually energized as the blob is battered by the mhd propeller.

Here it can be seen how the flux density diminishes with expansion and the turning point moves to lower frequencies. The flux levels from these blobs drop too fast and this would mean a lot of blobs (> 100) would have to be included to simulate the observed flux levels. The aim of this model was to explain the radio emission with the least amount of blobs, since it is believed that only a small fraction of the ejected blobs may in fact be magnetized. As an alternative, in this model it is assumed that the field is highly tangled and can be estimated from the equipartition value with the particle energy density (E = 3/2NkT). This means that the field will diminish like $1/r^{3/2}$ (H. Spruit 2002, pers. comm.) in the simulations, instead of $1/r^2$. The blobs in the simulations were seen as thermodynamic systems doing work on an external environment wile being activated by a 'heat source'(the MHD propeller interaction between the magnetosphere and the blob). Therefore the proposed model in the thesis is therefore an adapted Van der Laan process, i.e. relying on continued re-acceleration of the non-thermal particle population in the blob as a result of the battering by the magnetosphere and an equipartition frozen-in chaotic and twisted magnetic field inside gas blobs. As an illustration of this effect the evolution of the flux density as a function of ρ for initial parameters B_o = 2000 G and peak electron energy of ε_e = 1 MeV which was kept constant as the blob expanded. This represents an electron population which is continually energized as the blob is battered by the mhd propeller (see Figure 22b). From Fig. 22b it can be seen how the emission from an expanding blob is sustained by continuous acceleration and a slower decaying equipartition magnetic field in the expanding blobs. This is a very positive result, since in our modelling of the radio flares the total integrated radio flux over all frequencies was simulated with a comparatively small fraction (less than 30 %) of the total mass outflow from the system being in the form of strongly magnetized ($B_o \geq$ 2000 G) synchrotron emitting blobs.

To simulate the observed radio spectrum (Abada-Simon et al. 1999,2002), two trial cases were considered depending on the initial magnetic fields of 2000 G and 3000 G respectively. In both cases a small number ($\leq$ 20) were sufficient to account for the total radio-to-IR flux from AE Aqr. The step length in terms of the expansion was kept constant for simplicity. The flux density was calculated (see §3.3.2) for a 'freshly'magnetized blob with $r_o = 10^9$ cm. For each new r (or ρ) (due to the expansion), N_o and ν_m was calculated using chosen parameters. The choice of the parameters, specifically E_c and δ, was done in order to get a reasonable fit to the average spectrum. The emission from each individual blob was integrated with the other blobs' emission over a broad frequency range taking into account the absorption of radio intensity below the plasma frequency in each blob. Electromagnetic radiation is absorbed for all frequencies below $\nu_p = 9 \times 10^3 n_e^{1/2}$ with $n_e(\mathrm{cm}^{-3})$ the electron density. The calculated flux density was put equal to zero for frequencies

below the plasma frequency.

The scenario sketched above to explain the average radio-to-IR spectrum can be quantitatively represented by a range of parameter combinations. This is demonstrated by the simulated spectra in Figures 24 and 25a. The first spectrum was obtained by integrating the flux from 16 blobs at different stages of expansion and an initial frozen in field of 2000 G. The second spectrum (Fig. 25a) is from only 10 blobs with an initial field of 3000 G. The trend of the parameters used in the two simulations can be seen in Table 3. The increase of the electron energy E_c, was done at a decreasing rate with expansion as the acceleration mechanisms become less effective.This is visualized in Fig. 23.

B_o = 2000 G			B_o = 3000 G		
ρ	E_c(MeV)	δ	ρ	E_c(MeV)	δ
1	1	2.8	1	1	3.2
1.5	1	2.8	1.95	1	3.2
2.25	1	2.8	4	1	3.0
3.4	2	2.75	7	1.5	3.0
5	2	2.75	14	2	2.8
8	3	2.75	28	2.6	2.8
11	3	2.7	55	2.6	2.6
17	4	2.7	100	4	2.2
25	4	2.65	210	5.5	2.2
38	5.5	2.65	400	7	2.0
58	5.5	2.65			
87	8	2.65			
130	8	2.6			
195	11	2.6			
292	13	2.6			
400	15	2.6			

Table 3. This table contains the parameter values used in simulating the average radio spectrum of AE Aquarii.

The spectrum simulated in this model, by changing the parameters on a trial-and-error basis, is presented in Figure 24 with the observed averages from Abada-Simon et al. (1999,2002) (see §1.3.2). It can be seen how the plasma frequency (calculated for each blob individually) cuts up the spectrum as the optical depth gradually increases for blobs in a more advanced stage of expansion,

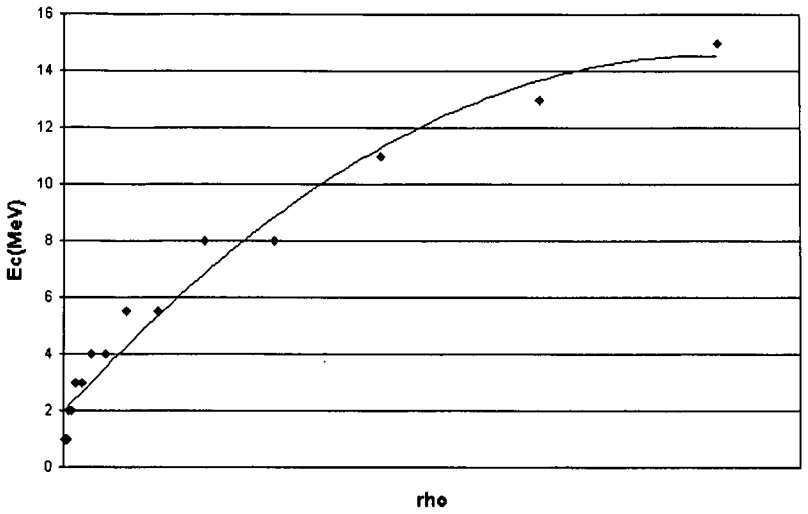

Figure 23 : The electron energies (E_c) in the simulations were increased at a declining rate with expansion of a blob and asymptotically approaches a maximum. (The fitted curve only aids the eye.)

resulting in a gradual shift in the observable integrated flux towards lower frequencies. The lower frequency emission therefore comes from older blobs, i.e. blobs that are in an advanced stage of their evolution. The turning point is expected to vary and not all of the spectrum, especially the high frequency end, will be visible at all times since the peak flux is dominated by the emission from blobs in the initial stages of their evolution, which changes upon expansion as the peak observable flux migrates to the lower frequency regime in terms of the VDL description (see Figure 22). An important result of the model is that variable non-thermal emission in the frequency region ν = (0.3-3.0) $\times$ 10^{13} Hz at the 10-160 mJy level (below *IRAS* sensitivity limit) is predicted (see Figure 22b and Figure 24a). This frequency range is below the IR frequencies ($\nu \sim 3 \times 10^{14}$ Hz) dominated by the thermal black body spectrum of the secondary star.

The chosen parameters for the blobs all lie in non-extreme ranges. The attractive feature of this model is that it links the non-thermal outbursts in the system with the propeller outflow of magnetized gas blobs from the system which is also connected to optical outbursts in terms of blobs that cool radiatively as they expand.

However, significantly less non-thermal ($\leq$ 20) than thermal (30-60) blobs are required at any given time in the system to account for the observed spectrum. Therefore a one-to-one correlation between radio and optical flares is not predicted, although both originate in the propeller driven mass outflow.

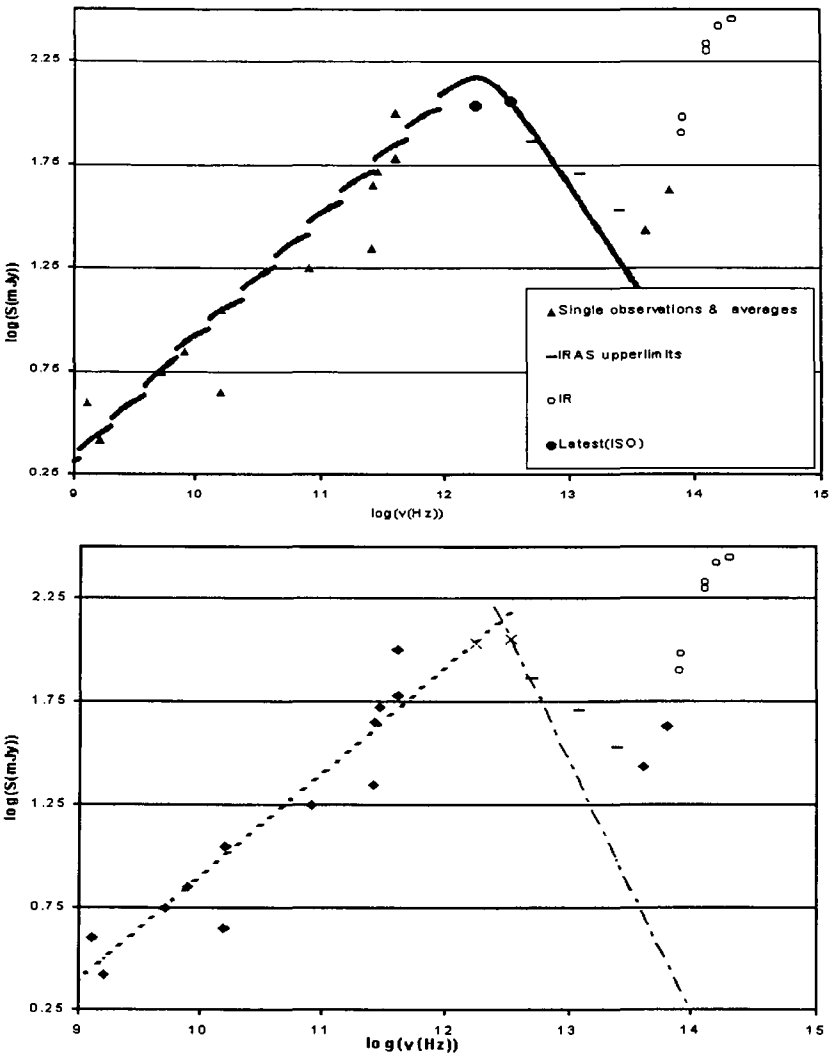

Figure 24a: The simulated radio to IR spectrum representing the total integrated flux from approximately 20, initially highly magnetic, synchrotron emitting blobs in different stages of their evolution. The spectrum represents the total integrated flux above the plasma frequency in each blob. Also indicated in this figure are time averaged radio measurements, reported by Abada-Simon et al. (1999,2002). It can be seen that the latest detection at 3333 GHz, according to our model, corresponds to emission after the turning point of the spectrum, i.e. where the blobs are optically thin.

Figure 24b: The spectrum shown in this figure represents a fit to the radio measurements, adapted form Abada-Simon et al. (1999). This fit represents a typical self absorbed spectrum, which is reconcilable with the fact that the radio outbursts are a superposition of several synchrotron emitting blobs in different stages of expansion.

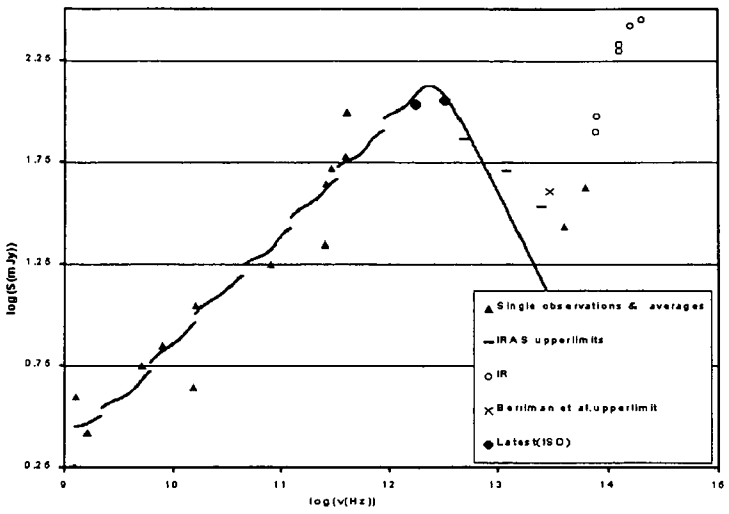

Figure 25a : Simulated spectrum from 10 blobs with $B_o = 3000$ G. The spectrum illustrates another valid parameterization of the model for the radio emission of AE Aqr.

The lower frequency end of the spectrum ($\leq$ 10 GHz) of the simulated VDL spectrum is superimposed on the quiescent flux of a remnant of magnetized gas (expanded magnetized blobs) as a result of the confluence of the blobs at late stages of expansion. The flux density expected from this optically thin synchrotron source is given by (Lang 1998)

$$S(\nu) = 0.933 \times 10^{-23} \alpha(\delta) C.l.B^{(\delta+1)/2} \left(\frac{6.26 \times 10^{18}}{\nu}\right)^{(\delta-1)/2} \left(\frac{\pi r_s^2}{D^2}\right) \text{erg s}^{-1}\text{cm}^{-2}\text{Hz}^{-1} \qquad (4.1)$$

where C is the constant in the electron energy distribution (par. 3.1) and l is the dimension of the source along the line of sight. The parameter $\alpha(\delta)$ is a slowly varying function of δ and of order unity. The parameters for this optically thin source were chosen for blobs that had expanded to ρ = 700–1000 to obtain estimates of the density and the magnetic field present at $\rho > 500$. The density of relativistic electrons was taken as ~ 0.01 cm^{-3} and energies of 1–5 MeV for $\delta = 3$ was sufficient to boost the low frequency end of the spectrum above the Razin frequency ν_R, for the assumed parameters. The flux calculated from Eq. 4.1 is highly dependent on the value of E_c and is not well constrained. The spectrum calculated for this quiescent ring is shown in Fig. 25b. The two simulated spectra(Fig. 24a and 25a) includes this background radiation, contributing only in frequencies around a few GHz.

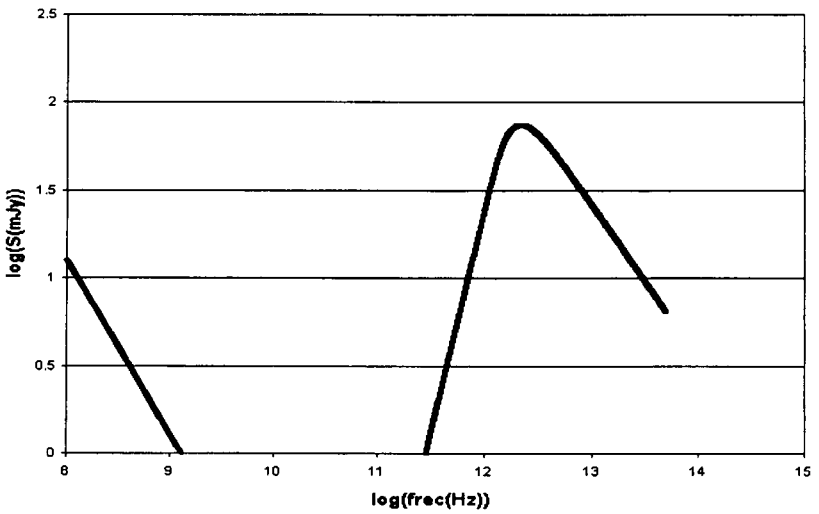

Figure 25b : The simulated spectra was superimposed on a quiescent emission level from a remnant-like ring around the system. The contribution of the remnant is only in the low GHz frequency range. It is compared here to the single blob spectrum from a young blob (compare also Fig. 22a).

Chapter 5

Conclusions

It is proposed that the observed radio spectrum which represents a self absorbed $S_\nu \propto v^\alpha$ power law is a superposition of several (≤ 20) expanding, strongly magnetized ($\beta \leq 1$) blobs in different stages of their evolution. The model assumes that blobs possessing highly disordered tangled magnetic fields with strengths up to $B_o \approx 2000$ G may be present among those leaving the L1 region. These blobs are then propelled out of the system by the propeller mechanism. The estimate for the blob magnetic fields is obtained from an estimate of the angular momentum losses through magnetic braking as a result of an ordinary Mestel & Spruit (1987) stellar wind, which allows an estimate of the coronal base surface field strength of the secondary star.

Turbulence in the mass transfer process from the secondary star in the initial phase of mass transfer, as well as the interaction between the blob and the propeller may excite turbulent fluid motions in the blob that may induce fast Petschek type magnetic reconnection with associated heating of electrons to energies of the order of $\varepsilon_e \approx$ 1-2 MeV. In this initial phase, synchrotron losses dominate expansion losses in the blobs. However, it was shown that reconnection can occur on time scales that are shorter than the synchrotron loss time scales on length scales of the order of $l \sim 10^{-2}\ r_o$, where $r_o \approx 10^9$ cm is assumed to be the initial blob size. As the blobs expand the synchrotron loss timescale increases significantly to timescales of the order of 30 - 60 minutes. Continuous interaction between the propeller and the blobs up to $\rho = (r/r_o) \approx 400$ may excite shocks in the magnetized plasma, resulting in continuous acceleration in blobs with $\beta \leq 1$ via mechanisms like shock drift acceleration (fast Fermi process), adiabatic compression and scattering from Alfvén waves. These acceleration mechanisms rely on the magnetic intensity for confining particles in the acceleration site.

A radio spectrum from the model is a superposition of several ($\leq$ 20) (gyro-)synchrotron emitting bubbles (Van der Laan mechanism) in different stages of expansion from $\rho = 1$ - 400, containing electron populations with energies between $\gamma \approx 2$ ($\rho = 1$) and $\gamma \approx 20$ ($\rho \approx 400$). Expanding blobs with dimensions corresponding to $\rho = 400$ have been observed at GHz frequencies during a VLBI observation of AE Aquarii's close surroundings (A.E. Niell, personal communication). The spectrum follows a self absorbed power law $S_\nu = S_o\ \nu^\alpha$, with $S_o \approx 1.9$ and $\alpha \approx 0.6$, very similar to the values reported by Abada-Simon et al. (2002). From Figure 23 it can be seen that the latest 5 sigma detection reported by Abada-Simon et al. (2002) already lies on the optically thin part of the radio spectrum and that the model excludes the possibility of detection by *IRAS* due to its sensitivity. The detectability of AE Aquarii as a strong variable radio source may depend on the magnetic field strength of the blobs, which in turn may depend on the magnetic cycle of the secondary K4-5 star. Continuous long term monitoring of AE Aquarii may provide a means to determine the magnetic cycle of the secondary star of AE Aquarii, which in turn may provide answers as to the behaviour of magnetic activity in other short period binaries.

A realistic model ?

The modelling of the radio-IR outbursts or varying emission in these frequency ranges by the superposition of synchrotron clouds in an adapted VDL scenario, relying on continuous acceleration, is a new approach. The results are encouraging since relatively good agreement is found with the average observed spectrum from AE Aquarii. The parameters used to simulate the emission from a single blob are also not extreme, for example electron energies between 1-15 MeV are quite moderate.

Furthermore, the blob scenario with integration of the emission from different blobs, leave room for a qualitative explanation of the variability of the observed emission. The blob parameters may also be highly variable. The magnetic fields of the blobs are dependent on the supply by the red dwarf's dynamo and the flow of blobs is also determined by instabilities in the flow from the red dwarf and the interaction with the magnetic propeller. The acceleration of electrons and their continued re-acceleration depend on the complicated interaction of the mass flow, the propeller and shocks created in the blobs in the ejection process. The resulting energy distribution of the particles in the blobs can therefore vary substantially in different blobs as well as over time. This means that the highly variable emission that fluctuates around a longer term average can be understood within the proposed model.

A possible next step is to model the detailed evolution of the emission from a synchrotron blob with expansion. This would also require including a detailed investigation of the plasma emission and absorption in blobs as well as the interaction of all the competing processes in the source itself. All aspects must then be combined with a time dependence built into each. The system should then also be observed with better time and spatial resolution to get a clearer picture of the time evolution from the youngest to the oldest radio blobs. The highest flux density is expected from the youngest blobs and then in the IR-(far)IR frequency range. Modelling and observations of the emission in this range will thus potentially be most illuminating in the continuing focus on AE Aquarii.

.ooOoo.

Appendix A

Synchrotron radiation

(Rybicki & Lightman 1979)

A.1 Total emitted power

Synchrotron radiation concerns the motion of a charged particle in a magnetic field. Motion of a charge q, relative to a magnetic field induces the Lorentz force.

$$F^{\mu} = \mathrm{q/c} F^{\mu}_{\nu} U^{\nu} \tag{A.1}$$

with F^{μ} the Lorentz four-force and F^{μ}_{ν} the electromagnetic fields in the field tensor. U^{μ} is the four-velocity. The components of the equation give

$$\begin{aligned} 1)\, F^{\circ} &= \mathrm{q/c} F^{\circ}_{\nu} U^{\nu} \\ 2)\, F^{i} &= \mathrm{q/c} F^{i}_{\nu} U^{\nu}. \end{aligned} \tag{A.2}$$

This then gives 1)

$$\begin{aligned} F^{\circ} &= \frac{d\mathrm{P}^{\circ}}{d\tau} = \gamma \mathrm{q/c} \bar{E}.\bar{v} \\ \frac{1}{\gamma}\frac{d}{d\tau}[\gamma \mathrm{mc}] &= \mathrm{q/c} \bar{E}.\bar{v} \\ \frac{d\tau}{dt}\frac{d}{d\tau}[\gamma \mathrm{mc}^2] &= \mathrm{q} \bar{E}.\bar{v} \\ \text{therefore } \frac{d}{dt}[\gamma \mathrm{mc}^2] &= \mathrm{q} \bar{E}.\bar{v} \end{aligned} \tag{A.3}$$

Consider $\bar{E} = 0$, then

$$\frac{d}{dt}[\gamma \mathrm{mc}^2] = \mathrm{q} \bar{E}.\bar{v} = 0 \tag{A.4}$$

Also, 2) $F^i = \frac{dP^i}{d\tau} = \mathrm{q/c}F^i_\nu U^\nu$ which gives

$$\begin{aligned}\bar{F} &= \frac{d\bar{\mathrm{P}}}{d\tau} = \mathrm{q/c}\gamma[\bar{E} + (\bar{v} \times \bar{\mathrm{B}})] \\ &= \mathrm{q/c}\gamma(\bar{v} \times \bar{\mathrm{B}}) \ldots\ldots\ldots\ldots\ldots\ldots\ldots\ldots (\bar{E} = 0)\end{aligned}$$

Then

$$\begin{aligned}\frac{1}{\gamma}\frac{d\bar{\mathrm{P}}}{d\tau} &= \mathrm{q/c}(\bar{v} \times \bar{\mathrm{B}}) \\ \frac{d\tau}{dt}\frac{d\bar{\mathrm{P}}}{d\tau} &= \frac{d(\gamma m\bar{v})}{dt} = \mathrm{q/c}(\bar{v} \times \bar{\mathrm{B}}) \\ &\text{thus} \\ \frac{d}{dt}(\gamma m\bar{v}) &= \mathrm{q/c}(\bar{v} \times \bar{\mathrm{B}}) \qquad (A.5)\end{aligned}$$

Now $\frac{d}{dt}[\gamma \mathrm{mc}^2] = \mathrm{q}\bar{E}.\bar{v} = 0$ (eq. A.4) implies that γ is constant which in turn implies that the magnitude, $|\bar{v}|$ is constant. Therefore

$$\gamma \mathrm{m}\frac{d\bar{v}}{dt} = \mathrm{q}(\bar{v} \times \bar{\mathrm{B}}) \qquad (A.6)$$

This gives components of $\bar{v}_\parallel$, along the B-field and $\bar{v}_\perp$ perpendicular to the field with

$$\begin{aligned}\mathrm{m}\gamma(\frac{d\bar{v}_\parallel}{dt} + \frac{d\bar{v}_\perp}{dt}) &= \mathrm{q/c}[(\bar{v}_\parallel + \bar{v}_\perp) \times \bar{\mathrm{B}}] \\ 1) \ldots\ldots\ldots \mathrm{m}\gamma\frac{d\bar{v}_\parallel}{dt} &= \mathrm{q/c}(\bar{v}_\parallel \times \bar{\mathrm{B}}) \\ &= \mathrm{q/c}v_\parallel \mathrm{B}\sin\theta = 0 \ldots\ldots\ldots\ldots (\theta = 0) \\ &\text{and} \\ 2) \ldots\ldots\ldots \mathrm{m}\gamma\frac{\bar{v}_\perp}{dt} &= \mathrm{q/c}(\bar{v}_\perp \times \bar{\mathrm{B}}). \qquad (A.7)\end{aligned}$$

Eq.1 now implies that $v_\parallel$ is constant and since $|\bar{v}|$ is constant, $|v_\perp|$ must be constant as well. Uniform circular motion is characterized by acceleration normal to the velocity and of constant magnitude. The motion of the charge q, then is a combination of such a circular motion and a motion along the field. This results in a helical motion with a frequency of rotation or gyration (the Larmor frequency) of

$$\omega_B = \frac{\mathrm{qB}}{\gamma \mathrm{mc}}.$$

From Eq. 2 we find

$$\begin{aligned}\mathrm{m}\gamma\frac{d\bar{v}_\perp}{dt} &= \mathrm{q/c}(v_\perp \bar{\mathrm{B}}\sin\theta) \\ (\mathrm{m}\gamma\frac{d\bar{v}_\perp}{dt})\mathrm{max} &= \mathrm{q/c}(v_\perp \mathrm{B}) \ldots\ldots (\theta = 90^\circ)\end{aligned}$$

therefore

$$\omega_B = \left| \frac{(\frac{d\bar{v}_\perp}{dt})}{v_\perp} \right| = \frac{qB}{\gamma mc}(s^{-1}) \qquad (A.8)$$

The acceleration is directed to the centre of the circle that is the projection of the helical path onto a flat surface. This acceleration has a magnitude of

$$a_\perp = v_\perp \omega_B = v_\perp \frac{qB}{m\gamma c}$$

The total emitted radiation is then [Eq. 4.92 Rybicki & Lightman(R & L)]

$$\begin{aligned} P &= \frac{2q^2}{3c^3}\gamma^4(a_\perp^2 + \gamma^2 a_\parallel^2) \\ &= \frac{2q^2}{3c^3}\gamma^4 \frac{q^2B^2}{m^2\gamma^2c^2}v_\perp^2 \end{aligned}$$

or

$$\begin{aligned} P &= \frac{2q^4\gamma^2B^2}{3c^3m^2}(\frac{v_\perp}{c})^2 \\ &= \frac{2}{3}\left(\frac{q^4c}{m^2c^4}\right)\beta_\perp\gamma^2B^2 \quad .....(\beta_\perp = \frac{v_\perp}{c}) \\ &= \frac{2}{3}r_\circ^2 c\beta_\perp^2\gamma^2B^2 \quad ..... \quad r_\circ^2 = b_{min}^2 = \frac{q^4c}{m^2c^4}. \end{aligned} \qquad (A.9)$$

The parameter $r_\circ$ gives an idea of the size of a point charge and is known as the classical electron radius in the case of electrons. The parameter b_{min} is the minimum value of the so called impact parameter for a charge, in this case an electron. It indicates the perpendicular distance from the electron to the original path of the electron it had impacted upon.

The total radiation from an ensemble of particles now depends on the velocities present. An isotropic distribution in velocities may be assumed for a given speed β. The formula is therefore averaged over all angles. Let α be the pitch angle, i.e. the angle between the field and the velocity. Figure 25 shows this relationship.

Now we get $v_\perp = v\sin\alpha$ and $\beta_\perp = \frac{v_\perp}{c} = \beta\sin\alpha$.
Furthermore $< \beta_\perp^2 > = \beta^2 < \sin^2\alpha >$. .... β - constant

$$\begin{aligned} < \sin^2\alpha > &= \frac{\int \sin^2\alpha \, d\Omega}{\int d\Omega} \\ &= \frac{\int_0^{2\pi}\int_0^{\pi} \sin^2\alpha \sin\alpha \, d\alpha \, d\phi}{\int_0^{2\pi}\int_0^{\pi} \sin\alpha \, d\alpha \, d\phi} \\ &= 2/3 \end{aligned}$$

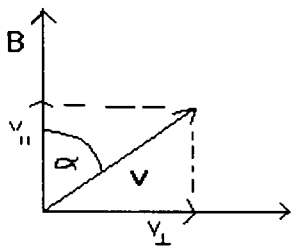

Figure 25

Therefore

$$< \beta_{\perp}^2 >= \frac{2}{3}\beta^2$$

and

$$\begin{aligned} < \mathrm{P} > &= \frac{2}{3} r_{\circ}^2 c < \beta_{\perp}^2 > \gamma^2 \mathrm{B}^2 \\ &= (\frac{2}{3})^2 r_{\circ}^2 c \beta^2 \gamma^2 \mathrm{B}^2. \end{aligned} \tag{A.10}$$

This may also be written as

$$\begin{aligned} \mathrm{P} &= \frac{4}{9} r_{\circ}^2 \beta^2 \gamma^2 \frac{\mathrm{B}^2}{8\pi} 8\pi \\ &= \frac{4}{3} \sigma_T c \beta^2 \gamma^2 \mathrm{U}_B \end{aligned} \tag{A.11}$$

where $\mathrm{U}_B = \frac{\mathrm{B}^2}{8\pi}$ is the magnetic energy density and $\sigma_T = \frac{8\pi}{3} r_{\circ}^2$ is the Thomson cross-section.

A.2 The spectrum

The power radiated by a synchrotron source is frequency dependent and therefore a spectrum of a specific source can give valuable information regarding the source parameters.

The spectrum that is observed is dependent on the time variation of the orientation of the electric field with respect to the observer. The magnetic field mimics the electric field and can therefore be ignored in the discussion of the spectrum. The velocities of the particles are relativistic and therefore beaming effects are important. Beaming causes the emitted radiation field to appear directionally concentrated about the particle's velocity. The velocity and acceleration are perpendicular and thus Figure 26 is applicable to show the beaming effect. This narrow beam causes the duration of a pulse of radiation from a particle to be shorter than the gyration period, $\frac{2\pi}{\omega_B}$. This means that radiation will be present at higher frequencies than, ω_B in the spectrum.

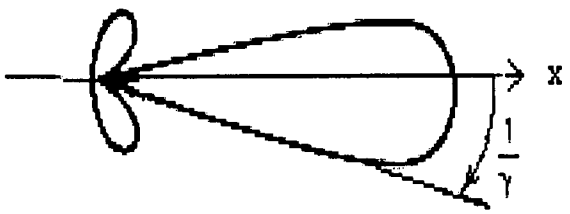

Figure 26 : The angular distribution of radiation from a particle with $a_\perp \perp v$.
(Rybicki & Lightman)

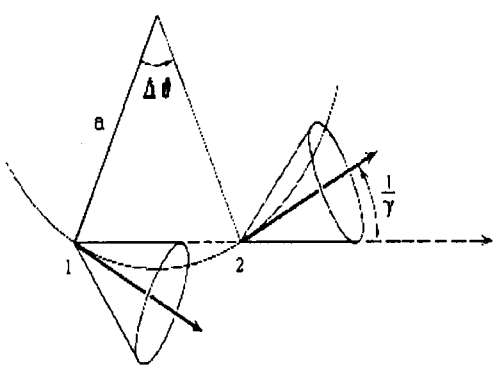

Figure 27 : The emission from a single particle traces out a cone as it circles a B-field line.
(Rybicki & Lightman)

Figure 27 shows the scenario for a single particle. The characteristic angle for beaming from highly relativistic particles is $\sim 1/\gamma$ and thus a cone results within which the radiation is visible, i.e. a pulse is registered in the time it takes to move from position 1 to position 2. The distance Δs along the path is related to the radius of curvature of the path, $a = \frac{\Delta s}{\Delta \theta}$. We have $\Delta\theta = 2 \times \frac{1}{\gamma}$ and thus

$$\Delta s = a(2/\gamma).$$

The radius of curvature can be calculated from the equation of motion

$$\gamma \mathrm{m} \frac{\Delta \bar{v}}{\Delta t} = \frac{\mathrm{q}}{\mathrm{c}} \bar{v} \times \bar{\mathrm{B}}. \tag{A.12}$$

Also $|\Delta v| = \mathrm{v}\Delta\theta$ and $\Delta \mathrm{s} = \mathrm{v}\Delta \mathrm{t}$ to give

$$\frac{\Delta\theta}{\Delta s} = \frac{(\frac{|\Delta \bar{v}|}{v})}{v\Delta t}$$

Now we have

$$\begin{aligned} |\bar{v}| &= \frac{\mathrm{qvB}\sin\alpha}{\gamma \mathrm{mc}} \Delta t \\ \text{and} & \\ \frac{\Delta\theta}{\Delta s} &= \frac{|\Delta \bar{v}|}{v^2 \Delta t} \\ &= \frac{\mathrm{qB}\sin\alpha}{\gamma \mathrm{mcv}} \end{aligned} \tag{A.13}$$

but

$$\begin{aligned} \omega_B &= \frac{\mathrm{qB}}{\gamma \mathrm{mc}} \quad \text{.....thus} \\ \frac{\Delta\theta}{\Delta s} &= \omega_B \frac{\sin\alpha}{v} \end{aligned} \tag{A.14}$$

Therefore we get the radius of curvature of the path

$$a = \frac{\Delta s}{\Delta \theta} = \frac{v}{\omega_B \sin\alpha}$$

and Δs as

$$\Delta s = \frac{2a}{\gamma} = \frac{2v}{\gamma \omega_B \sin\alpha} \tag{A.15}$$

The particle passes points 1 and 2 at times t_1 and t_2, respectively to give
$\Delta \mathrm{s} = \mathrm{v}(\mathrm{t}_2 - \mathrm{t}_1)$ and

$$t_2 - t_1 = \frac{2}{\gamma \omega_B \sin\alpha}.$$

Let t_1^A and t_2^A be the arrival times of the radiation at the observer from the two points. The radiation travels between points 1 and 2 at speed c and therefore the time difference $\mathrm{t}_2^A - \mathrm{t}_1^A$ is

smaller than t_2 - t_1 by an amount of Δs/c. The radiation from the more distant point reaches the nearer point in a time of Δs/c while the particle travels to the nearer point in Δs/v where it then emits the radiation for that position. So with $t_1^A = \Delta$s/c + (to observer) and $t_2^A = \Delta$s/v + (to observer) one gets

$$\begin{aligned} t_2^A - t_1^A &= \Delta s/v - \Delta \mathrm{s/c} = (t_2 - t_1) - \Delta s/c \\ \Delta t^A &= \frac{2}{\gamma \omega_B \sin\alpha} - \left(\frac{2v}{\gamma \omega_B \sin\alpha}\right)/c \\ &= \frac{2}{\gamma \omega_B \sin\alpha}[1 - \frac{v}{\mathrm{c}}] \end{aligned} \tag{A.16}$$

$\gamma = (1 - \frac{v^2}{c^2})^{-1/2}$ and thus for $\gamma \gg 1$ or v$\rightarrow$ c, one gets

$$(1 - \frac{v}{\mathrm{c}}) \approx \frac{1}{2\gamma^2}.$$

Thus

$$\Delta t^A \approx \frac{1}{2\gamma^2}\frac{2}{\gamma \omega_B \sin\alpha} = \frac{1}{\gamma^3 \omega_B \sin\alpha} \tag{A.17}$$

The gyration period P, is approximately P $\sim \frac{\text{circumference}}{\mathrm{V}} \sim \frac{2\pi a}{\mathrm{V}}$ to give

$$\mathrm{P} \sim \frac{2\pi}{\omega_B \sin\alpha}.$$

Therefore the observed pulse width Δt^A is smaller than the gyration period by a factor of γ^3.

It is expected that the spectrum will be broad, cutting off at frequencies like $\Delta\omega = 1/\Delta t^A$. The smaller Δt^A, the broader the frequency spectrum. We can expect that the spectrum will extend to a critical frequency which we define as $\omega_c = 3/2(\frac{1}{\Delta t^A})$ or $\nu_c = \frac{\omega_c}{2\pi}$, and then to fall away.

The following is an approximated approach to solving for the time averaged power per unit frequency. Firstly the electric field, which determines the behaviour of the emission with respect to the observer, is dependent on the polar angle about the direction of motion θ, through the product $\gamma\theta$. This means

$$E(t) \propto F(\gamma\theta)$$

where t is time in the observer's frame and F is some function as yet unknown. The zero of time and the path length s is when the pulse is centred on the observer. The distance to the observer is R and the particle's trajectory goes through points A and B. The scenario is sketched in Figure 28.

θ = s/a (θ is a small angle). The time t (duration of the pulse) is as before the difference in travel time of the radiation and the particle over the distance s. Therefore t = $\frac{s}{v}$[1 - $\frac{v}{\mathrm{c}}$] and so

$$s = vt(1 - \frac{v}{\mathrm{c}})^{-1}.$$

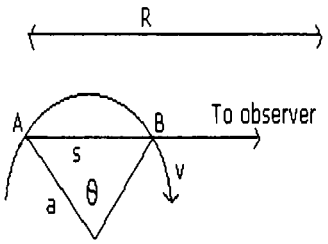

Figure 28

Thus

$$\begin{aligned} \gamma\theta &= \gamma\frac{s}{a} \\ &= \gamma\left[\frac{v}{(1-v/c)a}\right]t \\ \text{and with } (1-v/c) &= \frac{1}{2\gamma^2}; \quad \text{and} \quad a = \frac{v}{\omega_B \sin\alpha} \\ \gamma\theta &= 2\gamma^3\omega_B \sin\alpha t \qquad \text{(A.18)} \\ \text{which also gives } \gamma\theta &\propto \omega_c t \qquad \text{(A.19)} \end{aligned}$$

So now we see the electric field depends on time like

$$E(t) \propto g(\omega_c t).$$

Now a general dependence of the spectrum on ω can be searched for. The Fourier transform of the field is

$$\hat{E}(\omega) \propto \int_{-\infty}^{\infty} g(\omega_c t) e^{i\omega t} dt \qquad \text{(A.20)}$$

or change variables of integration to $\xi = \omega_c t$ and get

$$\hat{E}(\omega) \propto \int_{-\infty}^{\infty} g(\xi) e^{i\xi\omega/\omega_c} d\xi \qquad \text{(A.21)}$$

From (R & L, § 2.3) we have that

$$\frac{dW}{dt d\omega} = T^{-1}\frac{dW}{d\omega} \equiv P(\omega)$$

and $\frac{dW}{d\omega d\Omega} \propto (\hat{E}(\omega))^2$. Therefore integrate $\hat{E}$ over solid angle and divide by the orbital period, T . Thus

$$\frac{dW}{d\omega d\omega} \propto [\hat{E}]^2 \quad \text{.....so}$$

$$\int_0^{2\pi} \frac{d\mathrm{W}}{d\omega d\omega} d\Omega = \frac{\mathrm{W}}{d\omega}$$
$$= \int_0^{2\pi} (\hat{E})^2 d\Omega$$
$$= 2\pi[\hat{E}(\omega)]^2$$

and now

$$\frac{1}{\mathrm{T}} \frac{d\mathrm{W}}{d\omega} = \frac{d\mathrm{W}}{dtd\omega}$$
$$\frac{2\pi}{\mathrm{T}} (\hat{E})^2 = \frac{d\mathrm{W}}{dtd\omega}$$

to give

$$\mathrm{P}(\omega) = C_1 F(\frac{\omega}{\omega_c}) \tag{A.22}$$

The average power per unit frequency is thus a function of the ratio ω/ω_c like $\hat{E}$ is. To get the constant C_1, the total power over all ω can be compared to the previous result. The total power is

$$\mathrm{P} = \int_0^{\infty} \mathrm{P}(\omega) d\omega$$
$$= C_1 \int_0^{\infty} F(\frac{\omega}{\omega_c}) d\omega$$

or with variable $\mathrm{x} = \omega/\omega_c$

$$= \omega_c \times C_1 \int_0^{\infty} F(x) dx. \tag{A.23}$$

The integral is unknown until F(x) is specified, but since F(x) is dimensionless its value is not directly dependent on any physical parameters. C_1 therefore contains the influence of these parameters. So now from A.9

$$\mathrm{P} = \frac{2\mathrm{q}^4\mathrm{B}^2\gamma^2 v_\perp^2}{3\mathrm{m}^2\mathrm{c}^5} = \frac{2\mathrm{q}^4\mathrm{B}^2\gamma^2\beta^2 \sin\alpha^2}{3\mathrm{m}^2\mathrm{c}^3}$$

where $\beta = \mathrm{v}/\mathrm{c}$ and $\mathrm{v}_\perp = \mathrm{v}\sin\alpha$. Also

$$\omega_c = (3/2)\gamma^3\omega_B \sin\alpha = \frac{3\gamma^2 \mathrm{qB} \sin\alpha}{2\mathrm{mc}}$$

to give

$$\mathrm{P} = \omega_c \times \frac{4\mathrm{q}^3\mathrm{B}\sin\alpha(\beta)^2}{6\mathrm{mc}^2}.$$

Therefore $\mathrm{C}_1 \int F(x)dx = \frac{\mathrm{q}^3\mathrm{B}\sin\alpha}{\mathrm{mc}^2}(\frac{4}{6})$ and C_1 can be taken as

$$C_1 = \frac{\mathrm{q}^3\mathrm{B}\sin\alpha}{\mathrm{mc}^2}$$

with the non dimensional constant connected to F. Thus

$$\mathrm{P}(\omega) = \mathrm{k}\frac{\mathrm{q}^3\mathrm{B}\sin\alpha}{\mathrm{mc}^2}F(\frac{\omega}{\omega_c}) \tag{A.24}$$

with $\mathrm{P}(\nu) = 2\pi\mathrm{P}(\omega)$.

A.3 Details of the spectrum of synchrotron radiation

Figure 29 shows the trajectory of a particle (electron). The origin of the coordinates is the position of the particle at retarded time t' = 0 with a the radius of curvature of the trajectory. The particle has velocity $\mathbf{v}$ along the x-axis at time t' = 0(at the origin). $\epsilon_\perp$ is a unit vector along the y-axis in the x-y or orbital plane and $\epsilon_\parallel = \mathbf{n} \times \epsilon_\perp$. $\mathbf{n}$ points to the observer while $\epsilon_\parallel$ and $\epsilon_\perp$ respectively, are parallel and perpendicular to the projection of the B-field as seen by the observer. The 'new' coordinates with $\mathbf{n}, \epsilon_\perp$ and $\epsilon_\parallel$ has the same origin as the 'original' but $\epsilon_\perp$ and $\epsilon_\parallel$ form a natural reference to describe the polarization of the radiation.

From Figure 29 we have

$$\begin{aligned} \mathbf{v} &= v_x\mathbf{i}_x + v_y\mathbf{i}_z \quad ....(v_z = 0) \\ &= v\cos(\frac{vt'}{a})\mathbf{i}_x + v\sin(\frac{vt'}{a})\epsilon_\perp \quad ....(\mathbf{i}_y = \epsilon_\perp) \end{aligned} \tag{A.25}$$

$\mathbf{n}$ makes an angle of θ with $\mathbf{i_x}$ and this is also the angle between $\epsilon_\perp$ and $\mathbf{i_z}$. Thus we get $\mathbf{i_x} = \mathbf{n}\cos\theta - \epsilon_\parallel \sin\theta$ and

$$\begin{aligned} \mathbf{v} &= v\cos(\frac{vt'}{a})[\mathbf{n}\cos\theta - \epsilon_\parallel \sin\theta] + \mathbf{v}\sin(\frac{\mathbf{vt'}}{\mathbf{a}})\epsilon_\perp \\ &= v\left[\epsilon_\perp \sin(\frac{vt'}{a}) + \mathbf{n}\cos\theta\cos(\frac{vt'}{a}) - \epsilon_\parallel \sin\theta\cos(\frac{vt'}{a})\right] \end{aligned} \tag{A.26}$$

Now take $\mathbf{n} \times (\mathbf{n} \times \mathbf{v})$ with $\epsilon_\parallel = \mathbf{n} \times \epsilon_\perp$ and $\epsilon_\perp = -\mathbf{n} \times \epsilon_\parallel$.

$$\begin{aligned} \mathbf{n} \times \mathbf{v} &= \mathbf{n} \times v\left[\epsilon_\perp \sin(\frac{vt'}{a}) + \mathbf{n}\cos\theta\cos(\frac{vt'}{a}) - \epsilon_\parallel \sin\theta\cos(\frac{vt'}{a})\right] \\ &= v\sin(\frac{vt'}{a})\epsilon_\parallel + v\sin\theta\cos(\frac{vt'}{a})\epsilon_\perp \quad ....(\mathbf{n} \times \mathbf{n} = 0) \end{aligned}$$

and so

$$\mathbf{n} \times (\mathbf{n} \times \mathbf{v}) = v[-\sin(\frac{vt'}{a})\epsilon_\perp + \sin\theta\cos(\frac{vt'}{a})\epsilon_\parallel] \tag{A.27}$$

and with $\beta = \mathbf{v}/\mathrm{c}$:

$$\mathbf{n} \times (\mathbf{n} \times \beta) = \beta[-\sin(\frac{vt'}{a})\epsilon_\perp + \sin\theta\cos(\frac{vt'}{a})\epsilon_\parallel].$$

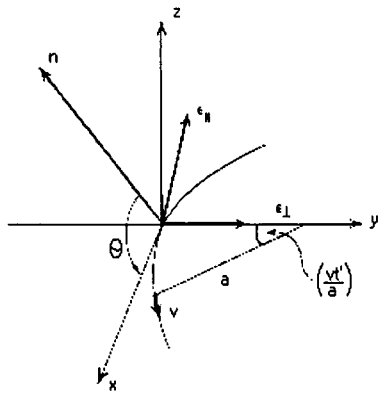

Figure 29 : The trajectory of a particle with velocity v. (Rybicki & Lightman)

This reduces to

$$\mathbf{n} \times (\mathbf{n} \times \beta) = -\epsilon_{\perp} \sin(\frac{vt'}{a}) + \epsilon_{\parallel} \cos(\frac{vt'}{a}) \sin\theta \tag{A.28}$$

for the highly relativistic case of v→c and $|\beta| = 1$.

From eq. 3.13 (R & L) we see that

$$\frac{dW}{d\omega d\Omega} = \frac{q^2\omega^2}{4\pi^2 c} \left| \int \mathbf{n} \times (\mathbf{n} \times \mathbf{v}) \exp[i\omega(\mathbf{t}' - \frac{\mathbf{n}.\mathbf{r}_o(\mathbf{t}')}{\mathbf{c}})]\mathbf{dt}' \right|^2 . \tag{A.29}$$

We need to find an expression for [t' - **n**.**r**(t')/c].

It can be seen from Figure 29 that $\mathbf{r}_o$(t') is the position vector of the particle in its orbit.

Consider $\mathbf{n}' = \frac{\mathbf{v}}{|\mathbf{v}|} = \epsilon_{\perp} \sin(\frac{vt'}{2a}) + \mathbf{n} \cos\theta \cos(\frac{vt'}{2a}) - \epsilon_{\parallel} \sin\theta \cos(\frac{vt'}{2a})$, then $\mathbf{r}(t') = a\mathbf{n}' \sin\theta$ where we *d*efine $\theta = (\frac{vt'}{2a}) < 90°$.

Now

$$\begin{aligned} \mathbf{r}(\mathbf{t}') &= 2a\mathbf{n}' \sin(\frac{vt'}{2a}) \\ &= 2a \sin(\frac{vt'}{2a})[\epsilon_{\perp} \sin(\frac{vt'}{2a}) + \mathbf{n} \cos\theta \cos(\frac{vt'}{2a}) - \epsilon_{\parallel} \sin\theta \cos(\frac{vt'}{2a})] \end{aligned} \tag{A.30}$$

Therefore

$$t' - \mathbf{n}.\mathbf{r}(t')/c = t' - \frac{2a \sin(\frac{vt'}{2a})}{c} \mathbf{n}[\epsilon_{\perp} \sin(\frac{vt'}{2a}) + \mathbf{n} \cos\theta \cos(\frac{vt'}{2a}) - \epsilon_{\parallel} \sin\theta \cos(\frac{vt'}{2a})]$$
$$[\mathbf{n}.\epsilon_{\parallel} = 0 \text{ and } \mathbf{n}.\mathbf{n} = 1]$$

$$
\begin{aligned}
&= t' - \frac{2a}{c}\sin^2(\frac{vt'}{2a})\mathbf{n}.\epsilon_\perp - \frac{2a}{c}\sin(\frac{vt'}{2a})\cos(\frac{vt'}{2a})\cos\theta \\
&= t' - \frac{2a}{c}\sin^2(\frac{vt'}{2a})n\epsilon_\perp\cos\theta - \frac{2a}{c}\sin(\frac{vt'}{2a})\cos(\frac{vt'}{2a})\cos\theta \\
&= t' - \frac{a}{c}[2\sin^2(\frac{vt'}{2a}) + 2\sin(\frac{vt'}{2a})\cos(\frac{vt'}{2a})]\cos\theta \quad ..[n = \epsilon_\perp = 1] \qquad \text{(A.31)}
\end{aligned}
$$

Now consider the identities:
$\sin(A/2) = \sqrt{\frac{1-\cos A}{2}}$ and $\cos(A/2) = \sqrt{\frac{1+\cos A}{2}}$

So now we have

$$
t' - \mathbf{n}.\mathbf{r}(t')/c = t' - \frac{a}{c}[1 - \cos(\frac{vt'}{a}) + \sin(\frac{vt'}{a})]\cos\theta
$$

and for (vt'/a) $\rightarrow$ 0 , cos(vt'/a) $\rightarrow$ 1 and the result is

$$
t' - \mathbf{n}.\mathbf{r}(t')/c = t' - \frac{a}{c}\cos\theta\sin(\frac{vt'}{a}). \qquad \text{(A.32)}
$$

The biggest contribution to the integral (eq.3.13 R & L) comes from the smallest values of (t' - $\mathbf{n}.\mathbf{r}$(t')/c), or when the exponential $\rightarrow$ 1. In the synchrotron process the radiation is strongly beamed in the direction of motion of the radiating electron. The distribution of the radiation is therefore dominated by small values of θ and correspondingly (vt'/a). Therefore we can expand the sine and cosine functions in [t' - $\mathbf{n}.\mathbf{r}$(t')/c] = t' - $\frac{a}{c}\cos\theta\sin(\frac{vt'}{a})$ for small θ and (vt'/a).
We then find

$$
\begin{aligned}
t' - \mathbf{n}.\mathbf{r}(t')/c &= t' - \frac{a}{c}[1 - \theta^2/2!][(vt'/a) - (vt'/a)^3/3!] \\
&= t' - \frac{a}{c}[(vt'/a) - (vt'/a)^3/3! - \frac{\theta^2}{2!}(vt'/a) + \frac{\theta^2}{2!}(vt'/a)^3/3!] \\
&\qquad\qquad \text{(last term negligible)} \\
&= t' - \frac{a}{c}(vt'/a) + \frac{a}{c}(vt'/a)^3/3! + \frac{a}{c}\frac{\theta^2}{2!}(vt'/a) \\
&= (1 - \frac{v}{c})t' + \frac{v^3}{6a^2c}t'^3 + \frac{v}{c}\frac{\theta^2}{2}t' \qquad \text{(A.33)}
\end{aligned}
$$

and now consider v $\approx$ c, then 1 -v/c $\approx \frac{1}{2\gamma^2}$, so set (1 - v/c) = $1/2\gamma^2$ and v = c elsewhere. Then

$$
\begin{aligned}
t' - \mathbf{n}.\mathbf{r}(t')/c &= \frac{1}{2\gamma^2}t' + \frac{v^3}{6a^2c}t'^3 + \frac{v}{c}\frac{\theta^2}{2}t' \\
&= \frac{1}{2\gamma^2}[t'(1 + \gamma^2\theta^2) + \frac{c^2\gamma^2t'^3}{3a^2}] \qquad \text{(A.34)}
\end{aligned}
$$

Reducing A.28 with v = c and θ and (vt'/a) $\rightarrow$ 0 gives

$$
\mathbf{n} \times (\mathbf{n} \times \beta) \approx -\epsilon_\perp(\frac{ct'}{a}) + \epsilon_\parallel\theta \qquad \text{(A.35)}
$$

Now we write down the radiation components for $\epsilon_\perp$ and $\epsilon_\parallel$ from eq. 3.13 using A.34 and A.35. Firstly,

$$\frac{dW}{d\omega d\Omega} = \frac{dW_\parallel}{d\omega d\Omega} + \frac{dW_\perp}{d\omega d\Omega}$$

and

$$\begin{aligned}
& \mathbf{n} \times (\mathbf{n} \times \beta) \exp[i\omega(t' - \frac{\mathbf{n}.\mathbf{r}_\circ(t')}{\mathrm{c}})] \\
= \; & -\epsilon_\perp(\frac{\mathrm{c}t'}{a}) + \epsilon_\parallel \theta \exp(i\omega[\frac{1}{2\gamma^2}[t'(1+\gamma^2\theta^2) + \frac{\mathrm{c}^2\gamma^2 t'^3}{3a^2}])] \\
= \; & -\epsilon_\perp(\frac{\mathrm{c}t'}{a}) \exp[\frac{i\omega}{2\gamma^2}[t'(1+\gamma^2\theta^2) + \frac{\mathrm{c}^2\gamma^2 t'^3}{3a^2}])] + \epsilon_\parallel \theta \exp[\frac{i\omega}{2\gamma^2}(t'(1+\gamma^2\theta^2) + \frac{\mathrm{c}^2\gamma^2 t'^3}{3a^2})]
\end{aligned} \tag{A.36}$$

This gives

$$\begin{aligned}
\frac{d\mathrm{W}}{d\omega d\Omega} &= \frac{\mathrm{q}^2\omega^2}{4\pi^2\mathrm{c}} \left| \int \mathbf{n} \times (\mathbf{n} \times \beta) \exp[i\omega(t' - \frac{\mathbf{n}.\mathbf{r}_\circ(t')}{\mathrm{c}})] dt' \right|^2 \\
&= \frac{\mathrm{q}^2\omega^2}{4\pi^2\mathrm{c}} \left| \int (\mathrm{c}t'/a) \exp[\frac{i\omega}{2\gamma^2}(t'(1+\gamma^2\theta^2) + \frac{\mathrm{c}^2\gamma^2 t'^3}{3a^2})] dt' \right|^2 |-\epsilon_\perp|^2 \\
&+ \frac{\mathrm{q}^2\omega^2\theta^2}{4\pi^2\mathrm{c}} \left| \int \exp[\frac{i\omega}{2\gamma^2}(t'(1+\gamma^2\theta^2) + \frac{\mathrm{c}^2\gamma^2 t'^3}{3a^2})] dt' \right|^2 |\epsilon_\parallel|^2 \quad ; [|-\epsilon_\perp|^2 = |\epsilon_\parallel|^2 = 1] \\
&= \frac{\mathrm{q}^2\omega^2}{4\pi^2\mathrm{c}} \left| \int (\mathrm{c}t'/a) \exp[\frac{i\omega}{2\gamma^2}(\theta_\gamma^2 t' + \frac{\mathrm{c}^2\gamma^2 t'^3}{3a^2})] dt' \right|^2 + \frac{\mathrm{q}^2\omega^2\theta^2}{4\pi^2\mathrm{c}} \left| \int \exp[\frac{i\omega}{2\gamma^2}(\theta_\gamma^2 t' + \frac{\mathrm{c}^2\gamma^2 t'^3}{3a^2})] dt' \right|^2
\end{aligned} \tag{A.37}$$

with $\theta_\gamma^2 = 1 + \gamma^2\theta^2$.

So we get

$$\frac{d\mathrm{W}_\perp}{d\omega d\Omega} = \frac{\mathrm{q}^2\omega^2}{4\pi^2\mathrm{c}} \left| \int \frac{\mathrm{c}t'}{a} \exp[\frac{i\omega}{2\gamma^2}(\theta_\gamma^2 t' + \frac{\mathrm{c}^2\gamma^2 t'^3}{3a^2})] dt' \right|^2 \tag{A.38}$$

$$\frac{d\mathrm{W}_\parallel}{d\omega d\Omega} = \frac{\mathrm{q}^2\omega^2\theta^2}{4\pi^2\mathrm{c}} \left| \int \exp[\frac{i\omega}{2\gamma^2}(\theta_\gamma^2 t' + \frac{\mathrm{c}^2\gamma^2 t'^3}{3a^2})] dt' \right|^2 \tag{A.39}$$

Most of the power is emitted for small θ and t' and therefore the integrals can be evaluated from -∞ to ∞. To get to standard integrals, a change in variables is made.

Let y = $\frac{\gamma \mathrm{c}t'}{a\theta_\gamma}$ which gives dt' = $\frac{a\theta_\gamma dy}{\gamma \mathrm{c}}$ and let $\eta = \frac{\omega a\theta^3}{3\mathrm{c}\gamma^3}$. So now

$$\begin{aligned}
\frac{d\mathrm{W}_\perp}{d\omega d\Omega} &= \frac{\mathrm{q}^2\omega^2}{4\pi^2\mathrm{c}} \left| \int_{-\infty}^{\infty} (\frac{\theta_\gamma y}{\gamma} \exp[\frac{i\omega}{2\gamma^2}(\theta_\gamma^2(\frac{ya\theta_\gamma}{\gamma\mathrm{c}}) + \frac{\mathrm{c}^2\gamma^2(\frac{a\theta_\gamma y}{\gamma\mathrm{c}})^3}{3a^2})] \frac{a\theta_\gamma}{\gamma\mathrm{c}} dy \right|^2 \\
&= \frac{\mathrm{q}^2\omega^2}{4\pi^2\mathrm{c}} (\frac{\theta_\gamma}{\gamma})^2 (\frac{a\theta_\gamma}{\gamma\mathrm{c}})^2 \left| \int_{-\infty}^{\infty} y \exp[\frac{3i}{2}(\frac{\omega a\theta_\gamma^3}{3\mathrm{c}\gamma^3})y + \frac{3i}{2}(\frac{\omega a\theta_\gamma^3}{3\mathrm{c}\gamma^3})\frac{2}{3}\frac{\gamma^2}{2\gamma^2}y^3] dy \right|^2
\end{aligned}$$

$$= \frac{q^2\omega^2}{4\pi^2 c}\left(\frac{a\theta_\gamma^2}{\gamma^2 c}\right)^2 \left|\int_{-\infty}^{\infty} y\exp[\frac{3}{2}i\eta(y+y^3/3)]dy\right|^2 \quad \text{(A.40)}$$

and also

$$\frac{dW_\parallel}{d\omega d\Omega} = \frac{q^2\omega^2\theta^2}{4\pi^2 c}\left|\int_{-\infty}^{\infty}\exp[\frac{3}{2}i\eta(y+y^3/3)]\frac{a\theta_\gamma dy}{\gamma c}\right|^2$$

$$= \frac{q^2\omega^2\theta^2}{4\pi^2 c}\left(\frac{a\theta_\gamma}{\gamma c}\right)^2\left|\int_{-\infty}^{\infty}\exp[\frac{3}{2}i\eta(y+y^3/3)]dy\right|^2 \quad \text{(A.41)}$$

These integrals can be further standardized using expressions from Abramowitz & Stegun (1972). But first consider the relations

$$a)\quad \exp[i\eta(3/2)(y+y^3/3] = \cos[(3/2)\eta(y+y^3)] + i\sin[(3/2)(y+y^3/3]$$

$$b)\quad y\exp[i\eta(3/2)(y+y^3/3] = y\cos[(3/2)\eta(y+y^3)] + iy\sin[(3/2)(y+y^3/3]$$

In (a) the real part dominates and in (b) the imaginary part, since if v→c, $\cos[(3/2)\eta(y + y^3/3)]\rightarrow 1$. All the 'real' emission is in a parallel direction to the motion.

Thus we have $\exp[i\eta(3/2)(y + y^3/3] = \cos[(3/2)\eta(y + y^3)]$

and $y\exp[i\eta(3/2)(y+y^3/3] = iy\sin[(3/2)(y+y^3/3]$.

The integrals can now be written in terms of Bessel functions as

$$\int_0^\infty \cos[\frac{3\eta}{2}(x+\frac{1}{3}x^3)]dx = \frac{1}{\sqrt{3}}K_{1/3}(\eta) \quad \text{(A.42)}$$

$$\int_0^\infty x\sin[\frac{3\eta}{2}(x+\frac{1}{3}x^3)]dx = \frac{1}{\sqrt{3}}K_{2/3}(\eta) \quad \text{(A.43)}$$

$K_{1/3}$ and $K_{2/3}$ are known as modified Bessel functions of order 1/3 and 2/3 respectively.

So now back to A.40 to get

$$\frac{dW_\perp}{d\omega d\Omega} = \frac{q^2\omega^2}{\pi^2 c}\left(\frac{a\theta_\gamma^2}{\gamma^2 c}\right)^2\left|\int_0^\infty ix\sin[\frac{3\eta}{2}(x+x^3/3)]dx\right|^2 \quad \text{(A.44)}$$

$$= \frac{q^2\omega^2}{3\pi^2 c}\left(\frac{a\theta_\gamma^2}{\gamma^2 c}\right)^2 K_{2/3}^2(\eta) \quad \text{(A.45)}$$

where the symmetric integrand was considered in changing the integration boundaries. The other integral is

$$\frac{dW_\parallel}{d\omega d\Omega} = \frac{q^2\omega^2\theta^2}{\pi^2 c}\left(\frac{a\theta_\gamma}{\gamma c}\right)^2\left|\int_0^\infty \cos[\frac{3\eta}{2}(x+x^3)]dx\right|^2$$

$$= \frac{q^2\omega^2\theta^2}{\pi^2 c}\left(\frac{a\theta_\gamma}{\gamma c}\right)^2[\frac{1}{\sqrt{3}}K_{1/3}(\eta)]^2$$

$$= \frac{q^2\omega^2\theta^2}{3\pi^2 c}\left(\frac{a\theta_\gamma}{\gamma c}\right)^2 K_{1/3}^2(\eta) \quad \text{(A.46)}$$

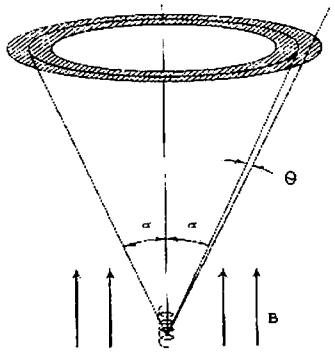

Figure 30 : The angular region of emission and gyration around a field line.
(Rybicki & Lightman 1979)

Now the task is to integrate over the angular distribution of the power. The radiation is, as has been said, strongly confined to a small angle θ with respect to the pitch angle α. Thus the angular region of the radiation from a particle in one gyration is $d\Omega = 2\pi \sin\alpha d\theta$. Figure 30 shows this angular region around a field line.

We have that $d\Omega = \int_0^{2\pi} \sin\alpha d\theta d\phi = 2\pi \sin\alpha d\theta$.

Therefore we get

$$\frac{dW_\perp}{d\omega} = \frac{2q^2\omega^2 a^2 \sin\alpha}{3\pi c^3\gamma^4} \int_{-\infty}^{\infty} \theta_\gamma^4 K_{2/3}^2(\eta) d\theta \qquad (A.47)$$

$$\frac{dW_\parallel}{d\omega} = \frac{2q^2\omega^2 a^2 \sin\alpha}{3\pi c^3\gamma^4} \int_{-\infty}^{\infty} \theta_\gamma^2\theta^2 K_{1/3}^2(\eta) d\theta \qquad (A.48)$$

Solutions to these integrals can be obtained from Westfold(1959) and leads to the following

$$A) \quad \int_{-\infty}^{\infty} \theta_\gamma^4 K_{2/3}^2(\eta) d\theta = \int \theta_\gamma^4 K_{2/3}^2(\frac{\omega a\theta^3}{3c\gamma^3}) d\theta$$
$$= \int \theta_\gamma^4 K_{2/3}^2(\frac{2\omega a\theta^3}{2.3c\gamma^3}) d\theta$$

and with $x = \frac{2\omega a}{3c\gamma^3} = \frac{\omega}{(3/2)\frac{\gamma^3}{a}} = \omega/\omega_c$

$$\int_{-\infty}^{\infty} \theta_\gamma^4 K_{2/3}^2(\eta) d\theta = \int_{-\infty}^{\infty} \theta_\gamma^4 K_{2/3}^2(\frac{x\theta_\gamma^3}{2}) d\theta$$
$$= \frac{\pi}{\sqrt{3}\gamma x}\left[\int_x^{\infty} K_{5/3}(z)dz + K_{2/3}(x)\right] \qquad (A.49)$$

and also

$$\begin{aligned}\int_{-\infty}^{\infty}\gamma^2\theta_\gamma^2\theta^2K_{1/3}^2(\eta)d\theta &= \int_{-\infty}^{\infty}\gamma^2\theta_\gamma^2\theta^2K_{1/3}^2\left(\frac{x\theta_\gamma^3}{2}\right)d\theta \\ &= \frac{\pi}{\sqrt{3}\gamma x}\left[\int_x^{\infty}K_{5/3}(z)dz - K_{2/3}(x)\right]\end{aligned} \tag{A.50}$$

We now let $F(x) = x\int_x^{\infty}K_{5/3}(z)dz$ and $G(x) = xK_{2/3}(x)$ to get

$$\begin{aligned}\frac{dW_\perp}{d\omega} &= \frac{2q^2\omega^2a^2\sin\alpha}{3\pi c^3\gamma^4}\left(\frac{\pi}{\sqrt{3}\gamma x^2}\right)\left[\int_x^{\infty}xK_{5/3}(z)dz + xK_{2/3}(x)\right] \\ &= \frac{2q^2\omega^2a^2\sin\alpha}{3\pi c^3\gamma^4}\frac{\pi}{\sqrt{3}\gamma}\left(\frac{3c\gamma^3}{2\omega a}\right)^2[F(x)+G(x)] \\ &= \frac{\sqrt{3}q^2\gamma\sin\alpha}{2c}[F(x)+G(x)]\end{aligned} \tag{A.51}$$

and

$$\begin{aligned}\frac{dW_\parallel}{d\omega} &= \frac{2q^2\omega^2}{2\pi c\gamma^2}\left(\frac{a}{\gamma c}\right)^2\sin\alpha\int_{-\infty}^{\infty}\gamma^2\theta_\gamma^2\theta^2K_{1/3}^2(\eta)d\theta \\ &= \frac{2q^2\omega^2}{2\pi c\gamma^2}\left(\frac{a}{\gamma c}\right)^2\sin\alpha\left(\frac{\pi}{\sqrt{3}\gamma x^2}\right)[x\int_x^{\infty}K_{5/3}(z)dz - xK_{2/3}(x)] \\ &= \frac{\sqrt{3}q^2\gamma\sin\alpha}{2c}[F(x)-G(x)].\end{aligned} \tag{A.52}$$

The orbital period is $T = \frac{1}{\nu_B} = \frac{2\pi}{\omega_B}$ and so therefore

$$P_\perp(\omega) = \frac{1}{T}\left(\frac{dW_\perp(\omega)}{d\omega}\right) = \frac{\sqrt{3}q^3B\sin\alpha}{4\pi mc^2}[F(x)+G(x)]$$

and

$$P_\parallel(\omega) = \frac{1}{T}\left(\frac{dW_\parallel}{d\omega}\right) = \frac{\sqrt{3}q^3B\sin\alpha}{4\pi mc^2}[F(x)-G(x)].$$

The total emitted power per frequency is the sum of the two components, giving

$$P(\omega) = P_\perp(\omega) + P_\parallel(\omega) = \frac{\sqrt{3}q^3B\sin\alpha}{2\pi mc^2}F(x) \tag{A.53}$$

which corresponds to A.24 . The total energy loss-rate of the electrons is the loss over all frequencies.

Thus

$$\begin{aligned}P &= \int_0^{\infty}P(\omega)d\omega \\ &= \int_0^{\infty}\frac{\sqrt{3}q^3B\sin\alpha}{2\pi mc^2}F(x)d\omega\end{aligned}$$

with $x = \omega/\omega_c$ and $d\omega = \omega_c dx$

$$\mathrm{P} = \frac{\sqrt{3}\mathrm{q}^3\mathrm{B}\omega_c \sin\alpha}{2\pi\mathrm{mc}^2} \int_0^\infty F(x)dx \tag{A.54}$$

Westfold(1959) showed that the integrals can be solved as follows

$$\int_0^\infty x^\mu F(x)dx = \frac{2^{\mu+1}}{\mu+2}\Gamma\left(\frac{\mu}{2}+\frac{7}{3}\right)\Gamma\left(\frac{\mu}{2}+\frac{2}{3}\right) \tag{A.55}$$

$$\int_0^\infty x^\mu G(x)dx = 2^\mu\Gamma\left(\frac{\mu}{2}+\frac{4}{3}\right)\Gamma\left(\frac{\mu}{2}+\frac{2}{3}\right) \tag{A.56}$$

where Γ(x) is the gamma function of argument x.

Now from A.55 and $\mu = 0$:

$$\int_0^\infty F(x)dx = \Gamma(7/3)\Gamma(2/3)$$

and then

$$\begin{aligned}
\mathrm{P} &= \frac{\sqrt{3}\mathrm{q}^3\mathrm{B}\omega_c \sin\alpha}{2\pi\mathrm{mc}^2}\Gamma(7/3)\Gamma(2/3) \\
&= \frac{\sqrt{3}\mathrm{q}^3\mathrm{B}[(3/2)\gamma^3\omega_B \sin\alpha]\sin\alpha}{2\pi\mathrm{mc}^2}\frac{8\pi}{9\sqrt{3}} \\
&= \left(\frac{8\pi\mathrm{q}^4}{3\mathrm{m}^2\mathrm{c}^4}\right)\frac{4}{3}\left(\frac{\mathrm{B}^2}{8\pi}\right)\gamma^2\mathrm{c}\sin^2\alpha \\
&= \frac{4}{3}\left(\frac{8\pi}{3}r_\circ^2\right)\mathrm{q}^2\mathrm{U}_B\gamma^2\mathrm{c}\sin^2\alpha \\
&= \frac{4}{3}\sigma_T\gamma^2\mathrm{cU}_B\sin^2\alpha
\end{aligned} \tag{A.57}$$

which corresponds to A.11 for $\alpha = 90°$.

The spectrum of a synchrotron source has a characteristic shape. The function F(x) has asymptotic forms of

$$F(x) = \frac{4\pi}{\sqrt{3}\Gamma(1/3)}\left(\frac{x}{2}\right)^{1/3} \quad ; \quad x \ll 1 \tag{A.58}$$

$$F(x) = (\pi/2)^{1/2}e^{-x}x^{1/2} \quad ; \quad x \gg 1 \quad (x = \omega/\omega_c) \tag{A.59}$$

The asymptotic emissivity in the low and high frequency ranges therefore are

$$\begin{aligned}
\mathrm{P}(\omega) &= \frac{\sqrt{3}\mathrm{q}^3\mathrm{B}\sin\alpha}{2\pi\mathrm{mc}^2}F(x) \\
&= \frac{\mathrm{q}^3\mathrm{B}\sin\alpha}{2\pi\mathrm{mc}^2}\frac{4\pi}{\Gamma(1/3)}\left(\frac{1}{2\omega_c}\right)^{1/3}\omega^{1/3} \quad ; \quad [x \ll 1]
\end{aligned}$$

$$= \frac{q^3 B \sin\alpha}{2\pi mc^2} \frac{4\pi}{\Gamma(1/3)} \left(\frac{1}{2.(3/2)\gamma^2 \frac{qB}{mc} \sin\alpha} \right)^{1/3} \omega^{1/3}$$

$$= \frac{2q^2}{3^{1/3}\Gamma(1/3)c} \left(\frac{qB \sin\alpha}{\gamma mc} \right)^{2/3} \omega^{1/3} \tag{A.60}$$

also

$$P(\nu) = \frac{2(2\pi)^2 q^2}{3^{1/3}\Gamma(1/3)c} \left(\frac{qB \sin\alpha}{\gamma mc} \right)^{2/3} \nu^{1/3} \; ; \; [\nu \ll \nu_c] [\omega = 2\pi\nu] \tag{A.61}$$

and for high frequencies

$$P(\omega) = \sqrt{\frac{3\pi}{2}} \frac{q^2 \gamma}{2\pi c} \left(\frac{qB \sin\alpha}{\gamma mc} \right) \left(\frac{\omega}{\omega_c} \right)^{1/2} e^{-\omega/\omega_c}$$

then also

$$P(\nu) = \sqrt{\frac{3\pi}{2}} \omega_B \frac{q^2 \gamma}{2\pi c} \left(\frac{\nu}{\nu_c} \right)^{1/2} e^{-\nu/\nu_c} \; ; \; [\nu \gg \nu_c] \tag{A.62}$$

We can now consider the influence of a power law electron energy distribution on the spectrum.

$$N(E)dE = CE^{-p}dE \; ; \; [E_1 < E < E_2] \tag{A.63}$$

$$\text{or} \quad N(\gamma)d\gamma = C\gamma^{-p}d\gamma \; ; \; [\gamma_1 < \gamma < \gamma_2] \tag{A.64}$$

We therefore have

$$P_{tot}(\omega) = \int_{E_1}^{E_2} P(\omega) N(E) dE = C \int_{E_1}^{E_2} P(\omega) E^{-p} dE \tag{A.65}$$

The radiation now comes from particles of different energies. Consider a distribution of electrons with fixed pitch angle α. The frequency ω can be related to energy E as follows

$$E = \gamma mc^2$$

and as before, $\omega_B = \frac{qB}{\gamma mc}$. This gives

$$x = \omega/\omega_c = \frac{\omega}{(3/2)\gamma^3 \omega B \sin\alpha}$$

$$= \frac{\omega}{(3/2)\left(\frac{E^2}{m^2c^4}\right) \frac{qB}{mc} \sin\alpha}$$

$$= \frac{2m^3c^5\omega}{3qBE^2 \sin\alpha} = \frac{A}{E^2} \tag{A.66}$$

So we get

$$E^2 = A/x \rightarrow dE = -(1/2)x^{-3/2}dx.$$

Back to A.65 and

$$\begin{aligned} \mathrm{P}_{tot}(\omega) &= C\int_0^\infty \mathrm{P}(\omega)N(E)dE = C\int_{E_1}^{E_2} \mathrm{P}(\omega)E^{-p}dE \quad ;[\mathrm{erg.cm^{-3}.s^{-1}.Hz^{-1}}] \\ &= C\int_0^\infty \mathrm{P}(x)\left[\left(\frac{A}{x}\right)^{1/2}\right]^{-p}[-(1/2)A^{1/2}x^{-3/2}dx] \\ |\mathrm{P}(\omega)| &= \frac{C}{2}A^{-p/2}A^{1/2}\int_0^\infty \mathrm{P}(x)x^{p/2}x^{-3/2}dx \\ &= \frac{C}{2A^{(p-1)/2}}\int_0^\infty \mathrm{P}(x)x^{(p-3)/2}dx \end{aligned}$$

and now using A.53

$$= \frac{\sqrt{3}C\mathrm{q}^3\mathrm{B}\sin\alpha}{4\pi\mathrm{mc}^2A^{(p-1)/2}}\int_0^\infty F(x)x^{(p-3)/2}dx \tag{A.67}$$

As before (A.55)

$$\int_0^\infty x^\mu F(x)dx = \frac{2^{\mu+1}}{\mu+2}\Gamma\left(\frac{\mu}{2}+\frac{7}{3}\right)\Gamma\left(\frac{\mu}{2}+\frac{2}{3}\right)$$

and now with μ = (p-3)/2 this results in

$$\begin{aligned} \int_0^\infty x^{(p-3)/2}F(x)dx &= \frac{2^{(\frac{p-3}{2}+1)}}{\frac{(p-3)}{2}+2}\Gamma\left(\frac{(p-3)/2}{2}+\frac{7}{3}\right)\Gamma\left(\frac{(p-3)/2}{2}+\frac{2}{3}\right) \\ &= \frac{2.2^{\frac{p-1}{2}}}{p+1}\Gamma\left(\frac{p}{4}+\frac{19}{12}\right)\Gamma\left(\frac{p}{4}-\frac{1}{12}\right) \end{aligned} \tag{A.68}$$

and therefore we get

$$\begin{aligned} \mathrm{P}_{tot}(\omega) &= \frac{\sqrt{3}C\mathrm{q}^3\mathrm{B}\sin\alpha}{4\pi\mathrm{mc}^2A^{(p-1)/2}}\frac{2.2^{\frac{p-1}{2}}}{p+1}\Gamma\left(\frac{p}{4}+\frac{19}{12}\right)\Gamma\left(\frac{p}{4}-\frac{1}{12}\right) \\ &= \frac{\sqrt{3}\mathrm{q}^3C\mathrm{B}\sin\alpha}{2\pi\mathrm{mc}^2(p+1)}\Gamma\left(\frac{p}{4}+\frac{19}{12}\right)\Gamma\left(\frac{p}{4}-\frac{1}{12}\right)\left(\frac{\mathrm{m}^3\mathrm{c}^5\omega}{3\mathrm{qB}\sin\alpha}\right)^{\frac{-(p-1)}{2}} \end{aligned} \tag{A.69}$$

This can also be written as

$$\begin{aligned} \mathrm{P}(\nu) &= \frac{\sqrt{3}\mathrm{q}^3C\sin\alpha}{2\pi\mathrm{mc}^2(p+1)}\Gamma\left(\frac{p}{4}+\frac{19}{12}\right)\Gamma\left(\frac{p}{4}-\frac{1}{12}\right)\left(\frac{2\mathrm{m}^3\mathrm{c}^5 2\pi\nu}{2.3\mathrm{q}\sin\alpha}\right)^{\frac{-(p-1)}{2}}\mathrm{B}.\mathrm{B}^{(p-1)/2} \\ &= \frac{\sqrt{3}\mathrm{q}^3C\sin\alpha}{2\pi\mathrm{mc}^2(p+1)}2^{\frac{p-1}{2}}\Gamma\left(\frac{p}{4}+\frac{19}{12}\right)\Gamma\left(\frac{p}{4}-\frac{1}{12}\right)\left(\frac{3\mathrm{q}}{4\pi\mathrm{m}^3\mathrm{c}^5}\right)^{\frac{(p-1)}{2}}(\sin\alpha)^{(p-1)/2}\mathrm{B}^{\frac{p+1}{2}}\nu^{-(p-1)/2} \\ &= \frac{\sqrt{3}\mathrm{q}^3C(\sin\alpha)^{(p+1)/2}}{2\pi\mathrm{mc}^2(p+1)}2^{\frac{p-1}{2}}\Gamma\left(\frac{p}{4}+\frac{19}{12}\right)\Gamma\left(\frac{p}{4}-\frac{1}{12}\right)\left(\frac{3q}{4\pi\mathrm{m}^3\mathrm{c}^5}\right)^{\frac{(p-1)}{2}}\mathrm{B}^{\frac{p+1}{2}}\nu^{-(p-1)/2} \end{aligned} \tag{A.70}$$

Now we can average over a whole isotropic pitch angle distribution. The average of the factor $(\sin\alpha)^{(p+1)/2}$ is calculated as follows.

In general we have

$$\begin{aligned}\frac{2}{\pi}\int_0^{\pi/2}\sin^{2n}x\,dx &= \frac{(2n)!}{2^{2n}n!}\\ &= \frac{\Gamma(n+1/2)}{\sqrt{\pi}\Gamma(n+1)}\end{aligned}$$

and with some steps

$$\frac{1}{2}\int_0^{\pi}\sin^{2n}x\,dx = \frac{\sqrt{\pi}}{2}\frac{\Gamma(n+1/2)}{\Gamma(n+1)} \tag{A.71}$$

Therefore now

$$\begin{aligned}<\sin^{\frac{p+1}{2}}\alpha> &= \frac{\int\sin^{\frac{p+1}{2}}\alpha\,d\Omega}{\int d\Omega}\\ &= \frac{\int_0^{2\pi}d\Phi\int_0^{\pi}\sin^{\frac{p+1}{2}}\alpha\,\sin\alpha\,d\alpha}{4\pi}\\ &= \frac{1}{2}\int_0^{\pi}\sin^{\frac{p+3}{2}}\alpha\,d\alpha\end{aligned} \tag{A.72}$$

and thus

$$<\sin^{\frac{p+1}{2}}\alpha> = \frac{\sqrt{\pi}}{2}\frac{\Gamma(\frac{p+5}{4})}{\Gamma(\frac{p+7}{4})} \tag{A.73}$$

This then results in

$$\begin{aligned}<\mathrm{P}_{tot}(\nu)> &= \frac{\sqrt{3}\mathrm{q}^3C<(\sin^{\frac{p+1}{2}}\alpha)>}{2\pi\mathrm{mc}^2(p+1)}2^{\frac{p-1}{2}}\Gamma\left(\frac{p}{4}+\frac{19}{12}\right)\Gamma\left(\frac{p}{4}-\frac{1}{12}\right)\left(\frac{3\mathrm{q}}{4\pi\mathrm{m}^3\mathrm{c}^5}\right)^{\frac{(p-1)}{2}}\\ &\quad\times\mathrm{B}^{\frac{p+1}{2}}\nu^{-(p-1)/2}\\ &= \frac{\sqrt{3}\mathrm{q}^3C2^{\frac{p-1}{2}}}{4\pi\mathrm{mc}^2(p+1)}\left[\frac{\sqrt{\pi}\Gamma\left(\frac{p}{4}+\frac{19}{12}\right)\Gamma\left(\frac{p}{4}-\frac{1}{12}\right)\Gamma\left(\frac{p}{4}+\frac{5}{4}\right)}{\Gamma\left(\frac{p}{4}+\frac{7}{4}\right)}\right]\left(\frac{3\mathrm{q}}{4\pi\mathrm{m}^3\mathrm{c}^5}\right)^{\frac{(p-1)}{2}}\\ &\quad\times\mathrm{B}^{\frac{p+1}{2}}\nu^{-(p-1)/2}\end{aligned} \tag{A.74}$$

Here we can see the most important parameters on which the emission is dependent.
We have

$$\mathrm{P}(\nu)\propto C\mathrm{B}^{\frac{p+1}{2}}\nu^{\frac{-(p-1)}{2}}$$

and from the electron spectrum $\mathrm{N(E)} = \mathrm{CE}^{-p} = \mathrm{N_o E}^{-p}$ ($\mathrm{N_o}$ is the electron density), we get

$$<\mathrm{P}_{(tot)}(\nu)>\propto\mathrm{N_o B}^{\frac{p+1}{2}}\nu^{\frac{-(p-1)}{2}}.$$

The power radiated by a synchrotron source is therefore dependent on the magnetic field in the source and the density of the radiating electrons in the source. The spectral index α = (p - 1)/2

is also characteristic of the spectrum when considering a power law electron energy distribution with index p.

A.4 Cyclotron to synchrotron radiation

The essential primary difference between cyclotron and synchrotron radiation emission is the energy of the radiating electrons. The transition from cyclotron to synchrotron involves the increase in energy from non-relativistic to highly relativistic. At low energies the electric field of the gyrating particle, as seen by the observer, varies sinusoidally with time at the frequency, ω_B. The power $P(\omega)$ has a single peak at this frequency. An increase in energy or an increase in (v/c) will cause the appearance of higher harmonics (multiples of the fundamental ω_B). A gyrating charge radiates at harmonics of the fundamental and the contribution at these harmonics is proportional to increasing powers of (v/c) for (v/c) $\ll 1$. When v$\rightarrow$ c a great number of harmonics are added to the spectrum and the electric field is sharply pulsed at intervals of $\frac{2\pi}{\omega_B}$. The envelope of the power spectrum, now containing all of these harmonics, takes on the shape of the function F(x). In general a synchrotron source will contain a distribution of γ values and since $\omega_B \propto 1/\gamma$, the particles will radiate at different fundamentals and harmonics. This will tend to fill in the gaps in the power spectrum and a continuous spectrum will result. The observed spectrum is just the superposition of pulses from individual particles.

A.5 Emitted and received power

A particle emitting synchrotron radiation is approximately moving towards the observer during part of its trajectory around a magnetic field line. This motion introduces a Doppler shift in the frequency of the received pulses.

Time delay effects (non-relativistic Doppler effect) cause the amended period of the arriving pulses to be

$$T_A = T[1 - \frac{v_{\|}}{c}\cos\alpha]$$

(eq.4.11; R & L) where $T = \frac{2\pi}{\omega_B}$. Then also $v_{\|} = v\cos\alpha$ and

$$\begin{aligned} T_A &= T[1 - \frac{v}{c}\cos^2\alpha] \\ &= T[1 - \frac{v}{c} + \frac{v}{c}\sin^2\alpha] \end{aligned} \tag{A.75}$$

and then for the limit v/c $\rightarrow$ 1:

$$T_A = \frac{2\pi}{\omega_B} \sin^2 \alpha \tag{A.76}$$

The observed fundamental frequency is then $\omega_B / \sin^2 \alpha$. The effect of this 'corrected' fundamental frequency concerns the difference between the emitted and the received power and spectrum. The emitted power is the energy divided by the period T of the gyration and thus the received power is the energy divided by T_A. This results in

$$P_r = \frac{\text{energy emitted}}{\frac{2\pi}{\omega_B} \sin^2 \alpha} = P_e / \sin^2 \alpha$$

The need to include the factor $\sin^2 \alpha$ when considering the usual astrophysical synchrotron source is minimal. This is the case since such an emission region is fairly localized in space and only moderately moves towards the observer. This means that any particle must at some time or other reverse its motion with respect to the observer simply to stay part of the source. The particles that are moving away do not contribute to the power due to the beaming effect. The result is that on average the power emitted is the power received, because the total number of emitted and received pulses are the same in the long run.

A.6 Synchrotron self-absorption

Synchrotron radiation is, like electromagnetic radiation from other processes, subject to absorption by the source itself. Radiating electrons absorb the radiation and this results in a modification of the observable spectrum from such a source. The absorption and emission processes walk hand in hand. It can be described as a two level system in which the electron makes transitions between the two states having different energy and momentum. A spontaneous transition from one state to the other occurs with a certain probability. If the electron loses energy it changes energy from E to E - dE and momentum from $\mathbf{p}$ to $\mathbf{p} - \mathbf{dp}$ and emits a photon. This photon has energy $E = h\nu$ and frequency ν. The probability of such a transition is indicative of the rate of emission of photons from an ensemble of electrons in the frequency interval ν to $\nu + d\nu$. Electrons in the lower energy state can also absorb a photon and this event also has a certain probability or occurs at a certain rate.

The description of these two state or level transitions is facilitated by the Einstein coefficients. The two energy levels considered are labeled 1 for the first energy E and 2 for energy $E + h\nu_o$. Three types of transition are distinguished, spontaneous and stimulated emission and absorption.

The Einstein A-coefficient for spontaneous emission is

$$A_{21} = \text{transition probability per unit time}(s^{-1}).$$

Absorption takes place of photons of energy $h\nu_o$ and the probability per unit time is proportional to the density of the photons at frequency ν_o. There is however a non-zero probability that photons of frequencies near ν_o may cause a transition (absorption). This leads to

$$B_{12}\bar{J} = \text{transition probability per unit time for absorption}$$

where B_{12} is an Einstein B-coefficient and $\bar{J}$ allows for the spread around ν_o. Stimulated emission is characterized by another Einstein B-coefficient

$$B_{21}\bar{J} = \text{transition probability per unit time for stimulated emission.}$$

These coefficients are used in a regime of transitions between discrete states, but this must be generalized to continuum states. Any two levels is possible in the synchrotron radiation process in a electron population with a spectrum of energies and emission frequencies. We therefore break up the continuous phase space in elements and consider transitions between these as being between discrete states. In the formula for the absorption coefficient the many possible transitions of size $h\nu$ must be accommodated. This is done by summing over all upper and lower states. Thus from eq.1.74(5) (R & L) the absorption coefficient is

$$\alpha_\nu = \frac{h\nu}{4\pi}\Sigma_{E_1}\Sigma_{E_2}[n(E_1)B_{12} - n(E_2)B_{21}]\phi_{21}(\nu) \qquad \text{(A.77)}$$

The profile function $\phi_{21}(\nu)$ limits the summation to those transitions between states that differ by $h\nu = E_2 - E_1$ and is thus a type of δ-function. A further assumption needed is that the emission and absorption is isotropic. In the case of synchrotron radiation this requires that the magnetic field is non-uniform or tangled with no net direction. A net direction would mean the radiating electrons have a net motion along the field and the emission is confined close to the velocity vector. The particle energy distribution also has to be isotropic.

Now we have $P(\nu, E_2) = 2\pi P(\omega)$, noting the energy E_2 of the radiating electron.

We have Kirchhoff's law $j_\nu = \alpha_\nu B_\nu(T)$. j_ν is the emission coefficient which is the energy emitted per unit time per unit solid angle and per unit volume. α_ν is the absorption coefficient.

Therefore

$$\begin{aligned}
\Sigma_{E_1}\Sigma_{E_2} j(\nu, E_2) &= \frac{h\nu}{4\pi}\Sigma_{E_1}\Sigma_{E_2} n(E_2) A_{21}\phi_{21}(\nu) \quad [\text{erg cm}^{-3}\text{s}^{-1}\text{Hz}^{-1}\text{sr}^{-1}] \\
\frac{\Sigma_{E_1}\Sigma_{E_2} 4\pi j(\nu, E_2)}{\Sigma_{E_2} n(E_2)} &= h\nu\Sigma_{E_1} A_{21}\phi_{21}(\nu) \quad [\text{erg s}^{-1}\text{Hz}^{-1}] \qquad \text{(A.78)}
\end{aligned}$$

and also

$$\mathrm{P}(\nu, E_2) = \mathrm{h}\nu\Sigma_{E_1} A_{21}\phi_{21}(\nu) \tag{A.79}$$

But $A_{21} = \frac{2\mathrm{h}\nu^3}{\mathrm{c}^2} B_{21}$ and thus

$$\mathrm{P}(\nu, E_2) = \frac{2\mathrm{h}\nu^3}{\mathrm{c}^2} h\nu\Sigma_{E_1} B_{21}\phi_{21}(\nu) \tag{A.80}$$

Now consider the part of the absorption coefficient due to stimulated emission $-\frac{h\nu}{4\pi}\Sigma_{E_1}\Sigma_{E_2} n(E_2) B_{21}\phi_{21}(\nu)$

and then using A.80

$$\begin{aligned} -\frac{1}{4\pi}\Sigma_{E_2} n(E_2)[\mathrm{h}\nu\Sigma_{E_1} B_{21}\phi_{21}(\nu)] &= -\frac{1}{4\pi}\Sigma_{E_2} n(E_2)[\frac{\mathrm{c}^2}{2h\nu^3}\mathrm{P}(\nu, E_2)] \\ &= -\frac{\mathrm{c}^2}{8\pi\mathrm{h}\nu^3}\Sigma_{E_2} n(E_2)\mathrm{P}(\nu, E_2) \end{aligned} \tag{A.81}$$

The true (pure) absorption (no stimulated emission) coefficient is the first term of A.77 or

$$\alpha_\nu^{true} = \frac{\mathrm{h}\nu}{4\pi}\Sigma_{E_1}\Sigma_{E_2} n(E_1) B_{12}\phi_{21}(\nu) \tag{A.82}$$

but $g_1 B_{12} = g_2 B_{21}$ which gives $B_{12} = B_{21}$ for elementary states.

So

$$\begin{aligned} \alpha_\nu^{\mathrm{true}} &= \frac{\mathrm{h}\nu}{4\pi}\Sigma_{E_2} n(E_2 - \mathrm{h}\nu)\Sigma_{E_1} B_{21}\phi_{21}(\nu) \\ &= \frac{1}{4\pi}\Sigma_{E_2} n(E_2 - \mathrm{h}\nu)[\mathrm{h}\nu\Sigma_{E_1} B_{21}\phi_{21}(\nu)] \\ &= \frac{\mathrm{c}^2}{8\pi\mathrm{h}\nu^3}\Sigma_{E_2} n(E_2 - \mathrm{h}\nu)\mathrm{P}(\nu, E_2) \end{aligned} \tag{A.83}$$

This can then combine with the stimulated emission part to give

$$\begin{aligned} \alpha_\nu &= \frac{\mathrm{h}\nu}{4\pi}\Sigma_{E_1}\Sigma_{E_2} n(E_1) B_{12}\phi_{21}(\nu) - \frac{\mathrm{h}\nu}{4\pi}\Sigma_{E_1}\Sigma_{E_2}[n(E_2) B_{21}\phi_{21}(\nu) \\ &= \frac{\mathrm{c}^2}{8\pi\mathrm{h}\nu^3}\Sigma_{E_2}[n(E_2 - \mathrm{h}\nu) - n(E_2)]\mathrm{P}(\nu, E_2) \end{aligned} \tag{A.84}$$

Taking a detour for a while, we have the distribution function for an isotropic electron population

$$\frac{\Delta N_j}{\Delta g_j} = \frac{N}{Z}\mathrm{e}^{-E_j/\mathrm{kT}} \tag{A.85}$$

where $Z = V[\frac{2\pi\mathrm{mkT}}{\mathrm{h}^2}]^{3/2}$.

For $g_j = 1$

$$\Delta N_j = \frac{N}{V}\left(\frac{2\pi\mathrm{mkT}}{\mathrm{h}^2}\right)^{-3/2}\mathrm{e}^{-E_j/\mathrm{kT}}$$

$$= K' e^{-E_j/kT}$$

and we have

$$n(E_j) = \frac{N(E_j)}{V} = K e^{-E_j/kT} \tag{A.86}$$

Then we get

$$\begin{aligned} \frac{\Delta N_j}{\Delta g_j} &= \frac{N}{V}\left(\frac{2\pi mkT}{h^2}\right)^{-3/2} e^{-E_j/kT} \\ &= \frac{N}{V}\left(\frac{1}{2\pi mkT}\right)^{3/2} h^3 e^{-E_j/kT} \end{aligned} \tag{A.87}$$

This gives the particle density per quantum state.

The number of quantum states per unit volume is

$$\begin{aligned} \Delta G_j &= \frac{4\pi m^3 V}{h^3} v^2 \Delta v \\ \frac{\Delta G_j}{V} &= \frac{4\pi m^3 V}{h^3} v^2 \Delta v \\ &= \frac{4\pi p^2 \Delta p}{h^3} \quad [dp = d(mv) = m dv;\ \text{non-relativistically}] \\ \frac{\Delta G_j}{V} &= \frac{d^3 p}{h^3} \end{aligned} \tag{A.88}$$

Now consider

$$\begin{aligned} n(E) &= \frac{\Delta N(E_j)}{V} \\ &= \frac{\Delta N(E_j)}{\Delta G_j}\frac{\Delta G_j}{V} \\ &= K h^3 e^{-E_j/kT}\frac{d^3 p}{h^3} \quad ;\ [\text{from A.87}] \\ &= K e^{-\frac{p_j^2/2m}{kT}} d^3 p \\ &= f(p) d^3 p \end{aligned} \tag{A.89}$$

From this we can get

$$\Sigma n(E) = \Sigma f(p) d^3 p \Rightarrow \int f(p) d^3 p.$$

We can now return to A.84 to find the following

$$\begin{aligned} \alpha_\nu &= \frac{c^2}{8\pi h\nu^3}\Sigma_{E_2}[n(E_2 - h\nu) - n(E_2)]P(\nu, E_2) \\ &= \frac{c^2}{8\pi h\nu^3}\int [f(p_2^*)d^3 p_2 - f(p_2)d^3 p_2]P(\nu, E_2) \\ &= \frac{c^2}{8\pi h\nu^3}\int [f(p_2^*) - f(p_2)]d^3 p_2]P(\nu, E_2) \end{aligned} \tag{A.90}$$

We also find

$$\begin{aligned} f(p_2^*) - f(p_2) &= Ke^{-\frac{E_2-h\nu}{kT}} - Ke^{-E_2/kT} \\ &= Ke^{-E_2/kT}[e^{h\nu/kT} - 1] \\ &= f(p_2)[e^{h\nu/kT} - 1] \end{aligned} \tag{A.91}$$

and thus

$$\begin{aligned} \alpha_\nu &= \frac{c^2}{8\pi h\nu^3}\int f(p_2)[e^{h\nu/kT} - 1]d^3p_2]P(\nu, E_2) \\ &= \frac{c^2}{8\pi h\nu^3}[e^{h\nu/kT} - 1]\int f(p_2)P(\nu, E_2)d^3p_2. \end{aligned} \tag{A.92}$$

The integral gives the total power per unit volume per frequency range or

$$4\pi j_\nu = \int f(p)d^3pP(\nu, E_2) = \int P(\nu, E_2)dn(E_2)\ ; \quad [\text{erg cm}^{-3}\text{s}^{-1}\text{Hz}^{-1}]$$

Therefore

$$\alpha_\nu = \frac{c^2}{2h\nu^3}[e^{h\nu/kT} - 1]j_\nu \tag{A.93}$$

But $B_\nu(T) = \frac{2h\nu^3}{c^2}\frac{1}{e^{h\nu/kT}-1}$
and thus

$$\alpha_\nu = \frac{j_\nu}{B_\nu(T)} \tag{A.94}$$

which is Kirchhoff's law. This gives the absorption coefficient for thermal emission.

The electron distribution is taken as isotropic and it is convenient to use the energy rather than the momentum in the distribution function. The power law electron spectrum looks like the following

$$\begin{aligned} N(E)dE &= CE^{-p}dE = f(p)d^3p \\ &= f(p)4\pi p^2dp \end{aligned} \tag{A.95}$$

This results (going back to A.90) in

$$\alpha_\nu = \frac{c^2}{8\pi h\nu^3}\int [N(E - h\nu)dE - N(E)dE]P(\nu, E) \tag{A.96}$$

Now consider the case of $h\nu \ll$ E. This would make the following true

$$\alpha_\nu \approx \frac{c^2}{8\pi h\nu^3}\int dEP(\nu, E)E^2\left[\frac{N(E - h\nu)}{(E - h\nu)^2} - \frac{N(E)}{E^2}\right] \tag{A.97}$$

We can now expand (Taylor expansion) this to first order in $h\nu$ to get

$$f(a) = f(x) - (x - a)\frac{\partial f(a)}{\partial x}$$

and then

$$\begin{aligned}
\frac{N(E-\mathrm{h}\nu)}{(E-\mathrm{h}\nu)^2} &= \frac{N(E)}{E^2} - (E^2-(E-\mathrm{h}\nu))\frac{\partial}{\partial E}\left[\frac{N(E-\mathrm{h}\nu)}{(E-\mathrm{h}\nu)^2}\right] \\
\frac{N(E-\mathrm{h}\nu)}{(E-\mathrm{h}\nu)^2} - \frac{N(E)}{E^2} &= -\mathrm{h}\nu\frac{\partial}{\partial E}\left(\frac{N(E)}{E^2}\right)\ ; \quad [\mathrm{h}\nu \ll E] \qquad \text{(A.98)}
\end{aligned}$$

Then

$$\begin{aligned}
\alpha_\nu &= \frac{\mathrm{c}^2}{8\pi\mathrm{h}\nu^3}\int \mathrm{P}(\nu,E)E^2\left[\frac{N(E-h\nu)}{(E-\mathrm{h}\nu)^2} - \frac{N(E)}{E^2}\right]dE \\
&= \frac{-\mathrm{c}^2}{8\pi\nu^2}\int \mathrm{P}(\nu,E)E^2\frac{\partial}{\partial E}\left(\frac{N(E)}{E^2}\right)dE \qquad \text{(A.99)}
\end{aligned}$$

The thermal contribution can be used to substantiate the results. The distribution of ultra-relativistic particles is

$$N(E) = KE^2\mathrm{e}^{-E/\mathrm{kT}}$$

and

$$\frac{\partial}{\partial E}\left(\frac{N(E)}{E^2}\right) = -\frac{K}{\mathrm{kT}}\mathrm{e}^{-E/\mathrm{kT}}$$

Therefore from A.98 and A.99 we get

$$\begin{aligned}
\alpha_\nu &= \frac{-\mathrm{c}^2}{8\pi\nu^2}\int \mathrm{P}(\nu,E)E^2\frac{\partial}{\partial E}\left(\frac{N(E)}{E^2}\right)dE \\
&= \frac{-\mathrm{c}^2}{8\pi\nu^2}\int \mathrm{P}(\nu,E)E^2\left[-\frac{K}{\mathrm{kT}}\mathrm{e}^{-E/\mathrm{kT}}\right]dE \\
&= \frac{\mathrm{c}^2}{8\pi\nu^2\mathrm{kT}}\int \mathrm{P}(\nu,E)KE^2\mathrm{e}^{-E/\mathrm{kT}}dE \qquad \text{(A.100)} \\
&= \frac{\mathrm{c}^2}{8\pi\nu^2\mathrm{kT}}\int \mathrm{P}(\nu,E)N(E)dE. \qquad \text{(A.101)}
\end{aligned}$$

Isotropic emission has the relation

$$\int \mathrm{P}(\nu,E)N(E)dE = 4\pi j_\nu$$

and again this results in

$$\alpha_\nu = \frac{\mathrm{c}^2 j_\nu}{2\nu^2\mathrm{kT}} = \frac{j_\nu}{B_\nu^{RJ}(\mathrm{T})}\ ; \quad [\mathrm{h}\nu \ll \mathrm{kT}]$$

where $B_\nu^{\mathrm{RJ}}(\mathrm{T}) = \frac{2\nu^2\mathrm{kT}}{\mathrm{c}^2}$ is the Rayleigh-Jeans limit ($\mathrm{h}\nu \ll \mathrm{kT}$)

A power law electron distribution can now be applied to get α_ν.

Let

$$
\begin{aligned}
-E^2\frac{\partial}{\partial E}\left(\frac{N(E)}{E^2}\right) &= -E^2\frac{\partial}{\partial E}\left[CE^{-p}E^{-2}\right] \\
&= -E^2C[-(p+2)E^{-(p+2)-1}] \\
&= C(p+2)E^{-(p+1)} \qquad \text{(A.102)} \\
&= \frac{(p+2)N(E)}{E} \qquad \text{(A.103)}
\end{aligned}
$$

The result then is

$$
\begin{aligned}
\alpha_\nu &= \frac{-\mathrm{c}^2}{8\pi\nu^2}\int \mathrm{P}(\nu,E)E^2\frac{\partial}{\partial E}\left(\frac{N(E)}{E^2}\right)dE \\
&= \frac{(p+2)\mathrm{c}^2}{8\pi\nu^2}\int \mathrm{P}(\nu,E)\frac{N(E)}{E}dE \\
&= \frac{(p+2)C\mathrm{c}^2}{8\pi\nu^2}\int \mathrm{P}(\nu,E)E^{-(p+1)}dE \qquad \text{(A.104)}
\end{aligned}
$$

Now we remember that $\mathrm{P}(\nu) = 2\pi\mathrm{P}(\omega)$ and $\mathrm{P}(\omega) = \frac{\sqrt{3}\mathrm{q}^3\mathrm{B}\sin\alpha}{2\pi\mathrm{mc}^2}F(x)$ and therefore

$$
\mathrm{P}(\nu,E) = \frac{2\pi\sqrt{3}\mathrm{q}^3\mathrm{B}\sin\alpha}{2\pi\mathrm{mc}^2}F(x).
$$

We substitute in A.104 and find

$$
\begin{aligned}
\alpha_\nu &= \frac{(p+2)C\mathrm{c}^2}{8\pi\nu^2}\int \frac{2\pi\sqrt{3}\mathrm{q}^3\mathrm{B}\sin\alpha}{2\pi\mathrm{mc}^2}F(x)E^{-(p+1)}dE \\
&= \frac{(p+2)\sqrt{3}\mathrm{q}^3\mathrm{B}\sin\alpha C}{8\pi\nu^2\mathrm{m}}\int F(x)E^{-(p+1)}dE \qquad \text{(A.105)}
\end{aligned}
$$

Now we have as before $\mathrm{x} = \omega/\omega_c = \nu/\nu_c$ and $\mathrm{x} = \mathrm{A}/\mathrm{E}^2$ with

$\mathrm{dE} = \text{-}1/2\mathrm{A}^{1/2}\mathrm{x}^{-3/2}\mathrm{dx}$.

We proceed with the integral from A.105 and thus

$$
\begin{aligned}
\int F(x)E^{-(p+1)}dE &= \int F(x)\left[(\frac{A}{x})^{1/2}\right]^{-(p+1)}[-\frac{1}{2}A^{1/2}x^{-3/2}dx] \\
&= -\frac{A^{-p/2}}{2}\int F(x)x^{\frac{p-2}{2}}dx
\end{aligned}
$$

and thus

$$
\int_0^\infty F(x)E^{-(p+1)}dE = -\frac{A^{-p/2}}{2}\int_0^\infty F(x)x^{\frac{p-2}{2}}dx \qquad \text{(A.106)}
$$

We continue with A.106 with use of A.55

$$
\begin{aligned}
\left|\int_0^\infty F(x)E^{-(p+1)}dE\right| &= \frac{A^{-p/2}}{2}\left[\frac{2^{\frac{p-2}{2}+1}}{\frac{p-2}{2}+2}\Gamma\left(\frac{p-2}{2}+\frac{7}{3}\right)\Gamma\left(\frac{p-2}{2}+\frac{2}{3}\right)\right] \\
&= \frac{A^{-p/2}}{2}\frac{1}{p+2}\Gamma\left(\frac{3p+22}{12}\right)\Gamma\left(\frac{3p+2}{12}\right) \qquad \text{(A.107)}
\end{aligned}
$$

This results in

$$\alpha_\nu = \frac{(p+2)\sqrt{3}q^3 B \sin\alpha C}{8\pi\nu^2 m}\left[\frac{A^{-p/2}}{2}\frac{1}{p+2}\Gamma\left(\frac{3p+22}{12}\right)\Gamma\left(\frac{3p+2}{12}\right)\right]$$

$$\text{and with } A = \frac{2m^3c^5\omega}{3qB\sin\alpha} = \frac{4\pi m^3c^5\nu}{3qB\sin\alpha}$$

$$\alpha_\nu = \frac{(p+2)\sqrt{3}q^3 B \sin\alpha C}{8\pi\nu^2 m(p+2)}\left[\frac{4\pi m^3c^5\nu}{6qB\sin\alpha}\right]^{-p/2}\Gamma\left(\frac{3p+22}{12}\right)\Gamma\left(\frac{3p+2}{12}\right)$$

$$= \frac{\sqrt{3}q^3 C}{8\pi m}\left[\frac{3q}{2\pi m^3c^5}\right]^{p/2}(B\sin\alpha)^{\frac{p+2}{2}}\Gamma\left(\frac{3p+22}{12}\right)\Gamma\left(\frac{3p+2}{12}\right)\nu^{-\frac{p+4}{2}} \tag{A.108}$$

The source function S_ν for an emitting region is defined as $S_\nu = \frac{j_\nu}{\alpha_\nu}$ where j_ν is the spontaneous emission coefficient. Therefore we have for an optically thick region

$$S_\nu = \frac{j_\nu}{\alpha_\nu} = \frac{P(\nu)}{4\pi\alpha_\nu} \quad [\text{erg cm}^2\text{s}^{-1}\text{Hz}^{-1}\text{sr}^{-1}]$$

We have from A 74 and A.108 the following

$$P(\nu) = \text{const.}\nu^{-\frac{p-1}{2}} \quad [\text{erg cm}^2\text{s}^{-1}\text{Hz}^{-1}]$$

and

$$\alpha_\nu = \text{const.}\nu^{-\frac{p+4}{2}}.$$

The source function for a self-absorbed or optically thick synchrotron source therefore is

$$S_\nu = \text{const.}\frac{\nu^{-\frac{p-1}{2}}}{\nu^{-\frac{p+4}{2}}}$$

$$= \text{const.}\nu^{5/2} \tag{A.109}$$

This result shows the effect of the plasma density in the emitting region on the synchrotron spectrum. The self-absorption causes the negative 'slope' of the radiated emission to change to a positive slope. This then means that the medium becomes increasingly optically thick and thus dim towards the lower frequency range.

The spectrum for an optically thick region is determined by the source function and for an optically thin region by $P(\nu) = K\nu^{-\frac{p-1}{2}}$.

The spectrum (log-log) therefore has the general form as in Figure 31.

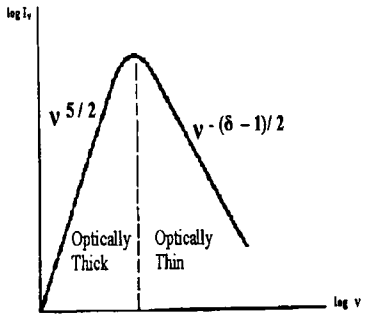

Figure 31 : The characteristic spectrum of a synchrotron source. (Rybicki & Lightman)

A randomly orientated magnetic field tends to isotropize the emission. Its influence on α_ν can be calculated by averaging over all pitch angles α in A.108 .
This means

$$\begin{aligned} < \sin^{\frac{p+2}{2}} \alpha > &= \frac{\int \sin^{\frac{p+2}{2}} \alpha d\Omega}{\int d\Omega} \\ &= \frac{\int_0^{2\pi} d\phi \int_0^{\pi} \sin^{\frac{p+2}{2}} \alpha \sin\alpha d\alpha}{4\pi} \\ &= 1/2 \int_0^{\pi} \sin^{\frac{p+4}{2}} \alpha d\alpha \end{aligned} \tag{A.110}$$

and with

$$1/2 \int_0^{\pi} \sin^{2n} x dx = \frac{\sqrt{\pi}}{2} \frac{\Gamma(n+1/2)}{\Gamma(n+1)}$$

we get

$$1/2 \int_0^{\pi} \sin^{\frac{p+4}{2}} \alpha d\alpha = \frac{\sqrt{\pi}}{2} \frac{\Gamma(\frac{p+6}{4})}{\Gamma(\frac{p+8}{4})} \tag{A.111}$$

The absorption coefficient then is

$$< \alpha_\nu > = \frac{\sqrt{3\pi} q^3 C}{16\pi m} \left[\frac{3q}{2\pi m^3 c^5}\right]^{p/2} (B)^{\frac{p+2}{2}} \frac{\Gamma(\frac{p+6}{4})\Gamma\left(\frac{3p+22}{12}\right)\Gamma\left(\frac{3p+2}{12}\right)}{\Gamma(\frac{p+8}{4})} \nu^{-\frac{p+4}{2}} \tag{A.112}$$

The importance of these results becomes apparent when observing synchrotron sources. The characteristic power law relations of the synchrotron spectrum in the optically thin and thick frequency ranges (for the specific source) makes it possible to get an idea of the source parameters. Electron energies, electron densities and magnetic field strengths combine to produce an observed spectrum. The slope of the optically thin part of the spectrum (-(p-1)/2) is indicative of the electron index p of the source.

The observable intensity I_ν which is expected can be calculated by considering a slab of thickness l. This gives (par. 1.4 R & L)

$$\frac{dI_\nu}{dx} = j_\nu - \alpha_\nu I_\nu$$

where dx is small distance along the path of the beam. A solution to this equation would give the intensity in an emitting and absorbing region.

The solution for a constant source function S_ν looks like the following

$$\begin{aligned} I_\nu(\tau_\nu) &= I(0)\mathrm{e}^{-\tau_\nu} + S_\nu - S_\nu \mathrm{e}^{-\tau_\nu} \\ &= S_\nu[1 - \mathrm{e}^{-\tau_\nu}]\ ; \quad [I(0) = 0] \end{aligned} \tag{A.113}$$

or

$$\begin{aligned} I_\nu(l) &= S_\nu[1 - \mathrm{e}^{-\alpha_\nu l}] \\ &= \frac{j_\nu}{\alpha_\nu}[1 - \mathrm{e}^{-\alpha_\nu l}] \end{aligned} \tag{A.114}$$

where τ_ν is the optical depth as defined by $d\tau_\nu = \alpha_\nu dx$.

If the source is optically thick or $\tau_\nu \sim \alpha_\nu l \gg 0$ then as before

$$I_\nu = S_\nu = \frac{j_\nu}{\alpha_\nu} = \frac{\mathrm{P}(\nu)}{4\pi\alpha_\nu} = K v^{5/2}.$$

If the source is optically thin ($\alpha_\nu l < 1$) we get

$$\begin{aligned} I_\nu &= \frac{j_\nu}{\alpha_\nu}[1 - \mathrm{e}^{-\alpha_\nu l}] \\ &= \frac{j_\nu}{\alpha_\nu}[1 - (1 - (\alpha_\nu l) + (\alpha_\nu l)^2/2 + ...)] \\ &= j_\nu l \quad ; \text{ [to first order]} \\ &= \frac{\mathrm{P}(\nu) l}{4\pi} \\ &= K\nu^{-\frac{p-1}{2}} \ ; \quad [\mathrm{erg\,cm^{-2}s^{-1}Hz^{-1}sr^{-1}}] \end{aligned} \tag{A.115}$$

Bibliography

[1] Abada-Simon M., Lecacheux A., Bookbinder J., Dulk G.A., 1993, ApJ, 406, 692

[2] Abada-Simon M., Bastian T.S., Horne K., Bookbinder J.A., 1995a, in Buckley D.A.H., Warner B., eds, ASP conf. Ser. Vol 85, Proc. Cape Workshop on Magnetic Cataclysmic Variables. Astron Soc. Pac., San Francisco, p. 355

[3] Abada-Simon M., Bastian T.S., Bookbinder A.J., Aubier M., Bromage G., Dulk G.A., Lecacheux A., 1995b, in Lecture Notes in Physics, 454, 268

[4] Abada-Simon M., Mouchet M., Aubier M., Barrett P., de Jager O.C., de Martino D., Ramsay G., 1999, in Cox, P. Kessler, M.F. eds., ESA SP-427, Proc. The Universe as seen by *ISO*. ESA, Paris, p.257

[5] Abada-Simon et al. 2002, in Combes F., Barret D. eds., Semaine de l' Astrophysique Francaise, EdP-Sciences

[6] Abada-Simon et al. 2003, A&A (in print)

[7] Abramowitz M., Stegun I.A., eds, Handbook of mathematical functions, NewYork: Dover Publications 1972

[8] Bastian T.S., Beasley A.J., Bookbinder J.A., 1996, ApJ, 461, 1016

[9] Bastian T.S., Dulk G.A., Chanmugam G., 1988, ApJ, 324, 431 (BDC)

[10] Bath G.T., Evans W.D. & Pringle J.E. 1974, MNRAS, 166, 113

[11] Beardmore A.P., Osborne J.P., 1997, MNRAS, 290, 145

[12] Beasley A.J., Bastian T.S., Ball L., Wu K., 1994, ApJ, 108, 2207

[13] Benz A., 1994, Plasma Astrophysics: Kinetic processes in the solar and stellar coronae, Kluwer Academic Publishers, Dordrecht, p. 285

[14] Biskamp D.,1988 in Meisenheimer K., Röser H.J., eds., Lecture Notes in Physics, Hot Spots in Extra Galactic Radio Sources. Springer, Berlin, p. 279

[15] Bookbinder J.A., Lamb D.Q., 1987, ApJ, 323, L131

[16] Bowden et al. 1992, Astropart. Phys, 1, 47

[17] Campbell C.G., 1997, Magnetohydrodynamics in Binary Stars, Kluwer Academic Publishers, Dordrecht, p. 251 - 293

[18] Chandrasekhar S., 1933, MNRAS, 93, 390

[19] Crawford J.A. & Kraft R.P. 1956, ApJ., 123, 44

[20] Cropper M., 1990, Sp. Sci. Rev., 54, 195

[21] de Jager O.C., 1991, ApJ., 378, 268

[22] de Jager O.C., Meintjes P.J., 1993 A&A, 268, L1

[23] de Jager O.C., Meintjes P.J., O' Donoghue D., Robinson A.L., 1994, MNRAS, 267, 577

[24] de Jager O.C., 1995, in Buckley D.A.H., Warner B., eds, ASP Conf. Ser. Vol. 85, Proc. Cape Workshop on Magnetic Cataclysmic Variables. Astron. Soc. Pac. San Fransisco, p. 373

[25] Dreicer H., 1959, Phys. Rev., 115, 242

[26] Dulk G.A., 1985, ARA&A, 23, 169

[27] Eilek J.A., Hughes P.A., 1991, Beams and Jets in Astrophysics, ed. P.A. Hughes, Cambridge University Press, Cambridge, p. 428 - 483

[28] Eracleous M., Horne K., Robinson E.L., Zhang E.-H., Marsh T.R., Wood J., 1994, ApJ, 433, 313

[29] Eracleous M., Horne K., 1996, ApJ, 471, 427

[30] Fermi E., 1949, Phys. Rev., 75, 1169

[31] Flannery, B. 1975, MNRAS, 170, 325

[32] Frank J., King A.R., Lasota J.P., 1988, A&A, 193, 113

[33] Frank J., King A.R., Raine D., 1992, Accretion Power in Astrophysics, Cambridge Univ. Press, Cambridge, p. 46-54

[34] Frank J., King A.R., Raine D., 2002, Accretion Power in Astrophysics(Third edition), Cambridge Univ. Press, Cambridge

[35] Ghosh P. & Lamb F. 1978, ApJ, 223, L83

[36] Ghosh P. & Lamb F. 1979a, ApJ, 232, 259

[37] Ghosh P. & Lamb F. 1979b, ApJ, 234, 296

[38] Hendry P.D. & Mochnacki S.W. 2000, ApJ, 531, 467

[39] Holman G.D., Pesses M.E., 1983, ApJ, 267, 837

[40] Iben I., 1967, ARASA, 5, 71

[41] Jackson J.D., 1975, Classical Electrodynamics, Wiley and Sons, New York

[42] Jameson R.F., King A.R., Sherrington M.R., 1980, MNRAS, 191, 559

[43] Joy A.H. 1954, ApJ., 120, 377

[44] King A.R. & Lasota J.P. 1991, ApJ, 378, 674

[45] King A.R., 1993, MNRAS, 261, 144

[46] King A.R., 1988, QJRAS, 29, 1

[47] Kopal Z., 1955, Am. d'Astrophys., 18, 379

[48] Kuijpers J.P., Pringle J.E., 1982, A&A, 114, L4

[49] Lang K.R. 1991, in Astrophysical Data: Planets and Stars, Springer-Verlag

[50] Lang K.R. 1998, Astrophysical Formulae, 3rd edition(Vol. 1), Springer-Verlag

[51] Lesch H., 1991, A&A, 245, 48

[52] Lubow S.H. & Shu F.H. 1975, ApJ, 198, 383

[53] McDermott P.N., Taam R.E., 1989, ApJ, 342, 1019

[54] Meintjes P.J., Raubenheimer B.C., de Jager O.C., Brink C., Nel H.I., North A.R., van Urk G., Visser B., 1992, APJ, 401, 325

[55] Meintjes P.J., de Jager O.C., Raubenheimer B.C., Nel H.I., North A.R., Buckley D.A.H., Koen C., 1994, ApJ,434, 292

[56] Meintjes P.J. & de Jager O.C. 2000, MNRAS, 311, 611

[57] Meintjes P.J. 2002a, in Flanagan C.S., Frescura F.A.M, Woerman B.,(eds.), Proceedings of the Pulsar studies in Africa workshop, African Skies no 7, 5

[58] Meintjes, P.J. 2002b, MNRAS, 336, 265

[59] Mestel L., Spruit H.C., 1987, MNRAS, 226, 57

[60] Mestel L., 1999, in Stellar Magnetism, Clarendon Press, Oxford

[61] Pacholzyk A.G. 1970, Radio Astrophysics (W.H. Freeman and Co.: San Francisco)

[62] Parker E.N. 1957, Phys. Rev. 107, 830

[63] Parker E.N. 1958, ApJ, 128, 664

[64] Parker E.N. 1976, The physics of non-thermal radio sources, G. Seti (ed.), D. Reidel Publishing company, Dordrecht-Holland, p. 137 - 167

[65] Parker E.N. 1963, ApJS, 8, 177

[66] Parker E.N. 1979, in Cosmical Magnetic Fields: Their Origin and Activity. Oxford Univ. Press, Oxford

[67] Patterson J., 1979, ApJ, 234, 978

[68] Patterson J., 1994, Publ. Asron. Soc. Pac., 106, 209

[69] Petschek H.E., 1964, AAS-NASA Symposium on the physics of solar flares, NASA Special publications SP-50, p.425

[70] Plavec M., 1958, Mem. Soc. R. Sci. Liege(4)., 20, 11

[71] Priest E.R., 1981, in Priest ed., Solar Flare Magnetohydrodynamics. Gordon & Breach, New York, p.139

[72] Priest E., Forbes T., 2000, Magnetic Reconnection: MHD Theory and Applications, p. 120-130, 460-509, Cambridge University Press, Cambridge

[73] Pringle, J.E. 1985, in Interacting Binaries, eds. J.E. Pringle & R.A. Wade, Cambridge Univ. Press, Cambridge, p.1

[74] Rybicki G.B., Lightman A.P., Radiative processes in astrophysics, New York, Wiley-Interscience 1979 (R & L)

[75] Saar S.H. 1991, in eds. Tuominen I., Moss D., Rudiger G., The sun and cool stars: activity, magnetism, dynamos. Springer, Berlin

[76] Sarris E.T., Krimigis S.M., 1985, ApJ, 298, 676

[77] Smak J., 1984, Publ. Amer. Astron. Soc. Pac., 96, 5

[78] Sweet P.A., 1958, Electromagnetic Phenomena in Cosmical Plasmas, IAU Aymp. 6, ed. B. Lehnert, Cambridge University Press, p. 123-134

[79] Tanzi E.G., Chincarini G, Tarenghi M., 1981, PASP, 93, 68

[80] Toptyghin I.N., 1980, Space Sci. Rev. 26, 157-213

[81] van der Laan, H., 1963, MNRAS, 126, 535

[82] van der Laan, H., 1966, Nature, 211, 1131

[83] Verbunt, F. 1982, Sp. Sci. Rev., 32, 379

[84] Wang Y.M. 1987, A&A, 183, 257

[85] Walker M.F., 1954, Publ. Astr. Soc. Pacific. 66, 230

[86] Warner B. & Wickramasinghe D.T. 1991, MNRAS, 248, 370

[87] Warner B., 1995, Cataclysmic Variable Stars, Cambridge Univ. Press, Cambridge

[88] Welsh W.F., Horne K., & Oke J.B., 1993, ApJ, 401, 229

[89] Welsh W.F., Horne K., & Gomer R., 1998, MNRAS 298, 285

[90] Westfold K.C., 1959, Ap.J. 130, 241

[91] Wood F.B., 1950, ApJ, 112, 196

[92] Woodsworth A.W., Hughes V.A., 1976, ApJ 208, 863

[93] Wynn G.A., King A.R., 1995, MNRAS, 275,9

[94] Wynn G.A., King A.R., Horne, K., 1997, MNRAS, 286, 436

[95] Zinner, E. 1938 Astron. Nach., 265, 345

Mon. Not. R. Astron. Soc. **341**, 891–900 (2003)

Modelling the continuous radio outbursts in AE Aquarii

P. J. Meintjes★ and L. A. Venter
Department of Physics, University of the Free State, Bloemfontein, 9300, South Africa

Accepted 2003 January 24. Received 2003 January 21; in original form 2002 October 17

ABSTRACT

In this paper an attempt is made to simulate the non-thermal radio spectrum of the enigmatic nova-like variable AE Aquarii. Earlier radio studies of AE Aquarii suggested that the radio flares originate from expanding synchrotron-emitting clouds in terms of a van der Laan process. Recent studies also indicate that expanding blob-like propeller-ejected outflow from the system may be the source of the optical flares from AE Aquarii. In this paper we model the radio to infrared flares from AE Aquarii in highly magnetized blob-like propeller-ejected outflow. We showed that the secondary star can possess surface magnetic fields of the order of $B_0 \geqslant 2000$ G. Through turbulence and subsequent reconnection, magnetic flux can be pinched off into a fraction of the mass transfer flow from the secondary star. These fields can be highly twisted, resulting in localized regions where the blob plasma is magnetically dominated, i.e. $\beta = (8\pi nk_{\rm B}T/B^2) < 1$. It was shown that the condition $\beta \leqslant 1$ constrains the frozen-in magnetic field in the blobs to $B_{\rm blob} \geqslant 2000$ G, which is of the same order of magnitude as the inferred stellar field. The total radio to infrared flare spectrum was modelled in terms of expanding magnetized synchrotron-emitting blobs in various stages of their evolution from $\rho = (r/r_0) = 1 \rightarrow 400$. In terms of our model we consider processes such as magnetic reconnection to provide a fast impulsive injection of 1–2 MeV electrons in regions where the condition for effective acceleration, i.e. $\beta \leqslant 1$, is satisfied. As these blobs expand ($\rho > 1$), mechanisms such as shock drift acceleration and magnetic pumping can further energize electrons, in regions where $\beta \leqslant 1$, to energies of the order of $\gamma \rightarrow 20$. It was shown that the total integrated flux during outbursts, over the frequency range from 1 to 50 000 GHz, can be the result of several (~10–20), initially highly magnetized ($B_0 \sim 2000$–3000 G) synchrotron-emitting blobs in different stages of their evolution. The simulated spectrum corresponding to $B_0 \approx 2000$ G (~20 blobs), showed that a peak flux of $S_\nu \sim 148$ mJy is produced at $\nu \sim 1805$ GHz (~166 μm), while a spectrum corresponding to $B_0 \approx 3000$ G (~10 blobs), results in a peak synchrotron flux of $S_\nu \sim 134$ mJy at $\nu \sim 2410$ GHz (~125 μm). In terms of a multiflare van der Laan superposition, these are obtained where the spectrum changes from a typical self-absorbed $S_\nu \propto \nu^\alpha$ to $S_\nu \propto \nu^{-(\delta-1)/2}$. In terms of the scenarios described above, this may place the latest detection (5σ level) at $\nu = 3333$ GHz ($S_\nu \approx 113$ mJy), already in the optically thin part of the spectrum.

Key words: accretion, accretion discs – binaries: general – stars: magnetic fields – stars: mass-loss – stars: winds, outflows – white dwarfs.

1 INTRODUCTION

The unique multiwavelength properties of the cataclysmic variable AE Aquarii have resulted in this source being the continuous focus of attention of multiwavelength studies, in wavelengths ranging from radio to TeV gamma-rays (e.g. Meintjes 1992, 2002a,b; Meintjes et al. 1992, 1994; Meintjes & de Jager 2000; Warner 1995). Since numerous reports on the multiwavelength emission properties of this system already exist (e.g. Meintjes 1992; Meintjes & de Jager 2000; Meintjes 2002a,b), only a short summary of the basic properties of the system, relevant to this study, will be presented.

Since the nova-like variable AE Aquarii displays similar properties in optical and X-ray wavelengths to DQ Her (e.g. Patterson 1979; Patterson et al. 1980), it was classified as a DQ Her-type cataclysmic variable during earlier studies. The system consists of a K4-5 secondary star and a white dwarf orbiting their common centre of mass with a period of $P_{\rm orb} = 9.88$ h. Faint $P_* = 33.08$ s

★E-mail: meintjpj@sci.uovs.ac.za

pulsations in the optical range are associated with the spin period of the white dwarf (Patterson 1979). This implies that AE Aquarii has the fastest rotating accreting white dwarf known to date. A long-term analysis of the spin period of the white dwarf in AE Aquarii (de Jager et al. 1994) shows that it is spinning down at a rate of $\dot{P} = 5.6 \times 10^{-14}$ s s^{-1}, resulting in an inferred spin-down power of $P_{sd} \approx 10^{34}$ erg s^{-1}. The system shows rapid flaring in the optical range (e.g. Patterson 1979; van Paradijs, Kraakman & van Amerongen 1989) with the optical intensity varying between $m_v = 10$ and 12 on a regular basis, initially believed to be the result of enhanced mass accretion on to the magnetic poles of the white dwarf. However, there is a peculiarly weak correlation between the amplitude of the 33-s oscillation and increased intensity during optical outbursts (e.g. Patterson 1979; Meintjes 1992; Meintjes et al. 1994; O'Donoghue et al. 1995), casting doubt on whether enhanced mass accretion on to the poles is the source of the optical outbursts. Cropper (1986) and later Beskrovnaya et al. (1995) reported circular polarization at the level of (0.05 ± 0.01) and (0.10 ± 0.03) per cent, respectively, in the optical light, which, if produced by cyclotron emission, may indicate a magnetic field in excess of $B_* \sim 10^6$ G (Chanmugam & Frank 1987). It was shown recently (Patterson 1994; Wynn, King & Horne 1995, 1997; Eracleous & Horne 1996; Meintjes & de Jager 2000) that the fast rotating (~33 s), highly magnetized (~10^6 G) white dwarf will act as a magnetohydrodynamic (MHD) propeller, ejecting a fragmented blob-like mass transfer flow of $\dot{M}_2 \sim (0.5\text{–}1.0) \times 10^{18}$ g s^{-1} (Eracleous & Horne 1996) from the system. Eracleous & Horne (1996) also showed that radiative cooling of ejected gas blobs is most probably the source of the optical outbursts in AE Aquarii, explaining the weak correlation between optical flaring and the amplitude of the 33.08-s optical oscillations during flares.

In this paper an attempt is made to model the nearly continuous radio outbursts in AE Aquarii, the nature of which will be discussed in detail in Section 2. The key ingredient of our model is that we propose that the mass transfer flow from the secondary star is fragmented into magnetized blobs, while earlier studies (e.g. King 1993; Wynn & King 1995) consider the mass transfer flow in the polar and intermediate polar subclasses of magnetic cataclysmic variables to be fragmented into diamagnetic blobs. We argue that the frozen-in magnetic flux of the fragmented mass flow (blobs) has its origin in a strongly magnetized secondary star. By using a Mestel & Spruit (1987) magnetic wind model, with accompanying magnetic braking, in tandem with the current converging evolution of the binary system (Meintjes 2002a,b), the surface magnetic field of the K4-5 secondary star in AE Aquarii is constrained to values of the order of $B_0 \approx 2000$ G. It is therefore possible that a fraction of the mass transfer flow from the secondary can possess strong frozen-in fields of similar magnitude that become tangled as a result of turbulence and reconnection in the blob (Priest & Forbes 2000; Spruit 2002, private communication). It will be shown that both synchrotron and adiabatic loss times in the propeller-ejected magnetized blobs are longer than realistic acceleration time-scales in regions where the blob is magnetically dominated, i.e. $\beta \leqslant 1$. Reconnection in blobs in the initial stages of their evolution, $\rho = (r/r_0) \approx 1$ can accelerate particles effectively to $\gamma \sim 2$, in $\beta \leqslant 1$ regions. Continued acceleration in $\beta \leqslant 1$ regions via several processes can result in the electron energies to approach $\gamma \sim 20$ as the blobs are propelled out of the system. Synchrotron emission from these expanding bubbles will then be the origin of the non-thermal flares. It will be shown that with this model the total non-thermal radio to infrared emission can be explained, as can the correct shape of the non-thermal spectrum.

The paper will be structured as follows. In Section 2 an overview is given of the nature of the non-thermal radio outbursts in AE Aquarii, deduced from observations. In Section 3 we discuss how the evolution of the system (Meintjes 2002a,b) and magnetic stellar wind theory are used to place constraints on the surface field strength of the K4-5 secondary star, which, according to our model, may play a vital role in the production of the radio flares in AE Aquarii. In Section 4 mechanisms of particle acceleration in magnetic blobs and the van der Laan (VDL) model used to model individual flares are briefly discussed. In Section 5 a detailed discussion of our modelling of the radio flares and the combined radio spectrum is presented, with a discussion following in Section 6.

2 RADIO OBSERVATIONS OF AE AQUARII

The first manifestation of the non-thermal properties of this system was the discovery of variable non-thermal radio emission (Bookbinder & Lamb 1987) at $\nu = 1.4$ and 5 GHz, respectively. Immediately after this first campaign, AE Aquarii was observed again with the VLA at 1.5, 4.9, 15 and 22.5 GHz, revealing nearly continuous radio synchrotron outbursts superimposed on a weak quiescent background emission (Bastian, Dulk & Chanmugam 1988), mimicking Cyg X-3, just on a lower scale. This variable radio emission was interpreted as non-thermal ($10^9 < T_B < 10^{12}$ K) incoherent flares involving relativistic electrons with energies $\gamma \approx 3\text{–}30$ (Bastian et al. 1988). The general time-averaged shape of the radio spectrum up to 15 GHz resembled a self-absorbed power law $S_\nu \sim S_0 \nu^\alpha$ with an index $\alpha = 0.3\text{–}0.4$ (Bastian et al. 1988). More recent radio and infrared (IR) observations (Abada-Simon et al. 1993, 1995a,b, 1999, 2002) to frequencies $\nu \sim 3333$ GHz revealed similar outbursts, and confirmed that the self-absorbed spectrum extends possibly up to $\nu \sim 3333$ GHz. However, the authors cautioned that the measured flux level at 3333 GHz is also consistent with the optically thin part of the radio spectrum after the turning point. The detection at 3333 GHz (90 μm) corresponds to a measured flux level (at 5 σ level) of $S_\nu \sim 113$ mJy (Abada-Simon et al. 2002), different from their earlier reports (Abada-Simon et al. 1999), which put the detection at the 3.1σ significance level and a flux close to $S_\nu \sim 180$ mJy. It is anticipated that the detection of the 3333-GHz emission must be very close to the turning point of the self-absorbed spectrum, since *IRAS* only obtained three ~200-mJy upper limits (Abada-Simon et al. 2002) at 12, 25 and 60 μm, respectively (i.e. 25 000, 11 538 and 5000 GHz). The time-averaged spectrum up to 3333 GHz is approximately $S_\nu = S_1(\nu/1\ \text{GHz})^{1/2}$, with $S_1 \approx 3.15$ mJy (Abada-Simon et al. 1999, 2002).

The variability of the observed radio emission and the resultant spectrum was explained in terms of a superposition of optically thick expanding magnetized synchrotron-emitting clouds ejected by the binary (Bastian et al. 1988). This model was first applied by van der Laan (1963, 1966) to explain variable radio emission in radio galaxies. Very long baseline interferometry (VLBI) observations of AE Aquarii during a radio flare indicate that the source expands with a velocity of the order of $v_{exp} \sim 0.01c$, where c is the speed of light (A. E. Niell, private communication), reaching sizes of ~4 orbital radii during large flares. As these plasmoids expand they become optically thin to the synchrotron emission, showing a spectrum $S \propto \nu^{-(\delta-1)/2}$, where δ is the spectral index of the electron spectrum. Extending the search to frequencies where the emission is optically thin will provide valuable information regarding the efficiency of the acceleration process in AE Aquarii. The frequency at which the spectrum turns over from optically thick to optically thin, i.e. ν_m,

will correspond to the maximum flux density S_0 which is related to the initial blob size r_0 and magnetic field B_0 of these plasmoids.

No information regarding the nature of the flaring is obtained with the latest detection at 90 μm (3333 GHz). However, the non-thermal spectrum (see Abada-Simon et al. 1999, 2002) indicates that the flux density is not compatible with flux densities obtained in the J, H, K and L bands (Tanzi, Chincarini & Tarenghi 1981), which is definitely the spectrum of the secondary star (Abada-Simon et al. 1999, 2002). This strengthens the conjecture of the non-thermal nature of the observed radio emission. The maximum observed non-thermal flux, $S_{\max} \sim 113\ (\nu_{\max}/3333\ \mathrm{GHz})^{1/2}$ mJy, results in a maximum non-thermal radio to IR luminosity of

$$L_{\mathrm{R-IR}} \approx 5 \times 10^{30} \left(\frac{\Omega}{4\pi}\right) \left(\frac{S_0}{113\,\mathrm{mJy}}\right) \left(\frac{D}{100\,\mathrm{pc}}\right)^2 \mathrm{erg\,s^{-1}}. \quad (1)$$

This maximum non-thermal radio luminosity inferred from the radio spectrum of AE Aquarii is several orders of magnitude lower than the spin-down power of the magnetized white dwarf, i.e.

$$\beta \sim \left(\frac{L_{\mathrm{R-IR}}}{I\Omega\dot{\Omega}}\right) \sim 5 \times 10^{-4} \left(\frac{I\Omega\dot{\Omega}}{10^{34}\,\mathrm{erg\,s^{-1}}}\right)^{-1} \left(\frac{L_{\mathrm{R-IR}}}{5 \times 10^{30}\,\mathrm{erg\,s^{-1}}}\right), \quad (2)$$

implying that only a small fraction of the spin-down power is converted to non-thermal power.

3 MAGNETIZED FRAGMENTED MASS TRANSFER

It was shown in previous papers (Meintjes 2002a,b) that the AE Aquarii binary system is currently most probably in a converging phase of its evolution (e.g. King 1988), resulting in the mass transfer between the secondary and the highly magnetized white dwarf being between $4 \times 10^{17} \leqslant \dot{M}_2 \leqslant 2 \times 10^{18}$ g s^{-1}. Mass transfer in this range is too low for the development of an accretion disc in the system given the fast rotation period of the spun-up highly magnetized white dwarf. The relatively low-mass transfer from the secondary in the current phase results in propeller-driven mass ejection from the system, with a total mechanical outflow power exceeding the power released by mass accretion by a factor of $\kappa =$ (outflow power/ accretion power) ≈ 250 (Wynn et al. 1997; Meintjes & de Jager 2000; Meintjes 2002a,b). In recent papers (Kuijpers & Pringle 1982; Frank, King & Lasota 1988; King & Lasota 1991; King 1993; Wynn & King 1995) it was pointed out that the mass transfer flow from the secondary to the primary in the intermediate polar and polar subclasses of magnetic cataclysmic variables may be clumpy or blob-like. A detailed study of the densities of the gas blobs from the secondary star in AM Her was carried out by Beardmore & Osborne (1997). They described the variability in the hard X-ray observations from AM Her, made by *Ginga*, as shot noise caused by inhomogeneous accretion of blobs with typical densities of $N_{\mathrm{blob}} \sim 10^{15}$–$10^{17}$ cm^{-3}. For these densities the blobs are probably diamagnetic, i.e. not easily penetrated by the magnetic field of the white dwarf. They may, however, be magnetized themselves, i.e. having a frozen-in magnetic field from the K4-5 secondary star, which may have a substantial surface magnetic field strength. Reconnection of flux loops in a blob in the mass transfer process, i.e. as the blobs leave the L1 region, can result in magnetic flux being pinched-off and confined to the blob, and initial particle acceleration.

The surface field of the K4-5 secondary star in AE Aquarii, i.e. the mass donor, is obtained from the condition of stable mass transfer in binary systems where the mass transfer process is driven by magnetic braking. For a mass losing system such as AE Aquarii, detailed calculations by Wynn & King (1995) and Meintjes (2002b) showed that stable mass transfer in the converging phase of the evolution of a binary system must satisfy the condition

$$\left(\frac{-\dot{J}_{\mathrm{mb}}}{J}\right) \geqslant \left[1 - q(1-\alpha) - \frac{\alpha}{2}\left(\frac{M_2}{M}\right) - \eta\left(\frac{M}{M_1}\right)^{1/2}\left(\frac{R_{\mathrm{circ}}}{a}\right)^{1/2}\right]\left(\frac{-\dot{M}_2}{M_2}\right), \quad (3)$$

where η is the fraction of the angular momentum, in terms of Roche lobe overflow across L1, being ejected from the binary (e.g. King & Lasota 1991; King 1993; Wynn & King 1995) and where α is the fraction of the mass overflow from the secondary being propelled out of the system by the propeller. In the current propeller phase of AE Aquarii we have $\eta \approx 1$ and $\alpha \approx 1$.

The mass transfer rate in AE Aquarii is constrained by the minimum required mass transfer that can explain the emission lines from the system, i.e. $\dot{M}_2 \geqslant 4 \times 10^{17}$ g s^{-1} (Eracleous & Horne 1996) and the maximum allowed rate that would still result in a converging evolution $\dot{M}_2 \leqslant 2 \times 10^{18}$ g s^{-1} (McDermott & Taam 1989; Meintjes 2002b). By adopting the Mestel & Spruit (1987) stellar wind model of magnetic braking in the fast rotator limit, i.e. $(\Omega_2/\Omega_\odot) = (\mathrm{P}_\odot/P_2) \gg 1$, assuming the rotation period of the secondary star is tidally locked with the orbital period of the system, the orbital angular momentum loss via stellar wind from the secondary in AE Aquarii, and hence magnetic braking, is derived from the basic stellar wind equations (e.g. Campbell 1997):

$$\frac{\dot{J}_{\mathrm{mb}}}{J_{\mathrm{orb}}} \approx 5.8 \times 10^{-21} \left(\frac{\bar{r}}{R_2}\right)^{-5/3} \left(\frac{P_{\mathrm{orb}}}{9.88\,\mathrm{h}}\right)^{8/3} \left(\frac{M_1}{0.9\,\mathrm{M}_\odot}\right)^{-1} \times \left(\frac{M_2}{0.6\,\mathrm{M}_\odot}\right)^{-4/3} \left(\frac{M}{1.5\,\mathrm{M}_\odot}\right)^{1/3} \left(\frac{B_0}{\mathrm{B}_\odot}\right)^{(4n+2)/3n} \quad (4)$$

for a stellar field depending on the dynamo number n. As an independent check, the same calculation was repeated for a model where the stellar field scales with the inverse turbulent Rossby number (Saar 1991; Campbell 1997)

$$\frac{\dot{J}_{\mathrm{mb}}}{J_{\mathrm{orb}}} \approx 4.2 \times 10^{-21} \left(\frac{\bar{r}}{R_2}\right)^{-5/3} \left(\frac{P_{\mathrm{orb}}}{9.88\,\mathrm{h}}\right)^{20/9} \left(\frac{M_1}{0.9\,\mathrm{M}_\odot}\right)^{-1} \times \left(\frac{M_2}{0.6\,\mathrm{M}_\odot}\right)^{-4/9} \left(\frac{M}{1.5\,\mathrm{M}_\odot}\right)^{1/3} \left(\frac{B_0}{B_\odot}\right)^{2}, \quad (5)$$

where in both models $\bar{r}/R_2$ represents the ratio of the wind dead zone to stellar radius for the secondary star (Mestel & Spruit 1987; Campbell 1997), and where $(B_0/\mathrm{B}_\odot)$ is the ratio of the stellar to solar surface polar magnetic field strength. The condition for stable mass transfer in AE Aquarii in the current propeller-driven mass losing phase ($\alpha \approx 1$; $\eta \approx 1$) is

$$\frac{\dot{J}_{\mathrm{mb}}}{J} \geqslant 5.25 \times 10^{-16} \left(\frac{\dot{M}_2}{2 \times 10^{18}\,\mathrm{g\,s^{-1}}}\right) \left(\frac{M_2}{0.6\,\mathrm{M}_\odot}\right)^{-1} \mathrm{s^{-1}}. \quad (6)$$

In the fast rotator limit $(\mathrm{P}_\odot/P_2) \approx 70$, applicable to AE Aquarii, the ratio $(\bar{r}/R_2) \approx 3$–5 (e.g. Campbell 1997). This results in estimates for the polar value of the magnetic field of the secondary star, for

a linear $n = 1$ dynamo model and the inverse Rossby number law, respectively, which are

$$B_0 \geqslant 1900 \left(\frac{\mathrm{B}_\odot}{2\,\mathrm{G}}\right)\left(\frac{\dot{M}_2}{2\times10^{18}\,\mathrm{g\,s^{-1}}}\right)^{1/2}\left(\frac{P_{\mathrm{orb}}}{9.88\,\mathrm{h}}\right)^{-8/6}\mathrm{G} \quad (7)$$

and

$$B_0 \geqslant 2245 \left(\frac{\mathrm{B}_\odot}{2\,\mathrm{G}}\right)\left(\frac{\dot{M}_2}{2\times10^{18}\,\mathrm{g\,s^{-1}}}\right)^{1/2}\left(\frac{P_{\mathrm{orb}}}{9.88\,\mathrm{h}}\right)^{-20/18}\mathrm{G} \quad (8)$$

using (M_2/0.6 $\mathrm{M}_\odot$), (M_1/0.9 $\mathrm{M}_\odot$) and (M/1.5 $\mathrm{M}_\odot$). Both estimates show that the polar value for the surface field of the secondary star can reach values up to $B_0 \approx 2000$ G for a Mestel & Spruit (1987) stellar wind model. Turbulent fluid motions near the L1 point can result in reconnection of the magnetic field frozen in the mass transfer flow, resulting in pinch-off of flux into the blobs that leave the L1 region. Turbulent fluid motions inside the blobs may also result in the field to obtain contorted and twisted, resulting in localized magnetic knots inside the blobs (Spruit 2002, private communication). In these regions the blob may be magnetically dominated, i.e. ratio of the gas pressure ($nk_{\mathrm{B}}\,T$) to the magnetic pressure ($B^2/8\pi$), i.e. $\beta = (P_{\mathrm{gas}}/P_{\mathrm{mag}}) \leqslant 1$. The minimum magnetic field for a $\beta \leqslant 1$ plasma can be obtained from equipartition between gas and magnetic pressure in the blob. There is observational evidence from *Ginga* data that the accretion flow may be clumpy, with particle densities of between $N_{\mathrm{p}} \approx 10^{15}$–$10^{17}$ cm^{-3} (Beardmore & Osborne 1997; Meintjes 2002b), with typical temperatures of the order of $T_{\mathrm{b}} \approx 10^4$ and 10^5 K (Eracleous & Horne 1996). Therefore, the minimum field strengths implying a $\beta \leqslant 1$ fluid inside blobs, which leave the L1 region with sizes comparable to the white dwarf radius ($r_0 \approx 10^9$ cm) are of the order of

$$B_{\mathrm{eq}} \geqslant 2300 \left(\frac{N_0}{10^{16}\,\mathrm{cm^{-3}}}\right)^{1/2}\left(\frac{T_{\mathrm{b}}}{10^5\,\mathrm{K}}\right)^{1/2}\left(\frac{\rho}{\rho_i}\right)^{-3/2}\mathrm{G}, \quad (9)$$

where the particle density in the expanding blobs is assumed to scale such as $N_{\mathrm{p}} = N_0\rho^{-3}$, where $\rho = (r/r_0)$ represents the blob size at any given instant. It is interesting to note that the minimum magnetic field satisfying $\beta \leqslant 1$ is of the same magnitude as the inferred polar coronal base field of the K4-5 secondary star, definitely what one would expect if a magnetic field of the magnitude of the surface field of the secondary ($B \sim 2000$ G) is transferred to the fragmented mass transfer flow through turbulence and accompanying reconnection. The attractive feature of magnetic knots inside the blobs is that the drop-off of magnetic intensity in their vicinity is approximately according to $B \geqslant B_0\rho^{-3/2}$, in contrast to blobs with a uniform isotropic magnetic intensity distribution, decreasing upon expansion according to $B = B_0\rho^{-2}$ (e.g. van der Laan 1963, 1966). This will have very important consequences for the radio emission from relativistic electrons inside the blobs since it will enable an electron population with moderate energies (1–10 MeV) to account for all the non-thermal radio to infrared emission up to ~50 000 GHz. These energies are much lower than the electron energies of the order of $E_{\mathrm{e}}{}^- \sim 100$ MeV, inferred from earlier studies (Abada-Simon et al. 1999, 2002; Meintjes & de Jager 2000). This is because synchrotron theory predicts that moderate energy electrons can still radiate to high frequencies in strong magnetic fields, i.e. $\nu_{\mathrm{c}} \propto \gamma^2 B_{\mathrm{blob}}$.

The magnetohydrodynamic interaction between the fast rotating white dwarf magnetic field and the clumpy mass transfer flow is most probably a very complex process, the exact details of which fall outside the scope of this paper. However, one can show that shearing of the white dwarf magnetic field in the propeller zone, i.e. close to the circularization radius $R_{\mathrm{circ}} \approx 2 \times 10^{10}(P_{\mathrm{orb}}/9.88\,\mathrm{h})^{2/3}$ cm (Wynn et al. 1995, 1997), can result in a highly sheared white dwarf magnetospheric field of the order of $B_\phi \approx (8\dot{M}_2 v_{\mathrm{ff}}/R_{\mathrm{circ}}^2)^{1/2}$ (Meintjes & de Jager 2000), derived from equipartition between the sheared magnetic field energy density and the ram pressure in the mass flow from the secondary star, resulting in field strengths of

$$B_\phi \approx 3500 \left(\frac{\dot{M}_2}{10^{18}\,\mathrm{g\,s^{-1}}}\right)^{1/2}\left(\frac{M_{\mathrm{wd}}}{0.9\,\mathrm{M}_\odot}\right)^{-1/4}\left(\frac{R}{R_{\mathrm{circ}}}\right)^{-5/4}\mathrm{G}. \quad (10)$$

It was shown (Meintjes & de Jager 2000) that the magnetohydrodynamic power dissipated in the propeller zone where the blobs are expelled from the binary system is of the order of

$$P_{\mathrm{MHD}} \sim 10^{34}\left(\frac{B_\phi}{3500\,\mathrm{G}}\right)^3\left(\frac{N_{\mathrm{p}}}{10^{16}\,\mathrm{cm^{-3}}}\right)^{-1/2}\mathrm{erg\,s^{-1}}, \quad (11)$$

where N_{p} represents the average blob gas particle density at R_{circ}. This dissipated magnetohydrodynamic power in the ejection zone is spinning the white dwarf down. As a result the spin-down power of the white dwarf, i.e. $P_{\mathrm{sd}} \approx 10^{34}$ erg s^{-1} (de Jager et al. 1994), inferred from the observed spin-down of the white dwarf, correlates well with the dissipated MHD power. The magnetohydrodynamic power that is dissipated in the propeller zone is sufficient to drive the mechanical mass outflow from the system at a rate of

$$P_{\mathrm{mech}} \leqslant 10^{34}\left(\frac{\dot{M}_2}{10^{18}\,\mathrm{g\,s^{-1}}}\right)\left(\frac{v}{v_{\mathrm{esc}}}\right)^2\mathrm{erg\,s^{-1}} \quad (12)$$

with an escape velocity $v_{\mathrm{esc}} \approx 1550$ km s^{-1}. As the blobs are ejected from the system they will cool radiatively, which is most probably the mechanism causing the optical flares seen from AE Aquarii (Eracleous & Horne 1996).

The severe interaction between the fast rotating magnetic propeller and the blobs may also result in a small fraction of the spin-down power of the white dwarf being pumped into particle acceleration in dense magnetized blobs, with resulting radio emission through the van der Laan process as these blobs expand. To an order of magnitude, one can estimate the energy pumped into expanding blobs as the white dwarf magnetic field sweeps over and compresses them. The MHD power pumped into expanding blobs by the rotating magnetic field of the white dwarf is

$$L_{\mathrm{blob}} \approx \left[\frac{B^2(r)}{8\pi}\right]\left(\frac{4\pi}{3}\right)R_{\mathrm{b}}^3\Omega_* \leqslant 10^{32}\left(\frac{B_*}{2\times10^6\,\mathrm{G}}\right)^2\left(\frac{P_{\mathrm{wd}}}{33\,\mathrm{s}}\right)^{-1}\left(\frac{R_{\mathrm{wd}}}{10^9\,\mathrm{cm}}\right)^3\mathrm{erg\,s^{-1}}. \quad (13)$$

This power is sufficient to excite processes resulting in particle acceleration and non-thermal radio emission from expanding blobs given that the maximum radio luminosity from AE Aquarii, derived from the Abada-Simon et al. (1999, 2002) spectrum, up to 3333 GHz is approximately $L_{\mathrm{R-IR}} \leqslant 10^{31}$ erg s^{-1}. These processes will be the focus of the rest of the paper.

4 PARTICLE ACCELERATION AND THE VDL MODEL

The model proposed in this paper is dependent on the fact that dense, strongly magnetized, gas blobs may be among the stream of ejected mass transfer propelled out of the system by the propeller mechanism. It is proposed that particle acceleration can occur in the blobs as a result of the severe battering from the propeller, leading to radio flares as these blobs expand. The model presented in this paper

differs from the model of Kuijpers et al. (1997) that links the radio flares to clouds of relativistic synchrotron-emitting electrons, magnetically pumped in the white dwarf magnetosphere and released through some magnetospheric instability.

It will be shown that processes such as magnetic reconnection can provide a quick impulsive energizing phase of the thermal electron population in these blobs to energies of approximately 1–2 MeV, and that continuous re-acceleration occurs in the blobs via processes such as shock drift acceleration in oblique shock fronts, adiabatic compression and magnetic pumping via Alfvén waves, resulting in heating of electrons to energies approaching $\gamma \approx 20$ as the blobs reach $\rho = (r/r_0) \approx 400$. The radio spectrum is then a superposition of several ($N \leqslant 20$) radio-emitting expanding blobs in different stages of their evolution. Since the initial acceleration and the continued re-acceleration of the electron population in the blobs play such an important role in the model, a qualitative but relevant discussion will be given of the various processes and stages that are of relevance to our model.

4.1 Particle acceleration processes in magnetized blobs

4.1.1 Phase I: magnetic reconnection

Magnetic reconnection as a mechanism to convert magnetic energy to particle energy in the from of thermal heating and possibly also acceleration is well documented e.g. Priest & Forbes (2000, and references therein). The mechanism occurs when field lines of opposite polarity merge at neutral points where $B = 0$. In the standard steady-state Sweet–Parker model (Sweet 1958a,b; Parker 1958, 1963) the rate at which magnetic fields merge in a highly conducting fluid scales as $M_m \propto (R_m)^{-1/2}$ (e.g. Priest & Forbes 2000 for a discussion), where R_m is the magnetic Reynolds number, which can be very large for perfectly conducting fluids. In terms of the Petschek model (Petschek 1964) the diffusion region of the magnetic field is much smaller than the global length-scale of the field, and merging of field lines are facilitated by shocks, accelerating the fluid from the diffusion region and therefore also accelerating the inflow of the fields of opposing polarity towards one another. This results in the rate of merging to scale according to $M_m \propto [\log(R_m)]^{-1}$ (e.g. Priest & Forbes 2000 for a discussion). This will dramatically increase the effectivity of reconnection as a mechanism for converting magnetic energy to thermal particle heating and possibly also acceleration.

We argue that magnetic reconnection through the fast Petschek (1964) mechanism as a result of turbulent fluid motions in fragments of the mass transfer flow can be initiated in localized regions. It can be shown (e.g. Parker 1976 for a discussion) that the electric field generated through this process is of the order of

$$E \approx -\frac{c}{4\pi\sigma}\left(\frac{\partial B}{\partial x}\right)_0, \tag{14}$$

where $\sigma \approx 3.22 \times 10^6 T^{1/2}$ esu (e.g. Benz 1994) is the Coulomb conductivity of the fluid, and $(\partial B/\partial x)_0$ represents the magnetic flux gradient near the neutral point in the reconnection zone. Since the electrical conductivity of astrophysical fluids is very high, the Petschek mechanism is only effective in producing strong electric fields if the magnetic reconnection takes place over a very small scalelength in comparison with the dimension of the blob (Petschek 1964; Parker 1976; Priest & Forbes 2000). To convert the magnetic field energy through reconnection to relativistic particles, instead of Ohmic heating of gas, reconnection has to occur in regions where the plasma is magnetically dominated instead of gas dominated, i.e. $\beta \leqslant 1$. Therefore, Petschek reconnection in localized regions in blobs where $\beta \leqslant 1$ (magnetic knots), satisfying the condition that the reconnection length ($l_{\rm rec}$) and acceleration length ($l_{\rm acc}$) should comprise a very small fraction of the initial blob size, e.g. $(l_{\rm rec}/r_0)$ and $(l_{\rm acc}/r_0) \leqslant 10^{-2}$, one can show for initial blob dimensions of the order of $r_0 \approx 10^9$ cm and a typical $\beta \leqslant 1$ blob field of $B_{\rm eq} \approx 2300$ G that magnetic reconnection can accelerate charged particles such as electrons to energies of the order of

$$\varepsilon_{\rm e} \leqslant 1.6\left(\frac{B_{\rm eq}}{2300\,{\rm G}}\right)\left(\frac{T_{\rm b}}{10^5\,{\rm K}}\right)^{-1/2}\left(\frac{l_{\rm rec}}{10^{-2}r_0}\right)^{-1}\left(\frac{l_{\rm acc}}{10^{-2}r_0}\right)\ {\rm MeV}. \tag{15}$$

Initially, in a highly magnetized $B_{\rm b,i} \approx 2000$ G, dense $N_{\rm p,i} \approx 10^{16}$ cm^{-3} plasma, synchrotron losses of mildly relativistic electrons will be the dominant energy loss mechanism. For sufficient acceleration initially, reconnection must occur on a shorter time-scale than the synchrotron loss time-scale for $\varepsilon_{\rm e} \sim 1$ MeV electrons, which is

$$t_{\rm s,i} \approx 1\left(\frac{\gamma}{2}\right)^{-1}\left(\frac{B}{2300\,{\rm G}}\right)^{-2}\ {\rm min}. \tag{16}$$

Reconnection can typically occur on time-scales $\tau_{\rm rec} \approx (l_{\rm rec}/v_i)$ where $l_{\rm rec}$ and v_i represent the length-scale of magnetic reconnection and speed at which the field lines approach one another, typically a fraction ($\beta \sim 0.1$) of the Alfvén speed [$v_{\rm A} = (B/\sqrt{4\pi\rho})$, i.e. $v_i \approx 0.1(B/\sqrt{4\pi\rho})$ (Parker 1976; Priest 1981)]. Since we consider $l_{\rm rec} \approx 10^{-2}r_0$, we can see that the reconnection and hence acceleration time-scale is approximately

$$\tau_{\rm rec} \approx 20\left(\frac{l_{\rm rec}}{10^{-2}r_0}\right)\left(\frac{v_i}{0.1v_{\rm A}}\right)^{-1}\ {\rm s}, \tag{17}$$

which is significantly shorter than the synchrotron loss time-scale.

4.1.2 Phase II: shock drift acceleration and magnetic pumping

As the battered magnetic blobs are heated and expand, the frozen-in magnetic field of the blob will decrease correspondingly as the blobs grow in size. Magnetic reconnection in regions where $\beta \leqslant 1$ could have energized a fraction of the electron population of the blobs, i.e. the suprathermal tail of the MB distribution in reconnection zones, which can be re-accelerated as the blobs expand. In this phase expansion losses ($t_{\rm exp} \sim r/v_{\rm exp}$) of the blobs take over from synchrotron losses as the dominant energy loss mechanism, i.e.

$$t_{\rm s} \approx 50\left(\frac{\gamma}{20}\right)^{-1}\left(\frac{B}{100\,{\rm G}}\right)^{-2}\ {\rm min} \tag{18}$$

$$t_{\rm exp} \approx 30\left(\frac{r(t)}{4a}\right)\left(\frac{v_{\rm exp}}{0.01c}\right)^{-1}\ {\rm min}, \tag{19}$$

where $t_{\rm exp}$ corresponds to a VLBI radio measurement (A.E. Niell, private communication) of a typical expanding synchrotron-emitting cloud, expanding with a speed $v_{\rm exp} \sim 0.01c$ until it reaches a size of approximately $\rho = (r/r_0) \rightarrow 400$, corresponding to a size of approximately four times the binary separation (a) of the system (e.g. Frank, King & Raine 1992), where the binary separation is approximately

$$a \approx 10^{11}\left(\frac{P_{\rm orb}}{9.88\,{\rm h}}\right)^{2/3}\ {\rm cm}. \tag{20}$$

These relatively slow losses during the expansion phase of the blobs may be instrumental in the net gain of electron energies through the processes described below.

Acceleration of electrons is often observed in astrophysical sites where strong oblique shocks (with respect to the magnetic field) are generated in $\beta \leqslant 1$ plasmas (i.e. Eilek & Hughes 1991; Benz 1994; Priest & Forbes 2000). This mechanism, sometimes referred to as shock drift acceleration or the fast Fermi process, is responsible for huge populations of mildly relativistic electrons at interplanetary shocks (Sarris & Krimigis 1985). The maximum energization of particles by this mechanism is caused by the reflection of a particle from a mirror or shock that propagates through a medium at an angle θ with respect to field lines (e.g. Holman & Pesses 1983). In the rest frame of a particle on a field line, the shock or mirror approaches with a speed $v_{\|} = v_s \sec\theta$, where v_s is the shock velocity. A condition for a particle to be reflected from the mirror is if $v_s \sec\theta < (B_u/B_d)v_i$, with B_u, B_d and v_i representing the upstream and downstream magnetic fields and the upstream particle speed, respectively. Reflection of thermal and mildly relativistic electrons (Toptyghin 1980) from a mirror point results in a maximum energy transfer per scattering of

$$\frac{\Delta E_{\max}}{E_i} = \left[4\left(\frac{B_d}{B_u}\right) - 3\right] \quad \text{(thermal)} \tag{21}$$

$$\frac{\Delta E_{\max}}{E_i} = \left[2\left(\frac{B_d}{B_u}\right) - 1\right] \quad \text{(relativistic)}. \tag{22}$$

Since for strong shocks $(B_d/B_u) \rightarrow 4$, this mechanism implies that the energy of thermal and mildly relativistic electrons can be increased, respectively, by factors of $(\Delta E_{\max}/E_i) \rightarrow 13$ and $(\Delta E_{\max}/E_i) \rightarrow 7$ in a single encounter with a strong shock. This can result in a relatively rapid energizing of the electron population that can compete with the energy loss time-scales in this phase of the evolution of the blobs. Given the short rotation period of the white dwarf ($P_{\rm rot} \approx 33$ s) and the strong white dwarf field ($B_{\rm wd} \approx 10^6$ G) it is probable that the fast periodic sweeping of the white dwarf field across blobs can generate intense shocks in the blobs that can result in effective acceleration of particles such as electrons in regions where the shocks are collisionless (de Jager 2002, private communication), i.e. where $\beta \leqslant 1$ in the blob. One can also see that the rate at which energy is pumped into the expanding blobs (e.g. equation 13) is sufficient to drive the total observed non-thermal radio to IR emission in AE Aquarii. In particular, because of the $\sec\theta$ factor, this mechanism can have a profound effect on the effective acceleration of particles with $v_{u,i} > v_s$, i.e. the suprathermal tail of the MB distribution. Shock fronts trapped in the blobs may result in fast repeated scattering of the electron population to energies of the order of $\gamma \leqslant 20$ for all $\rho \rightarrow 400$.

Additional acceleration mechanisms that may occur in tandem with the fast Fermi process in regions where $\beta \leqslant 1$ in the blob is electron heating through adiabatic compression in a magnetic field and scattering of electrons off Alfvén waves (e.g. Parker 1976). Both of these processes can, in principle, be considered as magnetic pumping of electrons. Magnetic pumping of electrons through adiabatic compression is, in principle, a reversible process, but it can be made irreversible by wave turbulence and scattering that may isotropize the pitch angle distribution, resulting in a net acceleration of particles, even during expansion. If the shock or magnetic mirror thickness is larger than the gyroradius of the particles, particles penetrating the shock will conserve their magnetic moment, resulting in

$$\frac{p_{\perp,d}^2}{B_d} = \frac{p_{\perp,u}^2}{B_u}. \tag{23}$$

Compression parallel to the field can also occur, resulting in

$$p_{\|,d} L_d = p_{\|,u} L_u, \tag{24}$$

where L represents the longitudinal space within which the particle is confined in the field. Magnetic pumping can also be produced by travelling Alfvén waves in the magnetized plasma. In this process, which is in principle, very similar to the processes described above, magnetic disturbances in the magnetic field take on the role of magnetic pumps. Electrons can be accelerated by this mechanism and subsequently scattered in pitch angle by whistler waves. This process will result in an average energy gain by the particles

$$\left[\frac{E(t)}{E_0}\right] = \left(\frac{B_w}{B_u}\right) \sin^2\theta_0(t_0) \tag{25}$$

before they tunnel through the magnetic disturbance. In this equation B_w, B_u and θ_0 represent the magnitude of the magnetic disturbance in the wave, the upstream unperturbed magnetic field and the initial pitch angle of the particle upstream of the approaching wave, respectively. The maximum gain in energy will occur for $\theta_0 \rightarrow \pi/2$ and $(B_w/B_0) \rightarrow 4$. For continued pumping and isotropizing of pitch angles by whistler waves or turbulence in the blobs, the particle population may be sufficiently heated to mildly relativistic energies $\gamma \leqslant 20$ while the blobs expand.

Since the blobs that are propelled out of the system will be subjected to continuous battering by the propeller, the mechanisms proposed above may all occur simultaneously to pump-up the electron energies to $\gamma \sim 20$ as the blobs expand. In our modelling of the radio outbursts of AE Aquarii the electron energy as a function of $\rho = (r/r_0)$ approached $\gamma \sim 20$ asymptotically in smaller increments as $\rho \rightarrow 400$. It can be shown that the electron gyro radii $r_e = 2.4 \times 10^9\ (\varepsilon/B)$ cm (e.g. Lang 1998) inside the blobs scale as

$$r_e \approx 1\left(\frac{\varepsilon}{1\,\text{MeV}}\right)\left(\frac{B_{eq}}{2300\,\text{G}}\right)^{-1} \text{cm} \quad (\rho \rightarrow 1) \tag{26}$$

$$r_e \approx 3 \times 10^5\left(\frac{\varepsilon}{20\,\text{MeV}}\right)\left(\frac{B_{eq}}{0.28\,\text{G}}\right)^{-1} \text{cm} \quad (\rho \rightarrow 400), \tag{27}$$

clearly showing that for all $\rho = 1 \rightarrow 400$, $r_e \ll r_{\rm blob}$, but for $\rho > 400$ the gyro radius is increasing, reaching sizes $r_e \gg 1$ km that may result in the electron no longer seeing shocks in the plasma as sharp discontinuities and hence limiting the energy increase per interaction. However, it will be shown that electron energies of the order of $\gamma = 20$ are more than adequate to simulate the observed non-thermal radio to infrared fluxes from 1 to 3000 GHz.

4.2 The van der Laan model

The model incorporates a power-law electron energy distribution $n(E)\mathrm{d}E = KE^{-\delta}\mathrm{d}E$, where K is related to N (the number density of electrons with $E > E_c$), as $K = (\delta - 1)E_c^{\delta-1}N$. A single flare is taken as a blob of relativistic electrons with a magnetic field frozen into the plasma. Bastian et al. (1988) give a parametrization for a single blob or flare according to the VDL model as

$$S(\nu, \rho) = S_{m0}\left(\frac{\nu}{\nu_{m0}}\right)^{5/2} \rho^3 \times \frac{\left\{1 - \exp\left[-\tau_m(\nu/\nu_{m0})^{-(\delta+4)/2}\rho^{-(2\delta+3)}\right]\right\}}{1 - \exp(-\tau_m)}, \tag{28}$$

where S_{m0} is the maximum flux density at initial time t_0, ν_{m0} is the frequency at this maximum and τ_m is the optical depth at this frequency. The frequency ν_m depends on the radius as

$$\nu(\rho) = \nu_{m0}\rho^{-(4\delta+6)/(\delta+4)}. \tag{29}$$

Therefore, the non-thermal flux, i.e. $S(\nu, \rho)$, depends asymptotically on ν and ρ as

$$S(\nu, \rho) = \begin{cases} S(\nu)\rho^3, & \nu \ll \nu_m, \\ S(\nu)\rho^{-2\delta}, & \nu \gg \nu_m. \end{cases} \tag{30}$$

The maximum flux density (zero expansion, $\rho = 1$) can be estimated from Dulk (1985), which is summarized in Bastian et al. (1988). For single flare events we have

$$S_{m,0} = A_1 \left[A_2 \frac{\delta - 1}{\delta + 2} \left(\frac{E_c}{1\text{MeV}} \right)^{\delta - 1} N_0 \right]^{3/(2\delta+3)} \times \left[r_0^{(4\delta+9)/3} B_0^{(\delta+3)/6} \right]^{3/(2\delta+3)} \nu_m^{(7\delta+3)/(4\delta+6)} \tag{31}$$

with $A_1 = 3.3 \times 10^6 \times 2^{-\delta/2} \pi k / c^2 D^2$, $A_2 = (2.8 \times 10^7)^{(\delta+4)/2}/10^{11}$ and

$$N_0 = A_3 \left[\frac{\delta + 2}{\delta - 1} \left(\frac{E_c}{1\text{MeV}} \right)^{-(\delta-1)} \left(\frac{B_0^{2\delta+9}}{r_0} \right) \right]^{1/(\delta+5)}, \tag{32}$$

where N_0 represents the electron number density assuming equipartition between the magnetic and relativistic electron energy densities. In this equation the constant $A_3 = [3.2 \times 10^4 \times 2^{\delta/2}(10^{11})^{1/(\delta+4)}]^{(\delta+4)/(\delta+5)}$. By substituting equations (31) and (32) into equation (28), the expected flux densities of individual flare events can be modelled.

5 MODELLING THE RADIO OUTBURSTS

5.1 Energetics and blob parameters

The energy density contained in a radio-emitting blob is a combination of the relativistic electron energy density and the magnetic energy density. The electron energy distribution is taken as a power law in the VDL model. The total volume emissivity of the synchrotron source is

$$L = \int n(E) \left(\frac{-\mathrm{d}E}{\mathrm{d}t} \right) \mathrm{d}E, \tag{33}$$

where $n(E)$ and $-\mathrm{d}E/\mathrm{d}t = 2 \times 10^{-3} B^2 E^2$ erg s^{-1} represent the relativistic electron number density and the synchrotron loss rate of a single electron, respectively (e.g. Pacholzyk 1970; Lang 1998). The critical frequency (e.g. Pacholzyk 1970; Lang 1998) is $\nu_c = c_1 B E^2 (c_1 = 6.27 \times 10^{18})$. Therefore,

$$E_e(\text{erg}) = \frac{L(\text{ergs}^{-1})}{2 \times 10^{-3}} \left(\frac{3 - \delta}{2 - \delta} \right) c_1^{1/2} B^{-3/2} \left[\frac{\nu_0^{(2-\delta)/2} - \nu^{(2-\delta)/2}}{\nu_0^{(3-\delta)/2} - \nu^{(3-\delta)/2}} \right]. \tag{34}$$

The total magnetic energy in the source is E_B (erg) $= B^2 R^3 \Phi / 6$, where Φ is the fraction of volume occupied by the field and relativistic particles (e.g. Pacholzyk 1970). Then ignoring particles other than electrons it can be shown (e.g. Pacholzyk 1970) that equipartition between the magnetic field and the particle energy, minimizing the energy, gives

$$B_{\min} = \left[\frac{3}{4} \frac{C_e(\delta)}{8\pi} \frac{L(\text{ergs}^{-1})}{V_{\text{source}}} \right]^{2/7}. \tag{35}$$

From the observed spectrum of AE Aquarii (Abada-Simon et al. 1999, 2002) the maximum synchrotron luminosity of AE Aquarii was estimated to be of the order of $L_{\text{R-IR}} \sim 5 \times 10^{30}$ erg s^{-1}. It is easy to show that for initial blob radii between $r_0 \approx 10^8$ and 10^9 cm, equipartition magnetic fields in the blobs of the order of $B_{\text{blob}} \geqslant 650\text{–}2 \times 10^4$ G are implied. This confirms our previous estimate that the magnetic field strength in the blobs can be large. Bastian et al. (1988) give ranges of $r_0 = 10^9\text{–}3 \times 10^{10}$ cm and $B_0 = 25\text{–}3000$ G ($E_c = 1$ MeV, $\delta = 2.5$) within which the activity can be explained. Using equation (32), one can show that, for $\delta \approx 2.75$, the maximum non-thermal radio to infrared luminosity, in the initial phase of radiation from a single blob, is compatible with a number density of mildly relativistic electrons in a single expanding blob in the initial stages of its evolution of

$$N_0 \approx 7 \times 10^{10} \left(\frac{\epsilon}{2\,\text{MeV}} \right)^{-0.2258} \left(\frac{B_0}{2300\,\text{G}} \right)^{1.8709} \times \left(\frac{r_0}{10^9\,\text{cm}} \right)^{-0.12903} \text{cm}^{-3}, \tag{36}$$

which is several orders of magnitude lower than the average thermal particle density in the blobs, which is $N_p \approx 10^{16}$ cm^{-3}. This result is encouraging since it implies that the maximum radio to infrared luminosity can be explained by the emission of a single blob with only a small fraction of the total number of particles having mildly relativistic energies. This confirms our initial assumptions that possibly only the suprathermal tail of the MB particle distribution will be accelerated to relativistic energies in the blobs.

5.2 Radio flares using a modified VDL model

It was shown earlier that the mass transfer flow from the secondary star can consist of a fragmented flow of strongly magnetized blobs satisfying $\beta \leqslant 1$ in the blob or parts of it where the magnetic field is tangled. It was shown that these tangled fields $B_0 \geqslant 2300$ G for $\beta \leqslant 1$ in the initial phases when $\rho \approx 1$. These blobs then become expelled by the magnetic propeller and thus the radio flares are viewed as originating in these expelled gas blobs, which are treated as spherical for simplicity. Based upon a shot noise analysis of *Ginga* data of AM Her, Beardmore & Osborne (1997) estimated the initial sizes of these blobs to be of the order of $r_{\text{blob}} \sim 10^9$ cm. Currently, the secondary loses mass at a rate of $-\dot{M}_2 \sim 5 \times 10^{17}$ g s^{-1} (Meintjes 2002b and references therein) and limits the number of blobs with densities of $N_p \sim 10^{16}$ cm^{-3} and $r_0 \sim 10^9$ cm (Beardmore & Osborne 1997; Meintjes 2002b), which must account for this mass loss. An estimate of 30–60 blobs ejected every 30 min will result in a mass outflow from the system of the order of $-\dot{M}_2 \sim 0.5\text{–}1.0 \times 10^{18}$ g s^{-1}, inferred by observations (Eracleous & Horne 1996), which is also consistent with the assumed evolution of the system (Meintjes 2002b). A single blob with magnetic field $B_0 \sim 2000$ G and $E_c = 1.2$ MeV quickly loses its synchrotron observability in terms of the van der Laan evolution. How the flux density diminishes with expansion can be seen in Fig. 1(a). Also noticeable is the migration of the maximum flux towards lower frequencies as a result of the expansion of the blobs. It was found that to explain the observed non-thermal radio to infrared emission through a standard van der Laan process, i.e. no re-acceleration and a ρ^{-2} decrease in magnetic flux in expanding blobs (van der Laan 1963, 1966; Bastian et al. 1988), an unrealistically large number of blobs have to be integrated to obtain the observed flux levels at the lower frequencies (~1–10 GHz). Our model, which is in principle, an adapted van der Laan process, i.e. relying on continued re-acceleration and an equipartition frozen-in chaotic and twisted magnetic field inside gas blobs, shows promising results in terms of the flux evolution as a function of ρ (see Fig. 1b). From Fig. 1(b) it can be seen how the emission from an expanding blob is sustained by continuous acceleration and a slower

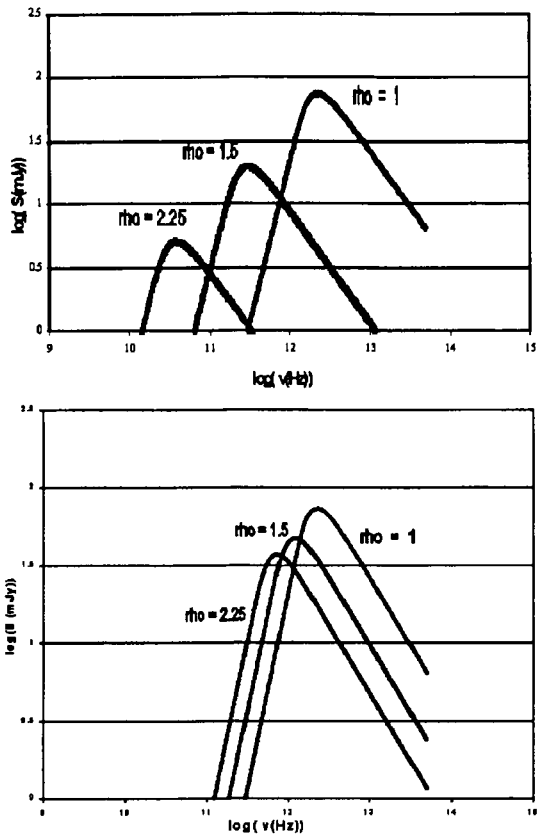

Figure 1. The simulated flux density (mJy) of a single blob as a function of $\rho = (r/r_0)$ for initial parameters $B_0 = 2000$ G and peak electron energy $\varepsilon_e = 1$ MeV. The upper panel represents a scenario where the electron energy diminishes with increasing ρ as a result of adiabatic losses. The lower panel represents an electron population that is continually energized as the blob is battered by the MHD propeller.

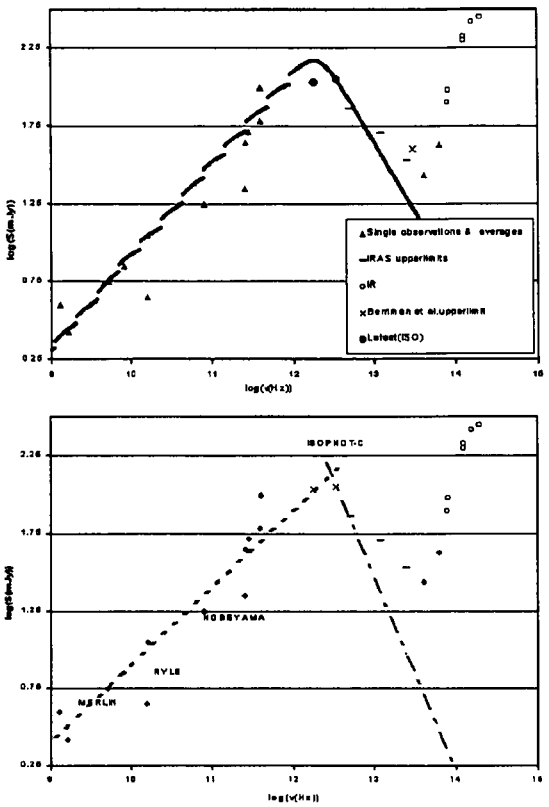

Figure 2. The top panel represents the simulated radio to IR spectrum representing the total integrated flux from approximately 20 initially highly magnetic, synchrotron-emitting blobs in different stages of their evolution. The spectrum represents the total integrated flux above the plasma frequency in each blob. Also indicated in this figure are time-averaged radio measurements, reported by Abada-Simon et al. (1999, 2002). It can be seen that the latest detection at 3333 GHz, according to our model, corresponds to optically thin emission after the turning point. The bottom panel represents a fit to the radio measurements, adapted form Abada-Simon et al. (1999). This fit represents a typical self-absorbed spectrum, which is reconcilable with the fact that the radio outbursts are a superposition of several synchrotron-emitting blobs in different stages of expansion. Noticeable from this figure is the good correlation between the measured and the simulated radio to infrared spectrum.

decaying equipartition magnetic field in the expanding blobs. This is a very positive result, since in our modulation of the radio flares the total integrated radio flux over all frequencies was simulated with a comparatively small fraction of the total mass outflow from the system being in the form of strongly magnetized ($B_0 \sim 2000$ G) synchrotron-emitting blobs.

To simulate the observed radio spectrum (Abada-Simon et al. 1999, 2002) approximately 16 blobs in different stages of evolution were used. The step length in terms of the expansion was kept constant for simplicity. The spectral flux density over a broad frequency range was integrated over all synchrotron-emitting blobs, taking into account the absorption of radio intensity below the plasma frequency in each blob. The spectrum simulated in this model is represented in Fig. 2. The observed averages from Abada-Simon et al. (1999, 2002) are included in Fig. 2 and it can be seen how the plasma frequency (calculated for each blob individually) cuts up the spectrum as the optical depth (for the radio band) decreases gradually for blobs in a more advanced stage of expansion, resulting in a gradual shift in the observable integrated flux towards lower frequencies. The lower-frequency emission therefore comes from older blobs, i.e. blobs that are in an advanced stage of their evolution. The turning point is expected to vary and not all of the spectrum, especially the high-frequency end, will be visible at all times since the peak flux is dominated by the emission from blobs in the initial stages of their evolution, which changes upon expansion as the peak observable flux migrates to the lower-frequency regime in terms of the VDL description (see Fig. 1). An important prediction forthcoming from our model is that variable non-thermal emission in the frequency region $\nu = (0.3\text{–}3.0) \times 10^{13}$ Hz at the 10–160 mJy level (below the *IRAS* sensitivity limit) is predicted (see Figs 1b and 2a). This frequency range is below the IR frequencies ($\nu \sim 3 \times 10^{14}$ Hz) dominated by the thermal blackbody spectrum of the secondary star.

The chosen parameters for the blobs all lie in non-extreme ranges. The attractive feature of this model is that it links the non-thermal outbursts in the system with the propeller outflow of magnetized gas blobs from the system that is also connected to optical outbursts in terms of blobs that cool radiatively as they expand. However, we showed that significantly less non-thermal ($\leqslant$20) than thermal (30–60) blobs exist at any given time in the system. Therefore, we do not predict a one-to-one correlation between radio and optical flares, although they both originate in the propeller-driven mass outflow.

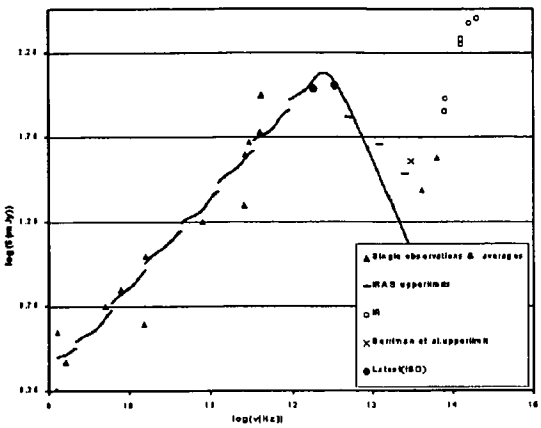

Figure 3. Simulated spectrum from 10 blobs with $B_0 = 3000$ G. The spectrum illustrates another valid parametrization of the model for the radio emission of AE Aqr.

Table 1. The first three columns pertain to a set of blobs with $B_0 = 2000$ G and the second with $B_0 = 3000$ G.

ρ	E_c (MeV)	δ	ρ	E_c (MeV)	δ
1	1	2.8	1	1	3.2
1.5	–	–	1.95	–	–
2.25	–	–	4	–	3.0
3.4	2	2.75	7	1.5	–
5	–	–	14	2	2.8
8	3	–	28	2.6	–
11	–	2.7	55	–	2.6
17	4	–	100	4	2.2
25	–	2.65	210	5.5	–
38	5.5	–	400	7	2.0
58	–	–			
87	8	–			
130	–	2.6			
195	11	–			
292	13	–			
400	15	–			

The scenario sketched above to explain the average radio-to-IR spectrum can be quantitatively represented by a range of parameter combinations. This is demonstrated by the simulated spectra in Figs 2 and 3. The first spectrum (Fig. 2) was obtained by integrating the flux from ~20 (16) blobs at different stages of expansion and an initial frozen-in field of 2000 G. The second spectrum (Fig. 3) is from only 10 blobs with an initial field of 3000 G. The simulated spectrum corresponding to $B_0 \approx 2000$ G (~20 blobs), showed that a peak flux of $S_\nu \sim 148$ mJy is produced at $\nu \sim 1805$ GHz (~166 μm), while a spectrum corresponding to $B_0 \approx 3000$ G (~10 blobs), results in a peak synchrotron flux of $S_\nu \sim 134$ mJy at $\nu \sim 2410$ GHz (~125 μm). The trend of the parameters used in the two simulations can be seen in Table 1. Note that our simulations include an effective hardening of the electron spectrum as a result of the continuous blob–propeller interaction, as is indicated in Table 1.

The lower-frequency end of the spectrum ($\leqslant$10 GHz) may be boosted by some quiescent flux from the ring of gas from the confluence of the blobs at late stages of expansion. The flux density expected from this synchrotron source is (Lang 1998)

$$S(\nu) = 0.933 \times 10^{-23} \alpha(\delta) K l B^{(\delta+1)/2} \times \left(\frac{6.26 \times 10^{18}}{\nu}\right)^{(\delta-1)/2} \left(\frac{\pi r_s^2}{D^2}\right) \text{erg s}^{-1}\,\text{cm}^{-2}\,\text{Hz}^{-1}, \quad (37)$$

where K is the constant in the electron energy distribution and l is the dimension of the source along the line of sight. The parameter $\alpha(\delta)$ is slowly varying with δ, and is of the order of unity. The physical parameters for the optically thin source, i.e. frozen-in magnetic field and particle density, were scaled from the expected values of expanding blobs at radii $\geqslant \rho = 700$–1000. The density of relativistic electrons was taken as ~0.01 cm^{-3} and energies of 1–5 MeV (for $\delta = 3$) were sufficient to provide a quiescent optically thin background, above the Razin frequency ν_R (i.e. Lang 1998), upon which the flares are superimposed. The two simulated spectra (Figs 2a and 3) include this background radiation, which contributes mainly in the frequency range around a few GHz.

6 DISCUSSION

In this paper a model is proposed to explain the observed non-thermal radio outbursts of AE Aquarii in terms of expanding radio-emitting magnetized blobs. It is proposed that the observed radio spectrum that represents a self-absorbed $S_\nu \propto \nu^\alpha$ power law is a superposition of several ($\leqslant$20) expanding, strongly magnetized ($\beta \leqslant 1$) blobs in different stages of their evolution. The model assumes that blobs possessing highly disordered tangled magnetic fields with strengths up to $B_0 \geqslant 2000$ G may be present among those leaving the L1 region. These blobs are then propelled out of the system by the propeller mechanism. The estimate for the blob magnetic fields is obtained from an estimate of the angular momentum losses through magnetic braking as a result of an ordinary Mestel & Spruit (1987) stellar wind, which allows an estimate of the coronal base surface field strength of the secondary star. Turbulence in the mass transfer process from the secondary star in the initial phase of mass transfer, and the interaction between the blob and the propeller may excite turbulent fluid motions in the blob that may induce fast Petschek-type magnetic reconnection with associated heating of electrons to energies of the order of $\varepsilon_e \approx 1$–2 MeV. In this initial phase synchrotron losses dominate expansion losses in the blobs. However, it was shown that reconnection can occur on time-scales that are shorter than the synchrotron loss time-scales on length-scales of the order of $l \sim 10^{-2} r_0$, where $r_0 \approx 10^9$ cm is assumed to be the initial blob size. As the blobs expand the synchrotron loss time-scale increases significantly to time-scales of the order of 30–60 min. Continuous interaction between the propeller and the blobs up to $\rho = (r/r_0) \approx 400$ may excite shocks in the magnetized plasma, resulting in a continuous acceleration in blobs with $\beta \leqslant 1$ via mechanisms such as shock drift acceleration (fast Fermi process), adiabatic compression and scattering from Alfvén waves. These acceleration mechanisms rely on the magnetic intensity for confining particles in the acceleration site (shocks and magnetic mirrors).

A radio spectrum in terms of our model is a superposition of several (~10–20) synchrotron-emitting magnetized bubbles ($B_0 \sim$ 2000–3000 G) (van der Laan mechanism) in different stages of expansion from $\rho = (r/r_0) = 1$–400, containing electron populations with energies between $\gamma \approx 2$ ($\rho = 1$) and $\gamma \approx 20$ ($\rho \approx 400$). Expanding blobs with dimensions corresponding to $\rho = 400$ have been observed at GHz frequencies during VLA observations of AE Aquarii (A.E. Niell, private communication). The simulated spectra follows a self-absorbed power law $S_\nu = S_0 \nu^\alpha$, with $S_0 \approx 2.1$ and

$\alpha \approx 0.55$ (for $B_0 \sim 2000$ G), and $S_0 \approx 2.2$ and $\alpha \approx 0.53$ (for $B_0 \sim 3000$ G), very similar to the values reported by Abada-Simon et al. (2002). For the choice of parameters, the simulations predict that the turning point may be anywhere between 125 and 166 μm. From Figs 2 and 3 it can be seen that the latest 5σ detection reported by Abada-Simon et al. (2002) already lies on the optically thin part of the radio spectrum, and that the model also excludes the possibility of detection by *IRAS*. The detectability of AE Aquarii as a strong variable radio source may depend on the magnetic field strength of the blobs, which in turn may depend on the magnetic cycle of the secondary K4-5 star. Continuous long-term monitoring of AE Aquarii may provide a means to determine the magnetic cycle of the secondary star of AE Aquarii, which in turn may provide answers as to the behaviour of magnetic activity in other short-period binaries.

ACKNOWLEDGMENTS

The authors wish to express their gratitude to Dr Henk Spruit (Max Planck Institute for Astrophysics) for valuable discussions regarding dynamo-generated fields in stars and the nature of associated magnetized mass flow. The authors also wish to thank Professor O.C. de Jager (PU for CHE) for valuable discussions regarding particle acceleration with shocks in $\beta < 1$ plasmas. The authors also wish to thank the referee for his positive comments, and his suggestions that helped to improve the quality of the paper.

REFERENCES

Abada-Simon M., Lecacheux A., Bookbinder J., Dulk G.A., 1993, ApJ, 406, 692
Abada-Simon M., Bastian T.S., Horne K., Bookbinder J.A., 1995a, in Buckley D.A.H., Warner B., eds, ASP Conf. Ser. Vol 85, Proc. Cape Workshop on Magnetic Cataclysmic Variables. Astron Soc. Pac., San Francisco, p. 355
Abada-Simon M., Bastian T.S., Bookbinder A.J., Aubier M., Bromage G., Dulk G.A., Lecacheux A., 1995b, in Lecture Notes in Physics, Vol. 454, Springer-Verlag, Berlin, 268
Abada-Simon M., Mouchet M., Aubier M., Barrett P., de Jager O.C., de Martino D., Ramsay G., 1999, in Cox P., Kessler M.F., eds, ESA SP-427, Proc. The Universe as seen by, *ISO*. ESA, Paris, p. 257
Abada-Simon M. et al., 2002, in Combes F., Barret D., eds, Semaine de l'Astrophysique Francaise. EdP-Sciences
Bastian T.S., Dulk G.A., Chanmugam G., 1988, ApJ, 324, 431
Beardmore A.P., Osborne J.P., 1997, MNRAS, 290, 145
Benz A., 1994, Plasma Astrophysics: Kinetic Processes in the Solar and Stellar Coronae. Kluwer, Dordrecht,, p. 285
Beskrovnaya N.G., Ikhsanov N.R., Bruch A., Shakhovskoy N.M., 1995, in Buckley D.A.H., Warner B., eds, ASP Conf. Ser. Vol. 85, Proc. Cape Workshop on Magnetic Cataclysmic Variables. Astron. Soc. Pac. San Fransisco, p. 364
Bookbinder J.A., Lamb D.Q., 1987, ApJ, 323, L131
Campbell C.G., 1997, Magnetohydrodynamics in Binary Stars. Kluwer, Dordrecht, p. 251
Chanmugam G., Frank J., 1987, ApJ, 320, 746
Cropper M., 1986, MNRAS, 222, 225
de Jager O.C., Meintjes P.J., O'Donoghue D., Robinson A.L., 1994, MNRAS, 267, 577
Dulk G.A., 1985, ARA&A, 23, 169
Eilek J.A., Hughes P.A., 1991, in Hughes P.A., ed., Beams and Jets in Astrophysics. Cambridge Univ. Press, Cambridge, p. 428
Eracleous M., Horne K., 1996, ApJ, 471, 427
Frank J., King A.R., Lasota J.P., 1988, A&A, 193, 113
Frank J., King A.R., Raine D., 1992, Accretion Power in Astrophysics. Cambridge Univ. Press, Cambridge, p. 46
Holman G.D., Pesses M.E., 1983, ApJ, 267, 837
King A.R., 1988, QJRAS, 29, 1
King A.R., 1993, MNRAS, 261, 144
King A.R., Lasota J.P., 1991, ApJ, 378, 674
Kuijpers J.P., Pringle J.E., 1982, A&A, 114, L4
Kuijpers J., Fletcher L., Abada-Simon M., Horne K., Raadu M.A., Ramsay G., Steeghs D., 1997, A&A, 322, 242
Lang K.R., 1998, Astrophysical Formulae, 3rd edn, Vol. 1. Springer-Verlag, Berlin
McDermott P.N., Taam R.E., 1989, ApJ, 342, 1019
Meintjes P.J., 1992, PhD thesis PU for CHE, Potchefstroom
Meintjes P.J., 2002a, in Flanagan C.S., Frescura F.A.M., Woerman B., eds, Proc. Pulsar Studies in Africa Workshop. African Skies, no, 7, 5
Meintjes P.J., 2002b, MNRAS, 336, 265
Meintjes P.J., de Jager O.C., 2000, MNRAS, 311, 611
Meintjes P.J., Raubenheimer B.C., de Jager O.C., Brink C., Nel H.I., North A.R., van Urk G., Visser B., 1992, ApJ, 401, 325
Meintjes P.J., de Jager O.C., Raubenheimer B.C., Nel H.I., North A.R., Buckley D.A.H., Koen C., 1994, ApJ, 434, 292
Mestel L., Spruit H.C., 1987, MNRAS, 226, 57
O'Donoghue D. et al., 1995, in Buckley D.A.H., Warner B., eds, ASP Conf. Ser. Vol. 85, Proc. Cape Workshop on Magnetic Cataclysmic Variables. Astron. Soc Pac., San Fransisco, p. 368
Pacholzyk A.G., 1970, Radio Astrophysics. Freeman, San Francisco
Parker E.N., 1958, ApJ, 128, 664
Parker E.N., 1963, ApJS, 8, 177
Parker E.N., 1976, in Seti G., ed., The Physics of Non-thermal Radio Sources. Reidel, Dordrecht, p. 137
Patterson J., 1979, ApJ, 234, 978
Patterson J., 1994, PASP, 106, 209
Patterson J., Branch D., Chincarini G., Robinson E.L., 1980, ApJ, 240, L133
Petschek H.E., 1964, AAS–NASA Symp. on the physics of solar flares. NASA Special publications SP-50, p. 425
Priest E.R., 1981, in Priest ed., Solar Flare Magnetohydrodynamics. Gordon and Breach, New York, p. 139
Priest E., Forbes T., 2000, Magnetic Reconnection: MHD Theory and Applications. Cambridge Univ. Press, Cambridge, pp. 120, 460
Saar S.H., 1991, in Tuominen I., Moss D., Rudiger G., eds, The Sun and Cool Stars: Activity, Magnetism, Dynamos. Springer, Berlin
Sarris E.T., Krimigis S.M., 1985, ApJ, 298, 676
Sweet P.A., 1958a, in Lehnert B., ed., IAU Symp. 6, Electromagnetic Phenomena in Cosmical Plasmas. Cambridge Univ. Press, Cambridge, p. 123
Sweet P.A., 1958b, Nuovo Cimento Suppl., 8, X., 188–196
Tanzi E.G., Chincarini G., Tarenghi M., 1981, PASP, 93, 68
Toptyghin I.N., 1980, Space Sci. Rev., 26, 157–213
van der Laan H., 1963, MNRAS, 126, 535
van der Laan H., 1966, Nat, 211, 1131
van Paradijs J., Kraakman H., van Amerongen S., 1989, A&AS, 79, 205
Warner B., 1995, Cataclysmic Variable Stars. Cambridge Univ. Press, Cambridge, pp. 7, 376, 417
Wynn G.A., King A.R., 1995, MNRAS, 275, 9
Wynn G.A., King A. R., Horne K., 1995, in Buckley D. A. H., Warner B., eds, ASP Conf. Ser. Vol. 85, Proc. Cape Workshop on Magnetic Cataclysmic Variables. Astron Soc. Pac., San Francisco, p. 196
Wynn G.A., King A.R., Horne K., 1997, MNRAS, 286, 436

This paper has been typeset from a TEX/LATEX file prepared by the author.

Opsomming

Die verhandeling stel 'n model voor vir die oorspong van die waargenome radio uitbarstings van die binêre ster AE Akwarius. Die sisteem bestaan uit 'n wit dwerg (WD) en rooi dwerg (RD) wat mekaar omwentel met 'n periode van P_{om} ~10 h. Die kompakte WD en sy relatief sterk magneetveld (magnetosfeer) spin om sy eie as met 'n periode van P_{WD} ~ 33 s. Plasma wolke val van die RD na die WD en 'n gedeelte van hierdie massa oordrag bereik die oppervlak van die WD waar X-strale en optiese straling vrygestel word. 'n Belangrike aspek van die sisteem is dat die meeste van die oordrag deur die snel tollende magnetosfeer van die WD uit die sisteem geslinger word.

'n Aanname van die model is dat 'n gedeelte van die oordrag gemagnetiseerd is met 'n veldsterkte tot ongeveer 3000 G, afkomstig van die oppervlak magneetveld van die RD. Die wolke ontstaan by die L1 punt van die Roche potensiaal waar die swaartekrag en sentripetale kragte van die twee-ster kombinasie in ewewig is en plasma deur drukgradiënte van die RD na die WD oorgestoot word. In die proses word van die RD se magneetveld in die wolke vasgevang en elektrone word ook versnel tot matig relativistiese energieë (1-15 MeV). Hierdie energieke elektrone in die magneetveld straal dan deur die synkrotron proses in die radio na infra-rooi frekwensie gebied.

Die straling verloor intensiteit soos die wolke uitsit, die veld verswak en die elektrone energie verloor. In die model word egter voorgestel dat die elektrone herversnelling ondergaan in die uitslinger proses. Tydens die slinger aksie word die elektrone geaktiveer deur die saampersende aksie van die magnetosfeer op die plasmawolke deur middel van versnellings meganismes soos skok-dryf versnelling en magnetiese pomping.

Verder word aanvaar dat die magneetveld in die wolke verstrengel is in 'n hoogs turbulente medium. Hierdie verstrengelde veld verseker knope van hoë magnetiese energie digtheid waar versnelling kan plaasvind, maar wat ook stadiger verswak met die uitsetting van die wolke. Die kombinasie van herversnelling van elektrone en die versterkte veld in die wolke verseker dat 'n wolk vir langer 'n stralingsbron kan bly. Hierdie langer 'leeftyd' vir 'n radio wolk is belangrik om die waargenome tydvariasie van die radio vloed van die sisteem te kan verklaar.

Die Van der Laan model beskryf die tydsverandering van die straling vanaf 'n synkrotron wolk wat uitsit. Dié idee word toegepas op die plasmawolke wat by AE Akwarius uitgegooi word en uitsit soos dit wegdryf. Die vloed word bereken vir 'n wolk in die radio tot infra-rooi frekwensie gebied. Die vloed van wolke in verskillende stadiums van uitsetting word dan gesommeer in elke frekwensie band bokant die plasma frekwensie van elke individuele wolk. Die resultaat is 'n spektrum wat vergelyk kan word met die gemiddelde waargenome spektrum.